U.S. ARMY RDECOM

SPECIAL REPORT RDMR-AF-14-01

DESIGN AND FLIGHT TEST OF A CABLE ANGLE FEEDBACK CONTROL SYSTEM FOR IMPROVING HELICOPTER SLUNG LOAD OPERATIONS AT LOW SPEED

Christina Ivler
Aeroflightdynamics Directorate
Aviation and Missile Research, Development, and Engineering Center

April 2014

AMRDEC

DESTRUCTION NOTICE

FOR CLASSIFIED DOCUMENTS, FOLLOW THE PROCEDURES IN DoD 5200.22-M, INDUSTRIAL SECURITY MANUAL, SECTION II-19 OR DoD 5200.1-R, INFORMATION SECURITY PROGRAM REGULATION, CHAPTER IX. FOR UNCLASSIFIED, LIMITED DOCUMENTS, DESTROY BY ANY METHOD THAT WILL PREVENT DISCLOSURE OF CONTENTS OR RECONSTRUCTION OF THE DOCUMENT.

DISCLAIMER

THE FINDINGS IN THIS REPORT ARE NOT TO BE CONSTRUED AS AN OFFICIAL DEPARTMENT OF THE ARMY POSITION UNLESS SO DESIGNATED BY OTHER AUTHORIZED DOCUMENTS.

TRADE NAMES

USE OF TRADE NAMES OR MANUFACTURERS IN THIS REPORT DOES NOT CONSTITUTE AN OFFICIAL ENDORSEMENT OR APPROVAL OF THE USE OF SUCH COMMERCIAL HARDWARE OR SOFTWARE.

REPORT DOCUMENTATION PAGE

Form Approved
OMB No. 074-0188

1. AGENCY USE ONLY	2. REPORT DATE	3. REPORT TYPE AND DATES COVERED
	April 2014	Final

4. TITLE AND SUBTITLE
Design and Flight Test of a Cable Angle Feedback Control System for Improving Helicopter Slung Load Operations at Low Speed

5. FUNDING NUMBERS

6. **AUTHOR**(S)
Christina Ivler

7. PERFORMING ORGANIZATION NAME(S) AND ADDRESS(ES)
Commander, U. S. Army Research, Development, and Engineering Command
ATTN: RDMR-ADF
Redstone Arsenal, AL 35898-5000

8. PERFORMING ORGANIZATION REPORT NUMBER
SR-RDMR-AF-14-01

9. SPONSORING / MONITORING AGENCY NAME(S) AND ADDRESS(ES)

10. SPONSORING / MONITORING AGENCY REPORT NUMBER

11. SUPPLEMENTARY NOTES

12a. DISTRIBUTION / AVAILABILITY STATEMENT
Approved for public release; distribution is unlimited.

12b. DISTRIBUTION CODE
A

13. ABSTRACT ***(Maximum 200 Words)***

The ability of a helicopter to carry externally slung loads makes it very versatile for many civil and military operations. However, the piloted handling qualities of the helicopter are degraded by the presence of the slung load. This dissertation investigates the dynamics, handling qualities requirements, and control aspects of the helicopter/slung load system that contribute to the performance of piloted slung load operations. A control system is developed that integrates measurements of both slung load motions and conventional fuselage feedback to improve the handling qualities for hover/low speed operations. Despite the fact that this technology was developed 40 years ago, it has not been tested in a manned helicopter since the 1970s, due to problems with handling qualities and pilot perception. This dissertation leverages advances in fly-by-wire, complex control design procedures (direct multi-objective optimization), and recently developed work that relates handling qualities to dynamic response (specifications) to successfully flight test cable angle feedback technology in a manned helicopter. The key contributions of this work are developing an understanding of the handling qualities trade-offs for cable angle/rate control system design, implementing an approach to solve the problem with a novel task-tailored control system, and performing extensive piloted flight tests of the control system on a fly-by-wire Black Hawk. The flight tests demonstrated that average precision load set-down time was reduced by 50% for a light load, 30% for a heavy load, and the average handling qualities rating for the external load placement task was improved from Level 2 to Level 1 on the Cooper-Harper rating scale, a significant improvement.

14. SUBJECT TERMS
Rotorcraft Flight Control, External Load Control, Slung Load Control, Cable Angle Feedback, Handling Qualities, Active External Load Control, Slung Load Stabilization, Load Placement, Coupling Numerators

15. NUMBER OF PAGES
158

16. PRICE CODE

17. SECURITY CLASSIFICATION OF REPORT	18. SECURITY CLASSIFICATION OF THIS PAGE	19. SECURITY CLASSIFICATION OF ABSTRACT	20. LIMITATION OF ABSTRACT
UNCLASSIFIED	UNCLASSIFIED	UNCLASSIFIED	UNLIMITED

NSN 7540-01-280-5500

Standard Form 298 (Rev. 2-89)
Prescribed by ANSI Std. Z39-18
298-102

DESIGN AND FLIGHT TEST OF A CABLE ANGLE FEEDBACK CONTROL SYSTEM FOR IMPROVING HELICOPTER SLUNG LOAD OPERATIONS AT LOW SPEED

A DISSERTATION

SUBMITTED TO THE DEPARTMENT OF AERONAUTICS AND ASTRONAUTICS AND THE

COMMITTEE ON GRADUATE STUDIES

OF STANFORD UNIVERSITY

IN PARTIAL FULFILLMENT OF THE REQUIREMENTS

FOR THE DEGREE OF

DOCTOR OF PHILOSOPHY

Christina Ivler

December 2012

ACKNOWLEDGEMENTS

I am forever amazed and grateful for the large number of people who have offered their support, advice, and encouragement during the last 4 years that I have been working towards this degree. This doctorate has been the most difficult endeavor of my life, and I certainly could not have done it alone.

First, I would like to thank my advisor Prof. Dave Powell, for accepting me as one of your doctoral students. Dave, you have pushed me to think outside the box and have really helped me to bring my research to the next level. You are also an amazing mentor, and I have enjoyed our chats on engineering, life, and skiing.

I would also like to thank Dr. Mark Tischler for acting as a mentor at AFDD. You always have believed in me, and gave me the support and confidence I needed to go back to school and get this degree. Your insights always surprise me, and you keep me on my toes, which is much appreciated (even if I don't always show it).

There are many people at AFDD who have supported me along the way. Everyone in the flight control group has acted as a wonderful support system for me. Thanks to Hossein Mansur for being my biggest cheerleader and offering great reassurances in moments of doubt. I would like to thank Jeff Lusardi for providing some excellent advice and ideas to make the flight testing of this research successful. To the 'young punk' crowd in the trailer (Tom Berger, Eric Tobias, Brian Fujizawa, Ondrej Juhasz, Marcos Berrios, Lisa Fern) thanks for your friendship and your help along the way. Kenny Cheung, thanks for being a great office mate, and for all the software support you have given me. Thanks also to Luigi Cicolani for giving me access to your library of slung load references. The RASCAL group was critical to making the flight tests for this research happen. Thanks to Jay Fletcher, Kevin Kalinowski, Ernie Moralez, and Dennis Zollo for your hard work that extended into many late nights and early mornings. Thanks to Lieutenant Colonel Carl Ott for your insight and inputs during the development of the control system, and also your patience, attention to detail and ability to describe your observations in flight in a way that makes sense to an engineer. Thank you to Lieutenant Colonel Michael Olmstead for stepping in during the initial flight tests of this research, and for your willingness to jump in and do frequency sweeps with the slung load on your first flight with the external load, you really saved the day. The FPO and L3 flight operations groups in the hangar were also very helpful and played a key role in supporting these flight tests. Thanks to everyone who supported flight operations for your expertise, hard work, and time away from your families when flight tests extended into Friday afternoon and Saturday. Finally, the management at AFDD has been wonderfully supportive. Chris Blanken, Barry Lakinsmith and Dick Spivey - I feel very blessed to work for people who have made it possible to complete a PhD while still working full time. This is really a dream come true and I thank you so much.

My family has provided me with a huge amount of love and support during this process. I am so grateful to my parents, Dave and Cathy Spaulding, for pushing me to always do my best in school and

instilling in me the belief that anything is possible if you try hard enough. Sisters and brother-in-law Clara Leik, Nick Leik, and Kim Spaulding, thanks for believing in me and being excited for me, it has helped me through the tough spots. Additionally, I have to thank all my in-laws in 'The Ivler Family' for being proud of me (and letting me know it). Thank you to both the Spaulding and Ivler clans for offering your unconditional love and support.

Finally, my husband, Evan Ivler is the person who I must thank the most. Evan, you have given up so much to help me pursue my dream. You have been there during the long nights of homework, hours studying for quals, and days agonizing over flight test results. You have made dinners and cleaned house and run errands while I was busy with my academic pursuits. You gave me courage in moments of weakness, and picked me up when I thought I could not go on -- without you I would have never had the guts or the sanity to face and complete this very difficult goal. I love you.

December 2012

Moffett Field, CA

Christy Ivler

TABLE OF CONTENTS

LIST OF FIGURES

LIST OF TABLES

NOMENCLATURE

$\boldsymbol{A}, \boldsymbol{B}, \boldsymbol{C}, \boldsymbol{D}$	=	state-space description of vehicle dynamics
$\frac{D}{\bar{q}}$	=	drag normalized by dynamic pressure (ft2)
g	=	acceleration due to gravity (ft/s2)
I_L	=	inertia of slung load (slug-ft2)
$I_{xx}, I_{yy}, I_{zz}, I_{xz}$	=	moments of inertia (slug-ft2)
l	=	sling length (ft)
L, M, N	=	moment components about body-fixed x, y, and z directions (lb-ft)
m	=	mass (slug)
m_A	=	mass of aircraft (slug)
m_L	=	mass of load (slug)
$\boldsymbol{M}, \boldsymbol{F}, \boldsymbol{G}$	=	state-space description of vehicle dynamics with mass-matrix
p_c, q_c	=	lateral and longitudinal inertial cable rates (rad)
p, q, r	=	vehicle roll rate, pitch rate, yaw rate (rad/s)
${}^{A}R^{B}$	=	rotation matrix from coordinate system B to coordinate system A
s	=	Laplace variable
t	=	time (s)
T	=	cable tension (lb)
u, v, w	=	velocity components in the body-fixed x, y, and z directions (ft/s)
u_o, v_o, w_o	=	trim velocity components in body-fixed x, y, and z directions (ft/s)
V_o	=	trim aircraft velocity (ft/s)
$\vec{x}, \vec{y}, \vec{u}$	=	state vector, output vector, control vector
X, Y, Z	=	force components in the body-fixed x, y, and z directions (lb)
X,Y,H	=	longitudinal position, lateral position, and height (ft)
z_a	=	vertical offset from aircraft center-of-gravity to the hook (where sling connects to fuselage) (ft)
δ_a	=	actuator input (in)
$\delta_{lon}, \delta_{lat}, \delta_{col}, \delta_{ped}$	=	longitudinal cyclic, lateral cyclic, collective, pedal inputs (in)

Δ	=	characteristic equation
$\Delta\theta_{co}$	=	trim longitudinal cable angle relative to fuselage (rad)
Δ_{MAG}	=	depth of magnitude distortion of aircraft with external load, as compared to an unloaded aircraft on a Bode plot (dB)
$\Delta\dot{x}_c, \Delta\dot{y}_c$	=	velocity of the load in the cable-axis x and y directions, relative to the helicopter (ft/s)
$\Delta\phi_c, \Delta\theta_c$	=	lateral and longitudinal cable angles relative to the aircraft (rad)
ζ	=	damping ratio
θ_o	=	trim aircraft pitch attitude (rad)
ρ	=	air-density (lb/ft3)
$\bar{\tau}$	=	time delay vector (s)
ϕ, θ, φ	=	Euler angles (rad)
ϕ_c, θ_c	=	lateral and longitudinal inertial cable angles (rad)
ϕ_L, θ_L, ψ_L	=	load Euler angles with respect to the inertial frame (rad)
ω	=	frequency (rad/s)
ω_n	=	natural frequency (rad/s)
ω_{-135}	=	frequency where the phase of response crosses -135 degrees on a Bode plot (rad/s)

ACRONYMS

AC	=	Attitude Command control system response type
ALTHLD	=	ALTitude HoLD control system response type
CAF	=	Cable Angle/rate Feedback control system
DRB	=	Disturbance Rejection Bandwidth
EGI	=	Embedded GPS/INS
FCS	=	Flight Control System
GM	=	Gain Margin (dB)
HQR	=	Handling Qualities Rating
LMR	=	Load Mass Ratio - $m_A/(m_A + m_L)$
MTE	=	Mission Task Element
OBL	=	Optimized BaseLine control system
PH	=	Position Hold control system response type
PID	=	Proportional, Integral, Derivative type controller
PM	=	Phase Margin (dB)
RASCAL	=	Rotorcraft Aircrew Systems Concepts Airborne Laboratory (Fly-by-wire UH-60A Black Hawk)
RCHH	=	Rate Command Heading Hold
SAS	=	Stability Augmentation System
VH	=	Velocity Hold control system response type
XOVER	=	Cross-over frequency, where Bode magnitude is 0dB (rad/s)

1 Introduction

1.1 Motivation

The operation of helicopters carrying externally slung loads has an important role in military and civilian applications for many diverse tasks such as delivering supplies, search and rescue, construction, fire-fighting, and logging. The additional utility of operating with a slung load comes at the cost of higher piloted workload due to the nature of controlling a two-body dynamic system: helicopter and slung load. The pilot must maneuver the helicopter effectively in order to fly to the drop-off point, monitor load motions, and eventually place the load down in a precise location – often without visibility of the load from the cockpit. Precision load delivery requires extensive compensation from the pilot, because this task requires the pilot to adopt a strategy similar to a non-collocated [1] control system to indirectly control the load position though the rotor. It is well known that the presence of external loads causes degraded piloted handling quality characteristics, especially for configurations with long slings and heavy loads [2].

Slung load operations have a high rate of accidents. Manwaring et. al studied the 230 civil helicopter slung load accidents that occurred between 1980 and 1995, which accounted for 11% of all helicopter accidents [3]. One of the specific risk factors identified was the potential for overload in solo pilots. This is especially true in logging, where there is one pilot who flies all day long, and must divide attention between the engine temperatures, warning lights, fuel quantity, and various other gauges, as well as watching the load to keep it clear of obstacles and ground personnel, and keep the rotor blades clear of the trees [4]. Despite the recommendations of Manwaring in 1998 regarding the high workload of helicopter external load operations, this aspect of external load operations was not improved in the following 10 years, as noted by deVoogt's study of the 120 civilian helicopter external load accidents between 1995-2005 [5]. A key finding of deVoogt's study was that training and experience still cannot compensate for the demands on the solo pilot, and that the addition of crew (either flight or ground) could considerably reduce pilot workload.

The potential for high pilot workload is also prevalent in military external load operations. Key's study of military helicopter operations showed that marginal or deficient handling qualities, which result in higher pilot workload, had a strong correlation with pilot error mishaps [6]. The author of Ref. 6 comments that adverse circumstances such as blowing dust can result in very long hook-up times (10 to 15 min), and that a hook-up crewman could have difficultly when he is "standing in the dark, in a tornado of downwash with a 46,000lb helicopter drifting around inches above his head". In this study of military helicopter mishaps, approximately 10 out of 35 total pilot error mishaps on the CH-47D were slung load related (although often only damage was done to the load). Still, this represents a relatively high rate (28%) of mishaps related to slung load operations on the CH-47D.

Pilot experience also plays a heavy role in the potential for accidents and mishaps. Both Key's military study and deVoot's analysis of civilian data point out that accident rates increase as pilot experience falls. In addition, Horcher's case study which used GPS to track helicopter yarding (logging) operations indicated that an experienced pilot was 63% more productive than an inexperienced pilot [7].

A method of relieving pilot workload and compensating for pilot inexperience is to introduce a feedback flight control system, which augments the pilot's input to provide improved stability, handling qualities, and load damping. In fact, advanced control laws are a proven and recommended method of reducing pilot workload in military operations, as noted in the military's recent rotorcraft survivability study [8]. Key points out that a good flight control system that improves handling qualities demands less skill from the inexperienced pilot and improves safety in degraded visual environments for all pilots [6]. Advanced control laws typically include semi-autonomous modes such as velocity hold, altitude hold, and position hold, which are very applicable to external load operations. In addition, if the load motion were measured, it would be possible to control the external load automatically.

This dissertation describes the design and flight test of an advanced full authority fly-by-wire flight control system (FCS) with novel architecture that implements external load cable angle and cable rate feedbacks combined with conventional fuselage feedback in order to improve piloted handling qualities with an external load. The focus is on hover/low speed operations, as pilot interviews by the author have identified the load pick-up/placement as the most difficult aspect of slung load operations, requiring high pilot workload. In addition, DeVoogt identifies hover as the critical flight phase, which accounted for 41% of accidents [5]. Key also points out that military pilot-error mishaps from low speed maneuvering are significantly more prevalent [6]. The goal of this research is to improve hover/low speed pilot workload and increase load placement precision, both of which are critical to improving safety and efficiency of helicopter external load operations. These benefits are applicable and desirable in both military and civilian slung load operations.

1.2 Background

With the development of a prototype of the Heavy Lift Helicopter by Boeing in the 1970s came many ideas for automatically controlling helicopters with external loads. During this development period, before the program was canceled, two methods for providing active damping of the load emerged. The first method is a *direct* "on-load" control mechanism. The on-load actuator provides a direct control force (or moment) to the load or sling, which can damp the load motions independently of the fuselage motions. Many examples of this type of system were discussed in the literature of the 70s; including an active arm [9] installed on the hook, an active winch system [10] and an aerodynamically stabilizing fin on the load [11,12]. The second method is to *indirectly* control the load motion through load feedback to the rotor. To damp load motions, the helicopter must be used as an actuator to control the response of the load, and therefore the load cannot be damped independently of fuselage motions. The concept of using a feedback

system to the rotor to *indirectly* damp the load motions by utilizing cable angle feedback was pioneered in the 1970s by Dukes[13], Gupta[14,15], Liu[12] and Hutto[16]. Lui and Gupta focused on optimal control methods for full-state feedback including load motions. Dukes and Hutto used classical control methods to improve load damping. Reference 12 provides a comprehensive trade-off study comparing these direct and indirect load controlling methods. It was concluded that the indirect feedback systems were more complex in implementation due to electronic technological limitations at the time (1970s), but were more robust in their effectiveness to differing load configurations as compared to control devices installed directly on the external load.

Modern electronic control technology enables much easier implementation of an indirect feedback control system of load motions to the helicopter rotor. The indirect feedback method can be easily incorporated into an existing fly-by-wire system. It requires only a measurement of the load states, and flight control software changes, which demands relatively few hardware changes. In contrast, the direct method requires installation of additional actuators, which adds mechanical complexity and weight, and still requires the same sensors to measure the load motion. Therefore, the indirect method of cable angle/rate feedback to the rotor is the focus taken herein.

The modern flight-test research in the area of indirect external load feedback control for helicopters focuses on *unmanned* aerial vehicles (UAVs). The unmanned K-MAX helicopter uses cable angle feedback to aircraft controls (i.e. indirect control) to stabilize the load motions [17]. Another example of indirect control is given in Ref. 18 which applied a feed forward technique previously used on overhead cranes to reduce swing motion on an unmanned autonomous Bergen Industrial Twin (5.3 ft rotor diameter). Another study on small unmanned rotorcraft implemented delayed load state feedback to the rotor (indirect control) to damp load motions on the GT-Max (10.2 ft rotor diameter) and the indoor electric AAU Corona (2ft rotor diameter) [19]. Kang developed a system for autonomous precision airborne cargo delivery to moving platforms, and demonstrated it on the unmanned GT-Max helicopter [20]. The focus of these flight test studies has been on unmanned load damping and delivery, where handling qualities and pilot perception are not relevant.

Current literature on *manned* indirect external load feedback has shown analytical benefits of incorporating cable angle/rate feedback into a modern full-authority flight control system. One such study has shown that conventional fuselage feedback control systems for helicopters with heavy external loads cannot provide adequate stability margins and simultaneously meet the military helicopter handling qualities specification (ADS-33E-PRF [21]) requirements, particularly in the roll axis [22]. Reference 22 also analytically demonstrated for the CH-53K that adding an advanced feedback configuration including cable rate feedback can provide improved stability margins. Recently, the German Aerospace Center (DLR) has also begun analytically exploring the use of rotor-state feedback for helicopter sling load positioning [23], and helicopter sling load damping [24]. This work was motivated by the DLR's

experience with difficulty in load placement of an externally slung pioneer bridge on a CH-53G (with standard fuselage feedback). This task had a high workload due to poor load damping, and the inability of the pilot to see the load in the test aircraft (CH-53G), which resulted in long set-down times. Based on the analytical studies in Ref. 23 and Ref. 24, Brenner concludes that the cable angle feedback technology could improve piloted workload in load placement. The modern body of literature focuses on the analytical and lacks flight test studies to determine/address the effects of the load feedback on handling qualities and pilot perception.

Recent studies by the German Aerospace Center (DLR) address the problem of pilot perception by focusing on a flight director for the Bo-105 and CH-53G helicopters, which does not use cable angle feedback control, but instead provides a display aid to the pilot for damping pendulous load motion [25,26]. This method was flight tested and has proven very effective at damping unruly modes in forward flight, and leaves the pilot in full control thus eliminating handling qualities concerns associated with automatic load damping. However, this method requires the pilot to be looking at a cockpit display as opposed to out the window, which would make it difficult for low speed, low altitude operations such as precision load placement that often occur near obstacles (such as in logging). The DLR did not test this technology for load placement tasks. However, in 1974, DiCarlo [27] studied a similar technology, closed-circuit television as a pilot aid, for load placement. The closed-circuit television aid for load placement was compared to the conventional method of using a crew chief to call out load position (still the current method used when the pilot cannot see the load) and the use of a load-facing pilot (for load placement only). This study showed that the closed-circuit television had the highest pilot workload because the pilot was required to split attention between the display and the outside world. The pilots reported that the crew-chief and load-facing pilot methods had much lower workload and that the load-facing pilot had the highest precision overall.

Although the pilot aid is good solution in terms of pilot perception of the handling qualities, it would increase pilot workload by dividing pilot attention at hover/low speed. Automatic control of the load with cable angle feedback is a more appropriate solution for hover/low speed because the pilot can focus more fully on the situation outside of the cockpit. However, in order to do this successfully the issue of handling qualities must be addressed.

Pilot perception of handling qualities, in large part, has discouraged the use of cable angle feedback in flight over the past 40 years. Despite the analytical benefits of cable angle feedback, there are no recent *manned* flight tests of the technology. In fact, the last manned flight tests of this technology are from the 1970s work on the heavy lift helicopter demonstrator (a CH-47C) [16,28]. These flight tests demonstrated the ability to improve the damping of the load pendulum motions, but the load feedback generally had the effect of making the load feel heavier to the pilot [28]. This is not a desirable outcome because a heavier load is generally associated with poor maneuvering handling qualities [2].

In the years since the CH-47C cable angle flight tests fly-by-wire, handling qualities studies and handling qualities criteria for helicopters with slung loads have been developed [2,21]. Also modern tools are now available for multi-objective control design that optimize against many specifications simultaneously including load response, handling qualities and stability. In addition to applying these enabling technologies in a cohesive way, this dissertation takes a fundamentally different approach to previous literature in the development of an automatic control system for a manned application that addresses the pilot's perception. As opposed to the past focus on only load damping, handling qualities for maneuvering and load placement are considered to be of critical importance. This dissertation makes use of modern technology, specifications, control design techniques and handling qualities considerations to enable the first successful flight tests of cable angle feedback technology since the 1970s.

1.3 Contributions of Dissertation

The problem of handling qualities for external load operations is well known in the industry. In the 1970s external load feedback was demonstrated to improve load damping in flight, but was not able to win pilot acceptance and was very difficult to install at the time. Thus, the problem of how to effectively use cable angle/rate feedback to improve manned helicopter operations has plagued the industry for the last 40 years, resulting in no flight test demonstrations of the technology during this time. This dissertation leverages advances in fly-by-wire, complex control design procedures (direct multi-objective optimization), and recently developed work that relates handling qualities to dynamic response (specifications) to successfully flight test cable angle feedback technology in a manned helicopter. The key contributions of this work are developing an understanding of the handling qualities trade-offs for cable angle/rate control system design, implementing an approach to solve the problem with a novel task-tailored control system, and performing extensive piloted flight tests of the control system on a fly-by-wire Black Hawk. These three key contributions are described in detail below.

Key Contributions

1. *Identification of trade-off between handling qualities and load damping*

Coupling numerator analysis [29, 30, 31], which was used to provide an effective single input response for analysis of basic helicopter/load dynamics, indicates that a trade-off exists between load damping and handling qualities for a cable-angle feedback control system. Coupling numerator analysis was used to show that the load damping can be improved through cable feedback to the rotor only at the cost of degraded (predicted) handling qualities characteristics, and vice-versa. This is the first time such a trade-off is recognized in the literature. The trade-off was explored with root-locus and bode control design techniques.

2. *Development of a task-tailored technique for cable angle/rate feedback*

A full-order attitude command control system was developed starting from the coupling numerator analysis and tested in a piloted fixed-base simulator to demonstrate that the pilot's comments were

consistent with a trade-off between load damping and handling qualities. This analysis and piloted simulation led to the key contribution of this thesis, which is a task-tailored control system with fuselage and cable angle/rate feedback. The task-tailored control law is a novel technique which provides improvements to pilot handling qualities during maneuvering and provides load damping (which degrades pilot handling) in an automated hover-hold mode. The control feedbacks were designed using multi-objective optimization. This architecture enables pilots to have the advantages of improved load damping while also meeting the handling qualities goals.

3. *Significant, flight validated improvement in handling qualities and load placement*

The 40 hours of manned flight tests that were completed on an experimental fly-by-wire JUH-60 Black Hawk helicopter are an important contribution to the literature. The last manned flight test of such a system was performed in the 1970s. This research contributes the first full set (3 pilots) of handling qualities ratings for a cable angle/rate feedback control system using modern evaluation techniques such as ADS-33 mission task elements. In addition, a new precision load placement task was developed and tested by 5 pilots. This task is planned to be added to the military helicopter design standard, ADS-33E-PRF [21], because this important and high workload aspect of slung load operations was not previously included as a mission task element in the specification.

Overall, the task tailored control system contributes improved handling qualities ratings from Level 2 to Level 1 (Cooper Harper [32]), as compared to the legacy partial authority SAS used on the operational UH-60A/L. It also improves precision load placement times by 50% for a 1000lb load, and 30% for a 5000lb load. If implemented operationally, these handling qualities and precision load placement improvements would increase safety for pilots and ground personnel, and improve efficiency of external load operations.

Supporting Contributions

In addition to the key contributions that were made in this dissertation, there were some significant supporting contributions that enabled the successful development and flight testing of the cable angle/rate feedback control system. These supporting contributions are described below.

1. Explicit linear model structure for helicopter/slung load dynamics

This dissertation develops an analytical linear model structure for a helicopter with an externally slung load that can be appended to an existing unloaded helicopter model. This model structure is unique and also very useful for system identification because unknown terms such as helicopter stability and control derivatives are not lumped into known physical quantities associated with the slung load, such as sling length or load mass.

2. Derivation of state-space constrained coupling numerator analysis

Coupling numerator analysis has been used in the literature to calculate the effective single-input/single-output transfer function of a system with key off-axis responses tightly constrained by the

other control inputs [31]. These constrained coupling numerator solutions presented in the literature are limited because they can only provide a single SISO transfer function. For higher-order systems, this dissertation derives a state-space representation with multiple inputs and outputs, with some but not all, of these inputs and outputs constrained. The new solution for the constrained coupling numerator is presented in state-space form. The resulting system is employed to look at basic coupling effects of cable angle/rate feedbacks in the lateral axis.

3. *Key methods for successful flight test integration of cable angle/rate feedback*

Implementation for flight test such as the modeling and filters for sling dynamics, and equations for converting load angles to cable angles were developed. These methods are unique due to the limited flight testing of a cable angle/rate feedback system that has been performed in recent times. These flight test considerations are critical for the success of the flight test, and will be important for future use of cable angle/rate feedback control systems on other platforms.

1.4 Organization of Dissertation

The main body of the dissertation in Chapter 2 provides a derivation and validation of the linear dynamics of a helicopter with a slung load. Chapter 2 also describes the vehicle used to demonstrate cable angle feedback technology – the UH-60 RASCAL fly-by-wire flying laboratory. Chapter 3 introduces the recently developed handling qualities specification for helicopters external loads that was developed in Ref. 2, and drives the design of the control system. Then, a coupling numerator approach is used to explore the trade-offs between load damping and handling qualities for cable angle/rate and fuselage feedback in Chapter 4. Chapter 5 takes the results of the coupling numerator analysis and applies the lessons learned to the full order UH-60 dynamics and uses multi-objective optimization to design an attitude control system, using an explicit model following controller architecture. Three attitude command designs are developed in Chapter 5; a Baseline fuselage feedback design, a Pilot Handling design with cable angle feedback, and a Load Damping design with cable angle/rate feedback. Then Chapter 6 presents the results of a fixed base piloted simulation of the three attitude command designs. Chapter 7 describes the development of a task tailored control law that switches between Load Damping and Pilot Handling control laws based on the results of the fixed base piloted simulation. The flight test implementation details are then described in Chapter 8, and flight test results are given in Chapter 9. Chapter 10 gives conclusions and recommendations for future work.

2 System Description and Modeling

This chapter describes the test aircraft, a fly-by-wire JUH-60A Black Hawk, which will be considered herein as the example application for the cable angle/rate feedback technology. A description of the models that were used for control design, analysis, and simulation of this aircraft are provided. Additionally, the models are validated against UH-60 flight data.

2.1 Aircraft Description

The UH-60 helicopter, also known as the Black Hawk, is a utility helicopter that has been in operation since the late 1970s. Since then, over 3000 Black Hawks and its derivatives have been produced [33]. The external load capability of the Black Hawk has been widely used to deliver supplies in military operations, as well as in natural disasters [33]. The fact that this helicopter is widely in operation and commonly used for external slung load operations makes it a good test vehicle for cable angle/rate feedback control technology. The UH-60A/L variants (in regular operation) have a partial authority stability augmentation system (SAS) with a rate command architecture, which has been shown to have poor handling qualities for heavy slung loads with long slings in flight [2]. Additionally, precision load placement can be difficult because the pilot cannot see the external load from the cockpit (military helicopters are not typically designed with cockpit windows that allow visibility of the load). When pilots have divided attention, poor visual cues, or are under time constraints to deliver an external load, these factors can combine to create a high workload environment for the pilots during external load operations.

The US Army maintains a unique rotorcraft in-flight-simulator capability in the US, a full authority JUH-60A fly-by-wire flying laboratory – the Rotorcraft Aircrew System Concepts Airborne Laboratory (RASCAL) [34]. The RASCAL is operated by the Aeroflightdynamics Directorate of the US Army at Ames Research Center in Moffett Field, CA. This aircraft is shown with an external load in Figure 2-1. The RASCAL is a full authority, fly-by-wire system for the evaluation pilot, with a backup mechanical system for the safety pilot. It has been used over the last 10 years to research cockpit hardware, investigate rotorcraft handling qualities, and to develop and test new fly-by-wire control system architectures (some recent examples are [35], [36], and [37]). This aircraft is an excellent platform for safely testing new flight-by-wire control concepts, and therefore is suited for the development of an advanced control system with cable angle/rate feedback for external load operations. For these reasons, the RASCAL aircraft is considered herein.

Figure 2-1.UH-60 with external load.

The fly-by-wire capability of the JUH-60A RASCAL is an important aspect of this research because it represents the future of rotorcraft flight control. While fixed-wing transports and fighter aircraft commonly use this technology, the rotorcraft industry is just beginning to implement fly-by-wire. Major upgrades or new rotorcraft such as the S-92F/CH-148, UH-60M Upgrade, NH-90 and now the CH-53K have opted to use full-authority fly-by-wire. The fly-by-wire flight control system uses measurements of piloted control inputs and other sensors (typically aircraft responses), and processes them through the flight control computer, which makes an appropriate command to the main and tail rotor actuators. Fly-by-wire provides a more flexible, full-authority architecture than legacy mechanical partial authority (usually 10%) configurations used in previous manned literature on slung load control.

The RASCAL (m_A =15,000 lbs) can carry a load of m_L =5000lbs for approximately 1.5 flight-hours at hover low-speed. This is the heaviest load RASCAL can carry to efficiently perform a set of evaluations without refueling. A useful measure of helicopter load is the load-mass-ratio (LMR):

$$LMR = \frac{m_L}{m_A + m_L} \tag{2.1}$$

The LMR for the UH-60A with a 5000lb load is 0.25. LMR > 0.20 are known to result in significant effects on handling qualities. The UH-60 with a heavy load (5,000 lbs, LMR = 0.25) and a long sling (56ft), was found to have poor baseline handling qualities (with standard partial authority SAS in UH-60L) in Ref. 2, and therefore is good case for testing the benefits of cable angle feedback. Furthermore, the 56ft sling with a light load (1000lbs, LMR=0.06) has poor baseline handling qualities and long set-down times in flight test for precision load placement. As these two configurations, described in Table

2-1, could particularly benefit from additional technology to improve handling qualities and load placement, they were used for evaluation. However, the concept and conclusions developed here can be applied to any load configuration.

Table 2-1. JUH-60A RASCAL flight test configurations.

Configuration	Load Mass	Aircraft Mass	LMR
1	5000lbs	15,000lbs	0.25
2	1000lbs	16,000lbs	0.06

Another important parameter is the slung load pendulum frequency. Using a simple pendulum model, this natural frequency (ω_n) is a function of sling length (l) alone:

$$\omega_n = \sqrt{\frac{g}{l}} \tag{2.2}$$

A better approximation can be found in Tyson [38], which considers the inertia of the load. This is a function of sling length, load mass, and inertia of the load:

$$\omega_n = \sqrt{\frac{m_L g l}{m_L l^2 + I_L}} \tag{2.3}$$

Note that if the load is approximated as a point-mass, its inertia is zero ($I_L = 0$) and Eq. (2.3) is then equivalent to Eq. (2.2).

2.2 Description of Dynamic Models

The first step in designing a control system is to understand the underlying dynamic equations of motion. The model fidelity should be appropriate for the level of analysis and simulation that is being performed. This research required a wide range of analysis and simulation techniques – from simple modeling to ascertain basic analytical effects of feedback via root locus plots, to full non-linear pilot-in-the-loop simulation to support flight testing. Therefore, a wide range of models were used to support this research. Table 2-2 is a roadmap of these models, and provides an overview of their assumptions, fidelity, and which analyses they supported. Then, the subsequent sections of this dissertation describe each model in more detail (except the flexible cable model, which is described in Chapter 8).

Table 2-2. Model overview.

Model	Section	Description	Assumptions/Fidelity	Analyses Supported
Generic nonlinear Equations-of-Motion	2.2.1	Nonlinear model derived by author	Aerodynamics treated as generic forces and moments. Model is used to support development of a linear model. Cable is assumed to be rigid. Load is a point mass. Model cannot be used for simulation.	Supports development of analytical linear model structure in Sec. 2.2.2.
Analytical Linear Model	2.2.2	Linear model derived by author	Linear model is derived from generic nonlinear equations-of-motion. Assumes quasi-steady rotor dynamics. Cable is rigid, load is point mass.	Used to develop understanding of dynamics. Used for study of basic design trade-offs in Chapter 4.
GENHEL with external load [39,38]	2.2.3	Nonlinear real-time simulation model	Nonlinear, large angle simulation model. Uses blade element model for rotor aerodynamics. Cable is rigid. Slung load has inertia.	Used in piloted fixed based simulator and hardware in the loop simulation in Chapters 6, 8.
FORECAST/OVERCAST linear model for the UH-60 with Slung Load [2,40]	2.2.4	Linear perturbation model of GENHEL with external load	Linear equations-of-motion. Linear rotor flapping, lagging, coning dynamics states are used. Load is a point mass on a rigid cable.	Used as basis for linear analysis and control design optimization in Chapters 5, 7.
Flexible Cable Model	8.3	Flexible model of cable and slung load	Linear equations of motion. Load is a point mass on a flexible cable.	Used to predict frequencies of motion in load measurements related to sling flexibility in Chapter 8.

2.2.1 Derivation of Generic Nonlinear Equations of Motion

The derivation of helicopter/slung load equations of motion has been performed in many references, a sampling include Tyson [38], Cicolani [41], Gupta [14], and Wolkovitch [42]. Thus, the derivation herein is very similar to previous references, and therefore is included in Appendix A. The derived nonlinear EOMs in Appendix A support the development of a linear model structure. The key contribution in modeling is the structure of the analytical linear model, which is described in the following section.

2.2.2 Derivation of an Analytical Linear Model

The linearized model was developed from analytical perturbation and small angle approximation to the nonlinear equations described in Sec. 2.2.1, and Appendix A. This model is unique because it is derived in an analytical form that appends the load dynamics to an existing unloaded model structure based on the geometry and mass of the slung load. This linear model enables a very simple conversion from an unloaded to loaded aircraft model. The linear model structure is also an ideal setup for system identification, because none of the parameters that would typically be identified are lumped in with known geometric quantities. This model was used primarily to understand the dynamics of the helicopter/slung-load system and the complexity of the coupling terms between the two bodies. The

model was also used for studying the basic effects of cable angle/rate feedback on the helicopter/load coupling dynamics, in Chapter 4.

The basic two-body system, reference frames, and geometry of the model are defined in Figure 2-2. The sling is assumed to be rigid. The flexible sling modes are sufficiently frequency separated from the pendular mode that this is a reasonable assumption to make. Later, in Sec. 8.3 the flexible sling modes are modeled and identified, validating this assumption.

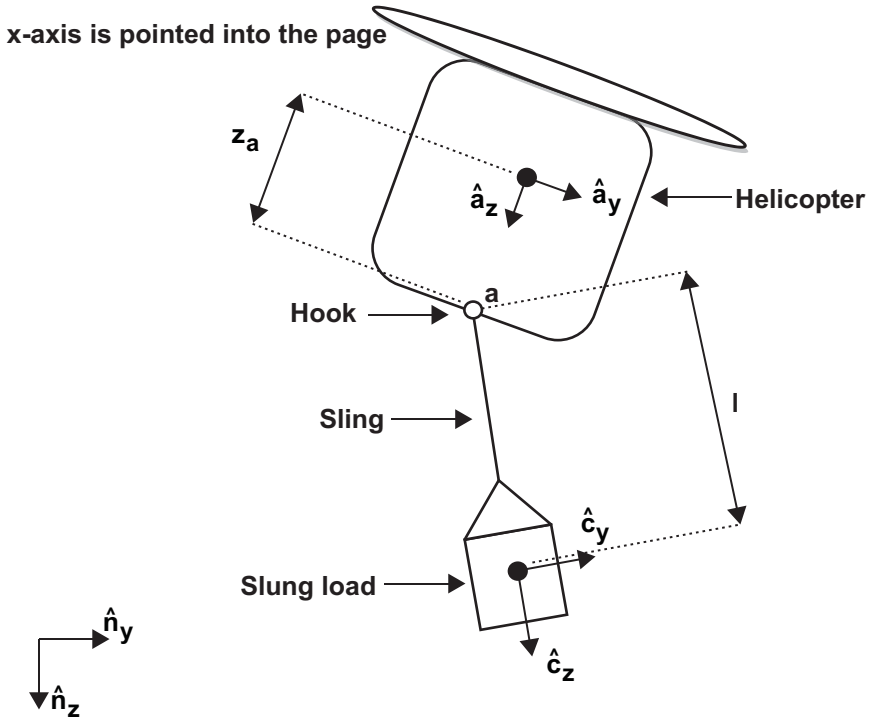

Figure 2-2. Reference frames and geometry for aircraft/slung load dynamics.

The model has the following structure, states and controls:

$$\boldsymbol{M}\dot{\vec{x}} = \boldsymbol{F}\vec{x} + \boldsymbol{G}\vec{u}(t-\vec{\tau}) \tag{2.4}$$

$$\vec{x} = \begin{bmatrix} u & v & w & p & q & r & \phi & \theta & \phi & \Delta\phi_c & \Delta\theta_c & \Delta\dot{x}_c & \Delta\dot{y}_c & \Delta T & T_{ox} & T_{oy} \end{bmatrix} \tag{2.5}$$

$$\vec{u} = \begin{bmatrix} \delta_{lat} & \delta_{lon} & \delta_{ped} & \delta_{col} \end{bmatrix} \tag{2.6}$$

The first nine states are the fuselage rigid-body states, where u, v, w represent fuselage velocities, p, q, r represent fuselage angular velocities, and ϕ, θ, ψ are fuselage Euler angles. The next four states are slung-load states, where the delta symbol indicates they are relative to the fuselage, so $\Delta\phi_c$, $\Delta\theta_c$ are lateral and longitudinal cable angles with respect to the fuselage and $\Delta\dot{x}_c$, $\Delta\dot{y}_c$ are lateral and longitudinal velocities of the center-of-gravity of the external load relative to the fuselage. The final three

states ΔT, T_{ox}, T_{oy} are dummy algebraic states (linear combinations of the other states) related to the cable tension, and are used to simplify and organize the equations. The controls are the standard helicopter controls (lateral cyclic, longitudinal cyclic, pedal, and collective). These states and control inputs represent perturbations around trim and this model structure uses a quasi-steady rotor (no explicit rotor states). The key effect of the unmodeled rotor-dynamics can be characterized by time delay $\vec{\tau}$ at frequencies below ~12 rad/s on the UH-60, as shown later in Sec. 2.3. A time invariant value of $\vec{\tau}$ should be identified for each control input by comparing the quasi-steady model to a full-order model with explicit rotor states, or flight data.

The aerodynamic forces and moments are approximated with 1st order Taylor series terms (stability and control derivatives) as in:

$$\frac{X_{aero}}{m_A} = X_u u + X_w w + X_q q + ... + X_{\delta_{lon}} \delta_{lon} + ... \tag{2.7}$$

where X_u,...., $X_{\delta_{lon}}$ are the conventional aircraft stability and control derivatives for the force in the x-direction of the body-fixed reference frame.

The longitudinal equations for the helicopter fuselage states with an external load are:

$$\begin{aligned} \dot{u} = {} & X_u u + X_w w + X_q q + X_{\delta_{lon}} \delta_{lon} + X_{\delta_{col}} \delta_{col} - w_o q + v_o r - g\cos(\theta_o)\theta \\ & - \frac{\sin(\Delta\theta_{co})}{m_A \sigma} \Delta T - \frac{\cos(\Delta\theta_{co})}{m_A \sigma} T_{ox} \end{aligned} \tag{2.8}$$

$$\begin{aligned} \dot{w} = {} & Z_u u + Z_w w + Z_q q + Z_{\delta_{lon}} \delta_{lon} + Z_{\delta_{col}} \delta_{col} + u_o q - v_o p - g\sin(\theta_o)\theta \\ & - \frac{\cos(\Delta\theta_{co})}{m_A \sigma} \Delta T + \frac{\sin(\Delta\theta_{co})}{m_A \sigma} T_{ox} \end{aligned} \tag{2.9}$$

$$\begin{aligned} \dot{q} = {} & M_u u + M_w w + M_q q + M_{\delta_{lon}} \delta_{lon} + M_{\delta_{col}} \delta_{col} - \frac{z_a \sin(\Delta\theta_{co})}{I_{yy} \sigma} \Delta T \\ & - \frac{z_a \cos(\Delta\theta_{co})}{I_{yy} \sigma} T_{ox} \end{aligned} \tag{2.10}$$

$$\dot{\theta} = q \tag{2.11}$$

$$\sigma = \frac{1}{m_A} + \frac{1}{m_L} \tag{2.12}$$

The model shown in Eqs. (2.8) – (2.12) treats the lateral and longitudinal dynamics as decoupled, and the rotor as quasi-steady (no explicit rotor-states). To develop a loaded model with coupled lateral/longitudinal dynamics and/or explicit rotor states, the ΔT and T_{ox} cable tension terms (and associated coefficients) can simply be appended to the unloaded model with the desired complexity. These two additional states are actually algebraic 'dummy states' that are used to separate these

complicated cable tension terms from the unloaded dynamics, and thus make the model easier to implement. Dummy states can be easily implemented using the ***M***-matrix in Eq. (2.4).

Dummy state T_{ox} represents the change in magnitude of the longitudinal component (fuselage axis) of the cable tension due to the load swing, where:

$$T_{ox} = \left\{ \frac{\sin(\Delta\theta_{co})F_{xo} + \cos(\Delta\theta_{co})F_{zo}}{m_A} + 0.5\frac{\rho}{m_L}\frac{D}{\bar{q}}V_o^2\left(\sin(\Delta\theta_{co}) + \sin(\theta_o)\right)\right\}\Delta\theta_c \tag{2.13}$$

$$F_{xo} = (m_A + m_L)\sin(\theta_o)g \tag{2.14}$$

$$F_{zo} = -(m_A + m_L)\cos(\theta_o)g \tag{2.15}$$

The trim cable tension due to gravity in the x-direction and z-direction are given by Eq. (2.14) and (2.15), respectively. Changes in cable tension due to changes in the aircraft states are represented by dummy state ΔT :

$$\Delta T = T_u u + T_w w + T_q q + T_{\delta_{lon}}\delta_{lon} + T_{\delta_{col}}\delta_{col} \tag{2.16}$$

$$T_u = \sin(\Delta\theta_{co})X_u + Z_u + (z_a)\sin(\Delta\theta_{co})M_u + \frac{\rho}{m_L}\frac{D}{\bar{q}}V_o\sin(\Delta\theta_{co}) \tag{2.17}$$

$$T_w = \sin(\Delta\theta_{co})X_w + Z_w + (z_a)\sin(\Delta\theta_{co})M_w + \frac{\rho}{m_L}\frac{D}{\bar{q}}V_o\cos(\Delta\theta_{co}) \tag{2.18}$$

$$T_q = \sin(\Delta\theta_{co})(X_q) + (Z_q) + (z_a)\sin(\Delta\theta_{co})M_q + \frac{\rho}{m_L}\frac{D}{\bar{q}}V_o\sin(\Delta\theta_{co})(z_a) \tag{2.19}$$

$$T_{\delta_{lon}} = \sin(\Delta\theta_{co})X_{\delta_{lon}} + Z_{\delta_{lon}} + (z_a)\sin(\Delta\theta_{co})M_{\delta_{lon}} \tag{2.20}$$

$$T_{\delta_{col}} = \sin(\Delta\theta_{co})X_{\delta_{col}} + Z_{\delta_{col}} + (z_a)\sin(\Delta\theta_{co})M_{\delta_{col}} \tag{2.21}$$

Note that if an unloaded model with explicit rotor states is used as the baseline model upon which the loaded dynamics are appended, Eqs. (2.16)-(2.21) should be calculated using the effective quasi-steady derivatives (as determined by performing a model reduction). Herein, a decoupled quasi-steady (rotor) model is used as the baseline unloaded model for simplicity.

The linear dynamics for the longitudinal load states (longitudinal velocity and cable angle) are described by:

$$\begin{aligned}\Delta\ddot{x}_c = &-\left(\sin(\Delta\theta_{co})u_o + \cos(\Delta\theta_{co})w_o\right)q + \sin(\Delta\theta_{co})\dot{w} - \cos(\Delta\theta_{co})\dot{u} \\ &-\left(\cos(\Delta\theta_{co})z_a + l\right)\dot{q} - g\left(\cos(\theta_o)\cos(\Delta\theta_{co}) - \sin(\theta_o)\sin(\Delta\theta_{co})\right)\theta \\ &+\left(\frac{\rho}{m_L}\frac{D}{\bar{q}}V_o^2\cos(\theta_o)\sin(\Delta\theta_{co}) - g\left(\cos(\theta_o)\cos(\Delta\theta_{co}) - \sin(\theta_o)\sin(\Delta\theta_{co})\right)\right)\Delta\theta_{co} \\ &-\frac{\rho}{m_L}\frac{D}{\bar{q}}V_o\left(\cos(\Delta\theta_{co})u - \sin(\Delta\theta_{co})w + \Delta\dot{x}_c + \left(\cos(\Delta\theta_{co})z_a + l\right)q\right)\end{aligned} \tag{2.22}$$

$$\Delta\dot{\theta}_c = \frac{1}{l}\Delta\dot{x}_c \tag{2.23}$$

The lateral helicopter fuselage dynamics are similar, but simpler in form than the longitudinal equations. The key effect of the slung load are the changes in magnitude of the lateral component (fuselage axis) of the cable tension due to the load swing, T_{oy}. The lateral aircraft states do not affect the cable tension (no ΔT term as in the longitudinal equations) because these terms are small and drop out of the linear equations of motion. Thus, only term T_{oy} is appended to unloaded dynamics to model the effect of the slung load on the lateral fuselage states:

$$\dot{v} = Y_v v + Y_p p + Y_r r + Y_{\delta_{lat}}\delta_{lat} + Y_{\delta_{ped}}\delta_{ped} + w_o p - u_o r + g\cos(\theta_o)\phi - \frac{1}{m_A\sigma}T_{oy} \tag{2.24}$$

$$\dot{p} = L_v v + L_p p + L_r r + L_{\delta_{lat}}\delta_{lat} + L_{\delta_{ped}}\delta_{ped} + \left\{\frac{\frac{z_a\cos(\Delta\theta_{co})}{I_{xx}\sigma}}{1-\frac{I_{xz}^2}{I_{xx}I_{zz}}}\right\}T_{oy} \tag{2.25}$$

$$\dot{r} = N_v v + N_p p + N_r r + N_{\delta_{lat}}\delta_{lat} + N_{\delta_{ped}}\delta_{ped} + \left\{\frac{-\frac{I_{xz}}{I_{zz}}\left(\frac{z_a\cos(\Delta\theta_{co})}{I_{xx}\sigma}\right)}{1-\frac{I_{xz}^2}{I_{xx}I_{zz}}}\right\}T_{oy} \tag{2.26}$$

$$\dot{\phi} = p + \tan(\theta_o)r \tag{2.27}$$

$$\dot{\psi} = \frac{r}{\cos(\theta_o)} \tag{2.28}$$

Where σ is defined by Eq. (2.12).

Similarly to the longitudinal case, the model shown in Eqs. (2.24) – (2.28) treat the lateral and longitudinal dynamics as decoupled, and the rotor as quasi-steady (no explicit rotor-states). To develop a loaded model with coupled lateral/longitudinal dynamics and/or explicit rotor states, the T_{oy} state (and associated coefficients) can simply be appended to the unloaded model with the desired complexity. A simplified unloaded model was used herein for brevity.

Then the change in magnitude of the lateral (fuselage axis) cable tension force due to lateral load swing, T_{oy}, is given by:

$$T_{oy} = -\left\{\frac{\sin(\Delta\theta_{co})F_{xo} + \cos(\Delta\theta_{co})F_{zo}}{m_A} + 0.5\frac{\rho}{m_L}\frac{D}{\bar{q}}V_o^2\left(\sin(\Delta\theta_{co}) + \sin(\theta_o)\right)\right\}\Delta\phi_c \tag{2.29}$$

Where the trim cable tension due to gravity in the x-direction, F_{xo}, and z-direction, F_{zo}, are given by Eqs. (2.14) and (2.15), respectively.

The linear equations for the lateral load velocity and cable angle states are:

$$\begin{aligned}\Delta\ddot{y}_c &= w_o p - u_o r - \dot{v} + \left(z_a + l\cos(\Delta\theta_{co})\right)\dot{p} - \left(l\sin(\Delta\theta_{co})\right)\dot{r} + g\cos(\theta_o)\phi \\ &+ g\cos(\theta_o)\Delta\phi_c - 0.5\frac{\rho}{m_L}\frac{D}{q}V_o\left(v + \Delta\dot{y}_c - \left(z_a + l\cos(\Delta\theta_{co})\right)p + \left(l\sin(\Delta\theta_{co})\right)r\right) \\ &- 0.25\frac{\rho}{m_L}\frac{D}{\bar{q}}V_o\left(\sin(\theta_o) + \sin(\Delta\theta_{co})\right)\Delta\phi_c\end{aligned} \tag{2.30}$$

$$\Delta\dot{\phi}_c = -\frac{1}{l\cos(\Delta\theta_{co})}\Delta\dot{y}_c \tag{2.31}$$

Eigenvalues of Derived Linear Model for UH-60

The analytical linear model is applied to the UH-60 dynamics for $m_A = 15000$ lb, $m_L = 5000$ lb load and *l*=56ft sling. The stability and control derivates were taken from a validated internally loaded physics-based UH-60 model (generated by FORECAST [43]). The internally loaded model has a total mass of 20,000lbs. The analytical slung load states were then appended to the model using the equations from Sec. 2.2.2. The resulting eigenvalues of the loaded UH-60 model are shown in Table 2-3. Eigenvalues for analytical linear model of coupled helicopter/slung load system. As expected, there are unstable lateral and longitudinal Phugoid modes, which couple with the lateral and longitudinal short period modes to create the so called "hovering cubic". The hovering cubic is characteristic of helicopter dynamics at hover. There are also the expected yaw and heave modes. The presence of the load adds oscillatory pendulum modes in the pitch and roll axes, as expected.

Table 2-3. Eigenvalues for analytical linear model of coupled helicopter/slung load system.

Mode Description	Eigenvalue	Damping	Frequency (rad/s)
Psi integrator	0	1.00	0.00
Yaw/Heave	-2.36e-001 +/- 8.26e-002i	0.94	0.25
Longitudinal Phugoid	2.19e-001 +/- 4.23e-001i	-0.46	0.48
Lateral Phugoid	2.28e-002 +/- 5.01e-001i	-0.045	0.50
Pitch Mode	-0.943	1.00	0.94
Longitudinal Pendulum	-5.10e-002 +/- 1.11e+000i	0.047	1.11
Lateral Pendulum	-8.22e-001 +/- 1.25e+000i	0.55	1.50
Roll Mode	-2.68	1.00	2.68

2.2.3 Nonlinear Flight-Validated GenHel Model with External Load

The development of the non-linear model in Appendix A treats the aerodynamics of the rotor as generic forces and moments. These modeling efforts are developed to provide understanding and insight into the dynamics problem and support analytical linearization. This dissertation does not attempt to re-

derive the complex rotor dynamics and aerodynamics of the UH-60 considering the vast prior work on the subject (some examples include [39] and [44]). As this work focuses on control system analysis and design, it made sense to use tools that have been validated and developed over the last 20 years for the UH-60. Therefore, the General Helicopter Flight Dynamics Simulation (GenHel) was used for nonlinear simulation of the unloaded UH-60A aircraft [39]. This model is used in a piloted fixed base simulator (Chapter 6), and hardware in the loop simulation in Chapter 8.

GenHel is a full flight envelope, nonlinear, large angle model, with rigid blades and fuselage [39]. It is a physics-based model that represents the rotor blades as hinged beams without flexibility, and models the rotor aerodynamics using conventional blade element theory. The inflow is represented by a Pitt-Peters inflow model. The model also makes use of extensive wind tunnel and flight based corrections. The slung load dynamics are added via a module that simulates the load motion as a function of the helicopter states, and transmits hook forces and moments imparted by the external load up to the helicopter [38]. This process is depicted by Figure 2-3. The model of helicopter and slung load is extensively validated against flight data in Ref. 38.

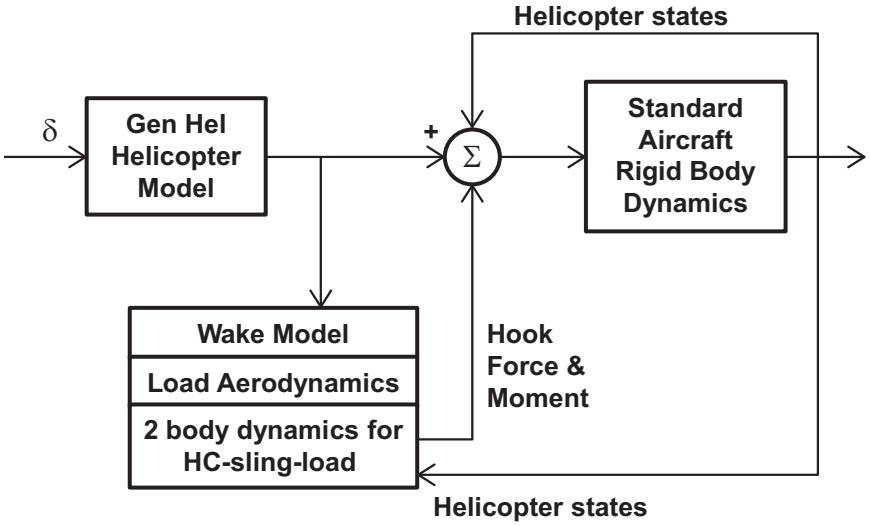

Figure 2-3. Slung load simulation diagram (Ref. 38).

2.2.4 FORECAST/OVERCAST Linear Model with External Load

The analytical linear model presented in Sec. 2.2.2 is useful for system identification, developing simple linear models of the helicopter/slung load dynamics, and studying basic feedback control trade-offs (in Chapter 4). However, it does not include explicit rotor-dynamics in the form presented herein. To support the flight control design optimization (in Chapters 5-7), a more complex model with rotor-dynamics was extracted via perturbation methods from the non-linear GENHEL simulation described in Sec. 2.2.3. The tools used to extract these linear models are called FORECAST/OVERCAST [2,40]. The linear model extracted for the hovering externally loaded UH-60 has 30 states: 9 fuselage, 4 slung load, 6 main rotor flap, 6 main rotor lag, 3 main rotor inflow, and 2 engine states. The resulting dynamic modes

of the model are shown in Table 2-4. The fuselage and pendular dynamics of the system have similar modes to those from the analytical linear model presented in Table 2-3. This is due to use of the same unloaded aircraft stability and control derivatives, and similar assumptions for the added slung load dynamics. This model adds complexity in the addition of rotor flapping, lead-lag and inflow modes. It is important to include these modes when developing a control system design that has high cross-over frequencies that could potentially destabilize the rotor modes.

The presence of the rotor modes however, does not significantly affect the load mode or other dynamics below 12 rad/s, except for the presence of an effective time delay. So simple design trade-offs can be developed using a simple model such as the analytical linear model or reduced order FORECAST/OVERCAST model that eliminate rotor modes, but one must be careful to account for the effective time delay (typically 70ms) of the rotor. This will become apparent in the Bode plot overlays in the following section of this dissertation.

Table 2-4. Dynamic modes for 15,000lb UH-60 carrying a 5000lb external load on 56ft sling.

Mode Description	Eigenvalues	Damping	Frequency (rad/s)
Psi Integrator	0	1.00	0.00
Yaw/Heave	-2.45e-001 +/- 5.80e-002i	0.97	0.25
Pitch Phugoid	2.24e-001 +/- 4.11e-001i	-0.48	0.47
Roll Phugoid	4.20e-002 +/- 5.03e-001i	-0.08	0.51
Pitch Short Period	-1.01	1.00	1.01
Longitudinal Pendulum	-6.20e-002 +/- 1.12e+000i	0.06	1.12
Lateral Pendulum	-7.70e-001 +/- 1.18e+000i	0.55	1.41
Collective Lag	-2.58e+000 + 1.01e+000i	0.93	2.77
Roll Short Period	-2.89	1.00	2.89
Engine Response	-4.64	1.00	4.64
Regressive Flap	-4.11e+000 +/- 4.53e+000i	0.67	6.11
Constant Inflow	-12.3	1.00	12.30
Regressive Lag	-5.78e+000 +/- 2.02e+001i	0.28	21.00
1st Harmonic Inflow	-2.04e+001 +/- 9.15e+000i	0.91	22.40
Collective Flap	-9.45e+000 + 2.56e+001i	0.35	27.30
Progressive Lag	-8.47e+000 +/- 3.61e+001i	0.23	37.10
Progressive Flap	-4.56e+000 +/- 4.87e+001i	0.09	48.90
Power Turbine Response	-90.8	1.00	90.80

2.3 Validation of Linear Models against Flight Data

The two linear models described herein (analytical linear model of Sec. 2.2.2 and FORECAST/ OVERCAST linear model of Sec. 2.2.4) are compared against flight data to assess their validity. A 70ms time delay was added to the analytical linear model to account for effective rotor dynamics. The flight data were recorded during frequency sweep maneuvers with the 5K load and 56ft sling. The frequency

responses were calculated from the time domain flight data using a ChirpZ-transform (similar to FFT) and composite windowing technique using CIFER® software [45]. This method was used to identify on-axis frequency responses of the aircraft. The frequency sweeps were recorded with the RASCAL fly-by-wire flight control system on, which makes it impossible to identify off-axis responses due to correlation in the controls from the mixer. Therefore, only on-axis responses were validated. There were no flight data for the pedal and collective axes for this flight condition, so the two linear models are simply overlaid. Herein the validation of the linear derived model against the OVERCAST/FORECAST model is considered to be sufficient. These responses also tend to have very light coupling with the external load.

The longitudinal response validations are given in Figure 2-4 - Figure 2-6. The linear models agree well with each other and with the flight data for the on-axis longitudinal responses. The flight data is valid over the frequencies where the coherence is greater than 0.5 [45]. The fuselage longitudinal velocity and pitch attitudes are well modeled by both linear models and the effect of the load around 1 rad/s is also well modeled. In addition, the cable angles (relative to the fuselage) are in good agreement with the flight data. It is important to point out that the analytical linear model and FORECAST/OVERCAST models have good correlation with each other over the frequency range of 0.1-12 rad/s because the effect of the rotor dynamics included in the FORECAST/OVERCAST model is not important over this frequency range. The effect of the rotor dynamics are modeled by a simple 70ms time delay in the analytical linear model responses, which works well up to 12 rad/s. This indicates that the rotor/body dynamics are lightly coupled in this frequency range, and therefore well characterized by a time delay. Additionally, this indicates that the analytical linear model is sufficient for simple control design trade-off studies that focus on handling qualities and load response, which are mostly effected by dynamics below 12 rad/s.

The lateral models have good agreement with flight data as shown in Figure 2-7 - Figure 2-9. The fuselage responses are well modeled over the 0.1-12 rad/s frequency range. The effect of the load on the aircraft, at the pendular frequency of ~1 rad/s is also accurately modeled. This is an important effect for handling qualities prediction. The load response is also well modeled, although the flight frequency-response quality is low, especially at low frequency, as indicated by the coherence (coherence of less than 0.5 is considered poor quality). Similarly to the longitudinal axis, the two linear models agree well over the frequency range shown, due to the validity of the quasi-steady rotor dynamics below 12 rad/s.

The collective and pedal responses shown in Figure 2-10 and Figure 2-11 are comparisons between the two linear models. This is a check that the analytical linear model matches the FORECAST/OVERCAST data (since no flight data were available). As shown in the figures, there is little coupling of the heave and yaw degrees of freedom with the external load, indicated by the relatively small distortion near the pendulum frequency at ~1 rad/s. The yaw rate to pedal response of the analytical model under predicts the damping of the helicopter/load coupling as compared to the

FORECAST/OVERCAST model, providing a conservative estimate of the damping of the modes at ~0.5 and ~1.0 rad/s.

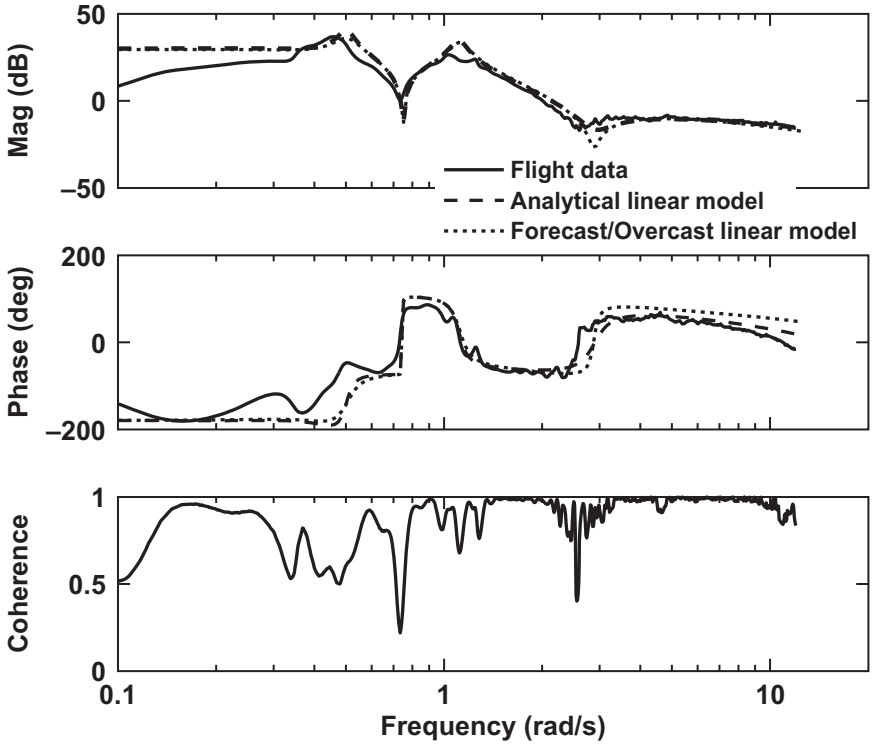

Figure 2-4. Flight validation for u/δ_{lon} .

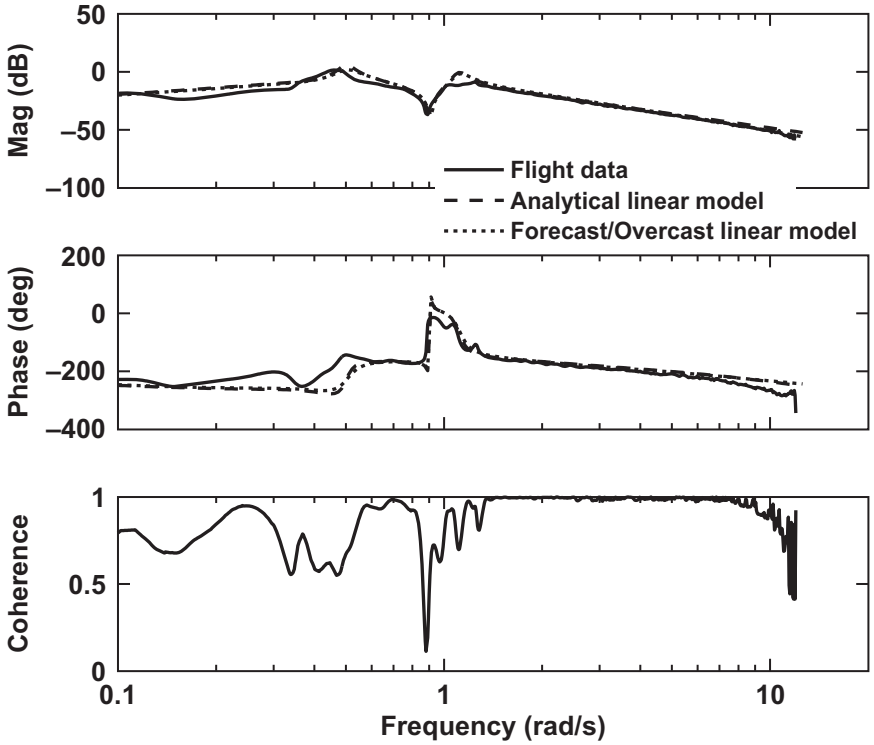

Figure 2-5. Flight validation for θ/δ_{lon} .

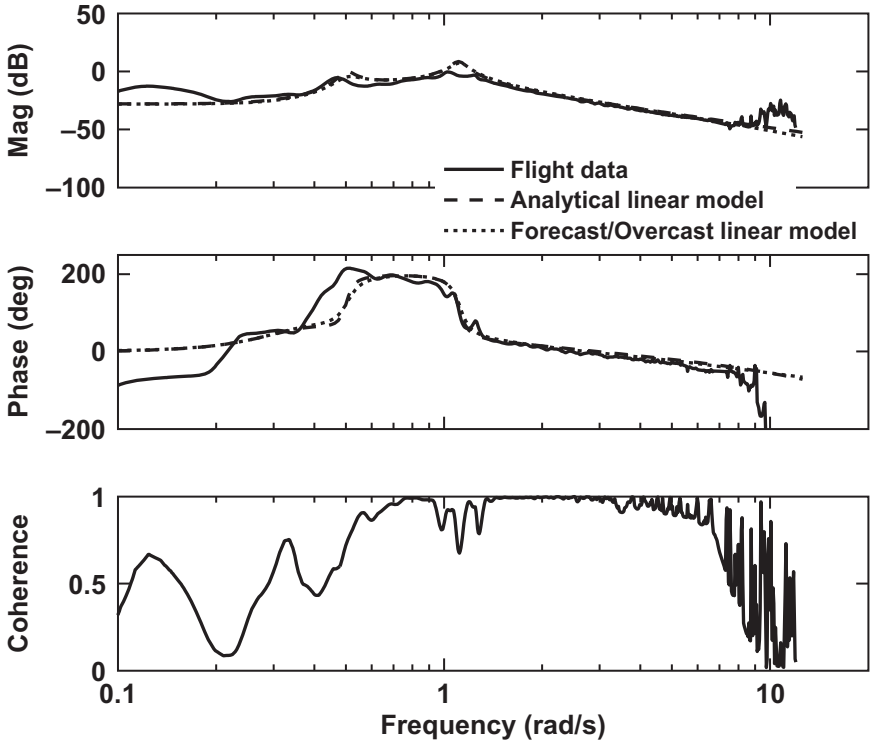

Figure 2-6. Flight validation for $\Delta\theta_c/\delta_{lon}$.

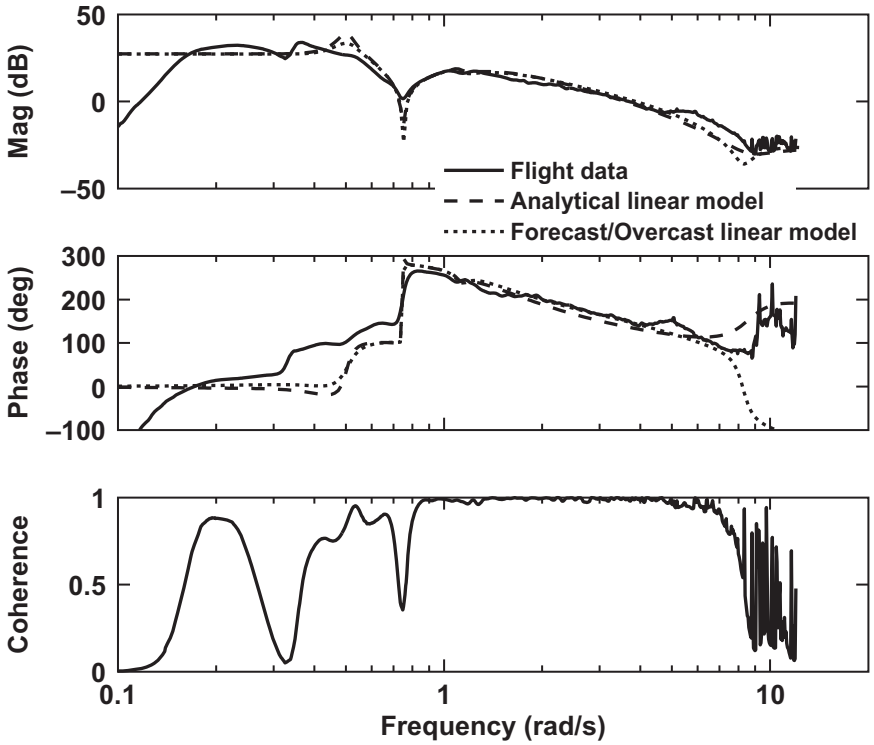

Figure 2-7. Flight validation for v/δ_{lat} .

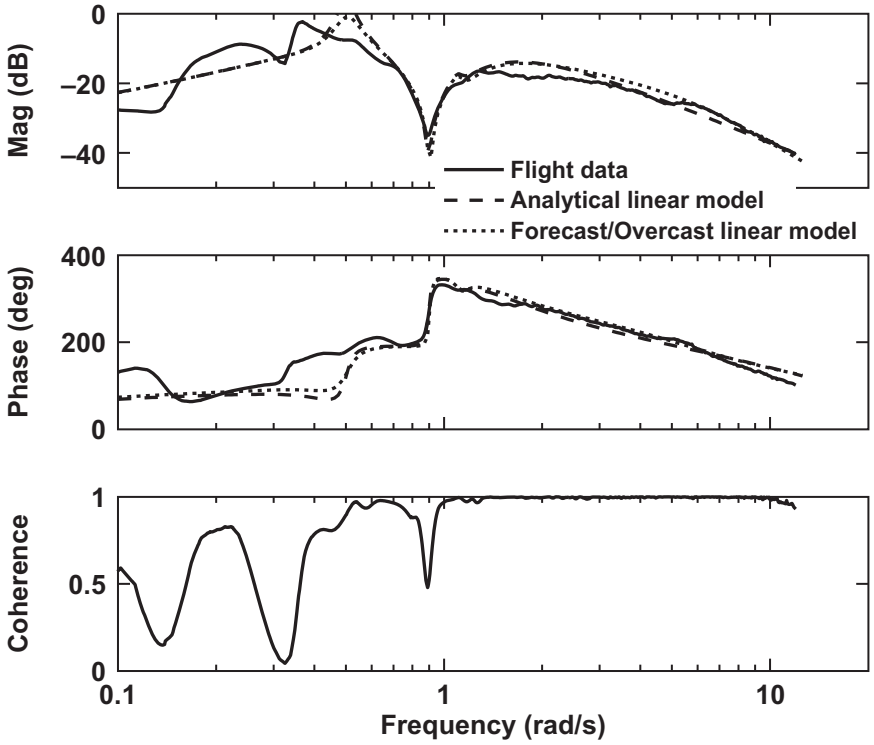

Figure 2-8. Flight validation for ϕ/δ_{lat} .

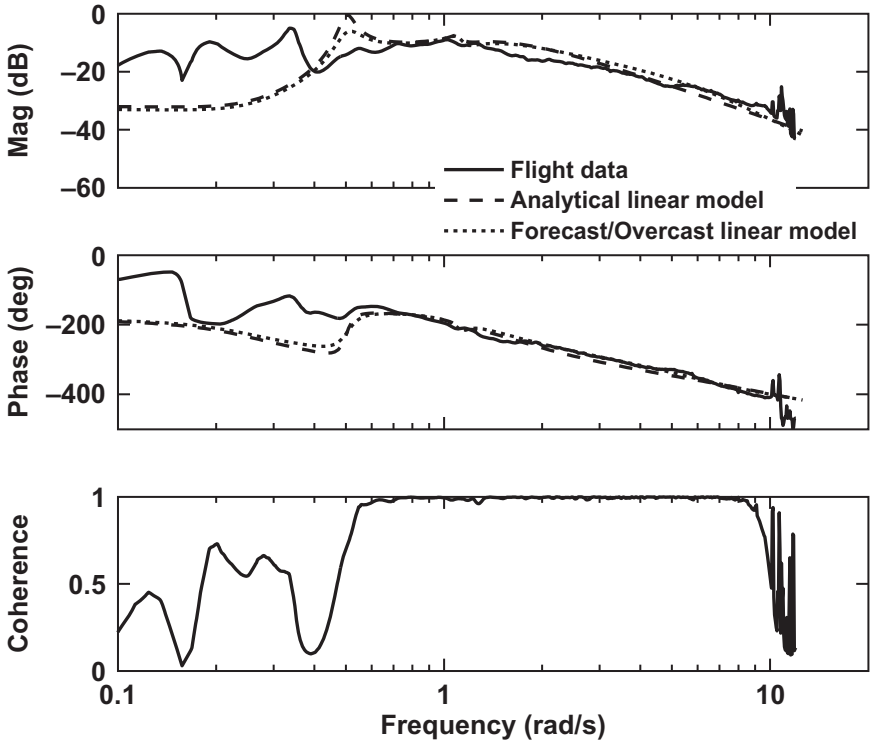

Figure 2-9. Flight validation for $\Delta\phi_c/\delta_{lat}$.

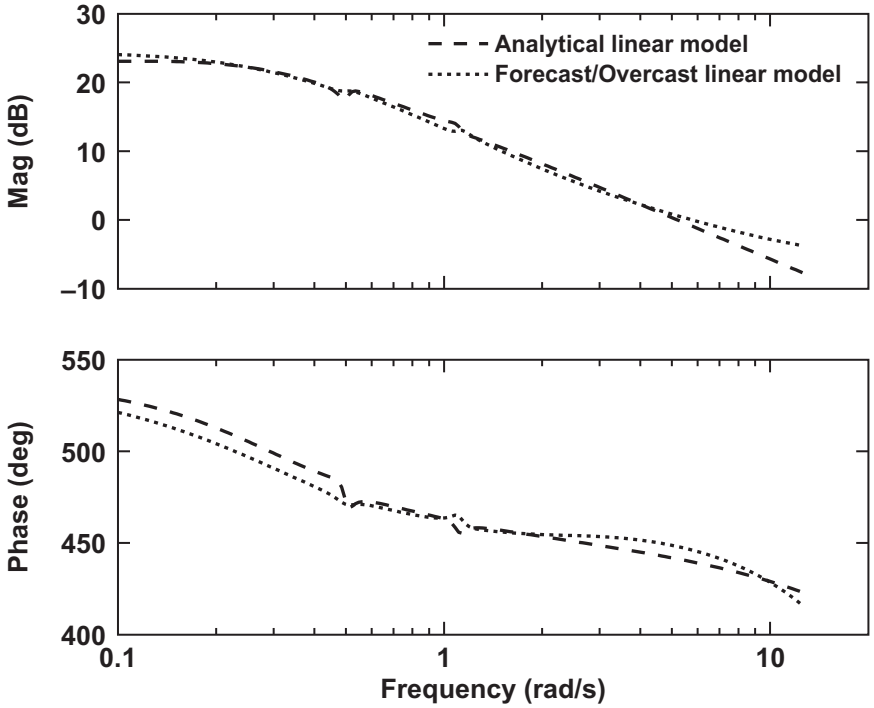

Figure 2-10. Model comparison for w/δ_{col} .

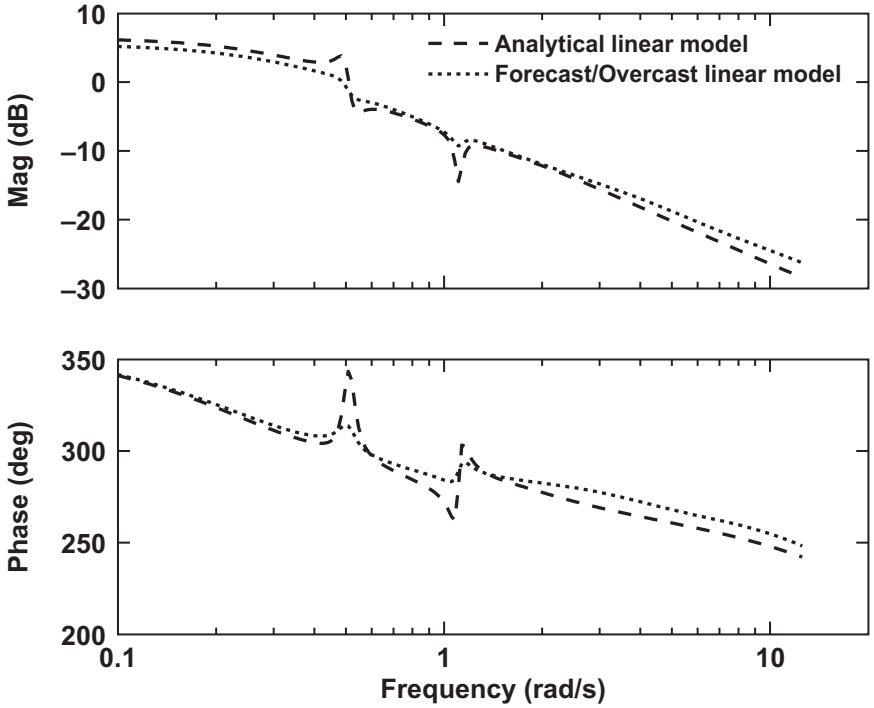

Figure 2-11. Model comparison for r/δ_{ped} .

2.4 Summary of Chapter 2

Chapter 2 describes the dynamic models that were used to support the control system design and analyses in this research. This chapter describes validation of these models, indicating that the models are of appropriate accuracy for development of a flight control system with fuselage and cable angle/rate feedback for a UH-60 helicopter with an external load. The key contributions of this chapter include:

1. Development of an analytical linear model structure for two-body helicopter slung-load system.
2. Validation of analytical linear model structure against flight data and the FORECAST/ OVERCAST model.

3 Slung Load Handling Qualities Specification

The recent development of a new slung load handling qualities criteria in Ref. 2 provides insight into how slung loads degrade handling qualities, and which aspects of the response the pilots find undesirable. This understanding shapes how the inclusion of the load feedbacks can be used to improve the pilot handling qualities with an externally slung load in this research. Thus, the control design and analysis in later chapters (Chapters 4, 5, and 7) relies heavily on these criteria. The slung load handling qualities specification is based on extensive flight test data where a variety of sling length and load masses were tested with the Mission Task Elements in ADS-33E-PRF [21]. Mission Task Elements are a set of stylized maneuvers for helicopters which are performed by the pilot and rated based on the Cooper-Harper scale.

The slung load handling qualities specification that was developed relates distortion in the shape of the attitude frequency responses of the externally loaded aircraft as compared to an internally loaded aircraft to the piloted handling qualities rating (HQR). An important characteristic of the response of an externally loaded helicopter is the depth of the notch in the attitude response (at 0.8 rad/s in Figure 3-1) that is associated with the attenuation of the attitude response to pilot stick inputs because of the load swing. This notch is non-existent for an internally loaded baseline helicopter (LMR = 0), and becomes deeper with increasing external load mass ratio (LMR, Eq. (2.1)) as shown in Figure 3-1.

Handling qualities were correlated to the distortion in the frequency response of the externally loaded aircraft by collecting handling qualities ratings (HQRs) in flight in a UH-60L Black Hawk [2]. A variety of LMR and sling length configurations were used in order to test a range of response distortions in Ref. 2. The depth of the notch (Δ_{MAG}) as compared to an internally loaded helicopter is the metric used in y-axis of the handling qualities prediction criterion shown in Figure 3-2. As indicated by the HQRs supporting this criteria (as plotted in Figure 3-2) a greater magnitude loss (i.e. increased distortion caused by a heavier load) is associated with degrading handling qualities ratings given by pilots in flight (HQR > 4), shown by the triangle symbols that converge in the upper left corner.

The x-axis criterion shown in Figure 3-2 is the frequency of the -135 degree crossing of the phase (ω_{-135}) response near the load mode (or the frequency of the minimum phase near the load mode if it does not cross -135 deg). The frequency where the phase crosses -135 degrees decreases with longer sling lengths, due to the lower frequency load pendulum mode (at approximately $\sqrt{(g/l)}$). This is associated with degraded handling qualities in Figure 3-2 as shown by the triangle symbols, which indicate poor handling qualities. The -135 degree frequency is important because it is used in standard helicopter bandwidth criteria since it better correlates to helicopter handling qualities ratings than the pure magnitude bandwidth (-3dB frequency) that is often used in text books [46]. This -135 deg point also represents the frequency where the pilot will have 45deg of phase margin with pure gain compensation.

Flight test HQRs from Ref. 2 (shown in Figure 3-2) show that the unaugmented configuration considered herein, UH-60 with LMR = 0.25 and a 56ft sling, has poor baseline handling qualities (HQR > 4) particularly in the lateral axis.

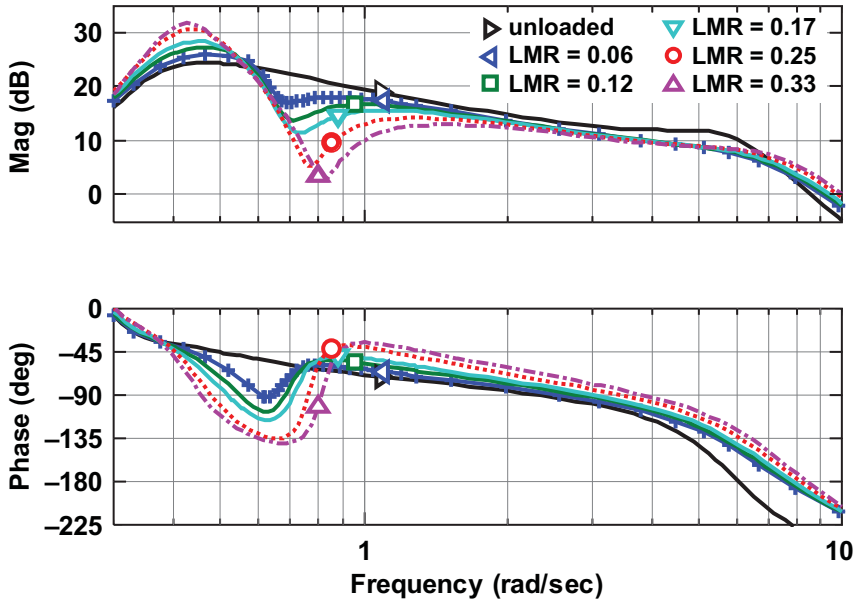

Figure 3-1. Roll attitude frequency response due to lateral cyclic ϕ/δ_{lat} for the 79ft sling with increasing LMR (Ref. 2).

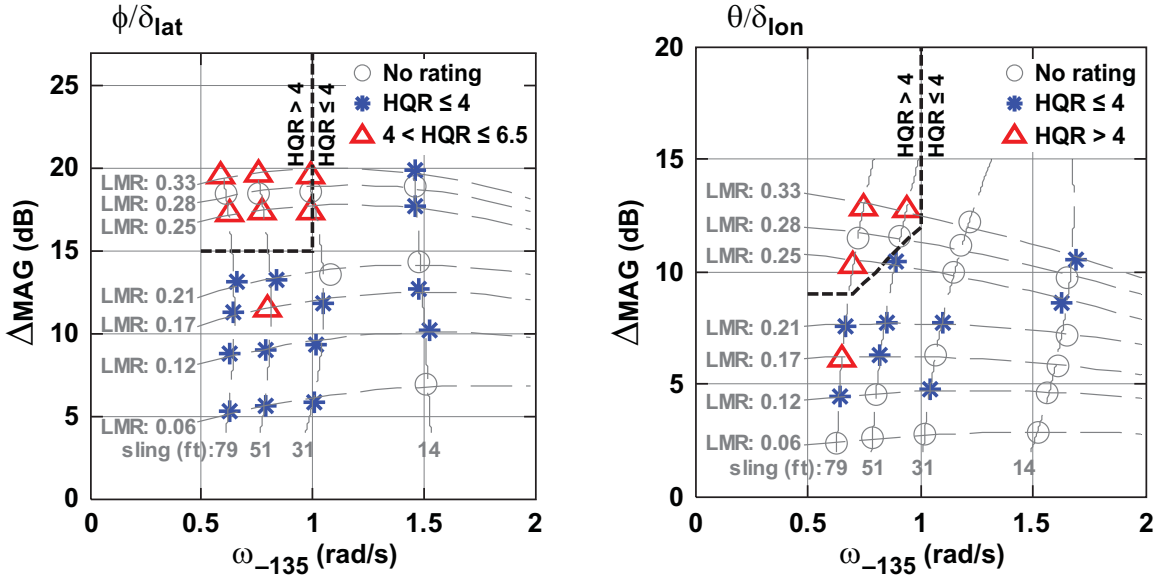

(a) Lateral Criteria (b) Longitudinal Criteria

Figure 3-2. Slung load handling qualities criteria (Ref. 2), where HQR>4 represents poor handling.

Based on these criteria, the shape of the attitude response due to piloted stick determines how the slung load affects the piloted handling qualities. These data indicate that by reshaping the magnitude response via feedback control, the handling qualities of the externally loaded helicopter could be improved by manipulating the depth of the magnitude notch and the frequency of the -135 crossing. This approach would effectively cause the pilot to feel like he/she is flying a lighter load on a shorter sling. Reducing the depth of the magnitude notch for the UH-60 with LMR=0.25 and therefore improving the predicted HQR is one of the key goals of the control system developed herein.

3.1 Summary of Chapter 3

Chapter 3 describes recently proposed handling qualities criteria for helicopters with external loads. These criteria show that degraded handling qualities are correlated with larger distortion of the magnitude response of the aircraft attitude at the load pendulum frequency. This distortion increases with the mass of the slung load. This handling qualities criterion is important because it indicates that using a feedback control system to change the distortion of the magnitude response near the load pendular mode can affect the handling qualities associated with an external load configuration. Chapter 4 performs analyses to look at the effect of fuselage, cable angle, and cable rate feedback on the predicted handling qualities.

4 Coupling Numerator Analysis of Control Feedbacks

The key components of the control system were initially developed in a single axis environment in order to explore the basic effects of cable angle feedback on the helicopter/load dynamics. However, due to heavily coupled helicopter dynamics, coupling effects due to off-axis loop closures could not be simply ignored. In this approach, coupling numerators [29,30] are used to calculate the effective aircraft dynamics between a particular input and output pair (for example p/δ_{lat}), while the off-axis response variables are assumed to be tightly constrained by feedback (e.g. $\delta_{lon} \to q$, $\delta_{ped} \to r$, $\delta_{col} \to w$). Then when designing control systems for the full order, fully coupled, multi-input multi-output system, where all the loops are simultaneously constrained by the control feedbacks, the analysis from the single-input coupling numerator is applicable. The first section of this chapter describes the traditional coupling numerator analysis developed by McRuer [29,30] to analytically calculate transfer functions of generic multi-loop systems. McRuer's analysis was later extended by Ref. 31 to the tightly constrained solution that provides the effective SISO transfer-function from a coupled multi-loop system. In the second section of this chapter, a new state-space derivation is presented for the constrained response, which is equivalent to the coupling numerator approach, but extends the solution to a more generic multi-input, multi-output state-space formulation, with the desired responses constrained. Then, this analysis is used to look at the first-principles effects of simple fuselage and cable-angle feedback with root-locus and Bode analyses.

4.1 Traditional Single-Input Single-Output Coupling Numerator Solution

Coupling numerators were developed in the 1960s to calculate transfer functions for multi-loop vehicular control systems [29]. This analytical method of calculating transfer functions for MIMO closed-loop systems is a useful tool for understanding the nature of the multi-loop problem in a coupled system. One key purpose of coupling numerator analysis is to allow insight into the effect of subsequent off-axis loop closures on the poles and zeros of the primary response. This was particularly important in the 1960s when the most common method of multi-loop control system design was trial and error using repetitive analysis on an analog computer, which did not provide much insight into the physical make-up of the modes [30]. In modern times, insight on multi-loop system dynamics can be achieved using software tools such as MATLAB's SIMULINK and various symbolic mathematical packages. However, the coupling numerator analysis is still relevant and interesting because it leads to a constrained solution which can provide an effective SISO transfer function while all other loops are assumed to be tightly controlled in a MIMO system. This is an important solution, which can simplify the response and provides the fundamental effects of feedback in a single axis, while accounting for the coupling effects on the response that will be present when all loops of the control system are simultaneously closed. Then, the MIMO design can be conducted using the effective SISO loop closures of the constrained transfer

functions. Using this method to design effective compensation in all the control axes will ensure a self-healing approximation once all loops are in place [47].

4.1.1 Example Case

As an example of multi-loop analysis using coupling numerators, consider the following notional 3 degree-of-freedom system:

$$\dot{\vec{x}} = \boldsymbol{A}\vec{x} + \boldsymbol{B}\vec{u} \tag{4.1}$$

$$\boldsymbol{A} = \begin{bmatrix} a_{11} & a_{12} & a_{13} \\ a_{21} & a_{22} & a_{23} \\ a_{31} & a_{32} & a_{33} \end{bmatrix}, \boldsymbol{B} = \begin{bmatrix} b_{11} & b_{12} & b_{13} \\ b_{21} & b_{22} & b_{23} \\ b_{31} & b_{32} & b_{33} \end{bmatrix} \tag{4.2}$$

$$\vec{x} = \begin{bmatrix} x_1 & x_2 & x_3 \end{bmatrix}^T \tag{4.3}$$

$$\vec{u} = \begin{bmatrix} \delta_1 & \delta_2 & \delta_3 \end{bmatrix}^T \tag{4.4}$$

Note that the ***A*** and ***B*** notation is used here to differentiate from the ***M***, ***F***, ***G*** formulation used later in Eq. (4.28), where $\boldsymbol{A}=\boldsymbol{M}^{-1}\boldsymbol{F}$ and $\boldsymbol{B} = \boldsymbol{M}^{-1}\boldsymbol{G}$. Eqs. (4.1) – (4.4) can be represented equivalently in the Laplace (s) domain:

$$\begin{bmatrix} s-a_{11} & -a_{12} & -a_{13} \\ -a_{21} & s-a_{22} & -a_{23} \\ -a_{31} & -a_{32} & s-a_{33} \end{bmatrix} \begin{bmatrix} x_1 \\ x_2 \\ x_3 \end{bmatrix} = \begin{bmatrix} b_{11} & b_{12} & b_{13} \\ b_{21} & b_{22} & b_{23} \\ b_{31} & b_{32} & b_{33} \end{bmatrix} \begin{bmatrix} \delta_1 \\ \delta_2 \\ \delta_3 \end{bmatrix} \tag{4.5}$$

Numerator Notation

A simple example of the notation used by McRuer [29] to represent an open loop transfer function numerator is demonstrated by the calculation of x_3/δ_3 with Cramer's rule:

$$\frac{x_3}{\delta_3} = \frac{N_{\delta_3}^{x_3}}{\Delta} = \frac{\begin{vmatrix} s-a_{11} & -a_{12} & b_{13} \\ -a_{21} & s-a_{22} & b_{23} \\ -a_{31} & -a_{32} & b_{33} \end{vmatrix}}{\begin{vmatrix} s-a_{11} & -a_{12} & -a_{13} \\ -a_{21} & s-a_{22} & -a_{23} \\ -a_{31} & -a_{32} & s-a_{33} \end{vmatrix}} \tag{4.6}$$

$N_{\delta_3}^{x_3}$ represents the numerator of x_3/δ_3, which is calculated by replacing the x_3 column in the ***A***-matrix with the δ_3 column of the ***B***-matrix and taking the determinant of the resulting matrix, as shown in Eq. (4.6).

Coupling numerator analysis introduces a type of numerator notation where more than one column in the A-matrix is replaced by columns in the B-matrix before calculating the determinant. This type of

numerator is called a "coupling-numerator" to distinguish it from the conventional numerator. For example:

$$N_{\delta_1\delta_2}^{x_1x_2} = \begin{vmatrix} b_{11} & b_{12} & -a_{13} \\ b_{21} & b_{22} & -a_{23} \\ b_{31} & b_{32} & s-a_{33} \end{vmatrix} \tag{4.7}$$

This notation can be used to represent any number of B-matrix column substitutions into the A-matrix, for any order system.

An additional property of the coupling numerator is that if two responses are feedback to the same control, or alternately if two controls are feedback to the same state, the coupling numerator is equal to zero:

$$N_{\delta_1\delta_1}^{x_1x_2} = 0 \tag{4.8}$$

$$N_{\delta_1\delta_2}^{x_1x_1} = 0 \tag{4.9}$$

Also, the order of the coupling numerator is immaterial:

$$N_{\delta_1\delta_2}^{x_1x_2} = N_{\delta_2\delta_1}^{x_2x_1} \tag{4.10}$$

Multi-loop Analysis

Now, imagine that system described in Eqs. (4.1) – (4.4) has two feedback loops as shown in Figure 4-1, with compensation G_{11} and G_{22}. Notice there are no cross-feeds in the analysis (e.g. no compensator G_{12} that would feedback x_2 to δ_1). The full generic analysis of Ref. 29 uses a fully propagated matrix of compensators between each input and output. However, for the sake of introducing coupling numerator analysis to the reader, the example shown herein is simplified to include only the diagonal terms in this matrix of compensators.

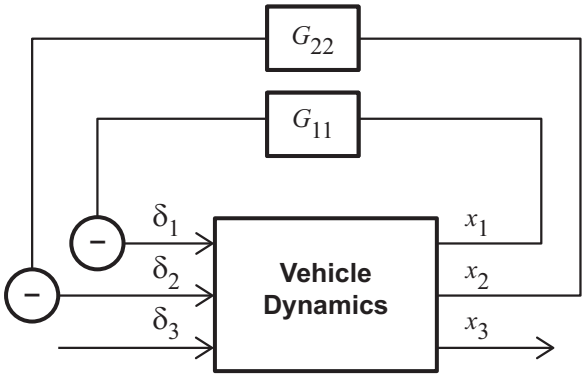

Figure 4-1. Block diagram for coupling numerator example.

The system in Figure 4-1 can then be represented by the following state-space equations where $\delta_1 = -G_{11}x_1$, $\delta_2 = -G_{22}x_2$:

$$\begin{bmatrix}\dot{x}_1\\ \dot{x}_2\\ \dot{x}_3\end{bmatrix}=\begin{bmatrix}a_{11} & a_{12} & a_{13}\\ a_{21} & a_{22} & a_{23}\\ a_{31} & a_{32} & a_{33}\end{bmatrix}\begin{bmatrix}x_1\\ x_2\\ x_3\end{bmatrix}-\begin{bmatrix}b_{11}\\ b_{21}\\ b_{31}\end{bmatrix}G_{11}x_1-\begin{bmatrix}b_{12}\\ b_{22}\\ b_{32}\end{bmatrix}G_{22}x_2+\begin{bmatrix}b_{13}\\ b_{23}\\ b_{33}\end{bmatrix}\delta_3 \tag{4.11}$$

Then, rearranging Eq. (4.11) and using LaPlace form:

$$\begin{bmatrix}s-a_{11}+G_{11}b_{11} & -a_{12}+G_{22}b_{12} & -a_{13}\\ -a_{21}+G_{11}b_{21} & s-a_{22}+G_{22}b_{22} & -a_{23}\\ -a_{31}+G_{11}b_{31} & -a_{32}+G_{22}b_{32} & s-a_{33}\end{bmatrix}\begin{bmatrix}x_1\\ x_2\\ x_3\end{bmatrix}=\begin{bmatrix}b_{13}\\ b_{23}\\ b_{33}\end{bmatrix}\delta_3 \tag{4.12}$$

In order to calculate the transfer function x_3/δ_3, with compensators G_{11} and G_{22} active, Cramer's rule can again be used:

$$x_3/\delta_3\Big|_{\substack{x_1\to\delta_1\\ x_2\to\delta_2}}=\frac{\begin{vmatrix}s-a_{11}+G_{11}b_{11} & -a_{12}+G_{22}b_{12} & b_{13}\\ -a_{21}+G_{11}b_{21} & s-a_{22}+G_{22}b_{22} & b_{23}\\ -a_{31}+G_{11}b_{31} & -a_{32}+G_{22}b_{32} & b_{33}\end{vmatrix}}{\begin{vmatrix}s-a_{11}+G_{11}b_{11} & -a_{12}+G_{22}b_{12} & -a_{13}\\ -a_{21}+G_{11}b_{21} & s-a_{22}+G_{22}b_{22} & -a_{23}\\ -a_{31}+G_{11}b_{31} & -a_{32}+G_{22}b_{32} & s-a_{33}\end{vmatrix}} \tag{4.13}$$

The notation $x_3/\delta_3\Big|_{\substack{x_1\to\delta_1\\ x_2\to\delta_2}}$ indicates that calculation of x_3/δ_3, taking into account active feedbacks of x_1 to δ_1, and x_2 to δ_2.

The key to McRuer's coupling numerator method is recognizing that the determinants, such as in Eq. (4.13), used to calculate the multi-loop transfer functions can be represented as a sum of simpler determinants. For example, the denominator in Eq. (4.13) can be represented as a sum of four simpler determinants:

$$\begin{aligned}&\begin{vmatrix}s-a_{11}+G_{11}b_{11} & -a_{12}+G_{22}b_{12} & -a_{13}\\ -a_{21}+G_{11}b_{21} & s-a_{22}+G_{22}b_{22} & -a_{23}\\ -a_{31}+G_{11}b_{31} & -a_{32}+G_{22}b_{32} & s-a_{33}\end{vmatrix}=\\ &\quad\begin{vmatrix}s-a_{11} & -a_{12} & -a_{13}\\ -a_{21} & s-a_{22} & -a_{23}\\ -a_{31} & -a_{32} & s-a_{33}\end{vmatrix}+\begin{vmatrix}G_{11}b_{11} & -a_{12} & -a_{13}\\ G_{11}b_{21} & s-a_{22} & -a_{23}\\ G_{11}b_{31} & -a_{32} & s-a_{33}\end{vmatrix}\\ &\quad+\begin{vmatrix}G_{11}b_{11} & G_{22}b_{12} & -a_{13}\\ G_{11}b_{21} & G_{22}b_{22} & -a_{23}\\ G_{11}b_{31} & G_{22}b_{32} & s-a_{33}\end{vmatrix}+\begin{vmatrix}s-a_{11} & G_{22}b_{12} & -a_{13}\\ -a_{21} & G_{22}b_{22} & -a_{23}\\ -a_{31} & G_{22}b_{32} & s-a_{33}\end{vmatrix}\\ &=\Delta+G_{11}\mathrm{N}_{\delta_1}^{x_1}+G_{11}G_{22}N_{\delta_1\delta_2}^{x_1x_2}+G_{22}N_{\delta_2}^{x_2}\end{aligned} \tag{4.14}$$

The characteristic equation (Δ), conventional numerators ($N_{\delta_1}^{x_1}$, $N_{\delta_2}^{x_2}$), and coupling numerator ($N_{\delta_1\delta_2}^{x_1x_2}$) in Eq. (4.14) are calculated based on Eq. (4.5). The numerator of Eq. (4.13) can also be expressed as a sum of four simpler determinants:

$$\begin{vmatrix} s-a_{11}+G_{11}b_{11} & -a_{12}+G_{22}b_{12} & b_{13} \\ -a_{21}+G_{11}b_{21} & s-a_{22}+G_{22}b_{22} & b_{23} \\ -a_{31}+G_{11}b_{31} & -a_{32}+G_{22}b_{32} & b_{33} \end{vmatrix} =$$

$$\begin{vmatrix} s-a_{11} & -a_{12} & b_{13} \\ -a_{21} & s-a_{22} & b_{23} \\ -a_{31} & -a_{32} & b_{33} \end{vmatrix} + \begin{vmatrix} G_{11}b_{11} & -a_{12} & b_{13} \\ G_{11}b_{21} & s-a_{22} & b_{23} \\ G_{11}b_{31} & -a_{32} & b_{33} \end{vmatrix}$$

$$+ \begin{vmatrix} G_{11}b_{11} & G_{22}b_{12} & b_{13} \\ G_{11}b_{21} & G_{22}b_{22} & b_{23} \\ G_{11}b_{31} & G_{22}b_{32} & b_{33} \end{vmatrix} + \begin{vmatrix} s-a_{11} & G_{22}b_{12} & b_{13} \\ -a_{21} & G_{22}b_{22} & b_{23} \\ -a_{31} & G_{22}b_{32} & b_{33} \end{vmatrix} \tag{4.15}$$

$$= \mathrm{N}_{\delta_3}^{x_3} + G_{11}N_{\delta_1\delta_3}^{x_1x_3} + G_{11}G_{22}N_{\delta_1\delta_2\delta_3}^{x_1x_2x_3} + G_{22}N_{\delta_2\delta_3}^{x_2x_3}$$

The open-loop numerator and coupling numerators in Eq. (4.15) are calculated based on Eq. (4.5). Finally, the transfer function, calculated via coupling numerators is:

$$x_3/\delta_3\big|_{\substack{x_1\to\delta_1 \\ x_2\to\delta_2}} = \frac{\mathrm{N}_{\delta_3}^{x_3} + G_{11}N_{\delta_1\delta_3}^{x_1x_3} + G_{11}G_{22}N_{\delta_1\delta_2\delta_3}^{x_1x_2x_3} + G_{22}N_{\delta_2\delta_3}^{x_2x_3}}{\Delta + G_{11}\mathrm{N}_{\delta_1}^{x_1} + G_{11}G_{22}N_{\delta_1\delta_2}^{x_1x_2} + G_{22}N_{\delta_2}^{x_2}} \tag{4.16}$$

This method is easier, faster, and more insightful to calculate the responses than directly from Eq. (4.13) because the effects of the additional loop closures are represented by simple summed terms. The generic solutions and rules for calculation of coupling numerators with cross-feeds and/or higher-order systems are given in Ref. 29.

Constrained Responses via Coupling Numerator Analysis

The coupling numerator results presented in the previous section are interesting, but have limited utility given the modern tools available to most engineers. However, there is an interesting result that comes out of the coupling numerator analysis, which is helpful for approximating a single-input single-output response, while considering other loops tightly constrained [31].

Start by rearranging Eq. (4.16):

$$x_3/\delta_3\big|_{\substack{x_1\to\delta_1 \\ x_2\to\delta_2}} = \frac{\dfrac{\mathrm{N}_{\delta_3}^{x_3}}{G_{11}G_{22}} + \dfrac{N_{\delta_1\delta_3}^{x_1x_3}}{G_{22}} + \dfrac{N_{\delta_2\delta_3}^{x_2x_3}}{G_{11}} + N_{\delta_1\delta_2\delta_3}^{x_1x_2x_3}}{\dfrac{\Delta}{\mathrm{G}_{11}G_{22}} + \dfrac{\mathrm{N}_{\delta_1}^{x_1}}{\mathrm{G}_{22}} + \dfrac{N_{\delta_2}^{x_2}}{\mathrm{G}_{11}} + N_{\delta_1\delta_2}^{x_1x_2}} \tag{4.17}$$

Now, considering that the responses are very tightly constrained, it is possible to calculate the response $x_3/\delta_3\big|_{\substack{x_1\to\delta_1\\x_2\to\delta_2}}$ as $G_{11}, G_{22} \to \infty$. Then, the constrained response can be represented by the coupling numerator terms:

$$x_3/\delta_3\big|_{\substack{x_1\to\delta_1\\x_2\to\delta_2}} \cong \frac{N^{x_1x_2x_3}_{\delta_1\delta_2\delta_3}}{N^{x_1x_2}_{\delta_1\delta_2}} = \frac{\begin{vmatrix} b_{11} & b_{12} & b_{13} \\ b_{21} & b_{22} & b_{23} \\ b_{31} & b_{32} & b_{33} \end{vmatrix}}{\begin{vmatrix} b_{11} & b_{12} & -a_{13} \\ b_{21} & b_{22} & -a_{23} \\ b_{31} & b_{32} & s-a_{33} \end{vmatrix}} \tag{4.18}$$

This is the classic limiting form of the coupling numerator as presented in Ref. 31. This result can be extended to higher order systems with any number of control inputs by including appropriate coupling numerators. For example, in a 4th order system with 4 control inputs:

$$\boldsymbol{A} = \begin{bmatrix} a_{11} & a_{12} & a_{13} & a_{14} \\ a_{21} & a_{22} & a_{23} & a_{24} \\ a_{31} & a_{32} & a_{33} & a_{34} \\ a_{41} & a_{42} & a_{43} & a_{44} \end{bmatrix}, \ \boldsymbol{B} = \begin{bmatrix} b_{11} & b_{12} & b_{13} & b_{14} \\ b_{21} & b_{22} & b_{23} & b_{24} \\ b_{31} & b_{32} & b_{33} & b_{34} \\ b_{41} & b_{42} & b_{43} & b_{44} \end{bmatrix} \tag{4.19}$$

$$\vec{x} = \begin{bmatrix} x_1 & x_2 & x_3 & x_4 \end{bmatrix} \tag{4.20}$$

$$\vec{u} = \begin{bmatrix} \delta_1 & \delta_2 & \delta_3 & \delta_4 \end{bmatrix} \tag{4.21}$$

The tightly constrained response $x_1/\delta_1\big|_{\substack{x_2\to\delta_2\\x_3\to\delta_3}}$ can be calculated by following the same general pattern as in Eq. (4.18):

$$\frac{x_1}{\delta_1}\bigg|_{\substack{x_2\to\delta_2\\x_3\to\delta_3}} = \frac{N^{x_2x_3x_1}_{\delta_2\delta_3\delta_1}}{N^{x_2x_3}_{\delta_2\delta_3}} = \frac{\begin{vmatrix} b_{11} & b_{12} & b_{13} & -a_{14} \\ b_{21} & b_{22} & b_{23} & -a_{24} \\ b_{31} & b_{32} & b_{33} & -a_{34} \\ b_{41} & b_{42} & b_{43} & s-a_{44} \end{vmatrix}}{\begin{vmatrix} s-a_{11} & b_{12} & b_{13} & -a_{14} \\ -a_{21} & b_{22} & b_{23} & -a_{24} \\ -a_{31} & b_{32} & b_{33} & -a_{34} \\ -a_{41} & b_{42} & b_{43} & s-a_{44} \end{vmatrix}} \tag{4.22}$$

This result can be used to design the control system axis-by-axis, while accounting for the effects of coupling due to multiple loop closures. When all loops are then closed with well designed feedbacks, the responses are as expected – "a self-healing assumption" [47].

4.2 Derivation of State-Space Solution for Constrained Coupling Numerators

The constrained coupling numerator solutions presented in the literature [30,31] are limited because they can only provide a single transfer function. For higher order systems, it would be useful to obtain a state-space representation with multiple inputs and outputs, with some but not all, of these inputs and outputs constrained. For example, it might be useful to obtain a state-space response with yaw rate constrained with pedal, and vertical velocity constrained by collective, and have outputs of lateral and longitudinal velocities, angular rates, and attitudes for lateral and longitudinal cyclic inputs.

Recent work by Hess in 2003 [48] derives a numerical solution for the constrained coupling numerator transfer function, which is compatible with modern tools and does not require analytical derivation, but still only provides a SISO transfer function, not a full state-space solution. Thus, the lack of a state-space method has motivated the derivation of the solution herein.

For the state-space approach, the derivation will be shown with the example from Sec. 4.4.1, as shown in Figure 4-1. Recall that the closed loop system is represented by the following state-space system (rearrangement of Eq. (4.12)):

$$\begin{bmatrix} \frac{s-a_{11}}{G_{11}}+b_{11} & \frac{-a_{12}}{G_{22}}+b_{12} & -a_{13} \\ \frac{-a_{21}}{G_{11}}+b_{21} & \frac{s-a_{22}}{G_{22}}+b_{22} & -a_{23} \\ \frac{-a_{31}}{G_{11}}+b_{31} & \frac{-a_{32}}{G_{22}}+b_{32} & s-a_{33} \end{bmatrix} \begin{bmatrix} G_{11}x_1 \\ G_{22}x_2 \\ x_3 \end{bmatrix} = \begin{bmatrix} b_{13} \\ b_{23} \\ b_{33} \end{bmatrix} \delta_3 \tag{4.23}$$

Now, for the tightly constrained solution $G_{11}, G_{22} \to \infty$:

$$\begin{bmatrix} b_{11} & b_{12} & -a_{13} \\ b_{21} & b_{22} & -a_{23} \\ b_{31} & b_{32} & s-a_{33} \end{bmatrix} \begin{bmatrix} G_{11}x_1 \\ G_{22}x_2 \\ x_3 \end{bmatrix} = \begin{bmatrix} b_{13} \\ b_{23} \\ b_{33} \end{bmatrix} \delta_3 \tag{4.24}$$

If solving this system of Eq. (4.24) using Cramer's Rule for x_3, the solution would be identical to the traditional method of Eq. (4.18):

$$x_3/\delta_3\big|_{Eq.(4.24)} = \frac{\begin{vmatrix} b_{11} & b_{12} & b_{13} \\ b_{21} & b_{22} & b_{23} \\ b_{31} & b_{32} & b_{33} \end{vmatrix}}{\begin{vmatrix} b_{11} & b_{12} & -a_{13} \\ b_{21} & b_{22} & -a_{23} \\ b_{31} & b_{32} & s-a_{33} \end{vmatrix}} = x_3/\delta_3\big|_{\substack{x_1 \to \delta_1 \\ x_2 \to \delta_2}} \tag{4.25}$$

Instead, algebraic "dummy" states x_1', x_2' are used to represent the model of Eq. (4.24) in the state space form, where:

$$\dot{x}_1' = G_{11} x_1 \tag{4.26}$$

$$\dot{x}_2' = G_{22} x_2 \tag{4.27}$$

$$\boldsymbol{M}\dot{\vec{x}}' = \boldsymbol{F}\vec{x}' + \boldsymbol{G}\vec{u}' \tag{4.28}$$

$$\begin{bmatrix} b_{11} & b_{12} & 0 \\ b_{21} & b_{22} & 0 \\ b_{31} & b_{32} & 1 \end{bmatrix} \begin{bmatrix} \dot{x}_1' \\ \dot{x}_2' \\ \dot{x}_3 \end{bmatrix} = \begin{bmatrix} 0 & 0 & a_{13} \\ 0 & 0 & a_{23} \\ 0 & 0 & a_{33} \end{bmatrix} \begin{bmatrix} x_1' \\ x_2' \\ x_3 \end{bmatrix} + \begin{bmatrix} b_{13} \\ b_{23} \\ b_{33} \end{bmatrix} \begin{bmatrix} \delta_3 \end{bmatrix} \tag{4.29}$$

Then the new $\boldsymbol{A}$ and $\boldsymbol{B}$ constrained coupling numerator matrices ($\boldsymbol{A}_{CN}$, $\boldsymbol{B}_{CN}$) can be calculated by multiplying the $\boldsymbol{F}$ and $\boldsymbol{G}$ matrices by $\boldsymbol{M}^{-1}$.

$$\boldsymbol{A}_{CN} = \begin{bmatrix} b_{11} & b_{12} & 0 \\ b_{21} & b_{22} & 0 \\ b_{31} & b_{32} & 1 \end{bmatrix}^{-1} \begin{bmatrix} 0 & 0 & a_{13} \\ 0 & 0 & a_{23} \\ 0 & 0 & a_{33} \end{bmatrix} \tag{4.30}$$

$$\boldsymbol{B}_{CN} = \begin{bmatrix} b_{11} & b_{12} & 0 \\ b_{21} & b_{22} & 0 \\ b_{31} & b_{32} & 1 \end{bmatrix}^{-1} \begin{bmatrix} b_{13} \\ b_{23} \\ b_{33} \end{bmatrix} \tag{4.31}$$

Then:

$$\dot{\vec{x}}' = \boldsymbol{A}_{CN}\vec{x}' + \boldsymbol{B}_{CN}\delta_3 \tag{4.32}$$

This produces the same solution for $x_3/\delta_3\big|_{\substack{x_1\to\delta_1 \\ x_2\to\delta_2}}$ as Eq. (4.18), as demonstrated by Eq. (4.25), but requires much less work manipulating transfer functions than those presented in Hoh [31], and in Hess [48].

The general procedure for determining the constrained state-space response for a generic system is:

1. Replace the column(s) of the constrained state(s) in the identity **M**-matrix with the **B**-matrix column(s) of the control(s) used to constrain the state(s).
2. To create the **F**-matrix, zero out the column(s) of the **A**-matrix that correspond to the constrained state(s).
3. The **G**-matrix is the **B**-matrix with column(s) of the constrained control(s) removed.
4. Calculate the $\mathbf{A_{CN}}$ and $\mathbf{B_{CN}}$ by left multiplying the **F** and **G** matrices by $\mathbf{M}^{-1}$.

This general constrained state-space 'coupling numerator' solution allows for MIMO design with some loops tightly constrained, rather than a strictly SISO transfer-function solution. As an example use of the state-space method to represent a MIMO system with any number of desired constrained input-output pairs, consider the 4th order system of Eqs. (4.19)-(4.21).

Then constraining $x_2 \to \delta_2$ and $x_3 \to \delta_3$, and using the general procedure outlined in Steps 1-4, the following state-space model structure results:

$$\begin{bmatrix} \dot{x}_1 \\ \dot{x}_2' \\ \dot{x}_3' \\ \dot{x}_4 \end{bmatrix} = \begin{bmatrix} 1 & b_{12} & b_{13} & 0 \\ 0 & b_{22} & b_{23} & 0 \\ 0 & b_{32} & b_{33} & 0 \\ 0 & b_{42} & b_{43} & 1 \end{bmatrix}^{-1} \begin{bmatrix} a_{11} & 0 & 0 & a_{14} \\ a_{21} & 0 & 0 & a_{24} \\ a_{31} & 0 & 0 & a_{34} \\ a_{41} & 0 & 0 & a_{44} \end{bmatrix} \begin{bmatrix} x_1 \\ x_2' \\ x_3' \\ x_4 \end{bmatrix} + \begin{bmatrix} 1 & b_{12} & b_{13} & 0 \\ 0 & b_{22} & b_{23} & 0 \\ 0 & b_{32} & b_{33} & 0 \\ 0 & b_{42} & b_{43} & 1 \end{bmatrix}^{-1} \begin{bmatrix} b_{11} & b_{14} \\ b_{21} & b_{24} \\ b_{31} & b_{34} \\ b_{41} & b_{44} \end{bmatrix} \begin{bmatrix} \delta_1 \\ \delta_4 \end{bmatrix} \tag{4.33}$$

This state space model can be used to calculate $x_1/\delta_1\big|_{\substack{x_2\to\delta_2 \\ x_3\to\delta_3}}$, identically to the conventional result shown in Eq. (4.22). In addition, the same state-space structure gives $x_1/\delta_4\big|_{\substack{x_2\to\delta_2 \\ x_3\to\delta_3}}$, $x_4/\delta_1\big|_{\substack{x_2\to\delta_2 \\ x_3\to\delta_3}}$, and $x_4/\delta_4\big|_{\substack{x_2\to\delta_2 \\ x_3\to\delta_3}}$. This state-space model can now be used directly for control system design of x_1 and x_4 responses, with the effects of coupling due to closure of the $x_2 \to \delta_2$ and $x_3 \to \delta_3$ loops taken into account.

4.3 Coupling Numerators for the UH-60

In a similar manner to that presented in Sec. 4.2, the effective single-axis responses are calculated for the lateral axis UH-60 with an external load. The state-space coupling numerator analysis described in the previous section is performed on the analytical linear model derived in Sec. 2.2.2. This model includes rigid-body, slung-load dynamics, and a 70ms time delay (Pade′ approximation) to represent effective rotor dynamics. This model with the time delay is valid from 0.1- 12 rad/s as shown in Figure 2-4 - Figure 2-11. The more complex FORECAST/OVERCAST model (Sec. 2.2.4) with explicit rotor-states will be used later in Chapters 5-7 to ensure that the rotor-modes are sufficiently damped. Here in Chapter 4, the simple analytical model (Sec. 2.2.2) is used to focus on the basic helicopter/load coupling dynamics without the added complication of the rotor modes, which are not needed to provide a valid frequency response over the frequency range of interest for load response and handling qualities (0.1 – 12 rad/s).

The use of coupling numerator analysis allows for the examination of basic dynamic effects of fuselage and cable angle/rate feedback in a single-axis, without the added complication of designing control systems for the off-axis responses (which are unstable and highly coupled). The coupling numerator analysis is important because the stability of control system near the load mode is very sensitive to changes in phase near the load mode notch in the attitude response. Given that this region of the response is heavily influenced by coupling, it is important to use a coupling numerator result to take into account the coupling effect of multiple loop closures. The lateral axis was chosen because it is more affected by the load motions than the longitudinal axis due to its lower inertial configuration. In this work, the following responses are of interest:

$$\frac{p}{\delta_{lat}}\bigg|_{\substack{q\to\delta_{lon} \\ r\to\delta_{ped} \\ w\to\delta_{col}}}, \quad \frac{\phi}{\delta_{lat}}\bigg|_{\substack{q\to\delta_{lon} \\ r\to\delta_{ped} \\ w\to\delta_{col}}}, \quad \frac{\Delta\phi_c}{\delta_{lat}}\bigg|_{\substack{q\to\delta_{lon} \\ r\to\delta_{ped} \\ w\to\delta_{col}}} \tag{4.34}$$

where the pitch rate is tightly constrained by longitudinal cyclic $\left(q \to \delta_{lon}\right)$, the yaw rate is tightly constrained by the pedal $\left(r \to \delta_{ped}\right)$, and vertical velocity is tightly closed by collective $\left(w \to \delta_{col}\right)$.

Comparisons of the bare airframe responses and the constrained (i.e. coupling numerator) responses for the roll attitude (ϕ) and load cable angle relative to the fuselage ($\Delta\phi_c$) are shown in Figure 4-2. The responses are not strongly affected by the closure of the off-axis loops over the 2-10 rad/s range, but are more influenced in the 0.1-1 rad/s where cross-axis coupling is prevalent. Most critically, the closure of off-axis loops effects the phase near the load mode (from 0.5 -1 rad/s), which strongly effects the stability of the load mode (because the broken loop typically has a 0dB crossing near this frequency due to the reduced magnitude near the load mode). Figure 4-2 also validates the state-space technique for determining the constrained coupling numerator result because the responses for the traditional transfer-function coupling numerators and the state-space solution are identical (e.g. the dash and dotted curves overlay in Figure 4-2).

An alternate method to coupling numerators can be to drop the coupling terms in the state-space matrix, to effectively calculate a SISO response. The results of this method are also shown in Figure 4-2. As seen in the figure, this method produces responses at low frequency that are not consistent with the bare airframe or the coupling numerator response. This is particularly true in the roll attitude response in Figure 4-2a, where the phase of the model with dropped coupling terms is not consistent with the coupling numerator result between 0.5-1.0 rad/s, which can greatly change the stability margin and damping of near the load mode. The coupling numerator result produces an effective single axis response that accounts for the coupling instead of eliminating it, which provides a better approximation for control design of multiple loops.

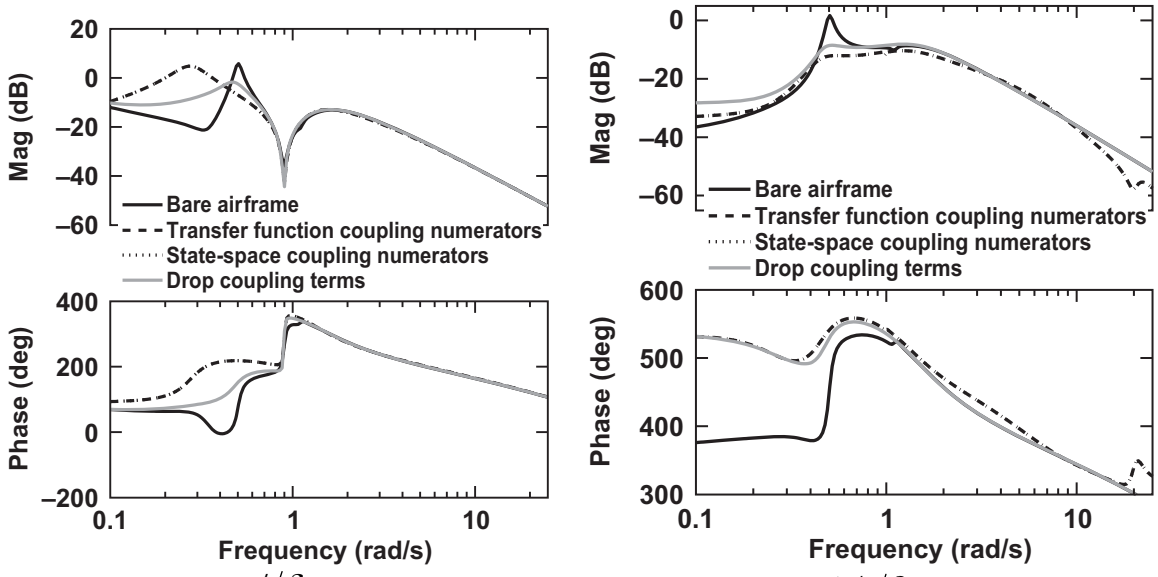

Figure 4-2. ϕ/δ_{lat} and $\Delta\phi_c/\delta_{lat}$ with and without coupling numerator closure of the off-axis.

4.4 Root Locus for Fuselage and Load Feedbacks on a UH-60

Now that the effective SISO coupling numerator responses have been determined, these responses can be used in any SISO control design technique. Herein, the single axis coupling numerator transfer functions for the lateral axis are used for compensator (H) design with root-locus and Bode plot techniques. The block diagram illustrating this method is shown in Figure 4-3. This method demonstrates the fundamental effects of different types of feedback on the helicopter/load dynamics, without needing to design a multi-loop system for the other control axes.

Three designs are examined:

- Fuselage Feedback Only
- Combination of Fuselage and Cable Angle Feedbacks
- Combination of Fuselage and Cable Rate Feedbacks

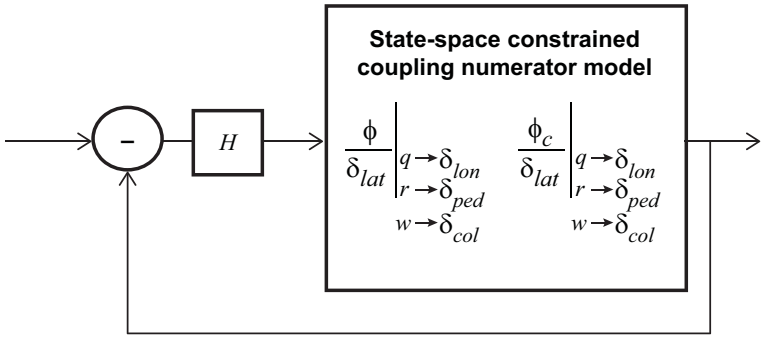

Figure 4-3. Control block diagram using constrained coupling numerator response.

4.4.1 Fuselage Feedback Only

The effects of conventional fuselage feedback on the dynamic modes of the aircraft are seen in Figure 4-4. As shown in Figure 4-4a, roll rate feedback tends to initially improve the roll mode, increasing its frequency (and therefore the effective bandwidth). Roll rate feedback also moves the Phugoid mode closer to the origin, but does not stabilize it, and tends to reduce the damping of the lateral load pendulum mode. Roll attitude feedback in Figure 4-4b tends to reduce the frequency of the roll mode (reducing the effective bandwidth), but stabilizes the Phugoid mode and damps the load pendulum mode. Due to multiple constraints such as stability margin, disturbance rejection bandwidth, piloted bandwidth, etc., a combination of roll rate (k_p), roll angle (k_ϕ), and the integral of roll angle feedbacks (k_{ϕ_i}) are required to provide a stable, and acceptably performing conventional control design for a helicopter [49]. As an example of a conventional feedback control system, combinations of these feedbacks are used to form a PID compensator (H) for roll attitude via classical control techniques. The compensator architecture has the following form:

$$H = k_\phi \left[1 + \frac{k_p}{k_\phi} s + \frac{k_{\phi_i}}{k_\phi} \left(\frac{1}{s} \right) \right] \tag{4.35}$$

The following gains proportions were used to provide the ideal k/s loop shape in the region of cross-over (1-3 rad/s):

$$\frac{k_p}{k_\phi} = 0.8 \,, \; \frac{k_{\phi_i}}{k_\phi} = 0.2 \tag{4.36}$$

Then the root locus was calculated to determine the proper value of k_ϕ in Figure 4-4c. The root locus indicates that increasing k_ϕ provides a higher frequency roll mode (improving the bandwidth), as well as considerable improvement in Phugoid stability. However, increasing gain in Figure 4-4c also results in a lightly damped load mode.

After choosing a gain of $k_\phi = 4$ for the conventional PID feedback from Figure 4-4c, the closed-loop bode plots for the aircraft roll attitude and lateral cable angle were plotted in Figure 4-5. The closed-loop bode plot of Figure 4-5a indicates that the shape of the attitude response near the load mode are mostly unchanged as compared to the bare airframe. Although the closed loop gain has changed, the depth of the magnitude notch of the slung load mode on the attitude is only slightly reduced, and the frequency of the load mode is unchanged (no crossing of -135deg near the load mode). Therefore, according to the slung load handling qualities specification, described in Chapter 3 and Ref. 2, the maneuvering handling qualities with the external load have not greatly improved from the unaugmented case. The inertial referenced load motion (ϕ_c) is larger and not as well damped as the unaugmented system, as indicated by the magnitude peak at the load mode (~1 rad/s) in Figure 4-5b. This analysis shows that fuselage feedback did not provide improved handling qualities characteristics or load damping.

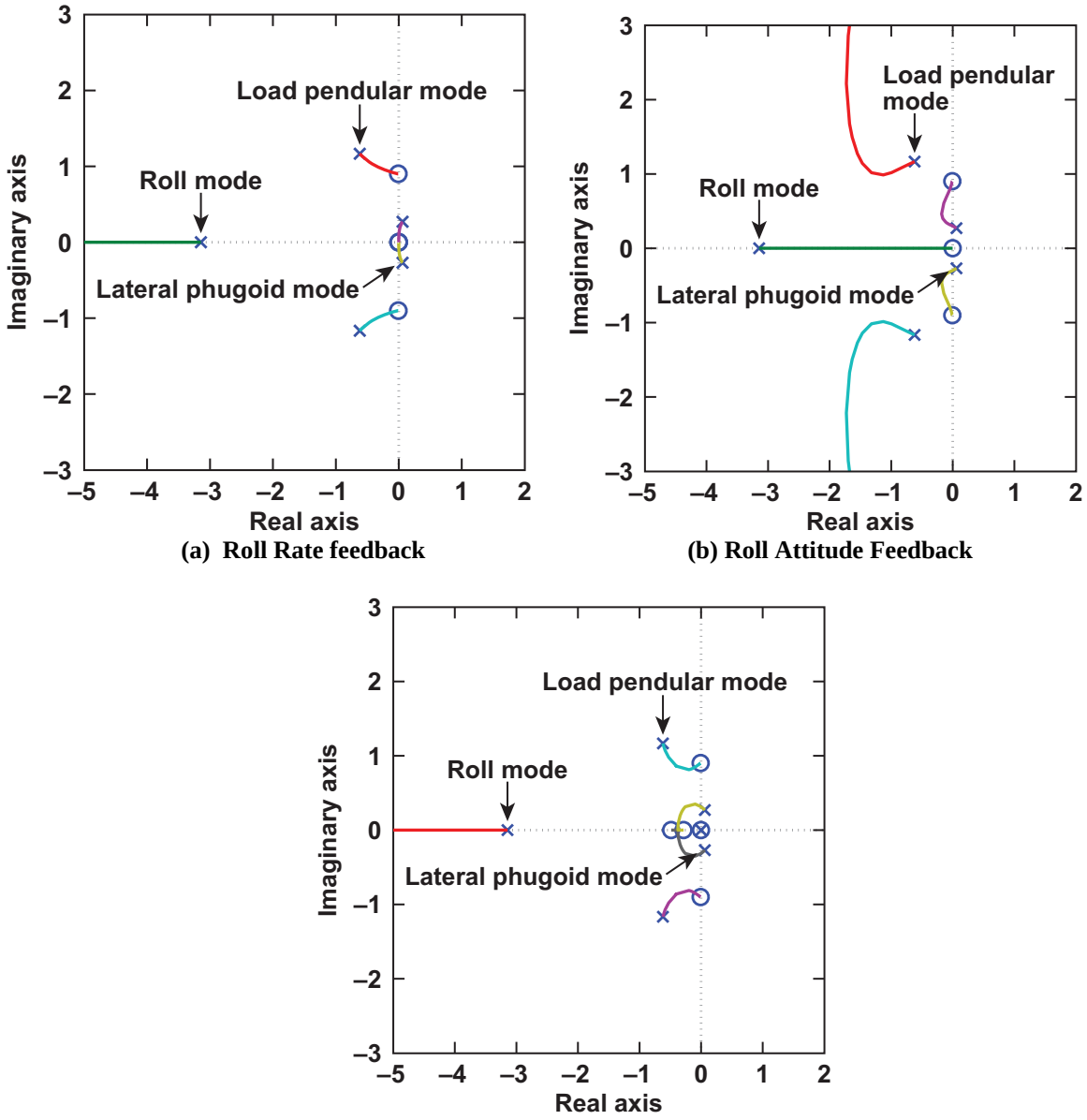

(a) Roll Rate feedback

(b) Roll Attitude Feedback

(c) Conventional combination of roll rate, roll attitude, and attitude integral feedback

Figure 4-4. Root loci for fuselage feedback using constrained coupling numerators.

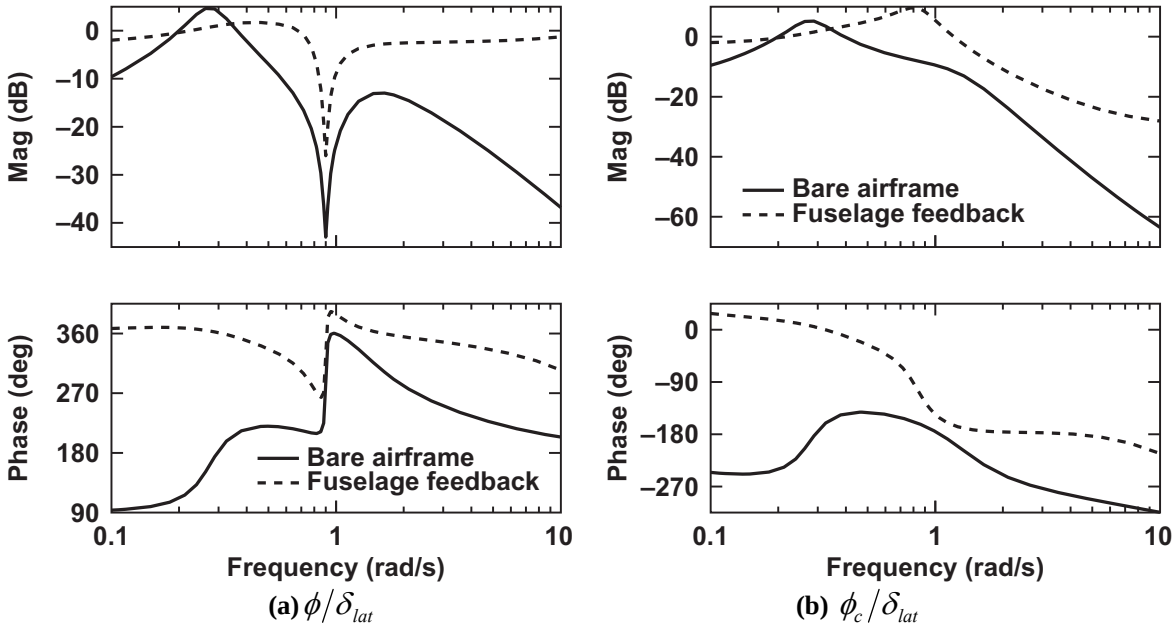

Figure 4-5. Bode plot comparison between bare airframe and fuselage feedback using constrained coupling numerators.

4.4.2 Fuselage and Cable Angle/Rate Feedback

Cable angle and cable rate feedbacks are now added to fuselage feedbacks from the previous section in order to determine if handling qualities characteristics and/or load damping can be improved. The model provides states for the load cable parameters in a reference frame with respect to the fuselage. In this work, the inertial referenced cable angle ϕ_c is used for control feedback, as opposed to cable angle measured in a reference frame relative to the fuselage. In the single-axis example, the fuselage referenced roll cable angle $\Delta\phi_c$ is simply:

$$\Delta\phi_c = \phi_c - \phi \tag{4.37}$$

The roll attitude, relative cable angle, and inertial cable angles of Eq. (4.37) are illustrated in Figure 4-6.

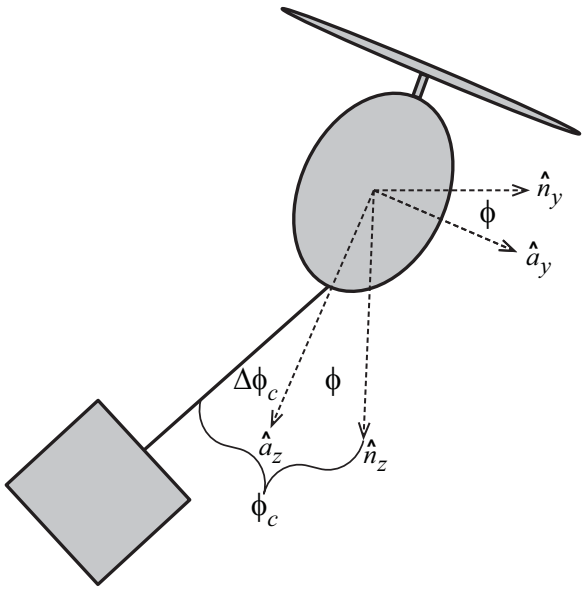

Figure 4-6. Illustration of roll attitude and cable angles.

In the single axis case, a combination of roll attitude feedback and *inertial* cable angle feedback can be algebraically manipulated to be equivalent to a compensator that uses roll attitude feedback combined with *relative* cable angle feedback via the relationship in Eq. (4.37). Although the two methods can be identically configured, the inertial cable angle feedback is used herein to isolate the effect of the load swing on the control system. This also makes sense physically because the earth referenced (inertial) load swing response should be minimized in the hover/low speed configuration for precision load placement. Inertial cable rate feedback was also utilized in this analysis.

Choosing $k_\phi = 4$ from the root locus diagram in Figure 4-4c, and using the ratios for the rate and integral gains from Eq. (4.36), the characteristic equation with inertial cable angle feedback k_c is:

$$1 + \frac{\phi}{\delta_{lat}} * k_\phi \left(1 + \frac{k_p}{k_\phi} s + \frac{k_{\phi_i}}{k_\phi} \left(\frac{1}{s} \right) + \frac{k_c}{k_\phi} \frac{\phi_c}{\phi} \right) = 0 \tag{4.38}$$

Solving in Evans Root Locus Form for the cable angle feedback term, to isolate k_C, results in Eq. (4.39):

$$1 + \left(\frac{k_c \dfrac{\phi_c}{\delta_{lat}}}{1 + \dfrac{\phi}{\delta_{lat}} * k_\phi \left(1 + \dfrac{k_p}{k_\phi} s + \dfrac{k_{\phi_i}}{k_\phi} \left(\dfrac{1}{s} \right) \right)} \right) = 0 \tag{4.39}$$

In this root locus of Figure 4-7, the poles represent the system with only the fuselage feedback control systems, $k_c = 0$. As cable angle feedback gain k_C increases, the closed loop poles change as shown in Figure 4-7a, which does not improve load damping but further improves Phugoid mode damping from the

baseline case. When using cable rate feedback $k_{\dot{c}}$ instead of angular feedback in Figure 4-7b, there is improved load damping, but a tendency for a lightly damped Phugoid mode.

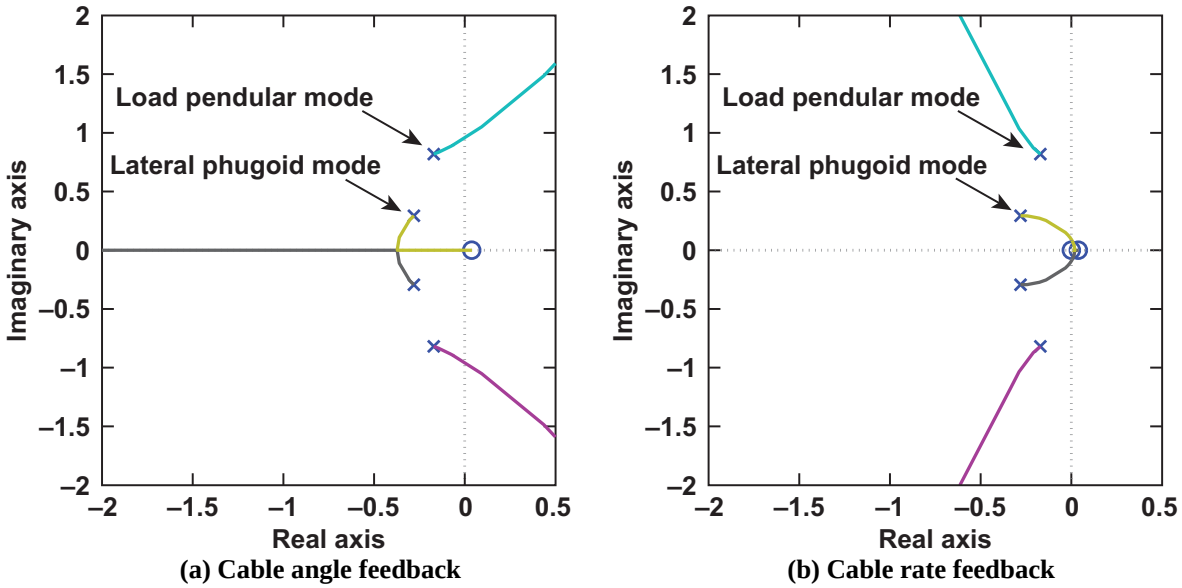

(a) Cable angle feedback (b) Cable rate feedback

Figure 4-7. Root loci for cable angle feedback using constrained coupling numerators.

The results of cable angle and cable rate feedback on the closed loop fuselage roll attitude are shown in Figure 4-8. Cable angle feedback in Figure 4-8a provides a reduction (i.e. improvement) in the notch depth (smaller Δ_{MAG}) as well as flattens the magnitude response between 0.2-0.9 rad/s. These effects combine to make a smoother attitude response which will provide better piloted handling qualities according to the slung load handling qualities specification (described in Chapter 3). This feedback should effectively make the load feel "lighter" to the pilot (a lighter load has a shallower distortion as shown in Figure 3-1). In Figure 4-8b, the cable rate feedback creates a slightly deeper magnitude notch (larger Δ_{MAG}), implying the load would feel effectively "heavier" to the pilot, but will be better damped for load placement as shown in Figure 4-7b.

So, despite the benefits of better load handling qualities related to the cable angle feedback, the load becomes poorly damped, as indicated by Figure 4-9a, which is consistent with the root locus shown in Figure 4-7a. The load response damping is improved with cable rate feedback, as indicated by the phase response in Figure 4-9b and the root locus of Figure 4-7a. There is also a large attenuation of the cable angle magnitude between 0.5-1.1 rad/s with increasing cable rate feedback as shown by Figure 4-9b. This indicates that the swing of the load will be much smaller with cable rate feedback.

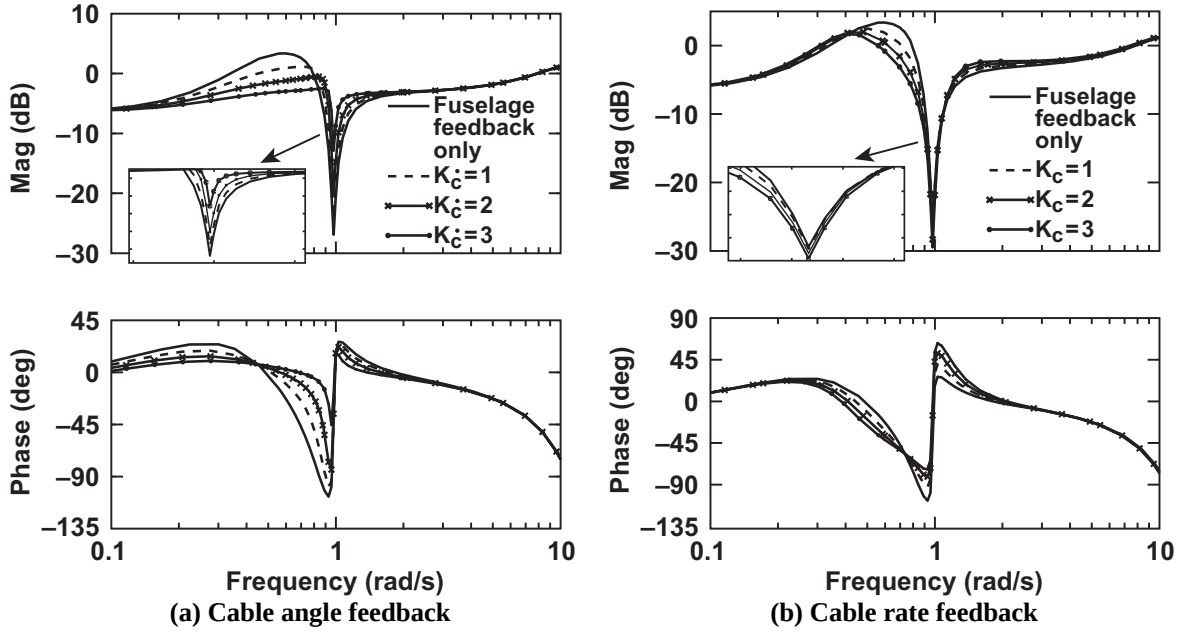

Figure 4-8. Aircraft response ϕ/δ_{lat} bode plot for combined fuselage and cable angle/rate feedback using constrained coupling numerators.

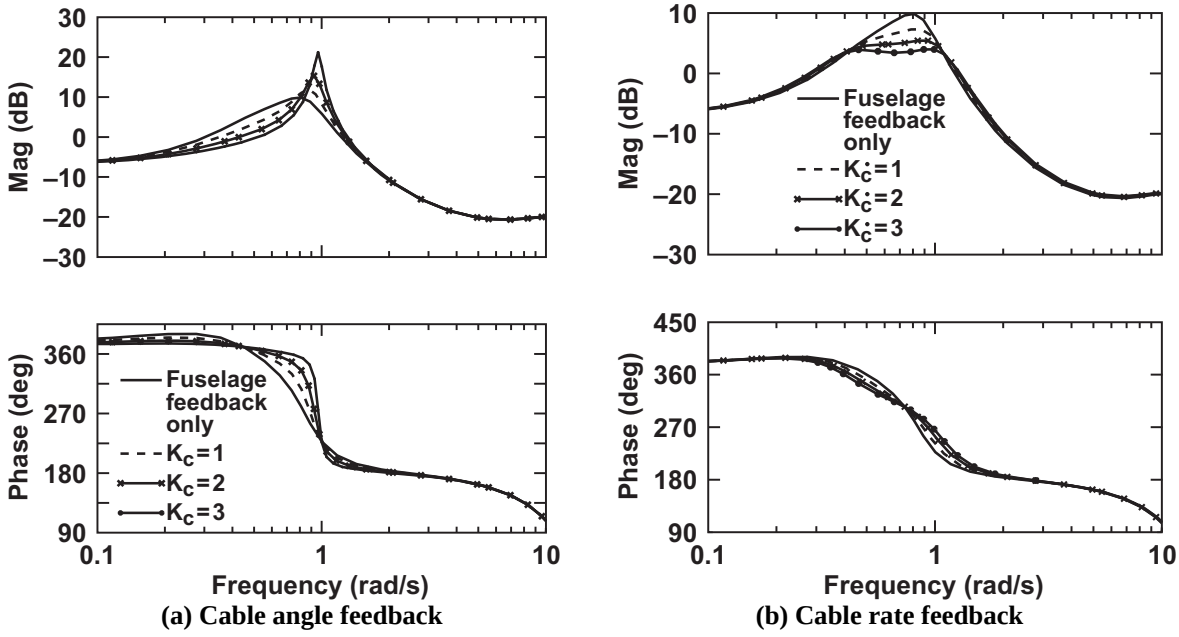

Figure 4-9. Load response ϕ_c/δ_{lat} bode plot for combined fuselage and cable angle/rate feedback using constrained coupling numerators.

These results indicate that cable angle feedback can be used to improve piloted handling qualities at the cost of a more lightly damped load response. The cable rate feedback does the opposite, providing a better damped load response, at the cost of degraded piloted handling qualities. This indicates that there is a fundamental trade-off between load damping and pilot handling qualities. The trade-off can be more fully explored via multi-objective optimization (in Chapter 5).

4.5 Summary of Chapter 4

In Chapter 4, the traditional constrained coupling numerator analysis for determining an effective SISO transfer function for a coupled MIMO system is described. This constrained coupling numerator analysis is then extended to a state-space solution which allows a MIMO analysis with some controls and states constrained. Finally, a basic analysis of helicopter/load dynamics was performed using Bode and Root-Locus methods for a simple feedback control system. This analysis explored how fuselage feedback, cable angle feedback, and cable rate feedback fundamentally affect the closed loop aircraft and slung load responses.

The key contributions of Chapter 4 are:

1. Development of a state-space solution for the constrained coupling numerator analysis.
2. Identification of a trade-off between lateral aircraft handling qualities and load damping for the lateral axis.
    a. Cable angle feedback is associated with reduced (improved) distortion of the aircraft attitude response, which is associated with better predicted piloted handling qualities. However, cable angle feedback also decreased load damping.
    b. Cable rate feedback improved load damping but caused larger (worse) distortion of the aircraft attitude response, which is associated with degraded piloted handling qualities.

5 Attitude Command Cable Angle/Rate Feedback Control Law Design and Analysis

The previous section explored the basic dynamics and trade-offs of a helicopter/slung load flight control system for a single-axis roll response with the off-axis responses tightly constrained. Now, the FORECAST/OVERCAST full-order, fully-coupled linear model presented in Sec. 2.2.4 is used for the control design of an explicit model following control system with fuselage, cable angle and cable rate feedbacks. The coupling numerator results from Chapter 4 are used to guide the control optimization design strategy. The FORECAST/OVERCAST model was used here in Chapter 5 because it contains the explicit rotor-states, as opposed to the quasi-steady rotor of the analytical linear model (Sec. 2.2.2) that was used to study basic control feedback trade-offs in Chapter 4. It is important to consider the effects on the rotor dynamic modes in control design optimization because it is possible to inadvertently de-stabilize these modes, particularly for high gain/high bandwidth designs.

The control system design in this chapter focuses on the piloted response. This section does not include the advanced hold modes such as velocity hold, position hold, or altitude hold that are included later on in Chapter 7. This chapter instead focuses on developing a well designed attitude command system, from which these advanced modes can be built upon.

5.1 Description of Architecture

The explicit model following control system architecture was chosen because it is an excellent approach for achieving handling qualities and feedback requirements for helicopters [49]. One key benefit of this architecture is that the bandwidth is set via the command model in the feed-forward path, independently of the feedback path, which sets disturbance rejection characteristics and stability margins. This is referred to as a two degree-of-freedom (2-DOF) architecture class [50]. In contrast, for a conventional single degree-of-freedom (1-DOF) feedback control system the bandwidth and disturbance characteristics are dependent upon one another, so increasing the disturbance rejection could result in an overly aggressive closed loop bandwidth.

5.1.1 Notational Examples of Control Architectures

In order to demonstrate the basic functionality and benefits of a model following architecture (2-DOF) as compared to a conventional feedback architecture (1-DOF), simple notional block diagrams are provided in Figure 5-1.

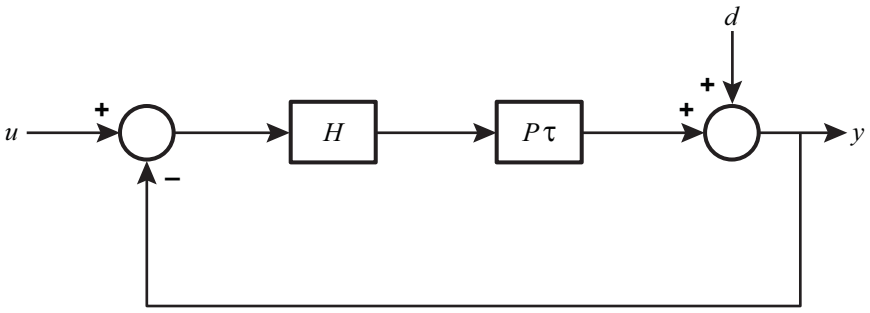

(a) Conventional feedback system (1-DOF)

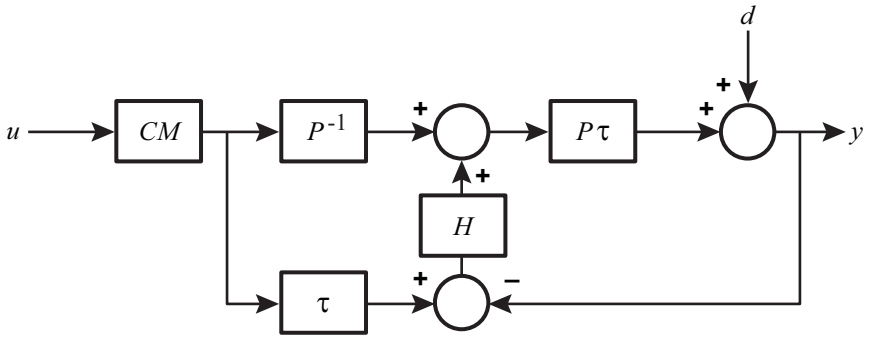

(b) Explicit model following control system (2-DOF)

Figure 5-1. Simplified 1- and 2- DOF control system block diagrams.

An example conventional 1-DOF block diagram is shown in Figure 5-1a. This 1-DOF block diagram has simple feedback compensation, with no feed-forward components. The system has a generic plant, $P\tau$, and compensator, H. High frequency dynamics of the plant such as actuators, rotor, sensor and filter dynamics are represented by an effective time delay block, τ . The control (y/u) and the disturbance (y/d) response characteristics are inherently coupled via the parameters of the compensator (H):

$$\frac{y}{u} = \frac{HP\tau}{1+HP\tau} \tag{5.1}$$

$$\frac{y}{d} = \frac{1}{1+HP\tau} \tag{5.2}$$

The inherent coupling (both have dependence on $HP\tau$) of the disturbance and control responses are characteristic of a 1-DOF system described in Ref. 50.

A simple example of the 2-DOF explicit model following architecture is shown in Figure 5-1b. The command model, CM, describes the desired response. The inverse plant model P^{-1} inverts the dynamics of P in the feed-forward path. In order to explain the model following concept, assume that the inverse plant model P^{-1} perfectly inverts the plant dynamics, e.g. $PP^{-1}=1$. Then the control response is independent of the compensator H and the plant P, and is set by the command model (and non-inverted time delays):

$$\frac{y}{u} = CM\tau \tag{5.3}$$

Note that the time delay block τ is not inverted in P^{-1}, to avoid overdriving the actuator. Thus, the use of the time delay in the command path is critical to ensure that the command and the response remain synchronized, when time delays are present.

The disturbance response characteristic for the 2-DOF system is set by the plant P and compensator H dynamics (equivalent to 1-DOF disturbance response):

$$\frac{y}{d} = \frac{1}{1 + HP\tau} \tag{5.4}$$

Thus, the disturbance and control response characteristics are decoupled, which is consistent with the 2-DOF model structure of Ref. 50. Thus, one key benefit of this architecture is the ability to set disturbance rejection and command model bandwidths independently. An additional benefit of the model following architecture is that the feed-forward inverse plant off-loads the feedback, which is not needed except in the case of the disturbances and, in practice, to compensate for errors in the inverse plant.

5.2 Explicit Model Following Architecture with Cable Feedback

The explicit model following architecture used in this work has the structure of Figure 5-2 - Figure 5-5, as implemented with cable angle/rate feedbacks in the lateral and longitudinal axes. There are no cable angle/rate feedbacks to the pedal and collective. Although each axis of the controller is shown independently in Figure 5-2- Figure 5-5, for clarity, all controllers are simultaneously closed around the MIMO bare airframe state-space UH-60 model.

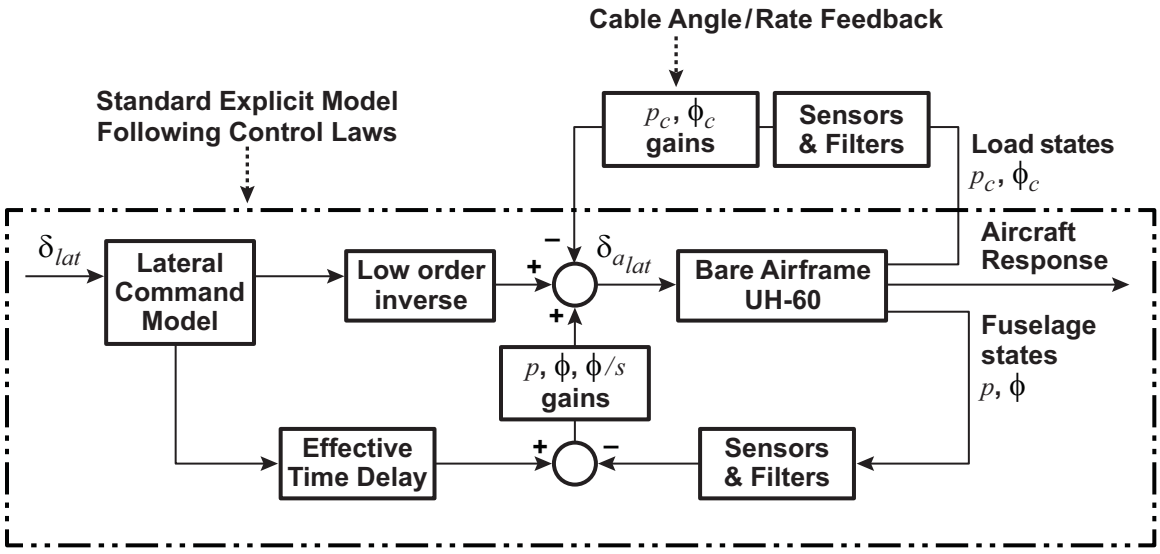

Figure 5-2. Lateral controller architecture.

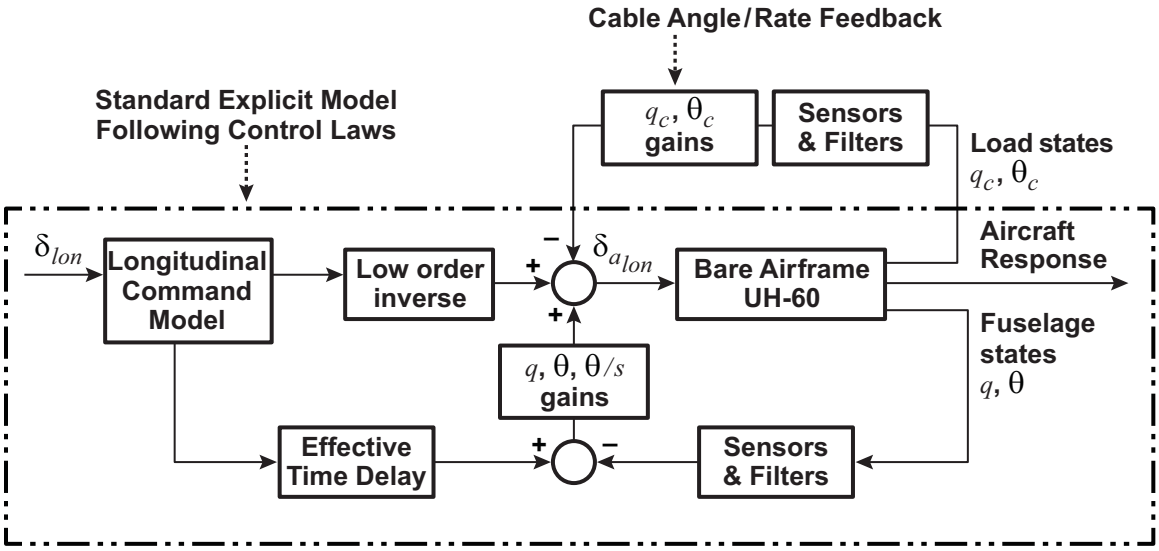

Figure 5-3. Longitudinal controller architecture.

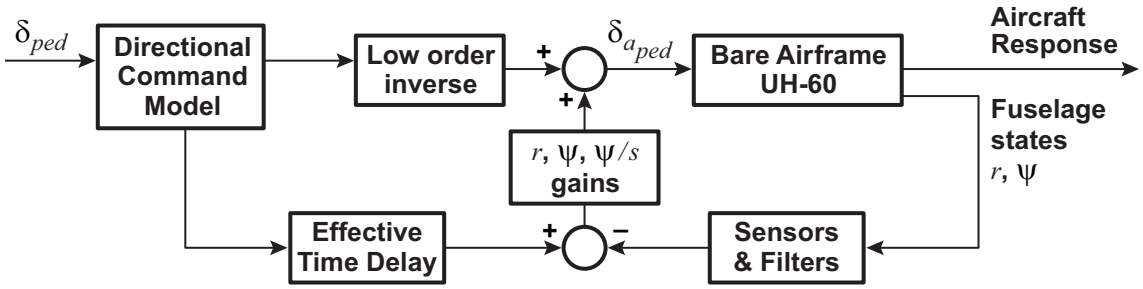

Figure 5-4. Yaw controller architecture.

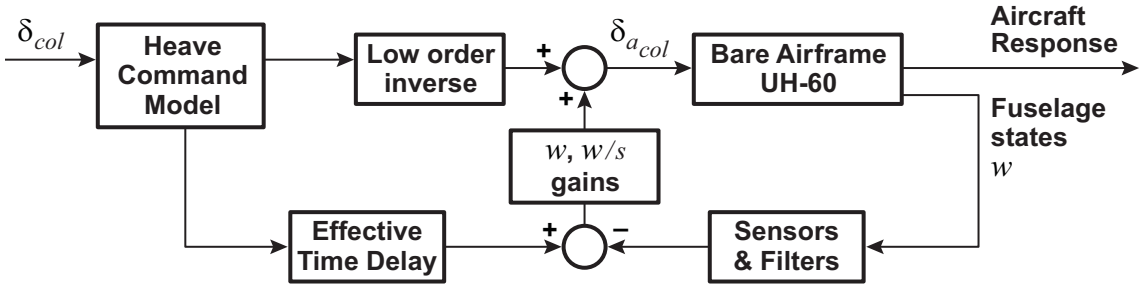

Figure 5-5. Heave controller architecture.

The structure of the model following controller and the purpose of each block are described in detail in Ref. 36. The following sub-sections provide a brief overview of the elements of the model following control system as implemented herein.

5.2.1 Command Model

The command model calculates the desired fuselage response for a given stick input. The command model sets the steady-state value of response per inches of pilot input (stick sensitivity), dictates the response type, and determines the desired closed loop bandwidth of the system. The response types, maximum response attitudes/rates (which can be used to set the stick sensitivity), and bandwidths that

have been found to produce good handling qualities in rotorcraft are described in ADS-33E-PRF [21]. The command models herein were developed to adhere to the guidelines in ADS-33E-PRF.

For the roll-attitude command (ϕ_{cmd}), a second order attitude command system is implemented via the command model:

$$\frac{\phi_{cmd}}{\delta_{lat}} = 12\left(\frac{2.5^2}{[\zeta = 1, \omega_n = 2.5]}\right) \text{(deg/in)} \tag{5.5}$$

The roll axis stick sensitivity is 12 deg/in. The lateral cyclic has a throw of +/-5 inches, which allows for piloted commands of +/-60 deg of roll attitude at maximum. This meets the ADS-33 moderate agility Level 1 requirement for +/-60 deg of large amplitude attitude change for roll [21]. The natural frequency and damping ratios are from ADOCS (Advanced Digital Optical Control System), as they provided acceptable handling qualities in flight [51].

The pitch-attitude command (θ_{cmd}) also uses a command model that is second-order and the attitude command response type:

$$\frac{\theta_{cmd}}{\delta_{lon}} = 6\left(\frac{2^2}{[\zeta = 1, \omega_n = 2]}\right) \text{(deg/in)} \tag{5.6}$$

The pitch sensitivity is 6 deg/in, for a total maximum command of +/-30 deg/in of pitch attitude (+/- 5 inches longitudinal cyclic travel). This meets the ADS-33 moderate agility requirement for +20,-30 degrees of large amplitude pitch attitude response [21]. Again the command model natural frequency and damping are based on the ADOCS control laws.

The yaw axis is a rate command/heading hold response type. This provides the pilot the ability to command a yaw rate for a given pedal input, and then hold the desired heading upon releasing the pedals. This is a natural method for heading control and is recommended by ADS-33E-PRF. The yaw rate command (r_{cmd}) model is first order:

$$\frac{r_{cmd}}{\delta_{ped}} = 8.8\left(\frac{1}{0.4s + 1}\right) \text{deg/s/in} \tag{5.7}$$

The control sensitivity of 8.8 deg/s/in provides a maximum yaw rate of +/-22deg/s (+/- 2.5 inches of pedal travel). This meets the requirement for moderate agility in ADS-33 for large amplitude directional response. For the yaw axis, the ADOCS command model time constant is not used. The time constant in the present control laws is higher than ADOCS to meet the bandwidth requirements of ADS-33E-PRF with the slung load configuration.

The heave axis response type is vertical velocity command/pseudo altitude hold. The collective input provides a proportional response in vertical velocity. Then at trim the altitude is held with a pseudo altitude hold, which is implemented via an integrator in the control feedback loop. In the section on the

task-tailored advanced control laws (Chapter 7), a true altitude hold is included by wrapping an altitude feedback loop around the vertical velocity loop. The vertical velocity command (w_{cmd}) model is first order:

$$\frac{w_{cmd}}{\delta_{col}} = (-6.667)\frac{1}{s+1} \text{ ft/s/in} \tag{5.8}$$

The collective sensitivity is set to allow for a maximum climb or descent rate of +/-2000ft/min (+/- 5 inches of collective travel). This collective control sensitivity was tuned based on pilot opinion. The time constant was set to meet the ADS-33 heave response requirement for hover/low speed.

5.2.2 Low Order Inverse

The low order inverse provides an estimate of the control input (e.g. $\delta_{lon_{est}}$) required to achieve the desired response (e.g. q_{cmd}). This inverse is a feed-forward component that provides a faster initial response, and then errors in the resulting response are eliminated via the feedback path. The inverse is first-order for all axes. A first-order model fit is chosen due to its simplicity, and because a second-order inverse tends to produce a jerky response on the UH-60 [36]. This first-order inverse is calculated from a low order fit of the aircraft response in the frequency domain, which is then inverted. An example first-order model fit is shown in Figure 5-6 for the pitch rate. Note that an additional time delay is also included in this model fit shown in Figure 5-6 in order to better match the phase, but this time delay is used on the command path only (and is not inverted) as described in the following section (Sec. 5.2.3). The slung load mode was not inverted in the longitudinal and lateral responses because the inverse model would have to be gain scheduled with different load mass and sling lengths. This results in a mismatch between the inverse plant model and the aircraft response near the pendular frequency, as exemplified in Figure 5-6 from 0.5-1.5 rad/s.

For this first-order inverse model, the pitch axis inverse has the form:

$$\frac{\delta_{lon_{est}}}{q_{cmd}} = \frac{s+B}{A} \tag{5.9}$$

Although this is an improper frequency response, it is easily implemented through block diagram arithmetic:

$$\delta_{lon_{est}} = \frac{1}{A}\left(\dot{q}_{cmd} + Bq_{cmd}\right) \tag{5.10}$$

Where q_{cmd} is approximated by the derivative of Eq. (5.6), and $\dot{q}_{cmd}$ is the 2nd-derivative of Eq. (5.6). This is easily implemented via block diagram manipulation as shown in Fujizawa [36]. The roll, yaw, and heave inverse models follow a similar form to the pitch axis example shown in Eqs. (5.9)-(5.10). The inverse models used herein are given in Table 5-1.

Table 5-1. Inverse parameters.

Control Axis	A	B
Lateral	1.95	4.69
Longitudinal	.406	.533
Pedal	.453	.2423
Collective	-6.31	.319

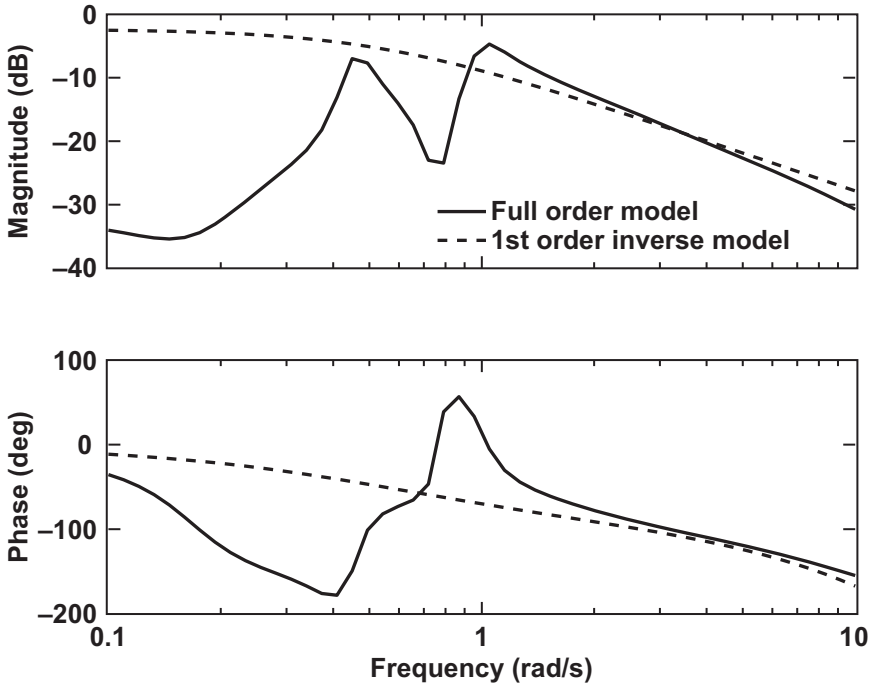

Figure 5-6. First order model fit for pitch rate.

5.2.3 Effective Time Delay

The effective time delay in the command path (that sums with the feedback) accounts for the rotor, filter, and computational delays that are inherent in the aircraft. The time delay is not used on the inverse path as shown in Figure 5-2 - Figure 5-5. This time delay does not effect stability margins because it is in the forward command path (not feedback). The actual time delay in the feedback path is part of the dynamics of the system (not the controller), and does effect stability margin. The presence of the command delay improves overshoot, reduces actuator activity, and increases model following performance [52]. For rotorcraft these values can be rather large due to the effective ~70ms time delay of the rotor and the heavy filtering that must be performed on the feedback paths (due to the high vibration environment). The time delays used herein are given in Table 5-2.

Table 5-2. Command path time delays.

Commanded variable	Time delay on command (s)
ϕ_{cmd}, p_{cmd}	0.093, 0.13
θ_{cmd}, q_{cmd}	0.097, 0.12
ψ_{cmd} , r_{cmd}	0.099, 0.12
w_{cmd}	0.10

5.2.4 Fuselage Feedback

Fuselage feedback is used to compensate for errors in the inverse model, provides gust rejection and stabilizes the hovering cubic (low frequency unstable Phugoid-type mode). The architectures of the fuselage feedbacks in the four control axes are shown by Figure 5-7 - Figure 5-10. The pitch, roll, and yaw axis control systems are effectively proportional, integral, derivative (PID) type compensators. The heave axis control system is a proportional, integral (PI) type compensator.

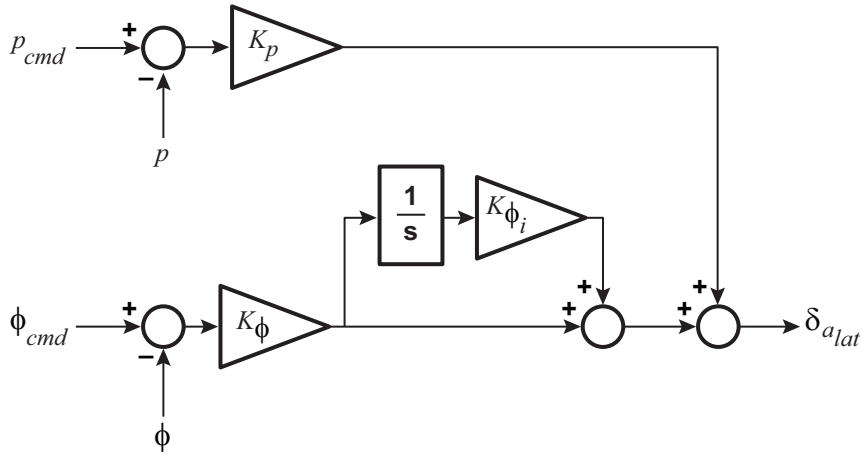

Figure 5-7. Lateral fuselage feedback.

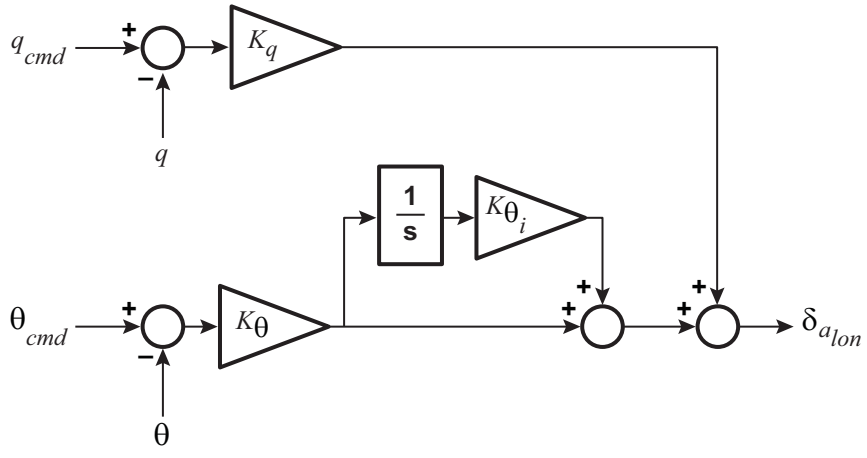

Figure 5-8. Longitudinal fuselage feedback.

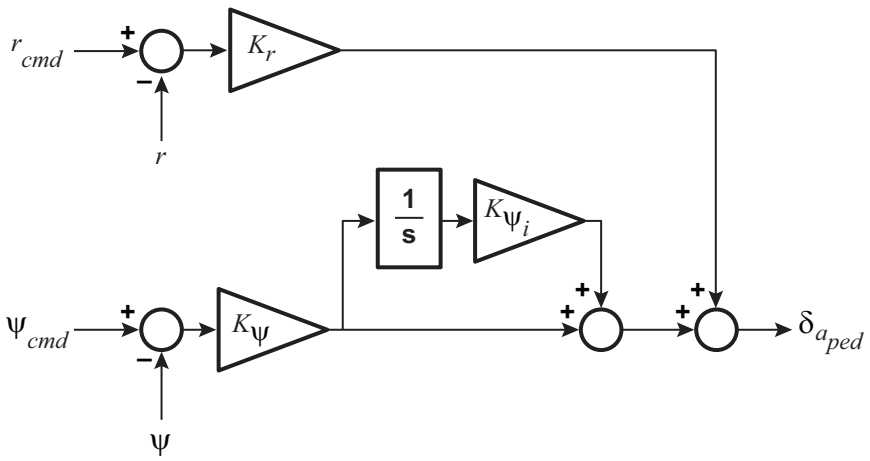

Figure 5-9. Directional fuselage feedback.

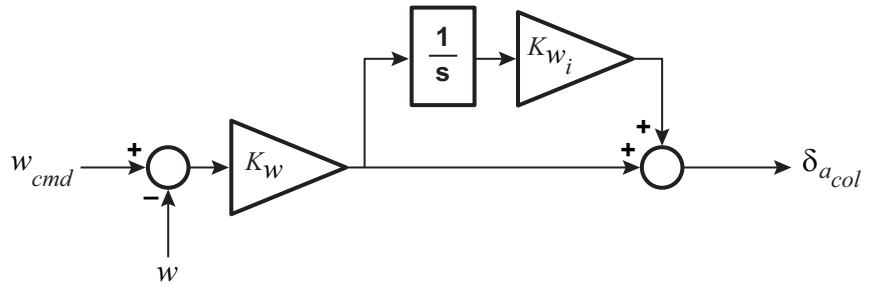

Figure 5-10. Heave fuselage feedback.

5.2.5 Load Cable Angle/Rate Feedback

The feedbacks of measured load states are used to improve handling qualities and stability margin with an external load, and also increase load damping. The architectures for the cable angle/rate feedbacks, which are only used in the lateral and longitudinal axes, are shown in Figure 5-11 and Figure 5-12. The controller uses inertial cable angle and rate feedback. The cable angle feedback is fed through a washout to eliminate feedback of the trim non-zero cable angle that occurs due to drag as the aircraft increases forward speed. The output of the load feedback controller sums with the output of the fuselage feedback controller as shown in Figure 5-2 and Figure 5-3.

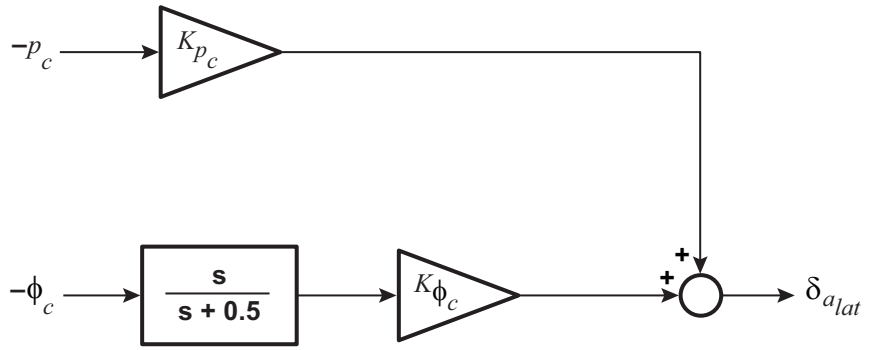

Figure 5-11. Lateral cable angle/rate feedback.

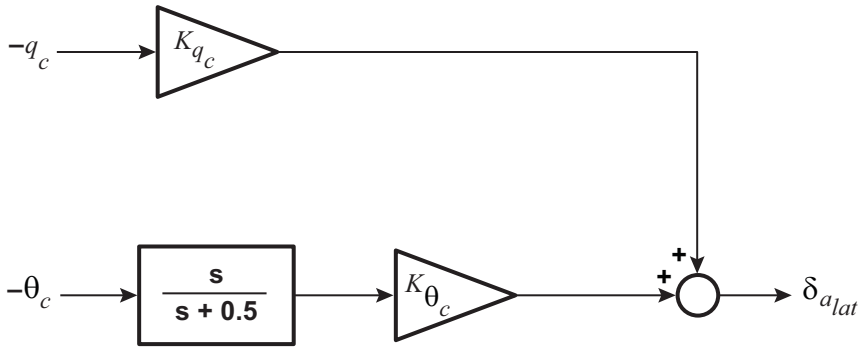

Figure 5-12. Longitudinal cable angle/rate feedback.

5.3 Control Design Requirements

The control system was designed to meet the requirements for ADS-33E-PRF Level 1 handling, stability margins, disturbance rejection, and external load handling qualities (described in Chapter 3). The design specifications of Table 5-3 were chosen to ensure that the control system would have the desired flying qualities. More background on many of these specifications is provided in Ref. 49.

There are many specifications that must be simultaneously achieved in order to provide a system with desirable flying qualities and a total of 15 feedback gains that must be chosen to meet these requirements. This is a difficult problem to be solved with classical control techniques, which offers no direct way to assess and tune all these requirements simultaneously. Therefore, the control gains are determined with a direct multi-objective parameter optimization technique. This technique provides a Pareto-optimal solution that meets the requirements while minimizing actuator usage [49].

Table 5-3. Control system design specifications.

Specification (CONDUIT ® Name)	Description	Constraint Type	Axes
EigLcG1	Eigenvalues in left-half plane [1]	Hard	Pitch, Roll, Yaw, Heave
StbMgG1	Gain and phase margin (45 deg, 6 dB) [53]	Hard	Pitch, Roll, Yaw, Heave
BnwPiH1	Pitch bandwidth for acquisition and tracking, attitude command requirements (ADS-33) [21]	Soft	Pitch
BnwRoH2	Roll bandwidth for other M.T.E.'s, attitude command requirements (ADS-33) [21]	Soft	Roll
BnwYaH1	Yaw bandwidth for acquisition and tracking (ADS-33) [21]	Soft	Yaw
BnwPiS1	Pitch external load handling qualities criteria (Chapter 3) [2]	Soft	Pitch
BwnRoS1	Roll external load handling qualities criteria (Chapter 3) [2] Relaxed boundaries allow slightly into Level 2 if needed for Load Damping case	Soft	Roll
CouPRH2	Coupling between pitch and roll [21]	Soft	Pitch/Roll
CouYaH2	Coupling between collective and yaw [21]	Soft	Yaw
DmpTmG1	Time domain load damping criteria [21]	Soft	Pitch, Roll
DstBwG1	Disturbance rejection bandwidth [54]	Soft	Pitch, Roll, Yaw, Heave
DstPkG1	Disturbance rejection peak magnitude[49]	Soft	Pitch, Roll, Yaw, Heave
EigDpG2	Damping ratio [21]	Soft	Pitch, Roll, Yaw, Heave
FrqHeH1	Heave response bandwidth [21]	Soft	Heave
HldNmH1	Normalized attitude hold response to disturbances [21]	Soft	Pitch, Roll, Yaw
ModFoG2	Performance of aircraft as compared to command model (model following) [36]	Soft	Pitch, Roll, Yaw, Heave
OlpOpG1	Open loop onset point specification for pilot PIO due to actuator rate limiting [55]	Soft	Pitch, Roll, Yaw, Heave
TrkErG1	RMS of load response in turbulence	Soft	Pitch, Roll
CrsLnG1	Minimizes cross-over frequency [49]	Summed Objective	Pitch, Roll, Yaw, Heave
RmsAcG1	Minimizes actuator RMS [49]	Summed Objective	Pitch, Roll, Yaw, Heave

5.4 Optimized Control Design

The CONDUIT® software is used to optimize the fuselage and load feedback gains. CONDUIT®, the Control Designers United Interface, is a computational software package for aircraft flight control design, evaluation and integration [56]. CONDUIT® is a useful tool that combines the control system design

process with the handling qualities requirements and servo-loop specifications compliance into one step. The control system is designed to meet these specifications with minimal control usage.

CONDUIT® solves the design problem in 3 phases with associated specifications grouped into the three categories that define how the optimization prioritizes each requirement. The categories are known as Hard Constraints, Soft Constraints, and Summed Objectives. The specifications used for the optimization of the flight control system in this research are grouped into these categories as indicated by the Constraint Type in Table 5-3. Hard constraints are considered in the first phase of the optimization. The set of Hard Constraints included requirements crucial to the stability of the aircraft (Eigenvalues in left-half plane and stability margins). This limits all potential designs to those that are stable. During the second phase of the optimization soft constraints, which include handling qualities and performance criteria, must be satisfied while simultaneously ensuring that the Hard Constraints remain satisfied. The last phase of the optimization begins once all of the Hard and Soft Constraints are met. The optimization minimizes a set of Summed Objectives during this phase while ensuring that all other specifications continue to be met, a Pareto-optimal solution. Actuator RMS and crossover frequency are chosen as summed objectives to minimize control usage.

Based on the results of the coupling numerator study in Sec. 4.4, the trade-off between load damping and handling qualities is used to guide the design optimization strategy. The results of the coupling numerator study indicated that two separate control systems for cable angle/rate feedback should be designed, one focused on pilot handling and one focused on load damping, because these two configurations could not be simultaneously achieved in the coupling numerator study. Ultimately three flight control systems (two cable angle/rate systems, and one fuselage only system) were optimized to the required specifications in Table 5-3:

1. “Baseline Control System” – This control system is optimized to provide the best control system possible with conventional fuselage feedback only. This system does not use cable angle feedback because it is meant to provide a baseline for comparison against the cable angle feedback control systems. By using the same architecture and optimizing against the same requirements, it provides the best possible comparison case for the two cable angle feedback designs.
2. “Load Damping Control System” – This control system attempts to meet the specifications while maximizing the external load damping. This control system uses fuselage, cable angle, and cable rate feedback.
3. “Pilot Handling Control System” – This control system provides the best piloted handling qualities possible by using the cable angle and rate feedback to smooth the attitude response, such that it better tracks the command model response and thus minimizes the effect of load swing on

the helicopter's attitude response. The control system must also simultaneously meet all other design specifications.

5.4.1 Explanation of Configuration

The configuration optimized for the purpose of these initial attitude command studies was a 79ft configuration with a 5000lb sling. This configuration represents a very poor handling qualities configuration as shown in Figure 3-2. Thus, the benefits demonstrated by including cable angle/rate feedback represent an extreme in possible improvements in handling qualities, due to the very poor baseline configuration. This configuration was chosen for the piloted simulation in Chapter 6 to ensure that the effect of the load would be very noticeable to the pilot in the fixed base environment. In Chapter 7 and beyond, a shorter sling at 56ft is used for flight control design and flight test, which also has poor handling qualities but is slightly better than the 79ft configuration. The switch of configurations was performed for practical flight test safety reasons, but the same general trade-offs and trends are very similar, as described in Chapter 7.

5.4.2 Optimized Results – 79ft Sling, 5000lb Load

Comparisons of key specifications are provided for the three optimized designs in Table 5-4 and Table 5-5 for the pitch and roll axes (which use cable angle/rate feedback). The heave and yaw results are shown in Table 5-6 and Table 5-7. The three designs are nearly identical in the yaw and heave axes because the control system was optimized with the same feedback gains (no cable angle/rate feedback in yaw or heave) to the same requirements for all three designs in these axes. All stability margins and cross-over frequencies of Table 5-4 - Table 5-7 are for responses with loops broken at the actuators. The closed-loop model following cost described in these tables is a weighted, least-squared average of the magnitude and phase errors between the commanded and actual responses [36]. A lower model following cost indicates a better match between the commanded and actual responses. In general a cost below 100 is desired for an unloaded aircraft, but for the external load case the response generally has some distortion near the load mode, which results in model following costs higher than 100.

Table 5-4. Key pitch axis metrics.

	Gain Margin	Phase Margin	Cross-over	Model Following	Δ_{MAG} Load HQ spec	ω_{-135} Load HQ spec	Load Damping Ratio
	dB	deg	rad/s	Cost	dB	rad/s	nondim
Baseline	14.24	45.74	2.23	330.33	9.23	0.72	0.12
Pilot Handling	13.77	45.77	2.26	178.02	7.16	0.72	0.13
Load Damping	13.15	49.09	2.28	384.49	12.15	0.69	0.29

Table 5-5. Key roll axis metrics.

	Gain Margin	Phase Margin	Cross-over	Model Following	Δ_{MAG} Load HQ spec	ω_{-135} Load HQ spec	Load Damping Ratio
	dB	deg	rad/s	Cost	dB	rad/s	nondim
Baseline	5.21	33.88	5.43	254.09	6.73	0.72	0.093
Pilot Handling	6.08	45.39	4.75	168.58	5.42	0.69	0.13
Load Damping	7.11	69.49	4.51	1233.58	13.77	0.46	0.27

Table 5-6. Key heave axis metrics.

	Gain Margin	Phase Margin	Cross-over	Model Following
	dB	deg	rad/s	Cost
Baseline	16.62	86.57	1.02	37.93
Pilot Handling	16.17	86.30	1.07	36.71
Load Damping	16.55	86.24	1.02	37.92

Table 5-7. Key yaw axis metrics.

	Gain Margin	Phase Margin	Cross-over	Model Following
	dB	deg	rad/s	Cost
Baseline	13.88	57.56	2.25	83.76
Pilot Handling	13.78	57.48	2.28	84.69
Load Damping	13.97	58.13	2.20	92.94

Table 5-5 shows the Baseline control system cannot achieve more than 33 degrees of phase margin in the lateral axis, and has 5.2dB of gain margin, which violates AS94900 [53]. In contrast, for both the Load Damping and Pilot Handling control systems the stability margins meet the requirement for 45 degrees of phase margin and 6dB of gain margin in AS94900 by introducing cable feedback. This indicates that cable angle/rate feedback can provide improved phase margins for the UH-60. The cross-over frequencies are not greatly affected by the cable feedback.

Figure 5-13 shows the predicted slung load handling qualities specification (described in Chapter 3) for the three control systems. Recall that the area in the upper left of the specification is the poor handling qualities region. The predicted handling qualities of Figure 5-13 for the Baseline control system are acceptable in the roll axis, but are at the boundary for poor predicted handling qualities in the pitch axis. As shown in the Table 5-4 and Table 5-5, the Pilot Handling control system has the lowest model following cost in both the pitch and roll axes, indicating that it performs the most like the desired low

order command model dynamics. The improved model following of the Pilot Handling case, and associated minimal distortion Δ_{MAG} contributes to improved predicted handling qualities for roll and pitch axis, bringing the pitch axis well into the acceptable region of Figure 5-13. The Pilot Handling control system has about the same load damping ratio as the Baseline case in the pitch axis but exhibits improved load damping ratio in the roll axis, as shown in Table 5-4 and Table 5-5. The Load Damping control system provides the highest load damping ratio, but very poor model following, as shown in the tables. The distortion Δ_{MAG} of the attitude response is much worse for the Load Damping control system, indicating degraded predicted handling qualities in Figure 5-13.

Example closed-loop frequency and time responses in Figure 5-14 and Figure 5-15 illustrate the trade-offs between the three control system designs. Figure 5-14a overlays the closed loop roll attitude and lateral cable angle responses in the frequency domain. As shown in the figure, the Baseline roll attitude frequency response has poor model following near the load mode, with an overshoot distortion between 0.2-0.7 rad/s, and a notch distortion from 0.7-1.3 rad/s. Figure 5-14a also shows that the closed-loop attitude response matches the command model best with the Pilot Handling control system. The Load Damping has a large notch in the magnitude response that causes the largest distortion of all three control systems with respect to the command model, and causes the associated poor model following cost (Table 5-5) and degraded predicted handling qualities (Figure 5-13). The roll attitude time responses of Figure 5-15a are consistent with the frequency domain results, where Pilot Handling has the response closest to the command model. The Load Damping roll attitude response has several oscillations during the time domain pulse maneuver of Figure 5-15a, and overall is very inconsistent with the command response.

In contrast to its poor attitude response characteristics, the Load Damping case demonstrates the best damped cable angle responses in the frequency and time domain, as shown in Figure 5-14b and Figure 5-15b. The Baseline case has the largest cable angle peak in the frequency domain (Figure 5-14b), and as expected, is poorly damped in the time domain (Figure 5-15b). The Pilot Handling case improves the peak load magnitude slightly as compared to the Baseline in Figure 5-14b, and demonstrates slightly improved load response over the Baseline in the time domain response of Figure 5-15b.

The time and frequency domain results demonstrate a clear trade-off between load damping ratio and piloted handling qualities for the cable angle/rate feedback designs. These two configurations cannot be achieved simultaneously. A simple physical explanation for this trade-off is that the single control actuator, the rotor, cannot simultaneously control the two bodies independently. These trade-off results are consistent with the simple single axis results in Figure 4-8 and Figure 4-9, where the Pilot Handling control laws closely resemble the cable angle feedback cases and the Load Damping results are similar to the cable rate feedback.

The optimized control gains for the three designs are given in Table 5-8 - Table 5-10. As indicated by Table 5-10, the Pilot Handling control system relies heavily on cable angle feedback, while the Load Damping control system uses both cable angle and rate feedbacks. For the Pilot Handling control system, the optimization of the cable angle rate feedback parameter results in a small value (1e-4).

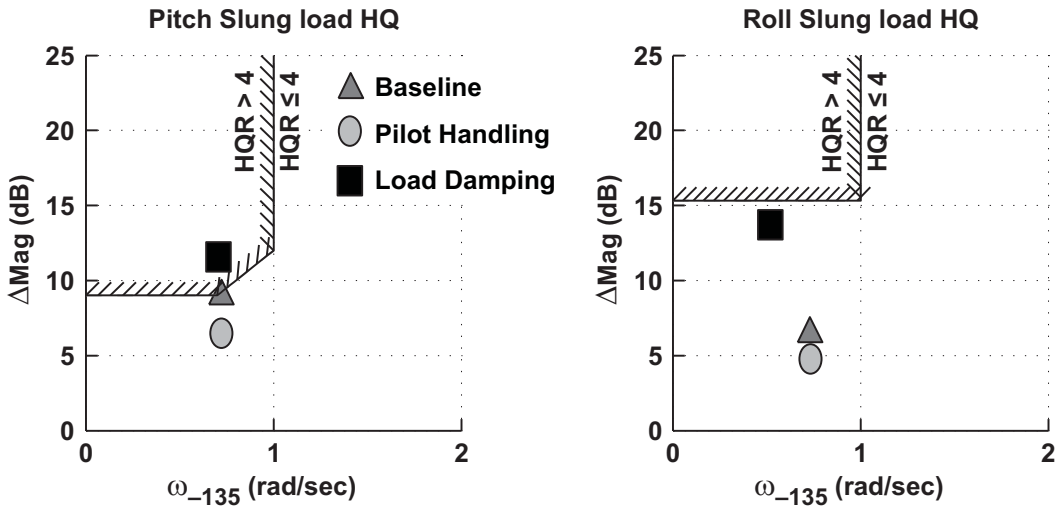

Figure 5-13. Slung load handling qualities specification for three optimized control systems.

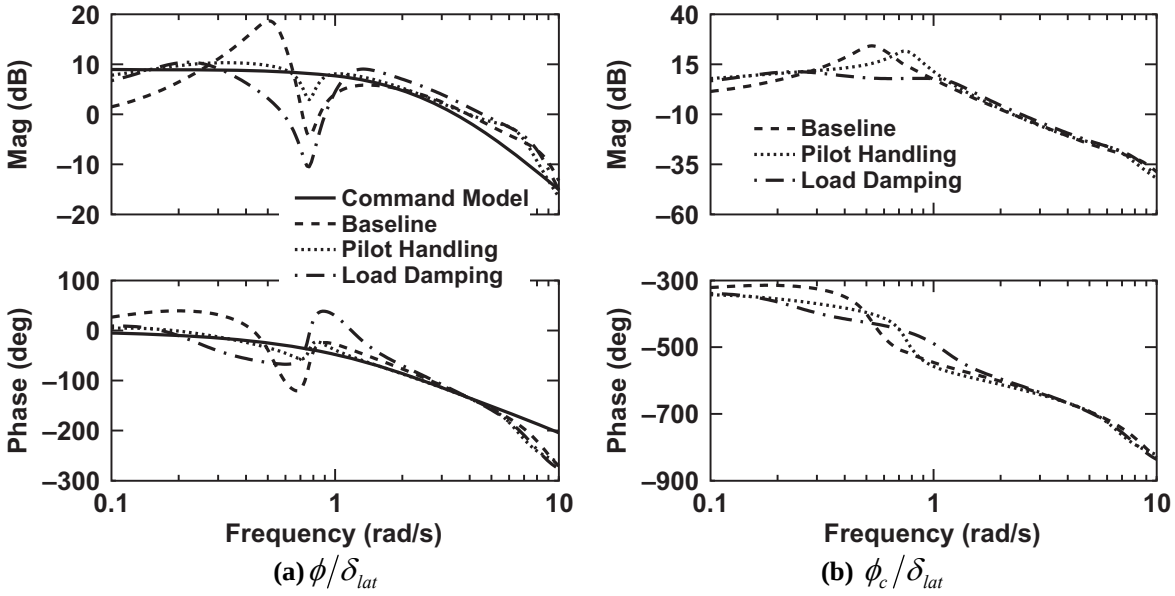

Figure 5-14. Closed loop Bode plot overlays for three optimized control systems.

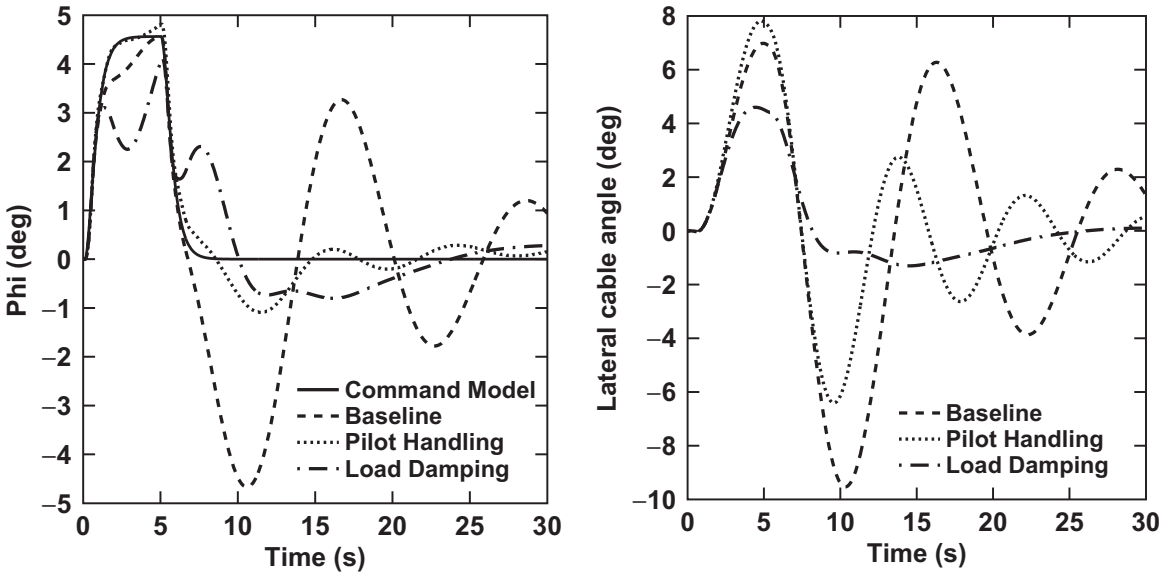

(a) ϕ/δ_{lat} **(b)** ϕ_c/δ_{lat}

Figure 5-15. Time responses for three optimized control systems.

Table 5-8. Fuselage feedback gains in the pitch and roll axes.

	Roll Axis Fuselage Gains			Pitch Axis Fuselage Gains		
	K_p (in-s/rad)	K_ϕ (in/rad)	K_{ϕ_i} (in/rad-s)	K_q (in-s/rad)	K_θ (in/rad)	K_{θ_i} (in/rad-s)
Baseline	1.86	14.40	0.10	3.59	7.64	0.30
Load Damping	2.98	8.32	0.10	4.52	7.28	0.30
Pilot Handling	1.40	13.44	0.10	3.93	7.83	0.30

Table 5-9. Fuselage feedback gains in the yaw and heave axes.

	Yaw Axis Fuselage Gains			Heave Axis Fuselage Gains	
	K_r (in-s/rad)	K_ψ (in/rad)	K_{ψ_i} (in/rad-s)	K_w (in-s/ft)	K_{w_i} (in-s/ft)
Baseline	4.28	5.85	0.5	0.22	0.125
Load Damping	4.32	5.99	0.5	0.23	0.125
Pilot Handling	4.21	5.91	0.5	0.23	0.125

Table 5-10. Load feedback parameters.

	Roll Axis Load Gains		Pitch Axis Load Gains	
	Cable Rate (in-s/rad)	Cable Angle (in/rad)	Cable Rate (in-s/rad)	Cable Angle (in/rad)
Baseline	0	0	0	0
Load Damping	7.89	8.07	1.41	2.56
Pilot Handling	0.0001	3.98	0.0001	1.24

5.4.3 Robustness of Optimized Results to Load Configuration

The three optimized control systems were designed for a single sling length (79ft) and load mass (5K). The stability robustness of the designs was analyzed for alternate sling length and load masses. The range of sling lengths analyzed for robustness was from 16ft to 96ft. Load masses from 1K to 6K were analyzed. The minimum stability margins considered safe for flight are 4dB and 30deg. For all cases analyzed, the gain margins were in the range acceptable for flight, greater than 4dB. The phase margin was the limiting factor, with some configurations having less than 30deg. The phase margins are shown for the three control system designs in Figure 5-16 - Figure 5-18.

The Baseline control laws are most sensitive to load mass as shown in Figure 5-16. The 6K load has the lowest margins for both the lateral and longitudinal axes for the Baseline control laws. In the lateral axis, the Baseline control laws generally do not meet margin requirement for the 6K load (just meets the requirement for 56ft sling), or the 16ft sling (only meets stability requirement for the 1K load). For the two cable feedback control systems, shown in Figure 5-17 and Figure 5-18, the stability is not as sensitive to load mass, but is quite sensitive to shorter sling lengths (16ft). Both the Pilot Handling and Load Damping control laws meet the margin requirements in both axes for 36ft – 96ft slings, for load masses between 1000-6000 lbs. This represents a wide range of configurations, and most importantly could be flown without gain scheduling by simply limiting the sling length to a minimum of 36ft for operations with cable angle feedback, as clearly the stability margins for the 16ft sling are not acceptable. The 16ft sling would require a separate set of control gains to meet stability margin requirements. Alternately, to use the Baseline control laws would require a limit on load mass and sling length to maintain acceptable margins without gain scheduling. A limit on load mass would effectively limit the operational capability of the aircraft.

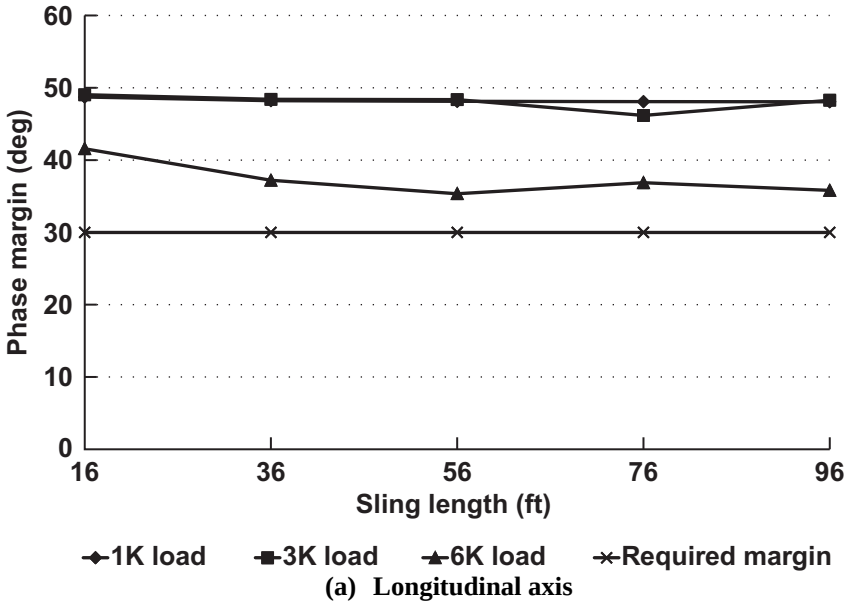

(a) Longitudinal axis

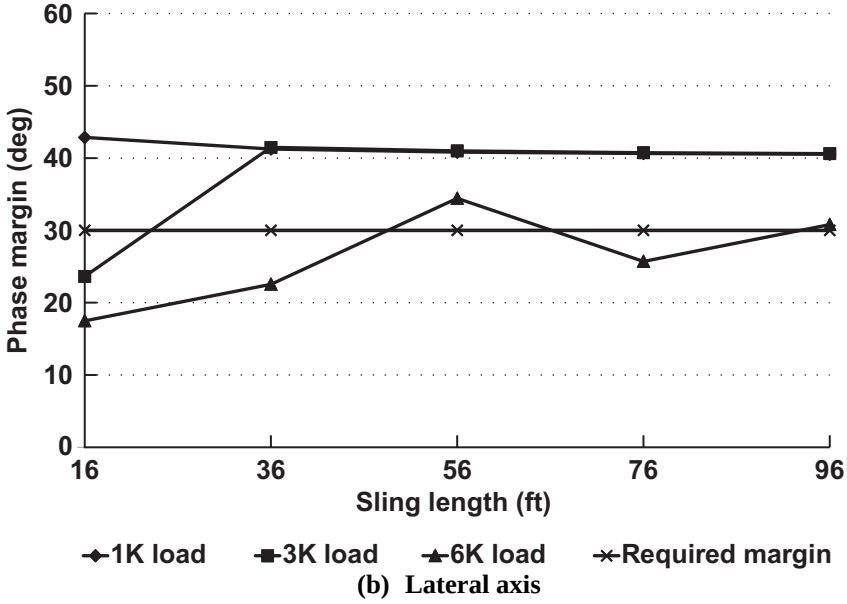

(b) Lateral axis

Figure 5-16. Robustness of Baseline control laws to external load configuration.

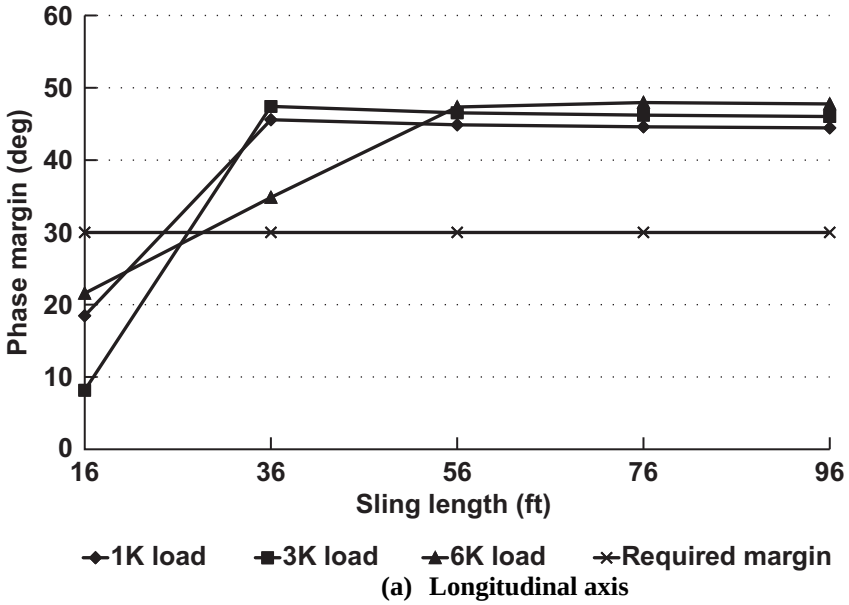

(a) Longitudinal axis

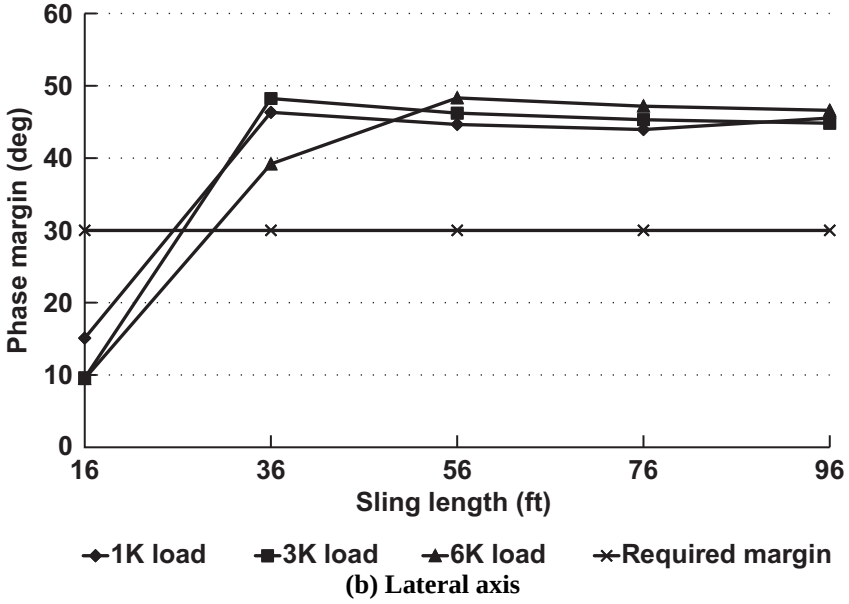

(b) Lateral axis

Figure 5-17. Robustness of Pilot Handling control laws to external load configuration.

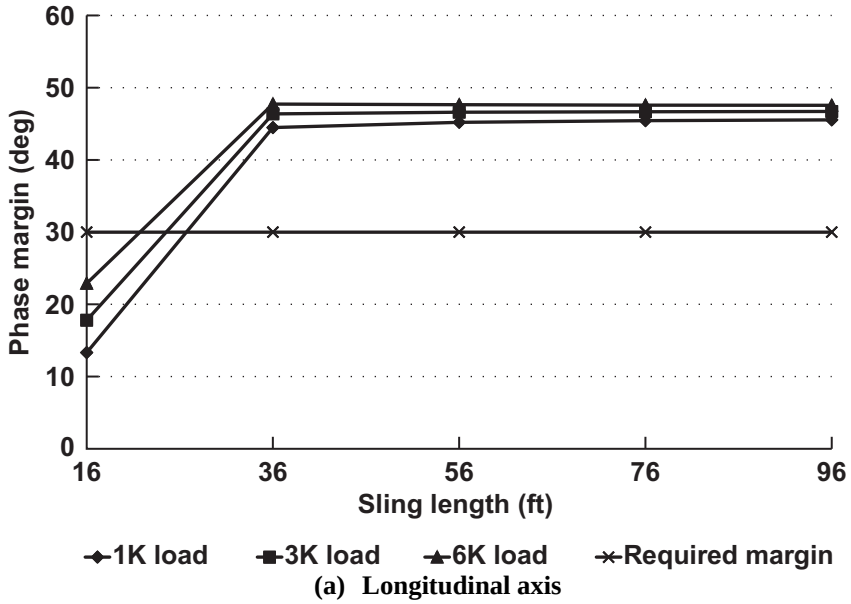

(a) Longitudinal axis

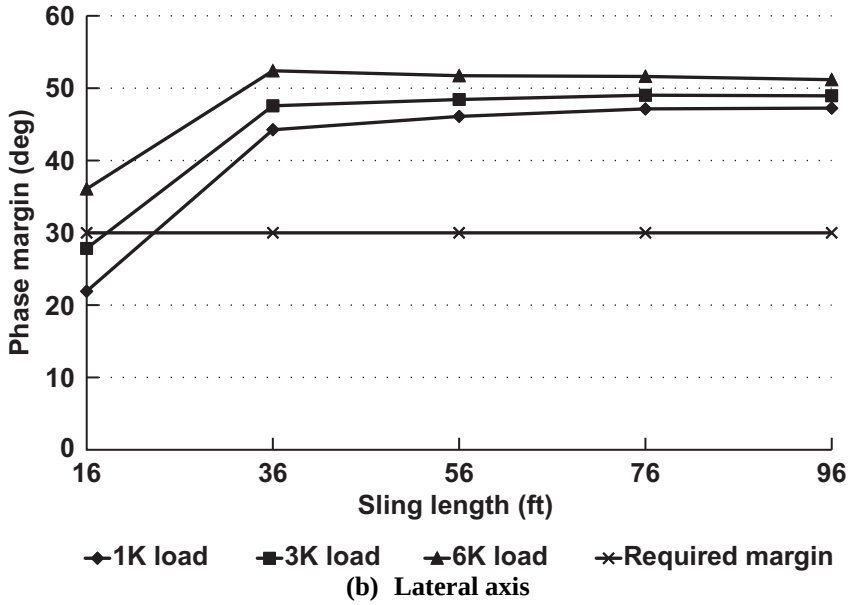

(b) Lateral axis

Figure 5-18. Robustness of Load Damping control laws to external load configuration.

5.5 Summary of Chapter 5

Chapter 5 describes the architecture and design methods for development of an explicit model following control system with fuselage, cable angle, and cable rate feedback. Multi-objective design optimization techniques are used to optimize the feedback gains to simultaneously meet the stability, handling qualities, and disturbance rejection requirements for a helicopter and minimize actuator activity. Three control systems are optimized: (1) Baseline configuration - Fuselage feedback only, (2) Pilot Handling configuration - Fuselage, cable angle, and cable rate feedback, optimized for pilot handling qualities, (3) Load Damping configuration - Fuselage, cable angle, and cable rate feedback, optimized for load damping.

The key contributions of this chapter include:

1. Handling-qualities/load-damping trade-offs for cable angle/rate feedback from the coupling numerator analysis in Chapter 4 using the simplified model are consistent with the full-order coupled MIMO design with explicit model following architecture used here in Chapter 5.
2. The required 45deg phase margin and 6dB gain margin is achieved when using cable angle/rate feedback for both Pilot Handling and Load Damping configurations. The Baseline configuration does not meet the requirement in the lateral axis.
3. Robustness studies of the three control system designs indicate that both Pilot Handling and Load Damping cable angle/rate feedback designs are more robust to changes in load mass than the Baseline fuselage feedback configuration.

6 Nonlinear Pilot in the Loop Simulation

Evaluation of the three control systems designed in Chapter 5 in a nonlinear environment was pursued with two objectives: to determine if benefits developed in the linear environment would transfer to a nonlinear full envelope flight simulation, and to perform realistic piloted simulation. Evaluating the performance of the system in a nonlinear environment was an important step to ensuring flight readiness. Additionally, the piloted simulation was important to collect pilot comments on perceived differences between the Baseline (fuselage only), Pilot Handling (cable angle) and the Load Damping (cable angle/rate) feedback systems.

The GenHel nonlinear model of the UH-60 and external load, discussed in Sec. 2.2.3, was used for the nonlinear dynamics simulation. To provide a visual environment, the RIPTIDE® software is used to realize real time, visual, full-flight-envelope pilot in the loop simulation [57]. RIPTIDE® provides the integration between the SIMULINK control system, GenHel, visual environment, and pilot inceptors.

6.1 Validation of Control System in Nonlinear Environment

To ensure that the nonlinear simulation with the control system engaged would behave as predicted in the linear environment, a validation of the nonlinear system against the linear system was performed by comparing responses in the frequency domain. In order to determine frequency responses from the nonlinear simulation, a frequency sweep was injected into the pilot inceptor. The aircraft and load responses were measured as a result of the sweep inputs. Then, the data is transformed to the frequency domain via the ChirpZ transform using the CIFER® software [45]. This method ensures that the linear frequency domain handling qualities predictions are consistent with the nonlinear simulation. In order to provide a good validation, the linear model must be an accurate representation of the nonlinear model, and the integration between the nonlinear model and control system must be correctly implemented in the nonlinear environment.

The validation was sufficiently accurate in all axes, as demonstrated for the roll attitude and cable angle responses in Figure 6-1 and Figure 6-2. There is excellent agreement near the load mode (~0.9 rad/s), which is of key importance to this study. The small discrepancy between 5-8 rad/s is due to an effectively more heavily damped rotor flap regressing mode in the nonlinear simulation. This should not have a large effect on the handling qualities because the differences are small in the frequency of predominate pilot operation, which typically does not exceed 1-3 rad/s (as verified by pilot cutoff frequencies calculated in Sec 6.5).

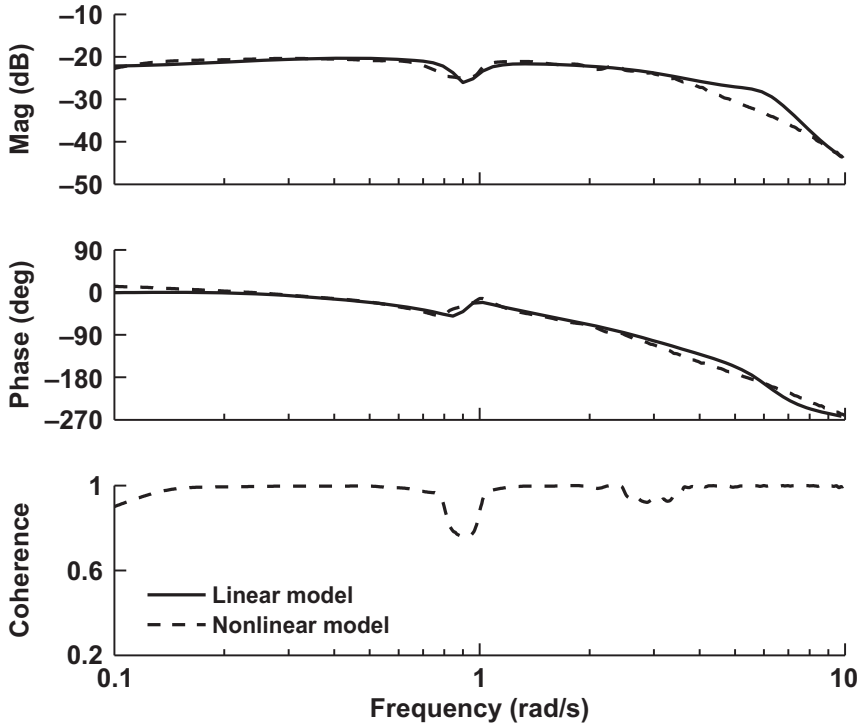

Figure 6-1. ϕ/δ_{lat} **closed loop validation of nonlinear responses for Pilot Handling FCS.**

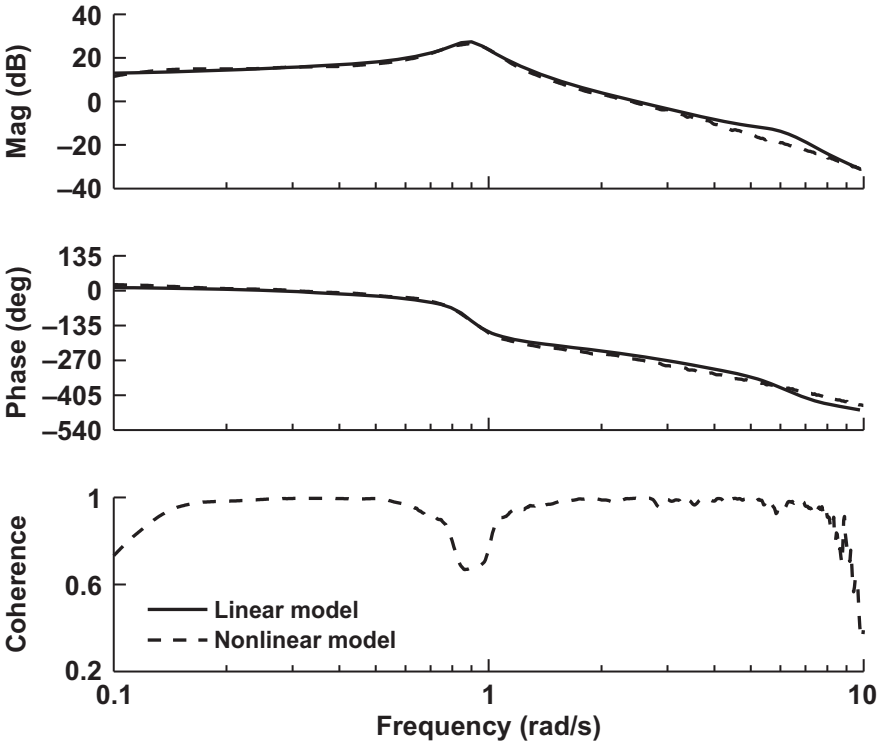

Figure 6-2. ϕ_c/δ_{lat} **closed loop validation of nonlinear responses for Pilot Handling FCS.**

6.2 Description of Fixed-Base Simulator

Given the good agreement between the linear and nonlinear simulation models, the next step was to test the control systems with a pilot in the loop to determine whether the predicted results from the linear analysis in Chapter 5 were realized. The simulation was performed at the US Army Aeroflightdynamics Directorate fixed-base Human Factors Simulation Cab at Ames Research Center. This cab uses a side-stick for longitudinal and lateral controls, and conventional pedal and collective. Although the actual RASCAL UH-60 helicopter has a center stick configuration, this simulation still allows compare and contrast of the relative performance of the control systems.

The simulator display is shown in Figure 6-3. There is a standard forward view (window A) and the UH-60 CAAS display panel (window B). The load is displayed to the pilot in a downward view (window C), as though a camera were looking down at the load. This is in fact the view as seen by the crew chief, who watches the load motion via an open hatch in the back of the UH-60. This display is used here to provide the pilot a load motion cue, since he/she cannot feel the load in the fixed base simulation. The downward view also gives the pilot visual cues for the lateral and longitudinal reposition maneuvers given the limited view out the forward window.

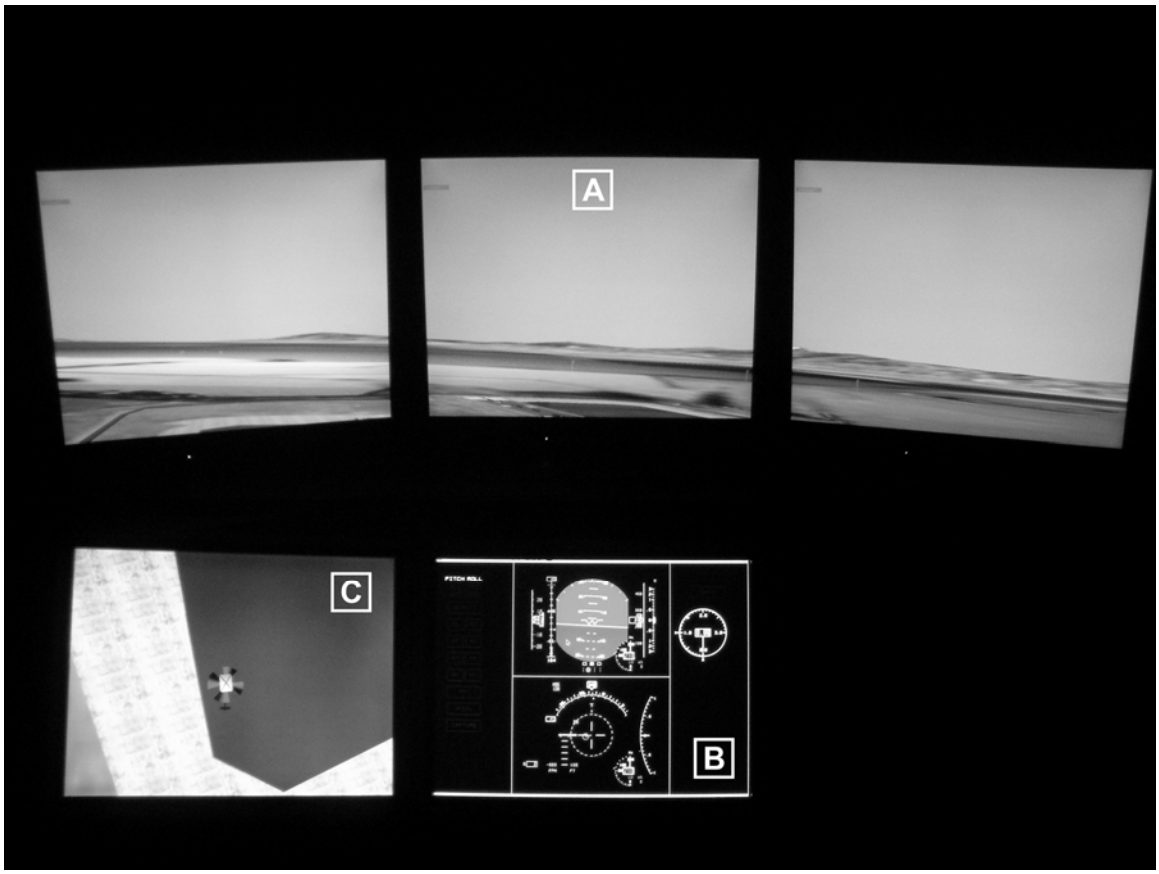

Figure 6-3. Simulator displays.

Due to the limitations of the fixed base environment for simulating slung load configurations, and the lack of sideward visual cueing (no side window), handling qualities ratings would not be valid and were not collected. Instead, pilot comments comparing the two cable angle feedback control systems to the Baseline, as well as statistical data (pilot stick cutoff frequency) are used to evaluate the relative drawbacks and benefits of the cable angle feedback control systems.

6.3 Piloted Tasks

The pilots were asked to complete a series of evaluation maneuvers and provide comments for each of the three control systems. The flight condition was hover/low speed, 15000lbs aircraft, 5000lbs load, and 79ft sling. Pilots first flew the Baseline control system, and then in random order, the two cable angle feedback control systems for the tasks given in Table 6-1. The pilots were not told whether they were in the Pilot Handling or Load Damping configuration. Comments were collected after each task in Table 6-1 for each control system. Pilots were instructed to provide comments comparing and contrasting the control systems and the relative ease of each of the tasks.

Four pilots were used in this study. All four pilots were test pilots, with UH-60 slung load experience. Pilots 1, 3, 4 are US Army experimental test pilots. Pilot 2 is a retired NASA test pilot.

Table 6-1. Pilot tasks.

Task #	Task	Description
1	Check out/ Familiarization	Pilot should become familiar with the response of the control system before performing the tasks.
2	Lateral Reposition	Fly 6kts laterally across the runway, and return to hover at the far end. This uses the downward display to provide visual references.
3	Longitudinal Reposition	Fly 6kts longitudinally across the runway, and return to hover at the far end. This uses the downward display to provide visual references.
4	Hover Boards	Hover in front of the hover board with and without turbulence.

6.4 Piloted Comments

The pilot comments provide good insight into the relative merits and drawbacks of the three control systems. A summary of comments are provided for each control system.

Baseline FCS

The pilots generally found the Baseline control system to have a reasonable response with respect to other external load configurations they have flown and did not find the responses objectionable:

"Control responses are reasonable" – Pilot 1

"Dynamics are appropriate to task" – Pilot 2

The lateral reposition task was found to be the most difficult with the external load:

"Better behaved longitudinally than laterally" – Pilot 2

"Lateral reposition task is more difficult if not anticipating load motion" – Pilot 3

The pilots also found that the load swing tended to cause a velocity response that was not as smooth and that the load took a long time to damp out:

"More difficult to maintain speed when starting maneuver while load is still swinging" – Pilot 3

"Load takes considerable time to damp, but does not affect workload" – Pilot 1

"Must accept load oscillations and correct for velocity changes due to load swing" – Pilot 4

Load Damping FCS

The pilots immediately noticed that the load damped more quickly:

"Load motions damp very quickly as compared to Baseline" – Pilot 3

"Work load roughly same as Baseline, but load damps more quickly" – Pilot 1

The tasks were generally considered easier or the same as Baseline, but the pilot must give up some control to the attitude control system:

"Control is not fine grained, but direction and speed of vehicle easier to control" – Pilot 2

"Overall maneuver is easier to perform than Baseline. [Periodically] got into load oscillations aggravated by the pilot during deceleration and had to back out of the loop" – Pilot 4

"Longitudinal and lateral repositioning tasks are easier but pilot must give up a lot of control" – Pilot 3

The uncommanded attitudes used to damp the load motions were found to be very unnatural by the 3rd pilot:

"Unnatural response, can get positive roll angle with negative lateral inputs at times" – Pilot 3

"Treat the control system like 'Attitude Suggestion' as opposed to attitude command" – Pilot 3

"Must take myself out of the loop, let the aircraft take care of the load" – Pilot 3

Pilot Handling FCS

This control system was found to provide a more stable response:

"More stable velocity response" – Pilot 1

"Load is more active but a/c is not as driven by the load dynamic, the attitude is more stable even though the load is swinging" – Pilot 2

Pilot 3 found this response to be much more natural than the damping control system:

"Aircraft is doing the same thing I want to do with the attitude, so more comfortable" – Pilot 3

"Very natural response" – Pilot 3

All four pilots felt that tasks were easier to complete using the Pilot Handling FCS as compared to the Baseline and Load Damping configurations:

"Good position hold, vehicle response is smooth" – Pilot 1

"By far the best performance of the three configurations" – Pilot 2

"This configuration was the easiest to fly, almost as easy as without an external load" – Pilot 3

"Slightly easier to perform tasks than damping configuration, much better than Baseline configuration" – Pilot 4

6.5 Statistics

The piloted cutoff frequency is a good measure of the bandwidth of the pilot's inputs and has been shown to closely track the pilot cross-over frequency [45]. Thus, the pilot cutoff frequency provides insight into the pilot's control strategy, and determines the fundamental frequency that the pilot used to control the helicopter/slung-load system during a task. The pilot cutoff frequency ω_1 is the half power frequency associated with σ_1:

$$\sigma_1^{\,2} = \frac{1}{2\pi}\int_0^{\omega_1} G_{\delta\delta}(\omega)d\omega \quad , \quad \left(\frac{\sigma_1}{\sigma_{tot}}\right)^2 = 0.5 \tag{6.1}$$

σ_{tot} is the pilot RMS calculated over the entire frequency range. The input autospectrum $G_{\delta\delta}$ is calculated via FFT of the input signal within the CIFER® software [45].

For external load operations, it has been observed that the pilot cutoff frequency is typically below the load mode for larger LMRs (including the LMR of 0.25 used here), indicating that the pilot adopts a control strategy to avoid exciting the load motion [2]. This implies that the pilot cannot fly aggressively with external loads which have long slings and thus low natural frequencies. This may limit the ability to fly some tasks successfully.

The pilot cutoff frequency for each pilot is shown in Figure 6-4, for the lateral cyclic during the lateral reposition maneuver. Figure 6-5 gives the cutoff frequencies for each pilot's longitudinal cyclic inputs during the longitudinal reposition maneuver. The results for the Load Damping control system indicate that all four pilots adopted a lower pilot cutoff frequency than for either the Baseline or Pilot Handling control systems in both the lateral (Figure 6-4) and longitudinal axes (Figure 6-5). This would indicate a diminished capability to achieve the same aggressiveness as the other two designs, which is consistent with the pilot comments indicating this configuration is not preferred. The Pilot Handling FCS had a consistently higher piloted cutoff frequency in both axes than the other control systems. In the longitudinal axis, the cut-off frequencies are in general much lower than in the lateral axis. However, the cutoff frequencies for the three control systems in the longitudinal axis still follow the same trend as the lateral axis. These results indicate that the Pilot Handling control system allows the pilots to be more aggressive even in the presence of the load motion. This is consistent with the pilot comments indicating that this was the preferred configuration.

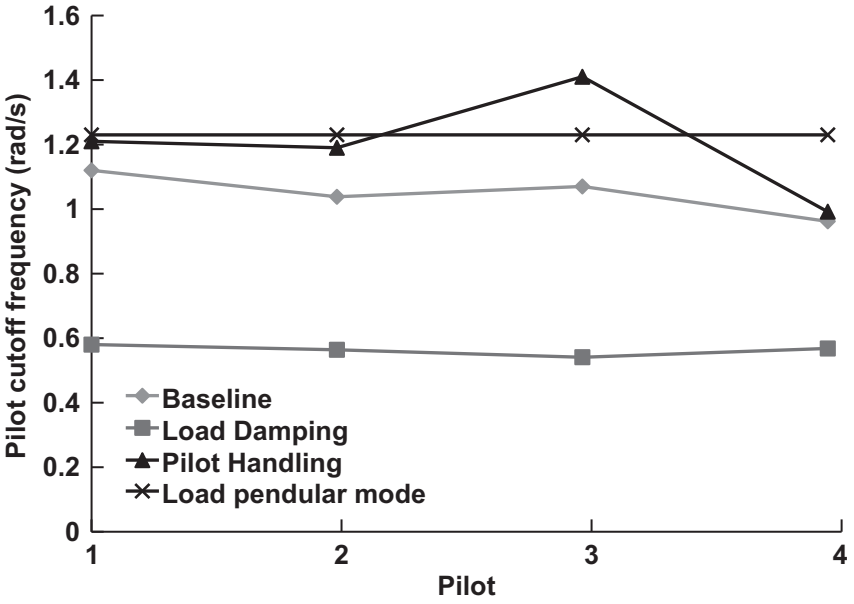

Figure 6-4. Lateral pilot cutoff frequencies.

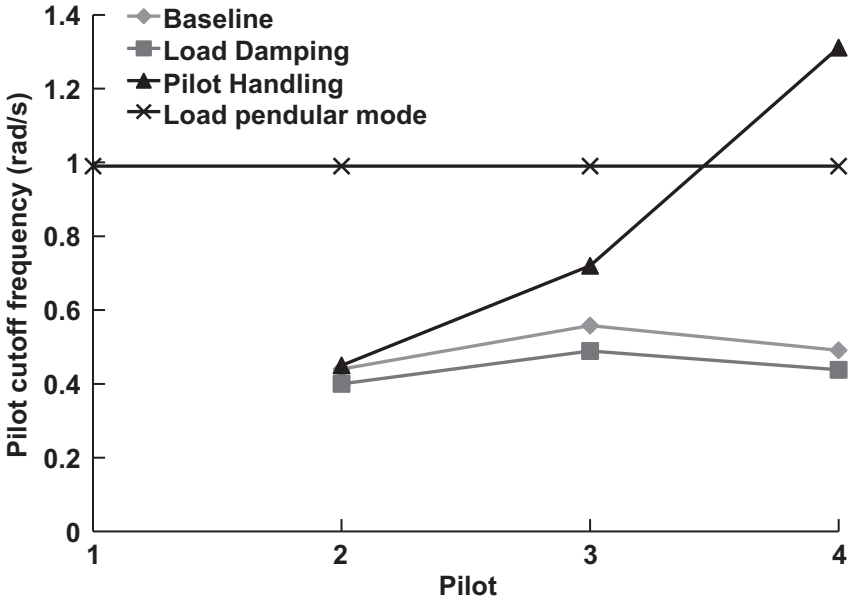

Figure 6-5. Longitudinal pilot cutoff frequencies (pilot 1 did not perform this task).

6.6 Discussion of Piloted Simulation Results

The results of the analytical and pilot simulation results are consistent with a trade-off between handling qualities and load damping for cable angle/rate feedback control laws. The piloted comments shows a preference for a cable angle feedback configuration that reduces the depth of the notch associated with the aircraft attitude attenuation at the load mode (Δ_{MAG}) over the Baseline and Load Damping configurations. However, for precision load placement, there are clearly operational advantages to being able to quickly damp load motions automatically, despite the cost paid in maneuvering handling qualities. As an example of the benefits of the Load Damping configuration, Figure 6-6 shows the lateral reposition maneuver from the fixed based piloted simulation (Pilot #3). In the first 30 seconds of the record, the pilot accelerates to ~10kts, translates across the runway, and decelerates to hover. In the recovery phase, which starts at about 30 seconds for all three cases, the pilot is attempting to hold a stable hover. The Load Damping case has no load swing nearly immediately after hover is achieved. The other two control laws still have significant load swing when the record ends. The Load Damping control laws would clearly be useful if the load was being delivered to a precise target location, where for the 79ft sling used herein even a seemingly small five degrees of load swing (in a steady hover) causes 7ft of load translation along the ground.

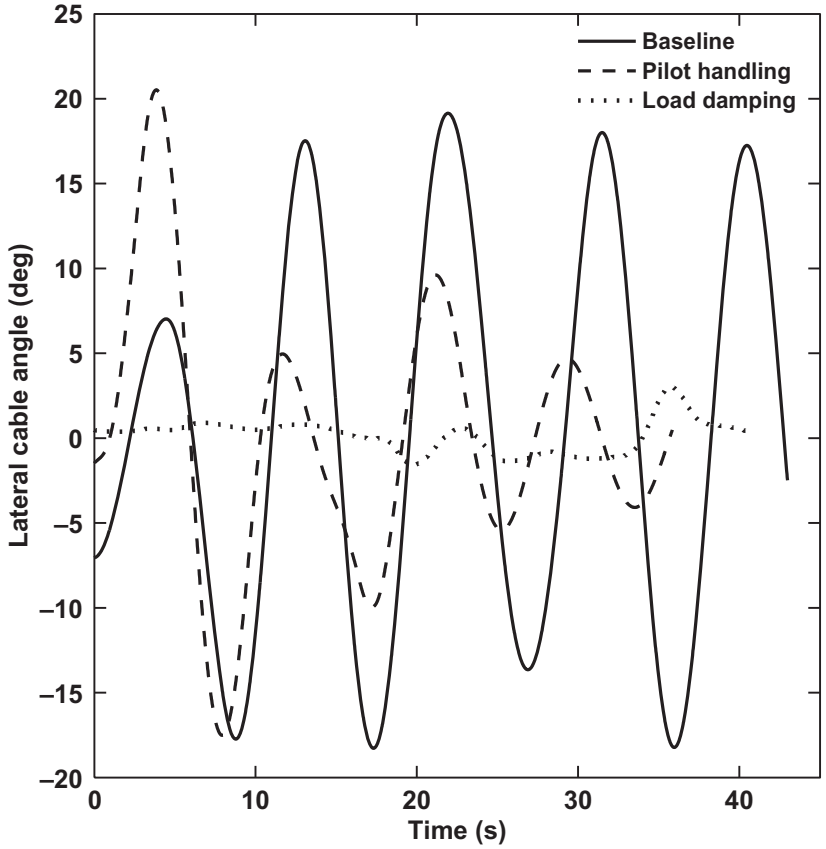

Figure 6-6. Lateral cable angle during lateral reposition maneuver in fixed based simulator.

There are two solutions to this fundamental tradeoff. The first is to choose a compromise design which is somewhere between the Pilot Handling and Load Damping control systems, but is not optimal for pilot handling or load damping. The second solution is to switch between the control laws in a task tailored strategy. This could be either a pilot selectable or an automatic Load Damping switch near hover but would default to the Pilot Handling control laws during maneuvering. This task tailored method would ensure that the control laws are optimal for the task, but comes at the cost of added complexity due to gain scheduling considerations. The task tailored approach is taken herein because the added software complexity is warranted given the improvements that can be achieved in maneuvering and load placement by implementing this method.

6.7 Summary of Chapter 6

Chapter 6 describes the fixed based piloted simulation of the three control system designs from Chapter 5 – Baseline (fuselage feedback only), Piloted Handling (fuselage and cable angle/rate feedback), and Load Damping (fuselage and cable angle/rate feedback) configurations. The key contributions of Chapter 6 include:

1. Validation of key trade-offs between load damping and pilot handling for cable angle/rate feedback control systems in the pilots' comments.
2. Quantitative results for pilot cut-off frequency are consistent with pilot comments indicating preference for the Pilot Handling control laws.
3. A task-tailored control law is suggested as a solution to the handling-qualities/load-damping trade-off for a cable angle/rate feedback control system.

7 Task Tailored Cable Angle/Rate Feedback Control Law Design and Analysis

In the previous chapters, a fundamental trade-off was identified between load damping and piloted handling qualities for feedback control systems with cable angle/rate feedback. This chapter develops a new task-tailored approach that uses a method of switching between a load damping mode and a piloted handling qualities mode based on the flight regime. This task-tailored control law is designed to be an integrated part of an advanced control system that builds on the attitude command architecture of Chapter 5 to add response types with higher levels of augmentation. These response types are implemented as 'outer-loop' velocity and position modes that pass attitude commands to the 'inner-loop' attitude command system. Due to a change of configuration from a 79ft sling in Chapter 5 to a 56ft sling in this chapter for safety of flight reasons and the requirement to maintain stability margins in the presence of the 'outer-loop' modes, the attitude command feedback gains are re-optimized in this chapter (as opposed to directly using the values from Chapter 5). This re-optimization uses the same design methods as in Chapter 5 to obtain 'Load Damping', 'Pilot Handling', and 'Baseline' control systems that are optimal for the new architecture and configuration used here in Chapter 7. Also, the velocity, position, and altitude feedback gains that implement the higher levels of augmentation are optimized.

7.1 Task Tailored Control Law Approach

ADS-33E-PRF [21] provides guidance on the required response types for Level 1 handling qualities, with more augmentation required as the usable visual cue environment [21] degrades (e.g. night). It is well known that the visual environment for hover/low speed tasks degrades with slung load operations because the pilot is higher from the ground (to avoid dragging the load), so cues are less available [2]. The response-types required for degraded visual cue environments are attitude command, translational rate command, position hold, yaw rate command with heading hold, and altitude hold. Furthermore, higher levels of augmentation generally improve the handling qualities of the aircraft [35], which should translate to improved handling qualities with an external load. The attitude command system studied in Chapters 5-6 did not include all the response types required, and instead focused on the pilot response trade-offs. Herein the attitude command architecture of Chapter 5 is built upon to include all the response types required for an advanced control system that can provide Level 1 handling qualities in the degraded visual environment.

The approach taken here to integrate all these response types into a single comprehensive control law is similar to that of the UH-60MU [35], where the mode of operation is based on ground-speed and pilot inceptor position. This type of control scheme is referred to as an "advanced" control law architecture, due to the complexity of the various control law modes of such a system, especially as compared to legacy civilian and military helicopters which feature only a simple rate feedback partial authority

stability augmentation system. In the case of the UH-60MU, the advanced control law architecture provided Level 1 handling qualities for an unloaded aircraft in the degraded visual environment [35]. The task-tailored control approach for cable angle/rate feedback is integrated into the moding architecture of the advanced control laws developed herein.

The task tailored design was developed to optimize the aircraft/load response characteristics as a function of the control task and aircraft state. To implement the task-tailored strategy, the Pilot Handling control laws are used when the pilot is in the loop (moving the controllers) to ensure that good handling qualities characteristics are active for maneuvering flight. Load Damping control laws are implemented only in the position hold and automatic deceleration modes because the pilot is not in the loop during these automated modes (and therefore response to pilot stick is not important). Also, the aircraft is at low speed in position hold/automatic deceleration, where the load motion is most important since the load is most likely to be placed on the ground from this flight condition.

7.2 Task Tailored Modes of Operation

The moding architecture that was developed to implement the task-tailored control strategy into an advanced control law architecture is shown in Figure 7-1 and Figure 7-2, as a function of lateral and longitudinal ground speed (V_x and V_y). The functionality is also dependent on the cyclic 'out of detent' and 'in detent', as shown by the left and right sides of the figures, respectively. The 'detent' of the cyclic is the center position. The maximum ground speed for this control law is 40kts because this study focuses on hover/low speed characteristics. The fuselage-based modes of the control system are shown in Figure 7-1, and the task-tailored cable angle/rate feedbacks are integrated into these control modes as shown in Figure 7-2.

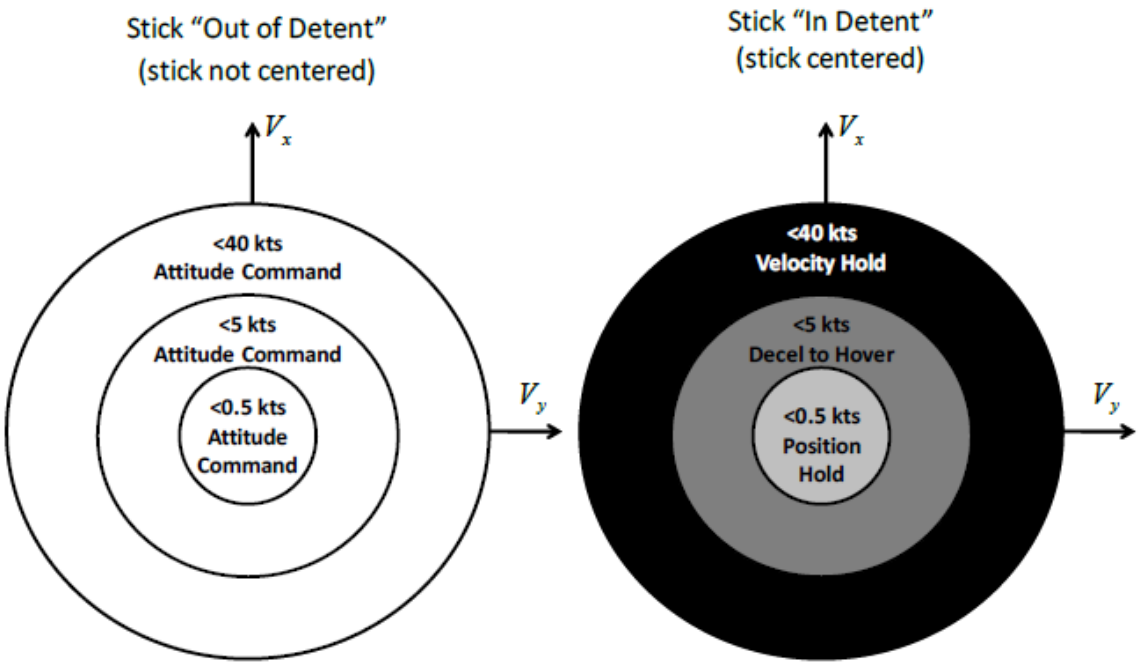

Figure 7-1. Fuselage-based control modes.

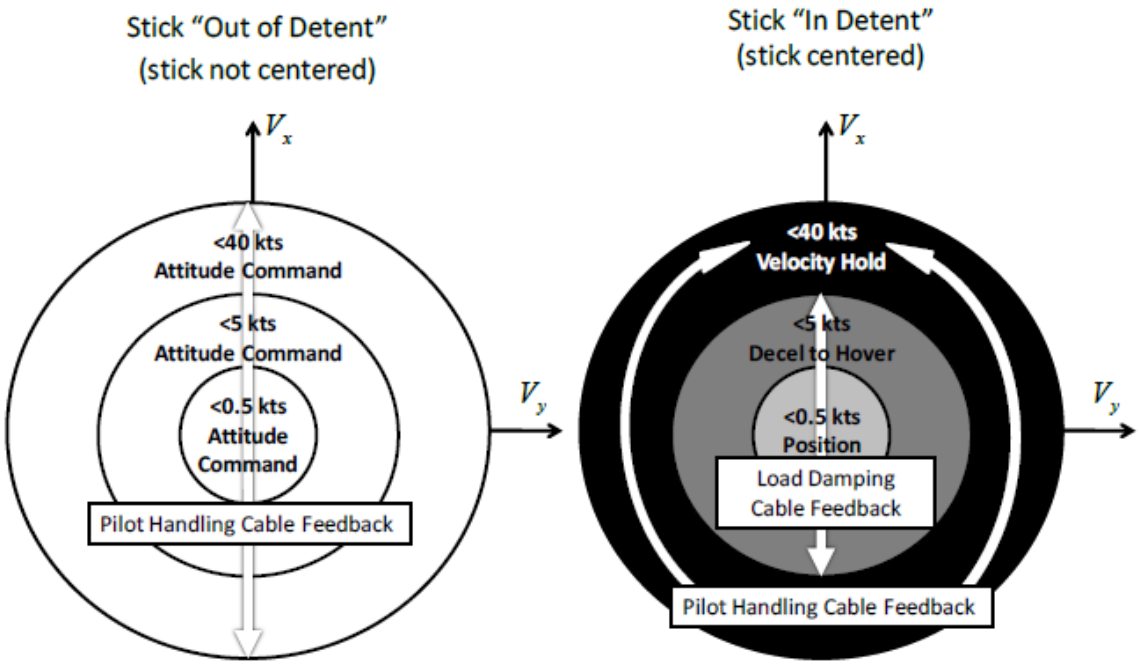

Figure 7-2. Task-tailored cable angle/rate feedback functionality.

The attitude command response type is used when the cyclic stick is 'out of detent', for all airspeeds from 0-40kts as shown on the left hand side of Figure 7-1. When the stick is 'in detent', the position hold, automatic deceleration, and velocity hold modes are applied depending upon the ground speed, as shown on the right hand side of Figure 7-1. For example, if the speed is above 5kts when the stick is placed into detent, the system will capture the current velocity, and maintain that velocity until the stick is removed from the detent position. Alternately, if the speed is less than 5kts when the stick is placed into the detent position, the aircraft will automatically decelerate to hover and once the ground speed is below 0.5kts the system will transition into position hold, capturing and maintaining position. The system switches back to attitude command immediately if the stick is moved out of the detent position during the velocity hold, automatic deceleration or position hold.

The task-tailored strategy for cable angle/rate feedback is integrated into the fuselage-based modes of operation as shown in Figure 7-2. In general, the strategy was to use Pilot Handling control laws when the pilot is in-the-loop and the Load Damping control laws when the pilot is *not* in-the-loop to minimize the undesirable effects of Load Damping on the perceived handling qualities. The Pilot Handling (cable angle feedback) control laws are active during maneuvering when the stick is 'out of detent' and the aircraft is in attitude command mode, as shown on the left side of Figure 7-2. The Pilot Handling control law was the preferred configuration for attitude command in the piloted simulation study of Chapter 6, and therefore is used for attitude command mode in this task-tailored strategy. This ensures the pilot has good handling qualities characteristics for maneuvering. The system switches to the Load Damping (cable angle/rate feedback) control laws during the deceleration and position hold modes, as shown on the right side of Figure 7-2. Thus, Load Damping control is used only when the stick is 'in detent'. This strategy ensures that Load Damping is only active near hover where it is most useful for load placement and that it is not used during pilot maneuvering. This is important to ensure that good handling qualities can be achieved for the overall system, considering that the piloted simulator comments were unfavorable toward the Load Damping control laws for maneuvering in Chapter 6. The Pilot Handling cable angle feedback is also used during the velocity hold mode, as shown on the right side of Figure 7-2, because this strategy provides a tighter velocity hold than the Load Damping system, and Load Damping is not needed when the aircraft is away from hover. Descriptions of all the modes are provided in Table 7-1.

Table 7-1. Description of control law modes.

Mode	Control Laws	Description
Attitude Command (AC)	CAF, OBL	Most basic mode of operation. Attitude of aircraft is proportional to pilot stick (stick out of detent).
Velocity Hold (VH)	CAF, OBL	Control system will hold the current ground velocity when the stick is in detent.
Automatic Decel	CAF, OBL	When ground speed is <5kts the aircraft will automatically decelerate to a hover if the stick is in detent. When speed is <0.5kts, system automatically captures position (PH).
Position Hold (PH)	CAF, OBL	Aircraft will hold position if aircraft speed is < 0.5 knots and stick is in detent. Position beepers: Short beep = +/-1ft Long beep = translation at +/-2kts
Altitude Hold (ALTHLD)	CAF, OBL	Aircraft will automatically hold altitude when collective is in the detent position. Altitude beeper: Short beep = +/-1ft Long beep = +/-90 ft/min
Rate Command, Heading Hold (RCHH)	CAF, OBL	Pedal will command yaw rate, and hold heading when pedal is in centered position.
Pilot Handling Load Feedback Mode	CAF only	Occurs when stick is out of detent position (pilot is maneuvering the aircraft).
Load Damping Load Feedback Mode	CAF only	Occurs during Automatic Decel and Position Hold when stick is in detent (pilot is not in the loop).

As described in Table 7-1, various 'beeper' modes are incorporated into the design. Position hold and altitude hold feature 'beeper' modes which provide additional functionalities that have been tailored to slung load operations. The position hold beeper allows the pilot to use a small 'joystick-like' beeper button that is on the cyclic to nudge the aircraft 1ft forward, aft, right, or left with a short click of this button. Multiple, consecutive short clicks of the beeper will command the aircraft to move the appropriate distance from the current position hold location (e.g. 5 clicks = 5ft), and hold the new position. The Load Damping mode stays on during beeper repositioning, ensuring that the load does not begin swinging. Additionally, by holding the beeper down (long beep) in a given direction, this commands a translational rate of 2kts in that direction. The beeper functionality was developed for making small adjustments to the position of the aircraft (and therefore the load) for precisely positioning a load before set-down. The collective beeper works similarly, with a button on the collective that moves up and down (with a thumb nudge). By giving a short click 'up' the aircraft will move up 1ft when in altitude hold mode (and multiple clicks moves aircraft multiple feet up). There is a similar functionality for downward beeps. Additionally, by holding the beeper up or down (a long beep), the aircraft will climb or descend at a rate of 90ft/min, which has been tuned for a reasonable load set-down speed. The collective beeper functionality was developed for controlled set-down of the load in the vertical axis.

As an example of how the task-tailored control law scheme of Figure 7-2 might be used, consider a precision load placement task, where the pilot must maneuver to the load set-down area, and quickly

deliver the load to a precise location. First, the task-tailored cable angle/rate feedback allows the pilot to maneuver with good handling qualities to the load set-down location in the Pilot Handling attitude command mode. Once near the load set-down location, the pilot hovers (or uses the automatic deceleration mode) at which time position hold is enabled and also automatic Load Damping control occurs. By using the position beeper and collective, the pilot can put down the load in the desired location, while staying in the Load Damping mode. If at any time the pilot wants to maneuver the helicopter, the control system automatically switches to the Pilot Handling cable angle/rate gains when the stick leaves the detent (center) position. The Load Damping mode returns when position hold or automatic deceleration is re-enabled (stick in detent and speed <5kts). Thus, the task tailored control law combines both the Load Damping and Pilot Handling control laws into a multi-mode control law architecture and will be henceforth be referred to as the Cable Angle/rate Feedback (CAF) control law.

An Optimized Baseline system with fuselage feedback only is described in Table 7-1. The Optimized Baseline was developed with the same command and hold modes in Figure 7-1, but does not use the load specific modes in Figure 7-2. The Optimized Baseline system does not switch gains in a task-tailored way because there are no cable feedbacks. This system provides a well designed and fair basis for comparison with the CAF system, since it has the same architecture (without cable feedback) and was designed against the same specifications. This control law extends the Baseline attitude command system described in Chapter 5 to include velocity and position hold modes, and optimizes the fuselage gains for this configuration. This control law is referred to as the Optimized BaseLine control law (OBL).

7.3 Task Tailored Control Law Architecture

The task-tailored control laws with modes shown in Figure 7-2 were implemented with architecture shown in Figure 7-3 for the lateral and longitudinal axes. The basic attitude command control system is an explicit model following control law [36], same as the system shown in Figure 5-2 and Figure 5-3. Attitude command is used when the stick is out of the detent (center) position. The load cable angle and rate feedback loops are also included the longitudinal and lateral axes (same as Figure 5-2 and Figure 5-3). The load feedback is inertial (ϕ_c , θ_c) as opposed to relative to the aircraft to provide faster load damping (it is desired to damp the load in the inertial frame, not in the relative frame). The velocity and position hold modes were added to this basic attitude command architecture from Chapter 5. These advanced control modes are implemented with nested velocity and position feedbacks as shown in Figure 7-3.

Figure 7-4 shows the vertical axis, which has the basic vertical velocity command developed in Chapter 5 (Figure 5-5) with an added altitude hold. The altitude hold comes on when the vertical velocity is less than 30 ft/min, and the collective is in the detent position. The yaw axis, which is rate command with heading hold, is identical to Figure 5-4. Load feedback is not active in the vertical or directional axes.

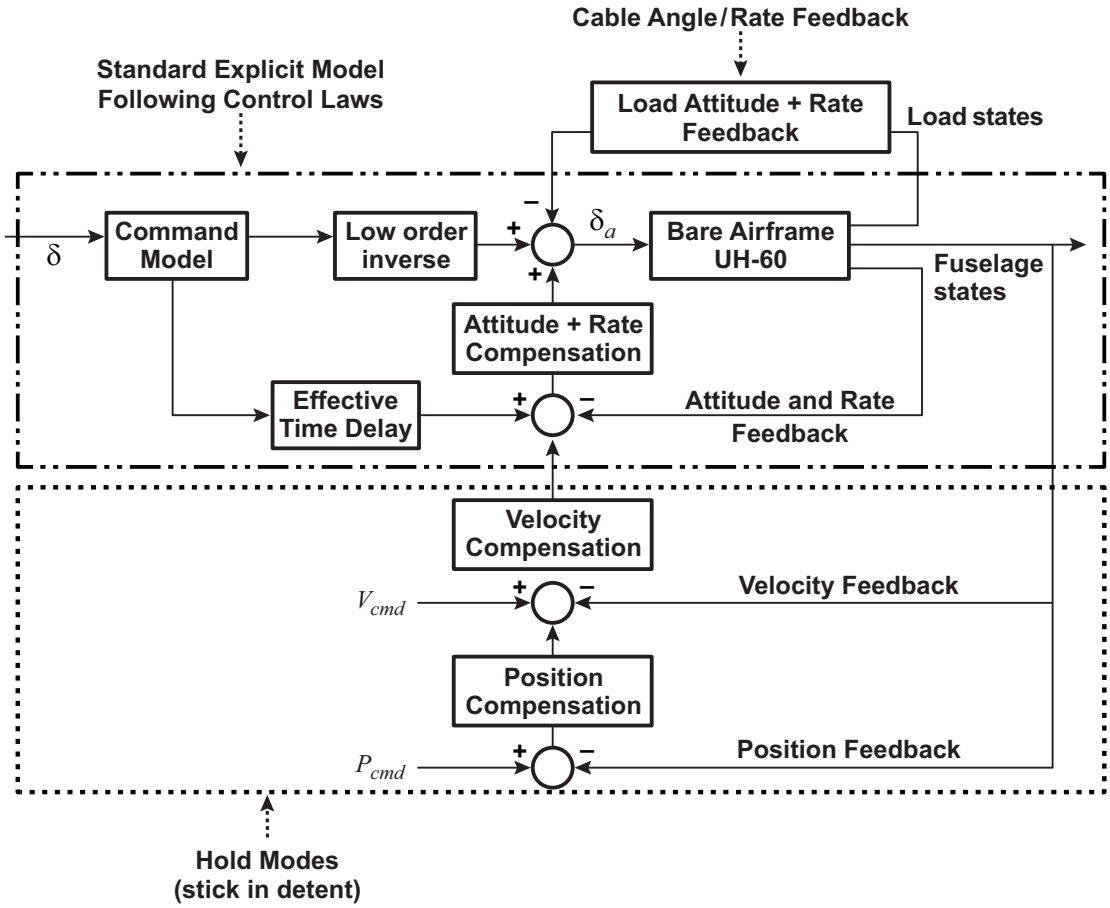

Figure 7-3. Control system architecture – lateral and longitudinal.

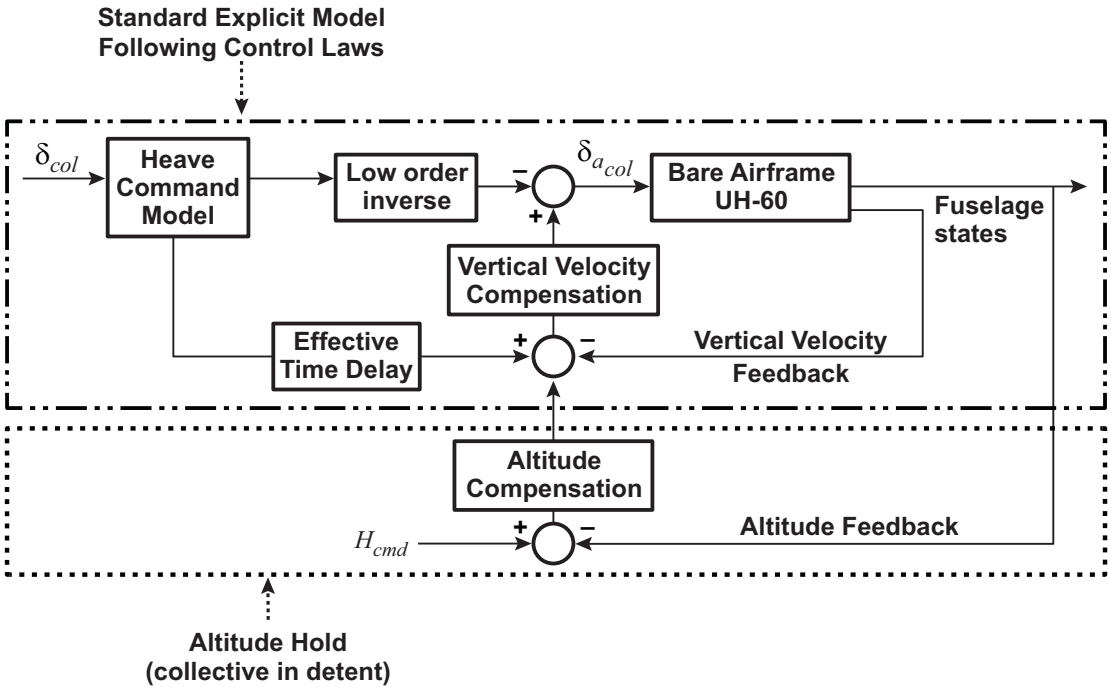

Figure 7-4. Control system architecture – vertical axis.

7.4 Control Law Optimization

Two control laws were designed using the multi-objective optimization technique for determining feedback gains:

1. Cable Angle/Rate Feedback (CAF) – task-tailored control laws that switch between Load Damping and Pilot Handling load feedback methods and makes use of fuselage, cable angle and cable rate feedbacks. The Load Damping and Pilot Handling attitude command gains are not used directly from Chapter 5, but instead are re-optimized here (in Sec. 7.4.2) to account for a change of sling length (described in Sec. 7.4.1) and to maintain stability in the presence of outer-loop velocity and position modes (shown in Figure 7-3 and Figure 7-4). The CAF control system is described in Table 7-1 and Figure 7-2.
2. Optimized Baseline (OBL) – uses fuselage feedback only, with the load feedback gains set to zero. This advanced control system is built on the Baseline architecture of Chapter 5, but the attitude command gains are slightly different than Chapter 5 because the feedback gains are re-optimized (as described later in Sec. 7.4.2). Similarly to the CAF control laws, OBL was re-optimized to account for a change in sling length (described in Sec. 7.4.1) and to maintain stability with the outer-loop velocity and position modes (shown in Figure 7-3 and Figure 7-4). This control system is described in Table 7-1 and Figure 7-1.

The multi-objective optimization technique is described in detail in Chapter 5 and Ref. 49. Due to the complicated nature of this problem with many modes, design specifications, in addition to gain scheduling and multiple configurations (e.g. different load masses) that must meet the requirements, this is a difficult control problem to tune by hand. Multi-objective optimization is useful to tune the gains to meet all the requirements using direct optimization techniques. The software used for the multi-objective optimization herein is CONDUIT® [56].

7.4.1 Aircraft and Load Configuration

The task-tailored control laws are optimized for the 56ft sling with 5000lb load, on a 15,000lb UH-60. The configuration was changed from the 79ft sling in Chapters 5-6 to a 56ft sling in order to accommodate safer flight testing. Additionally, the 56ft sling has poor handling qualities with a heavy load for maneuvering [2] and has poor handling qualities with a light load (1000lb) for load placement. The 79ft sling has slightly worse baseline handling qualities than the 56ft configuration, but otherwise the configurations display very similar characteristics and trade-offs.

7.4.2 Design Specifications

The goal for the CAF optimization is to ensure both modes (Load Damping and Pilot Handling) meet the stability and gust rejection requirements. In addition, the Pilot Handling mode must meet the Level 1 handling qualities requirements and the Load Damping mode must meet a load damping ratio greater than 0.2. The results from Chapter 5 are not used directly as the attitude loop gains herein because of the new

configuration (56ft sling), the desire to meet stability margins for VH and PH (without gain scheduling attitude and rate gains), and the desire to gain schedule as few gains as possible when transitioning in and out of the Load Damping mode. However, the overall strategy from Chapter 5 was used to optimize the Load Damping and Pilot Handling modes for the current configuration and constraints. For the OBL configuration, the goal was to optimize one gain set to obtain the best possible performance relative to the CAF design, but without load feedback. This gives a level field for comparison against which to determine the benefits of the cable angle/rate feedback task-tailored control law. Similarly to CAF, the OBL gains from Chapter 5 were not used for the attitude loop gains, but were instead re-optimized for the 56ft sling, and to maintain stability margins with velocity and position feedbacks.

The control law design was focused on one sling length (56ft) and load mass (5K), but was also required to meet stability margins for multiple load masses. The 56ft sling with a 5000lb load was chosen as the key design case because it represents the critical configuration (longest sling, heaviest load) that would be flown. The control laws were also required to meet stability margins for the unloaded configuration, which becomes relevant upon load set-down. The control laws also must revert to a system with acceptable margins if the cable angle sensors fail or are disconnected.

The control system was designed to meet the requirements for ADS-33E-PRF Level 1 handling qualities [21], stability margins [53], disturbance rejection [54], and handling qualities with an external load (described in Chapter 3). The design specifications of Table 7-2 were implemented in the multi-objective optimization to ensure that the control system would have the desired flying qualities. This set of specifications in Table 7-2 is a super-set of those given in Chapter 5, with the same specifications used to optimize the attitude command mode from Table 5-3, but with additional requirements for velocity and position hold modes.

A sequential optimization strategy, as described herein, was adopted in order to minimize the number of gain scheduled parameters needed to implement the task-tailored CAF control laws. The attitude command gains (including fuselage angular rate, attitude, and attitude integral gains, as well as cable angle and cable rate gains) for the Pilot Handling control mode were first optimized against the specifications. Then, a separate optimization was performed to optimize the attitude command gains for the Load Damping control laws, with some of the gains fixed to the Pilot Handling values, and the limited set of parameters $K_p, K_q, K_\phi, K_\theta, K_{p_c}, K_{q_c}, K_{\theta_c}$ available to optimize, such that the requirements of Table 7-2 including increased load damping ratio were met. This set of parameters ($K_p, K_q, K_\phi, K_\theta, K_{p_c}, K_{q_c}, K_{\theta_c}$) must be gain scheduled as the CAF system switches between Load Damping and Pilot Handling modes.

The outer loop modes were then optimized once the attitude command gains for both CAF modes were determined. Pilot Handling mode attitude and cable gains (vs. Load Damping gains) were used in

velocity hold because they provide a tighter velocity loop than the Load Damping gains. Thus, the Pilot Handling attitude command gain set was fixed for the optimization of the velocity hold gains. Then, during the optimization of the position hold mode, the position feedback gains were optimized with the Load Damping attitude command gains and the velocity hold gains fixed to the previously optimized values.

For the Optimized Baseline control system, the attitude command system was optimized and then the velocity hold and position hold gains were optimized around the fixed attitude command gains. This sequential optimization strategy for OBL eliminates the need for gain scheduled parameters, unlike the CAF control laws which need gain scheduling to handle the task tailored Load Damping and Pilot Handling switch in functionality. The 'outer loop' velocity and position gains for OBL are optimized to meet the requirements with the previously optimized 'inner loop' attitude gains. Therefore, the inner loop attitude gains do not need to be gain scheduled with each sequential loop closure. Slightly better performance might be obtained by gain scheduling all parameters with the addition of each outer loop closure, but adds unnecessary complexity for the OBL control laws because all requirements are met with the sequential strategy.

Table 7-2. Control system design specifications.

Specification (CONDUIT® Mnemonic)	Description	Constraint Type	Axes	Modes (defined in Table 7-1)
EigLcG1	Eigenvalues in left-half plane [1]	Hard	Pitch, Roll, Yaw, Heave	AC, VH, PH, ALTHLD, RCHH
StbMgG1	Gain and phase margin [53]	Hard	Pitch, Roll, Yaw, Heave	AC, VH, PH, ALTHLD, RCHH
BnwPiH1	Pitch bandwidth for acquisition and tracking, Attitude Command Requirements [21]	Soft	Pitch	AC
BnwRoH2	Roll bandwidth for other M.T.E.'s, attitude command requirements [21]	Soft	Roll	AC
BnwYaH1	Yaw bandwidth for acquisition and tracking [21]	Soft	Yaw	RCHH
BnwPiS1	Pitch external load handling qualities criteria [2]. Level 1 required for Pilot Handling CAF mode and OBL	Soft	Pitch	AC
BwnRoS1	Roll external load handling qualities criteria [2]. Level 1 required for Pilot Handling CAF mode and OBL	Soft	Roll	AC
CouPRH2	Coupling between pitch and roll [21]	Soft	Pitch/Roll	AC
CouYaH2	Coupling between collective and yaw [21]	Soft	Yaw	RCHH
DmpTmG1	Damping ratio of Load from log decrement method $\zeta > 0.08$ - AC, VH, PH for OBL $\zeta > 0.1$ - AC, VH for CAF (Pilot Handling mode) $\zeta > 0.2$ - PH for CAF (Load Damping mode)	Soft	Pitch, Roll	AC, VH, PH
DstBwG1	Disturbance rejection bandwidth [54]	Soft	Pitch, Roll, Yaw, Heave	AC, VH, PH, ALTHLD, RCHH
DstPkG1	Disturbance rejection peak magnitude [49]	Soft	Pitch, Roll, Yaw, Heave	AC, VH, PH, ALTHLD, RCHH
EigDpG1	Damping ratio requirements [21]	Soft	Pitch, Roll, Yaw, Heave	AC, VH, PH, ALTHLD, RCHH
FrqHeH1	Heave response bandwidth [21]	Soft	Heave	AC, ALTHLD
HldNmH1	Normalized attitude hold response to disturbances [21]	Soft	Pitch, Roll, Yaw	AC, RCHH
ModFoG2	Performance of Aircraft as compared to command model [36]	Soft	Pitch, Roll, Yaw, Heave	AC, RCHH
OlpOpG1	Open loop onset point specification for actuator rate limiting [55]	Soft	Pitch, Roll, Yaw, Heave	AC, VH, PH, ALTHLD, RCHH
TrkErG1	RMS of load response in turbulence	Soft	Pitch, Roll	AC, VH, PH, ALTHLD
CrsLnG1	Minimizes cross-over frequency [49]	Summed Objective	Pitch, Roll, Yaw, Heave	AC, VH, PH, ALTHLD, RCHH
RmsAcG1	Minimizes actuator RMS [49]	Summed Objective	Pitch, Roll, Yaw, Heave	AC, VH, PH, ALTHLD, RCHH

7.4.3 Control Law Optimization Results

Key attitude command characteristics for the optimized designs are shown for the 5000lb load, with a 56ft sling in Table 7-3 and Table 7-4. The tables show that the CAF control laws (in Pilot Handling mode for attitude command) have much improved stability margins and attitude disturbance rejection, in addition to slightly improved load damping as compared to OBL. Figure 7-5 shows that the CAF control laws in attitude command (Pilot Handling mode of task-tailored control law) have less magnitude distortion near the load mode than OBL, moving the predicted handling qualities deeper into the desired HQR$\leq$4 region for the stick-out of detent piloted response. These results are consistent with those in the attitude command optimization for the 79ft sling, in Table 5-4 and Table 5-5.

The improvements in the stability margins for CAF with respect to OBL are mainly due to changes in the broken-loop shape around the load mode as seen in Figure 7-6, which compares the broken loop responses of the two configurations. The figure shows that subtle changes near the load mode due to cable angle/rate feedback shift the cross-over frequency higher, where more phase margin is available. This improvement is more easily seen by plotting the broken loop response as a Nichols chart, in Figure 7-7. The arrow indicates considerably improved robustness of CAF as compared to OBL near the load mode because the response is much further from the exclusion zone. CAF also provides a modestly better robustness at higher frequency, as shown by increased distance from the exclusion zone on the lower right side of the diamond in Figure 7-7. Note that the diamond shaped exclusion zone is based on 35 degrees of phase margin and 6dB of gain margin. It is worth mentioning that cable feedback provides loop shaping at the frequency of the load mode and as such, it is robust to a variety of sling lengths and load masses as shown in Sec. 5.4.3. This is a large benefit over an inverse notch type compensator which could provide the same improvements in loop shape for one configuration, but would have to be scheduled with sling length and load mass to operate robustly.

Figure 7-6 shows that the OBL design has a crossing at ~0.8 rad/s, which is associated with low phase margin. The phase margin is 34.9 deg in this configuration, and cannot be increased within the constraints of the optimization. This manifests as a brief excursion into the exclusion zone of the Nichols chart in Figure 7-7 (near the start of the arrow). The CAF configuration changes the loop shape in order to have a low frequency crossing at 1 rad/s, and the highest cross-over at 4.69 rad/s is somewhat reduced from the OBL design, which is beneficial because it excites less high frequency actuator activity.

Another key improvement with the cable angle feedback in attitude command is the roll angle disturbance rejection bandwidth. The disturbance rejection bandwidth (DRB) improves considerably from .71 rad/s in OBL configuration to 2.24 rad/s in the CAF configuration, which indicates that attitude disturbances will be rejected much more quickly for the CAF configuration. This is due to attenuation of disturbances near the load mode with CAF, which is shown in Figure 7-8 in the circled area of the plot.

This causes the disturbance response to cross the -3dB line at a higher frequency, increasing the disturbance rejection bandwidth.

Table 7-3. Attitude command control law characteristics for lateral axis (5K, 56ft sling).

	Lateral				
	GM [dB]	PM [deg]	XOVER (at actuator) [rad/s]	Phi - DRB [rad/s]	Load Damping Ratio
OBL	5.89	34.90	5.41	0.71	0.08
CAF Pilot Handling Mode	6.78	47.55	4.69	2.24	0.14

Table 7-4. Attitude command control law characteristics for longitudinal axis (5K, 56ft sling).

	Longitudinal				
	GM [dB]	PM [deg]	XOVER (at actuator) [rad/s]	Theta - DRB [rad/s]	Load Damping Ratio
OBL	11.95	40.03	2.84	0.63	0.08
CAF Pilot Handling Mode	10.48	45.84	3.19	0.72	0.11

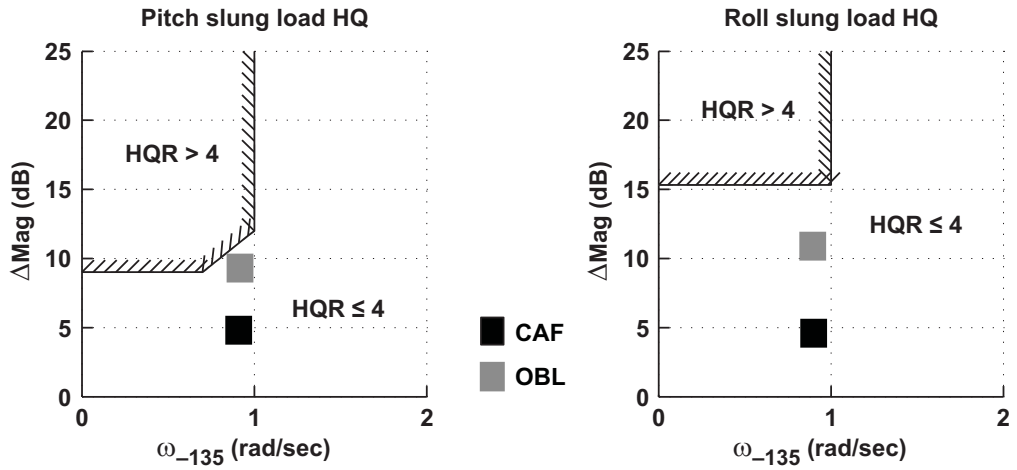

Figure 7-5. Handling qualities specification, attitude command mode (5K, 56ft sling).

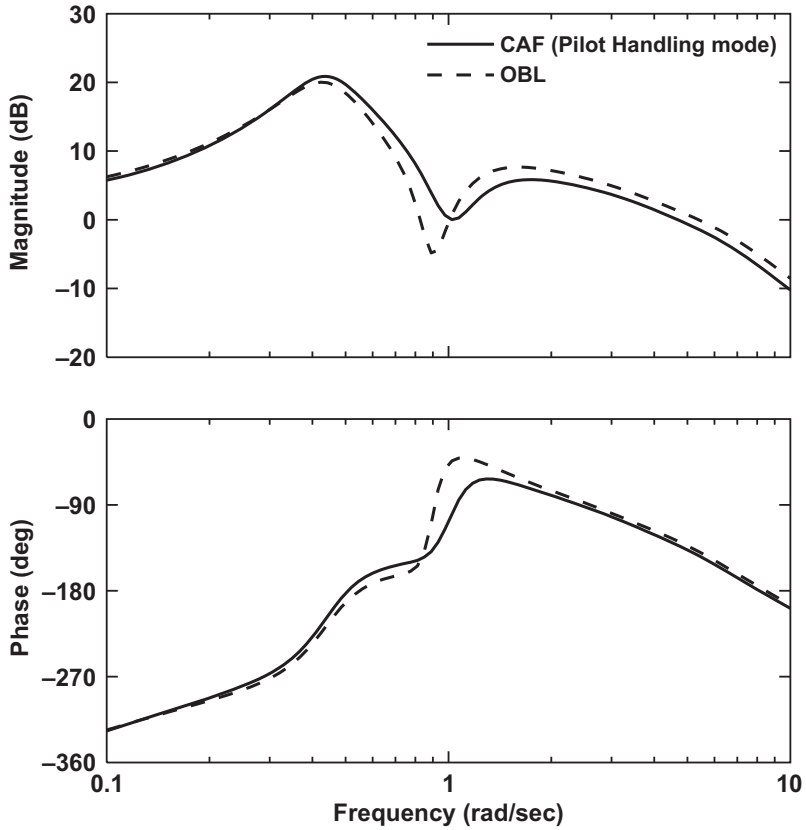

Figure 7-6. Lateral broken loop response, attitude command mode (5K, 56ft sling).

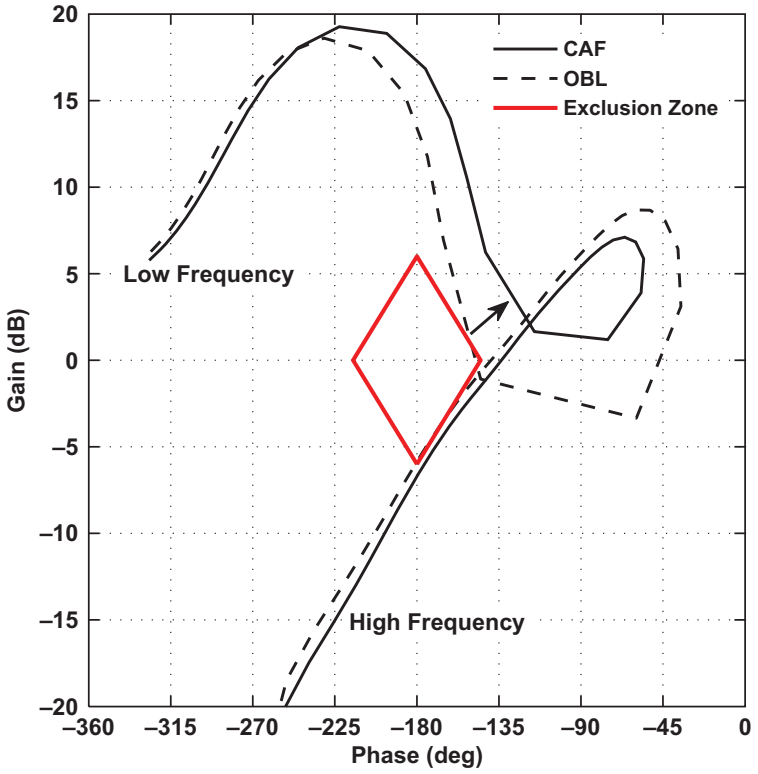

Figure 7-7. Nichols Chart for lateral broken loop response, attitude command mode (5K, 56ft).

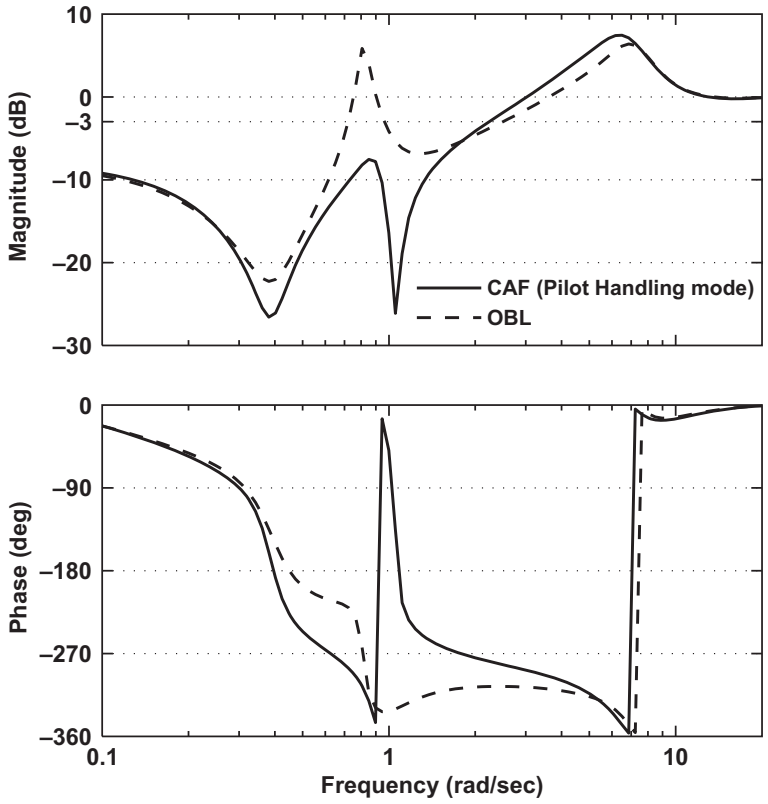

Figure 7-8. Roll attitude disturbance response (ϕ/ϕ_{gust}), attitude command mode (5K, 56ft sling).

The velocity and position hold characteristics of the optimized control systems are shown in Table 7-5 and Table 7-6. The stability margins shown in the tables are calculated with the loop broken at the actuator. The CAF system has better stability margins and greatly improved load damping, as well as similar velocity and position disturbance rejection bandwidth (DRB) characteristics to the OBL design. Recall that the longitudinal and lateral cable angles and rates, as well as pitch and roll attitude gains are scheduled with the Load Damping mode, which is active in position hold to provide a much improved load damping response.

The disturbance rejection bandwidth result in, for example, lateral position (Y) is defined as response to a disturbance in the lateral position feedback. This response is at low frequency (i.e. DRB~0.3), much lower than the load mode at ~1.0 rad/s, and thus the effect of load interaction is not present in these metrics. However, in the time responses, there is a trade-off with position hold performance and load damping for higher frequency disturbances that cause the load to swing, as shown for a pulse disturbance to roll attitude in Figure 7-9 - Figure 7-11. In this case, the OBL design does better at controlling the aircraft position, as shown in Figure 7-9, even though the CAF control laws have essentially the same position disturbance rejection bandwidth as the OBL design. However, the CAF design does much better at controlling the load motion, as shown in Figure 7-10. This relates to the key trade-off of cable angle/rate feedback to the rotor; that the system cannot control the aircraft and load motions

independently. This principle is further illustrated by Figure 7-11, which shows that the aircraft must actively position itself over the load to damp the load motions. In Figure 7-11a, the OBL aircraft position is out of phase with the load response, whereas for the CAF control system in Figure 7-11b the aircraft follows the load position, effectively damping the load at the cost of greater fuselage position variance.

The directional and vertical controller characteristics are given in Table 7-7. These axes do not have cable angle feedback so the designs are very similar for CAF and OBL. Also, the characteristics are nearly identical for Load Damping and Handling Qualities modes of CAF in the directional and vertical axes.

The optimized feedback gains are given in Table 7-8 - Table 7-11. Similarly to Chapter 5, the cable angle gains are used for the Pilot Handling CAF mode, whereas cable rate and cable angle feedback are needed for the Load Damping CAF mode. This is another reason that the two modes cannot occur simultaneously; in order to damp the load cable rate feedback is required, but it causes distortion in the attitude response of the aircraft. This is consistent with the coupling numerator results of Chapter 4, seen in Figure 4-8.

Table 7-5. Position and velocity control law characteristics for lateral axis (5K, 56ft sling).

	Lateral - in position hold					
	GM [dB]	PM [deg]	XOVER (at actuator) [rad/s]	v - DRB [rad/s]	Y - DRB [rad/s]	Load Damping Ratio
OBL	5.95	33.42	5.15	1.01	0.29	0.14
CAF Load Damping Mode	7.47	42.50	4.19	1.22	0.27	0.23

Table 7-6. Position and velocity control law characteristics for longitudinal axis (5K, 56ft sling).

	Longitudinal - in position hold					
	GM [dB]	PM [deg]	XOVER (at actuator) [rad/s]	u - DRB [rad/s]	X - DRB [rad/s]	Load Damping Ratio
OBL	8.08	47.86	2.80	1.04	0.22	0.17
CAF Load Damping Mode	9.12	46.50	2.34	1.12	0.21	0.25

Table 7-7. Directional and pedal control law characteristics (5K, 56ft sling).

	Pedal - yaw rate command/heading hold				Collective - in Altitude Hold				
	GM [dB]	PM [deg]	XOVER (at actuator) [rad/s]	Psi - DRB [rad/s]	GM [dB]	PM [deg]	XOVER [rad/s]	w - DRB [rad/s]	H - DRB [rad/s]
OBL	11.09	60.79	3.67	0.73	16.84	46.22	1.27	0.98	0.52
CAF (Both Modes)	11.09	60.69	3.68	0.76	13.77	47.71	1.66	1.26	0.68

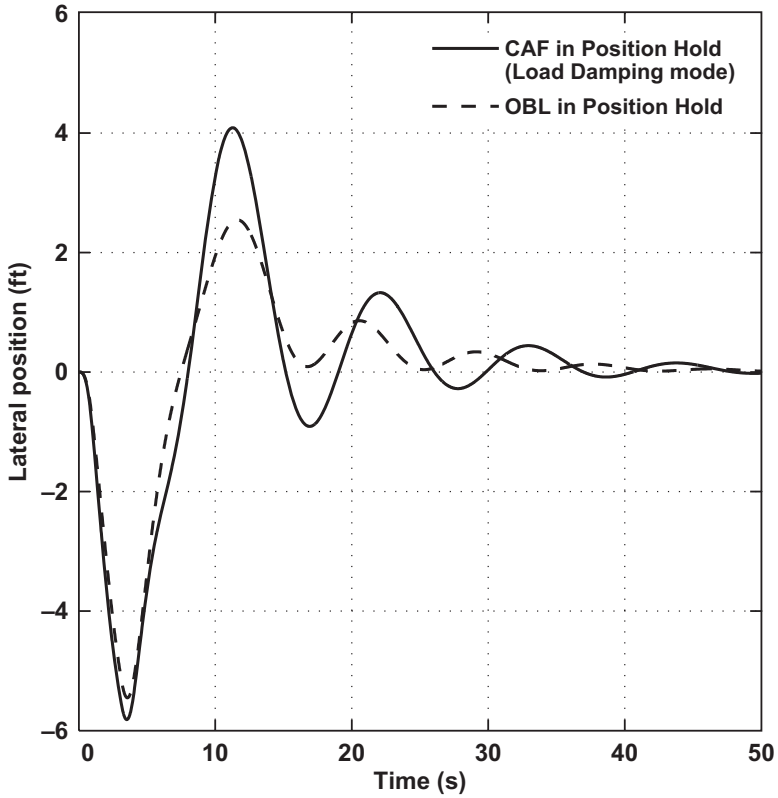

Figure 7-9. Lateral position response in position hold (PH) to 5 deg roll attitude pulse (5K, 56ft).

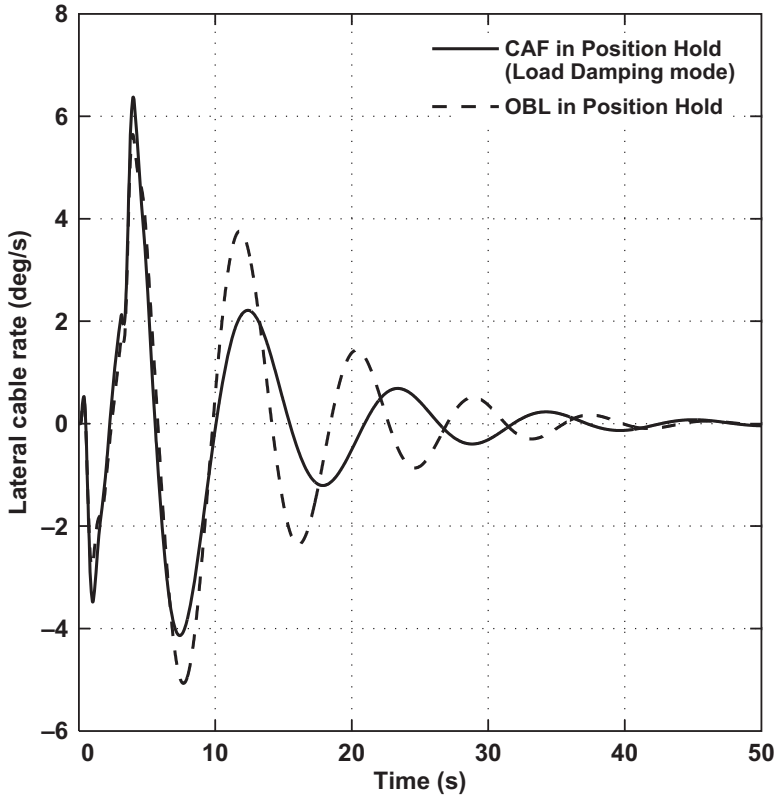

Figure 7-10. Load response in position hold (PH) to 5 deg roll attitude pulse (5K, 56ft).

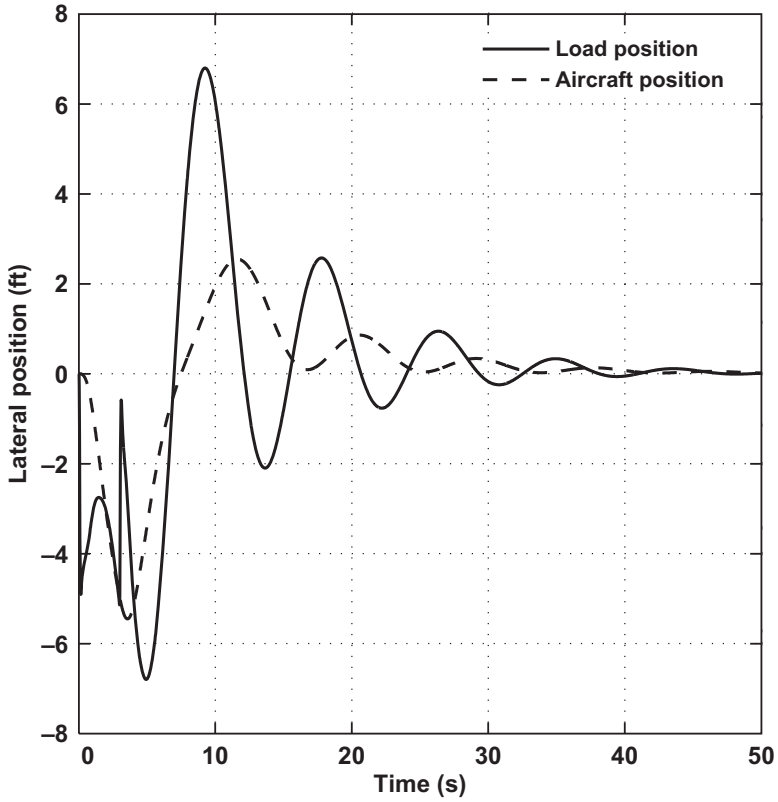

(a) OBL

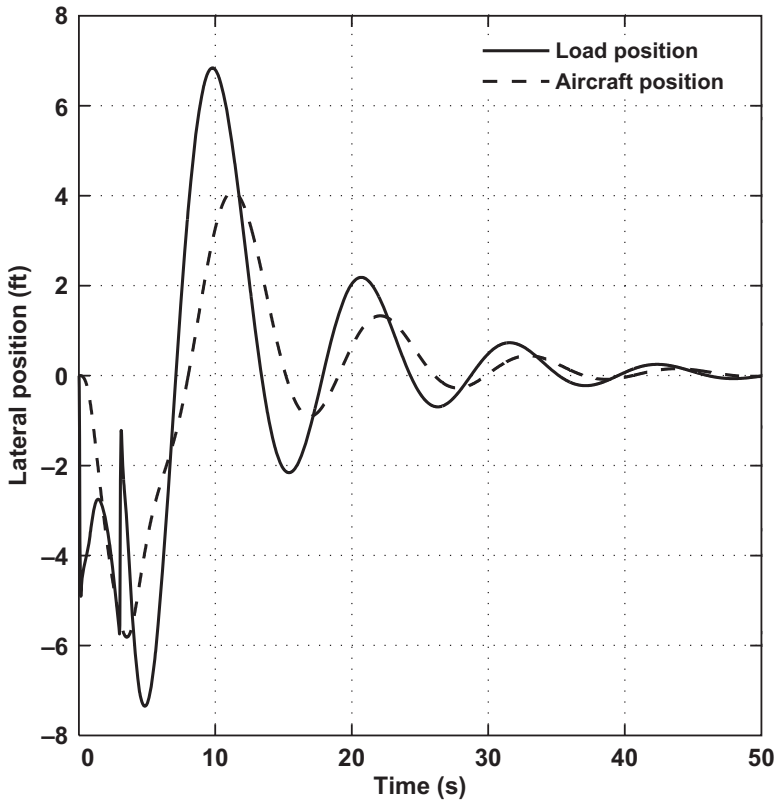

(b) CAF

Figure 7-11. Aircraft and load inertial position responses in position hold (Load Damping mode) to a pulse disturbance (5K, 56ft sling).

Table 7-8. Optimized roll axis fuselage gains.

	Roll Axis Fuselage Gains					
	K_p (in-s/rad)	K_ϕ (in/rad)	K_{ϕ_i} (in/rad-s)	K_v (rad-s/ft)	K_{v_i} (rad/ft)	K_Y (ft/s/ft)
OBL	1.86	14.40	0.10	0.019	0.13	0.39
CAF - Load Damping Mode	1.46	12.22	0.10	0.019	0.13	0.37
CAF - Pilot Handling Mode	1.40	13.44	0.10	0.019	0.13	n/a

Table 7-9. Optimized pitch axis fuselage gains.

	Pitch Axis Fuselage Gains					
	K_q (in-s/rad)	K_θ (in/rad)	K_{θ_i} (in/rad-s)	K_u (rad-s/ft)	K_{u_i} (rad/ft)	K_X (ft/s/ft)
OBL	5.81	8.84	0.30	0.015	0.062	0.34
CAF - Load Damping Mode	5.17	7.83	0.50	0.012	0.062	0.34
CAF - Pilot Handling Mode	7.06	9.77	0.50	0.012	0.062	n/a

Table 7-10. Optimized cable angle and cable rate feedback gains.

	Roll Axis Cable Gains		Pitch Axis Cable Gains	
	K_{p_c} (in-s/rad)	K_{ϕ_c} (in/rad)	K_{q_c} (in-s/rad)	K_{θ_c} (in/rad)
OBL	0	0	0	0
CAF - Load Damping Mode	0.81	3.98	0.60	1.24
CAF - Pilot Handling Mode	0.0001	3.98	0.0001	2.02

Table 7-11. Optimized yaw and heave axis fuselage gains.

	Yaw Axis Fuselage Gains			Heave Axis Fuselage Gains		
	K_r (in-s/rad)	K_ψ (in/rad)	K_{ψ_i} (in/rad-s)	K_w (in-s/ft)	K_{w_i} (in-s/ft)	K_H (ft/s/ft)
OBL	6.48	8.99	0.5	0.22	0.125	0.83
CAF - Load Damping Mode	6.49	9.00	0.5	0.31	0.125	1.03
CAF – Pilot Handling Mode	6.49	9.00	0.5	0.31	0.125	1.03

7.5 Summary of Chapter 7

A novel task-tailored technique is developed to switch between the Pilot Handling and Load Damping methods for CAF (cable angle/rate feedback with fuselage feedback). The task-tailored technique is developed as an integrated part of an advanced feedback control law that includes additional modes of augmentation such as altitude hold, velocity hold, automatic deceleration to hover, and position hold. An Optimized Baseline (OBL) control system was developed with fuselage feedback only with the advanced modes, to represent a modern control system without cable angle/rate feedback for comparison with the CAF control laws. The key contributions of this chapter are:

1. Development of a task-tailored control architecture optimized for maneuvering handling qualities when the pilot is moving the cyclic stick, and optimized for load placement in automated modes near hover (position hold).
2. The CAF control system provides improved stability margins in both Load Damping and Pilot Handling modes, as compared to OBL.
3. The CAF control system improves load damping by positioning the aircraft over slung load, which trades-off degraded position hold performance with load damping in the Load Damping mode.

8 Implementation for Flight Test

The preceding chapters of this dissertation described linear, analytical results of cable angle/rate feedback. In order to successfully integrate and flight test these cable angle/rate feedback control laws on the RASCAL fly-by-wire Black Hawk helicopter (described in Sec. 2.1), several engineering challenges had to be overcome. These challenges included:

1. Design, installation and integration of a cable angle/rate sensor
2. Development of equations to convert on-load sensor measurements into cable angles
3. Removal of load-sling interaction modes from the measured load motion
4. Elimination of vertical load bounce mode effects from the vertical motion measurements
5. Designing an effective filter for the aircraft radar altimeter

8.1 Cable Angle/Rate Sensor

The US Army Aeroflightdynamics Directorate researchers had previously employed an Embedded GPS/INS (EGI) in slung loads to measure inertial load motions and to calculate cable angles in post flight analysis. The high quality and reliability of the EGI data motivated the use of these sensors to calculate real-time cable angles for use by the CAF control laws. This led to the requirement to integrate the EGI in the load with the MIL-STD-1553b [58] data bus on RASCAL so that it could communicate with the flight control computer. A wired MIL-STD-1553b bus connection between the load EGI and the RFCS was implemented in order to minimize measurement latency and to maximize signal integrity (and safety). This configuration extends the 1553 muxbus up to 81ft outside of the aircraft fuselage along the path of the sling as shown in Figure 8-1. A dual-redundant electrical ground connection between the aircraft and the load has also been implemented to prevent excessive current travel along the 1553 bus and to protect the sensitive and expensive systems used for flight control. The sensors are not flight critical because RASCAL has a fail-safe flight control system. However, the RASCAL 1553 bus has also been modified to automatically reconfigure to an internally terminated configuration if electrical connection to the external load is severed.

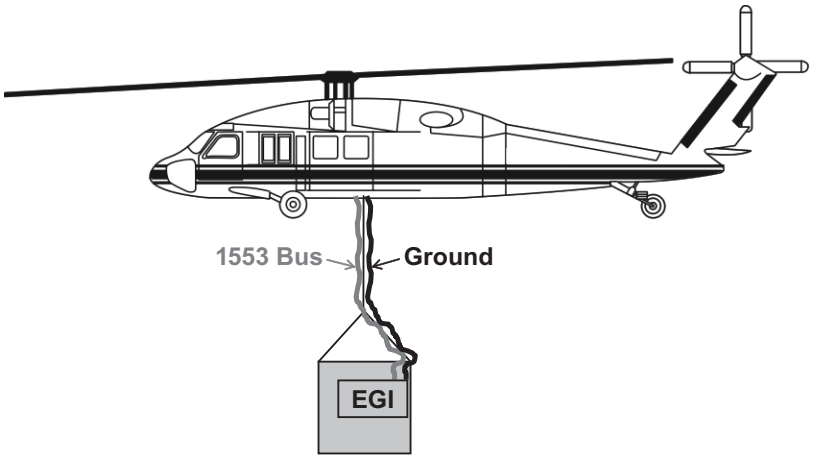

Figure 8-1. RASCAL 1553 muxbus extension.

8.2 Calculating Cable Angles from Load EGI Measurements

In a field application airworthy direct measurements of cable angle and rate would be desirable, but are only just now under development [59, 60]. In this research, the load Euler angles and angular rates were measured in an EGI unit on board the load as described in Sec 8.1. This means that load angles and rates will be measured with respect to the load body axes. Considering that the load can spin with respect to the helicopter and the helicopter can yaw with respect to the load, it is important to transform the load Euler angles and rates into a coordinate system that is aligned with the aircraft heading, which is referred to as the "inertial cable angle". This ensures that the lateral and longitudinal load motion with respect to the helicopter will be fed-back to the appropriate control axis, with the proper sign. Note that this should not be confused with the "relative cable angle", which is also aligned with the aircraft heading but cable angles are measured with respect to the fuselage body axes, as opposed to the inertial frame. Inertial cable angle and cable rate feedbacks are used herein (as described in Sec. 4.4.2).

For the transformation of load Euler angles to inertial cable Euler angles, it was assumed that the load does not pitch or roll about the cable. In fact, the load does rock about the cable axes, but these motions are systemic and can be removed from the measurement, as described in the following section (Sec. 8.3). Thus these calculations consider the cable to be rigid and the load rigidly attached to the cable, which indicates that the direction vector along the cable is equivalent in either the load or cable coordinate system, as shown in Figure 8-2. Then, resolving the cable direction ($\hat{c}_z$ and $\hat{l}_z$) into inertial coordinates using both the load Euler angles and the aircraft-aligned heading cable-angle transformation gives:

$$ {}^{N}R^{H} * {}^{H}R^{C} * \begin{bmatrix} 0 \\ 0 \\ 1 \end{bmatrix}_{\hat{c}_x,\hat{c}_y,\hat{c}_z} = {}^{N}R^{L} * \begin{bmatrix} 0 \\ 0 \\ 1 \end{bmatrix}_{\hat{l}_x,\hat{l}_y,\hat{l}_z} \tag{8.1} $$

The key coordinate systems are shown in Figure 8-2, and described in Table 8-1.

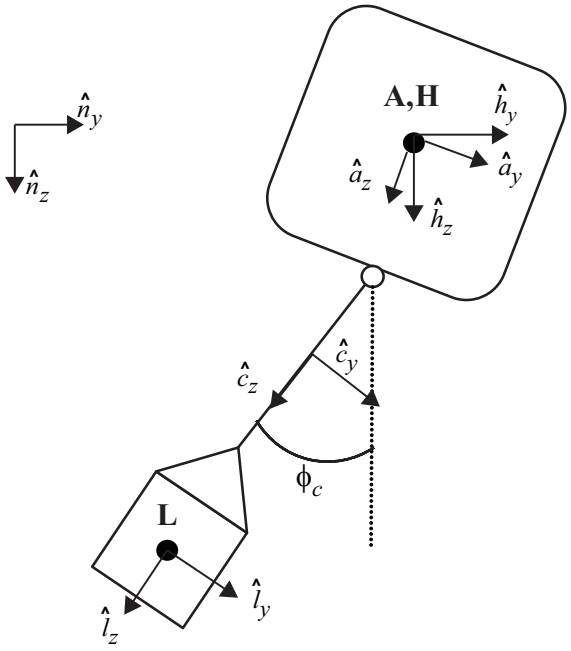

(a) View from behind

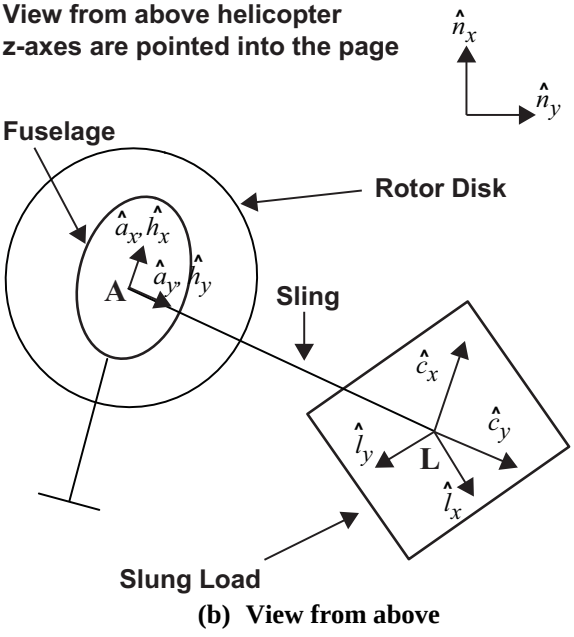

(b) View from above

Figure 8-2. Coordinate systems for cable angle feedback.

Table 8-1. Definition of reference frames.

Reference Frame	Description	Details
N	Inertial Frame	Standard inertial frame
H	Aircraft Level Heading Frame	Aligned with aircraft heading, but does not pitch or roll
A	Aircraft Body Axis Frame	Yaws, pitches and rolls with the aircraft
C	Cable Frame	Aligned with the cable (does spin relative to the aircraft)
L	Load Body Frame	Yaws, pitches and rolls with the load

${}^{N}R^{H}$ represents the rotation/transformation matrix from aircraft level heading (H) coordinate system to the inertial coordinate system (N). The level heading coordinate system is aligned with the aircraft heading, but does not pitch or roll with the fuselage.

$$ {}^{N}R^{H} = \begin{bmatrix} C_{\psi} & -S_{\psi} & 0 \\ S_{\psi} & C_{\psi} & 0 \\ 0 & 0 & 1 \end{bmatrix} \tag{8.2} $$

Herein a short notation is used for sine and cosine, where for example $S_{\psi} \equiv \sin\psi$ and $C_{\psi} \equiv \cos\psi$.

${}^{H}R^{C}$ represents the transformation matrix from the cable frame (C) to the aircraft level heading coordinate frame (H) and ${}^{N}R^{L}$ represents the rotations between the load frame (L) and the inertial coordinate frame (N). The load frame spins with the load body, whereas the cable coordinate system is aligned with the aircraft heading as shown in Figure 8-2.

$$ {}^{H}R^{C} = \begin{bmatrix} C_{\theta_c} & S_{\phi_c}S_{\theta_c} & C_{\phi_c}S_{\theta_c} \\ 0 & C_{\phi_c} & -S_{\phi_c} \\ -S_{\theta_c} & S_{\phi_c}C_{\theta_c} & C_{\phi_c}C_{\theta_c} \end{bmatrix} \tag{8.3} $$

$$ {}^{N}R^{L} = \begin{bmatrix} C_{\theta_l}C_{\psi_l} & S_{\phi_l}S_{\theta_l}C_{\psi_l} - C_{\phi_l}S_{\psi_l} & C_{\phi_l}S_{\theta_l}C_{\psi_l} + S_{\phi_l}S_{\psi_l} \\ C_{\theta_l}S_{\psi_l} & S_{\phi_l}S_{\theta_l}S_{\psi_l} + C_{\phi_l}C_{\psi_l} & C_{\phi_l}S_{\theta_l}S_{\psi_l} - S_{\phi_l}C_{\psi_l} \\ -S_{\theta_l} & S_{\phi_l}C_{\theta_l} & C_{\phi_l}C_{\theta_l} \end{bmatrix} \tag{8.4} $$

where ϕ_c and θ_c are the cable Euler angles with respect to the level heading frame. ϕ_l, θ_l, and ψ_l are the load Euler angles with respect to the inertial frame.

In this case, the aircraft heading and the load Euler angles are the measured quantities on the aircraft. Rearranging known quantities to the right half side of Eq. (8.1) gives:

$$ {}^{H}R^{C} * \begin{bmatrix} 0 \\ 0 \\ 1 \end{bmatrix}_{\hat{c}_x,\hat{c}_y,\hat{c}_z} = {}^{H}R^{N} * {}^{N}R^{L} * \begin{bmatrix} 0 \\ 0 \\ 1 \end{bmatrix}_{\hat{l}_x,\hat{l}_y,\hat{l}_z} \tag{8.5} $$

Which is equivalent to:

$$\begin{bmatrix} C_{\phi_c} S_{\theta_c} \\ -S_{\phi_c} \\ C_{\phi_c} C_{\theta_c} \end{bmatrix} = \begin{bmatrix} C_\psi & S_\psi & 0 \\ -S_\psi & C_\psi & 0 \\ 0 & 0 & 1 \end{bmatrix} * \begin{bmatrix} C_{\phi_l} S_{\theta_l} C_{\psi_l} + S_{\phi_l} S_{\psi_l} \\ C_{\phi_l} S_{\theta_l} S_{\psi_l} - S_{\phi_l} C_{\psi_l} \\ C_{\phi_l} C_{\theta_l} \end{bmatrix} \tag{8.6}$$

Solving for the cable angles gives the required angles for feedback, in terms of the measured load Euler angles and aircraft heading:

$$\phi_c = \sin^{-1}\left(-\begin{bmatrix} -S_\psi & C_\psi & 0 \end{bmatrix} * \begin{bmatrix} C_{\phi_l} S_{\theta_l} C_{\psi_l} + S_{\phi_l} S_{\psi_l} \\ C_{\phi_l} S_{\theta_l} S_{\psi_l} - S_{\phi_l} C_{\psi_l} \\ C_{\phi_l} C_{\theta_l} \end{bmatrix} \right) \tag{8.7}$$

$$\theta_c = \tan^{-1}\left(\frac{\begin{bmatrix} C_\psi & S_\psi & 0 \end{bmatrix} * \begin{bmatrix} C_{\phi_l} S_{\theta_l} C_{\psi_l} + S_{\phi_l} S_{\psi_l} \\ C_{\phi_l} S_{\theta_l} S_{\psi_l} - S_{\phi_l} C_{\psi_l} \\ C_{\phi_l} C_{\theta_l} \end{bmatrix}}{\begin{bmatrix} 0 & 0 & 1 \end{bmatrix} * \begin{bmatrix} C_{\phi_l} S_{\theta_l} C_{\psi_l} + S_{\phi_l} S_{\psi_l} \\ C_{\phi_l} S_{\theta_l} S_{\psi_l} - S_{\phi_l} C_{\psi_l} \\ C_{\phi_l} C_{\theta_l} \end{bmatrix}} \right) \tag{8.8}$$

It is simple to transform the load referenced angular velocities to give the cable angle rates in the cable axes, with the transformation between load and cable coordinates:

$${}^{C}R^{L} = \begin{bmatrix} \cos\Delta\psi & \sin\Delta\psi & 0 \\ -\sin\Delta\psi & \cos\Delta\psi & 0 \\ 0 & 0 & 1 \end{bmatrix} \tag{8.9}$$

where $\Delta\psi = \psi - \psi_l$.

Then the inertial cable rates are calculated from the measured load angular rates:

$$\begin{bmatrix} p_c \\ q_c \\ r_c \end{bmatrix}_{\hat{c}_x, \hat{c}_y, \hat{c}_z} = {}^{C}R^{L} * \begin{bmatrix} p_l \\ q_l \\ r_l \end{bmatrix}_{\hat{l}_x, \hat{l}_y, \hat{l}_z} \tag{8.10}$$

8.3 Elimination of Load-Sling Interaction Modes

The measurement of the load motion from the EGI on the load is particularly sensitive to any rocking motion of the load. These motions are measured as a load angular rate or attitude, but are not the pendular motions that the control system was designed to damp out. Once the EGI measurements of load angle are transformed to cable angles (which are in an axis system that is aligned with the aircraft heading) using the equations described in Sec. 8.2, these rocking motions show up as unwanted "noise" in the cable angles and rates. This "noise" would occur for any sensor located on the load (another example would be

a vision based sensor that tracks markings on the load [59, 60]), but can be minimized by taking measurements at the hook as in the case of the unmanned K-MAX [17] or by developing a method to remove this effect from the measured data, which is the approach taken herein.

The natural frequency of this rocking motion can be estimated by using a simple model of the sling that is modeled not as a single massless rigid cable, but instead as a cable with mass that is divided, for example, into three segments as shown in Figure 8-3. The resulting modes that arise from this model are a pendular mode and two sling modes. The linear equations of this system are:

$$\begin{bmatrix} 1 & 0 & 0 & 0 & 0 & 0 \\ 0 & l/3 & 0 & 0 & 0 & 0 \\ 0 & 0 & 1 & 0 & 0 & 0 \\ 0 & 2l/3 & 0 & l/3 & 0 & 0 \\ 0 & 0 & 0 & 0 & 1 & 0 \\ 0 & l & 0 & 2l/3 & 0 & l/3 \end{bmatrix} \begin{bmatrix} \dot{\phi}_1 \\ \ddot{\phi}_1 \\ \dot{\phi}_2 \\ \ddot{\phi}_2 \\ \dot{\phi}_3 \\ \ddot{\phi}_3 \end{bmatrix} = \begin{bmatrix} 0 & 1 & 0 & 0 & 0 & 0 \\ -g & 0 & g(m_2+m_L)/m_1 & 0 & 0 & 0 \\ 0 & 0 & 0 & 1 & 0 & 0 \\ -g & 0 & -g & 0 & gm_L/m_2 & 0 \\ 0 & 0 & 0 & 0 & 0 & 1 \\ -g & 0 & -g & 0 & -g & 0 \end{bmatrix} \begin{bmatrix} \phi_1 \\ \dot{\phi}_1 \\ \phi_2 \\ \dot{\phi}_2 \\ \phi_3 \\ \dot{\phi}_3 \end{bmatrix} \tag{8.11}$$

This model of Eq. (8.11) can be extended to divide the sling into as many (N) segments as desired. As shown in Figure 8-4, four masses (N=5 segments) are sufficient to accurately predict the first pendulum mode as well as the two sling modes. The model was compared against the flight data for N=1:500 sling segments to determine if further accuracy could be achieved. Ultimately the first two sling mode frequencies are largely unaffected by the inclusion of additional segments (beyond N=5), and therefore did not provide improved agreement. The model natural frequencies correlate well to the peaks in the power spectral density of the angular rate responses of the load from the flight data in Figure 8-4. The model predicts that the sling mode frequencies change slightly with the load weight (1000lb vs. 5000lb), which is consistent with the flight data. Additionally, the frequency separation between the pendulum mode and the sling modes indicate that it was a reasonable assumption to design the control system with a model that does not include sling dynamics.

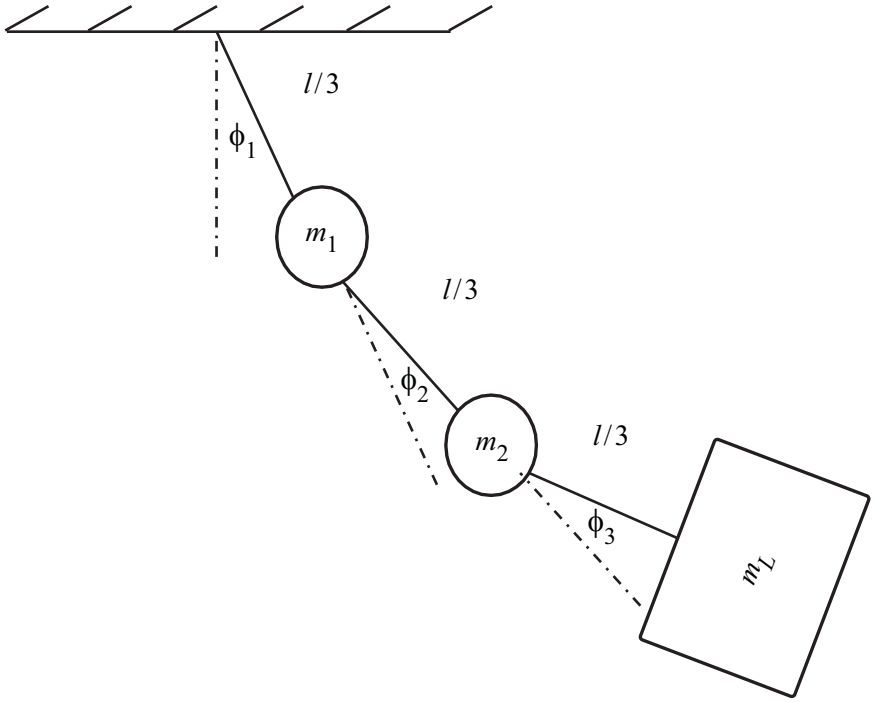

Figure 8-3. Sling model with 3 segments.

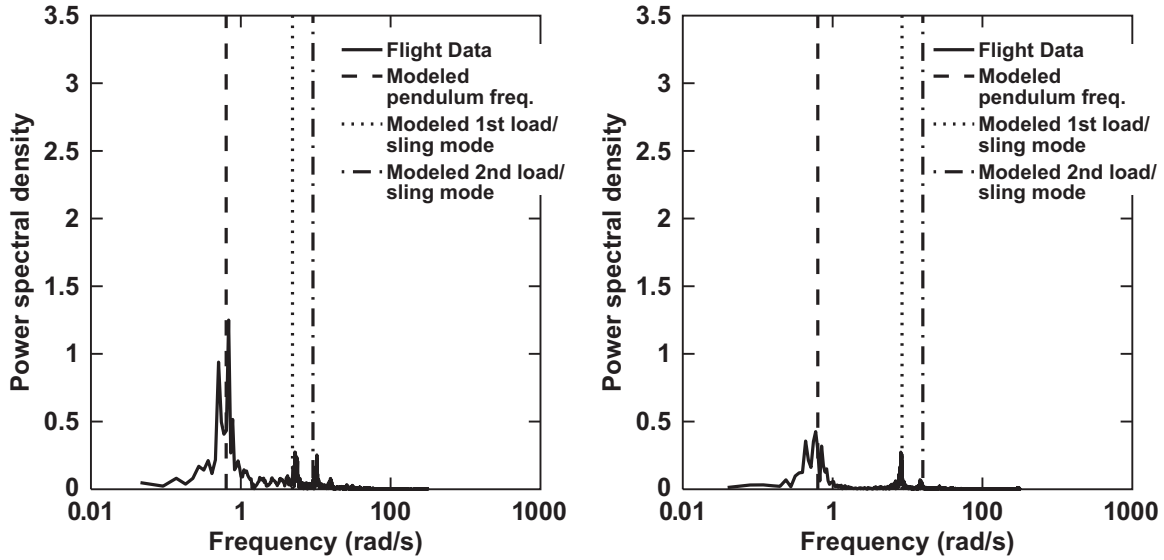

(a) 1000lb load, 4 mass model **(b) 5000lb load, 4 mass model**

Figure 8-4. Comparison of sling power spectral density from flight data, as compared to model.

These data in Figure 8-4 indicate that it is essential to eliminate the load rocking components from the cable angle measurements due to the frequency content. The first sling mode is not a desirable frequency to feedback, considering that it is near the coupled roll-flap mode for the UH-60A at ~6 rad/s (Sec. 2.2.4). This is also the frequency range in which the pilot would be very aware of additional uncommanded motions [61]. However, this motion is at too low a frequency to filter out using a low pass filter, which would add considerable lag to the load feedbacks. It would be possible to put a narrow notch filter, which

would reduce lag, but would have to be scheduled with load mass and sling length, since these two parameters affect the frequency of this mode quite strongly. Since neither a low pass nor notch filter are practical for this case, a simple estimator was designed to smooth the load measurements. The estimator uses measured load motions as well as aircraft accelerations, and requires knowledge of sling length (*l*). It is based on simple linear pendulum equations of motion, for a pendulum with an accelerating origin ($\ddot{x}_H$):

$$m_L(\ddot{x}_H + \dot{q}_c l) = -m_L g * \sin\theta_c \tag{8.12}$$

The sling degrees of freedom from Eq. (8.11) are not included in Eq. (8.12) because it is desired to ultimately eliminate these motions from the estimated load response. The linear state-space model of Eq. (8.12) is implemented in the estimator, and uses the acceleration of the hook (where the load attaches to the fuselage) as an input and the pendular motions of the load as outputs:

$$\begin{bmatrix}\dot{q}_c \\ \dot{\theta}_c\end{bmatrix} = \begin{bmatrix}0 & -g/l \\ 1 & 0\end{bmatrix}\begin{bmatrix}q_c \\ \theta_c\end{bmatrix} + \begin{bmatrix}-1/l \\ 0\end{bmatrix}\begin{bmatrix}\ddot{x}_H\end{bmatrix} \tag{8.13}$$

The hook accelerations are calculated by transferring the measured aircraft accelerations ($\ddot{x}_A$) in aircraft body axes from the CG to the hook with the measured aircraft angular rates ω_A, and the known CG-to-hook geometry $r^{H/A}$. This inertial acceleration is then transformed from the aircraft body axis coordinate system the cable coordinate system with ${}^C R^A$ and $\ddot{x}_H$ is the resulting x-component:

$$\ddot{x}_H = \left[{}^C R^A\left(\ddot{x}_A + \dot{\omega}_A \times r^{H/A} + \omega_A \times \omega_A \times r^{H/A}\right)\right]\cdot \hat{c}_x \tag{8.14}$$

Note that the measured cable angles (with the unwanted sling mode noise) are used to calculate the transformation ${}^C R^A$, but that this does not add significant noise to the estimated cable angles (as seen later in this section).

Then a state-estimator was designed:

$$\dot{\hat{x}} = (\mathbf{F} - \mathbf{LH})\hat{x} + \mathbf{G}u + \mathbf{L}y \tag{8.15}$$

Where:

$$\mathbf{F} = \begin{bmatrix}0 & -g/l \\ 1 & 0\end{bmatrix},\ \mathbf{G} = \begin{bmatrix}-1/l \\ 0\end{bmatrix} \tag{8.16}$$

$$\mathbf{H} = \begin{bmatrix}1 & 0 \\ 0 & 1\end{bmatrix},\ \mathbf{L} = \begin{bmatrix}0.5 & 0 \\ 0 & 0.5\end{bmatrix} \tag{8.17}$$

$$\hat{x} = \begin{bmatrix}\hat{q}_c \\ \hat{\theta}_c\end{bmatrix},\ y = \begin{bmatrix}q_c \\ \theta_c\end{bmatrix} \tag{8.18}$$

$$u = [-\ddot{x}_H] \tag{8.19}$$

The values of the **L** matrix are set very low in order to force the natural frequency of the estimator to be just slightly above the pendulum mode of the load. This ensures that the measured data is used for frequencies at and below the load mode. Then the model, which does not include the sling dynamics, dominates the estimated response at higher frequencies. Note that the washout on the cable angle feedback (see Figure 5-12) eliminates any problem with low frequency drift due to the low gain **L** matrix. This method succeeds in filtering the sling mode "noise" in the EGI data as shown in Figure 8-5. The state-estimator does not introduce lags such as in the heavily filtered raw data shown in Figure 8-5. The heavily filtered data uses a 2nd order Butterworth filter with cutoff frequency of 2 rad/s, which adds approximately 2 seconds of lag and would considerably degrade the stability margins of the CAF system. A similar estimator to that given in Eqs. (8.15)-(8.19) was used in the lateral axis.

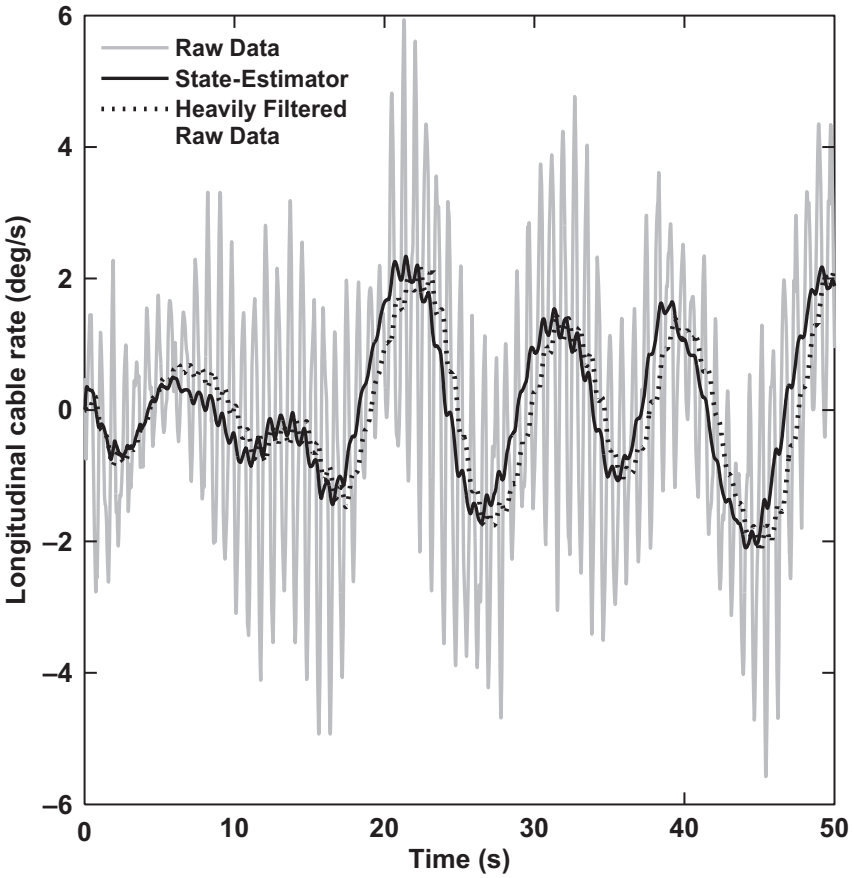

Figure 8-5. Longitudinal cable rate data from flight (5K, 56ft sling).

8.4 Load Bounce Mode Notch Filters

Another source of sensor "noise" which must be considered and addressed is the effect of the load "bounce" mode on the sensed aircraft vertical motion quantities. The load-sling dynamics also have a vertical mode where the sling stretches and contracts, similarly to a spring. This mode is at approximately 14.5 rad/s for the load configuration that was flown (5000lbs, 56ft sling), as seen in the autospectrum of

the vertical velocity in Figure 8-6. The initial flight tests of the control laws did not include a notch filter to eliminate this mode from the vertical velocity feedback. Consequently, this caused the load bounce mode to be fed-back through the collective in the vertical velocity command mode and altitude hold mode, resulting in small but very lightly damped oscillations at this frequency. The pilots could detect this vibration and found it unsettling. The oscillations were eliminated by including a notch filter (F_{notch}) on the vertical velocity feedback path:

$$F_{notch} = \frac{s^2 + 2(0.01)(14.5)s + (14.5)^2}{s^2 + 2(0.6)(14.5)s + (14.5)^2} \tag{8.20}$$

The notch filter was designed to be fairly wide (at the cost of additional phase lag at cross-over) because the frequency range of the load bounce mode was observed to vary from 14.5 to 17 rad/s depending on the load mass and sling length.

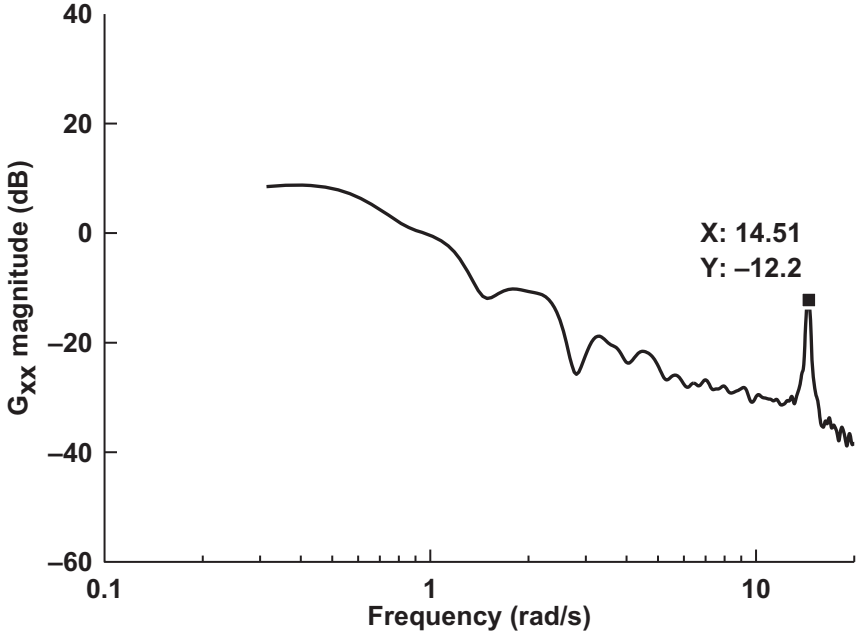

Figure 8-6. Autospectrum for vertical velocity from flight (5K, 56ft sling).

8.5 Radar Altitude Complimentary Filters

Radar altimeters are very noisy sensors. This is exacerbated when an external load is moving in its sensing area. A complimentary filter with integrated vertical velocity (w_{EGI}) from the EGI on RASCAL was developed and worked well to improve the altitude signal (H_{RadAlt}) for the unloaded configuration. A complimentary filter time constant of T_C=6s was found to work well in flight testing without a slung load:

$$H_{Filtered} = H_{RadAlt}\frac{1}{T_C s + 1} + \left(\frac{-w_{EGI}}{s}\right)\frac{T_C s}{T_C s + 1} \tag{8.21}$$

However, with an external load, this filtering is not sufficient when the load swings forward and blocks the radar altimeter. Depending upon on the sling length and altitude, the radar altimeter can jump hundreds of feet when the load swings beneath the radar altimeter. The external load angle measurement is used to change the time constant when the load is sensed to be swinging forward. The time constant is changed from T_C=6s to T_C=50s when the load sensor indicates that the load is swinging forward more than 4 degrees. This approach was used for both the CAF and OBL configurations. Since this does not affect the CAF/OBL comparison, the authors thought it was fair to use the load sensors for complimentary filtering on both configurations to increase safety in the vertical axis. The complimentary filter is beneficial because it does not add lag like a regular low pass filter, but it can become biased (i.e. steady-state error), particularly for large time constants. This is the motivation for switching the time constant with load swing instead of fixing the time constant at a value of T_C=50.

Examples of the raw and filtered signals are shown in Figure 8-7, for the depart-abort maneuver with a 5000lb load. During the maneuver the load swings forward, interfering with the radar, and causing a sharp downward spikes the in the radar altimeter signal at 4 and 11.5 seconds. The complimentary filter is effective at smoothing these spikes.

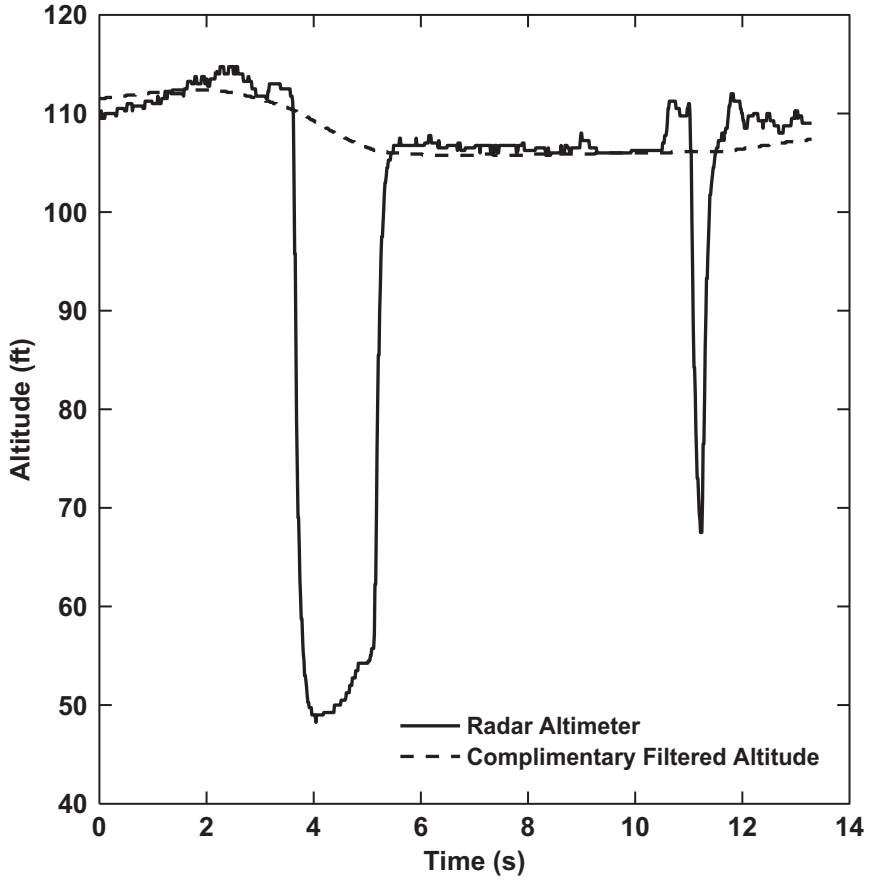

Figure 8-7. Complimentary filtered altitude during depart-abort maneuver in flight (5K, 56ft sling).

8.6 Flight Test Preparation

The flight control system code was generated using SIMULINK™ and RealTimeWorkshop™ auto-coding functionality. The flight control law code was then tested in the RASCAL software-in-the-loop development facility at Moffett Field, CA. The RASCAL development facility (DF) is pictured in Figure 8-8. The DF uses the nonlinear flight validated GENHEL model, described in Sec. 2.2.3, in the simulation of the aircraft dynamics. The flight control code is validated in the nonlinear GENHEL environment with frequency sweeps (similar to the results shown in Sec. 6.1), to ensure that broken loop and closed loop responses are as expected. The DF validation results are also shown later, against flight data and the linear model, in Figure 9-2. The DF uses the flight control computer in the loop, which is loaded with the validated flight control code, and is then used in flight. This ensures that the actual flight control code is tested in the DF, and thus minimizes configuration management problems. The pilot also is required to run through the flight test maneuvers as a practice in the DF before being cleared for flight test.

Figure 8-8. RASCAL software-in-the-loop development facility.

8.7 Summary of Chapter 8

Chapter 8 describes the analyses required to successfully integrate the cable angle/rate feedback control laws into the nonlinear flight environment. The key contributions of Chapter 8 include:

1. Development of equations to convert on-load sensor measurements into cable angles.
2. Design of an estimator to filter the sling modes from the measured on-load data.
3. A complimentary filter that improves the aircraft radar altimeter drop-out due to load swing obscuring the radar.

9 Flight Testing

The previous chapters of this dissertation described the design, simulation, and implementation of the control laws. Chapter 9 is the culmination of this work – flight testing. This is an important milestone because it represents the first time cable angle/rate feedback control laws have been tested in a manned full-authority fly-by-wire system. The flight test environment allows assessment of the validity of performance and handling qualities predictions from simulation. Additionally, flight testing provides concrete results in the form of measured flight responses of the aircraft and load, pilot comments, and handling qualities ratings. Flight testing also ultimately determines if the CAF control system provides an improvement in the ability of the pilot to carry out tasks with the load as compared to the OBL system.

The aircraft used for flight testing of the control system is the RASCAL JUH-60 experimental fly-by-wire helicopter, shown with an external load in Figure 2-1 and described in Sec. 2.1. Flight testing was performed with 1000lb (1K) and 5000lb (5K) external loads, on a 56ft sling. A total of 43.1 hours of flight testing were completed, with four Army experimental test pilots.

First, the responses of the system were validated in flight test using broken and closed-loop frequency responses. Then back-to-back single-blind pilot evaluations of the OBL and CAF designs were performed to determine how handling qualities were affected by cable feedback. The mission task elements (MTEs) that were used for this comparison were lateral reposition, depart-abort, precision hover, and precision load placement. The precision load placement task is a newly proposed MTE that focuses on placing the load on the ground in a precise delivery location.

9.1 Flight Validation

The flight testing began with validation of the flight-measured responses against the model for CAF and OBL using frequency sweeps, for the closed and broken loop responses. The frequency sweeps were input by the pilots for closed loop sweeps. The broken-loop frequency sweeps were injected electronically at the actuator. This method is illustrated by Figure 9-1, where the broken loop response $PH\tau(s)$ is calculated by calculating the frequency response for measured input signal, *i*, and measured output signal, *o* (broken loop = $\frac{-o}{i}(s)$). Note that the pilot is instructed not to put in any inputs during this maneuver such that the broken loop response can be calculated.

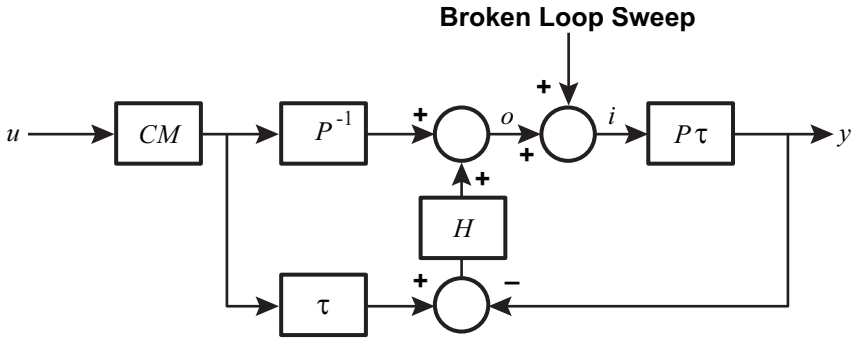

Figure 9-1. Broken loop sweep inputs.

Then, the software CIFER® [45] was used to calculate the flight frequency responses from the data. Finally, the flight frequency responses were compared to the model responses, to ensure that the responses of the closed and broken loop systems were as expected. This ensures that the model of the aircraft and flight control system used to predict stability margins and handling qualities is valid. This validation was performed before formal piloted evaluations, because model validity is critical to interpreting and understanding a correlation between the analytical specifications, and pilot comments/handling-qualities ratings.

9.1.1 Validation Results

The broken loop responses for the 1000lb (1K) and 5000lb (5K) loads were validated in order to ensure the stability margins were consistent with the model predictions. Figure 9-2 shows the 5K broken loop response compared with the linear model for OBL (a) and CAF (b). The broken-loop frequency sweeps were performed in PH mode, so CAF is in Load Damping mode. As shown in the figures, the flight test broken loop responses closely track both the CONDUIT linear model response and the non-linear simulation development facility (DF) response. The DF is a hardware in the loop simulator which uses the GenHel non-linear flight validated model [39] of the UH-60 dynamics (described in Sec. 2.2.3).

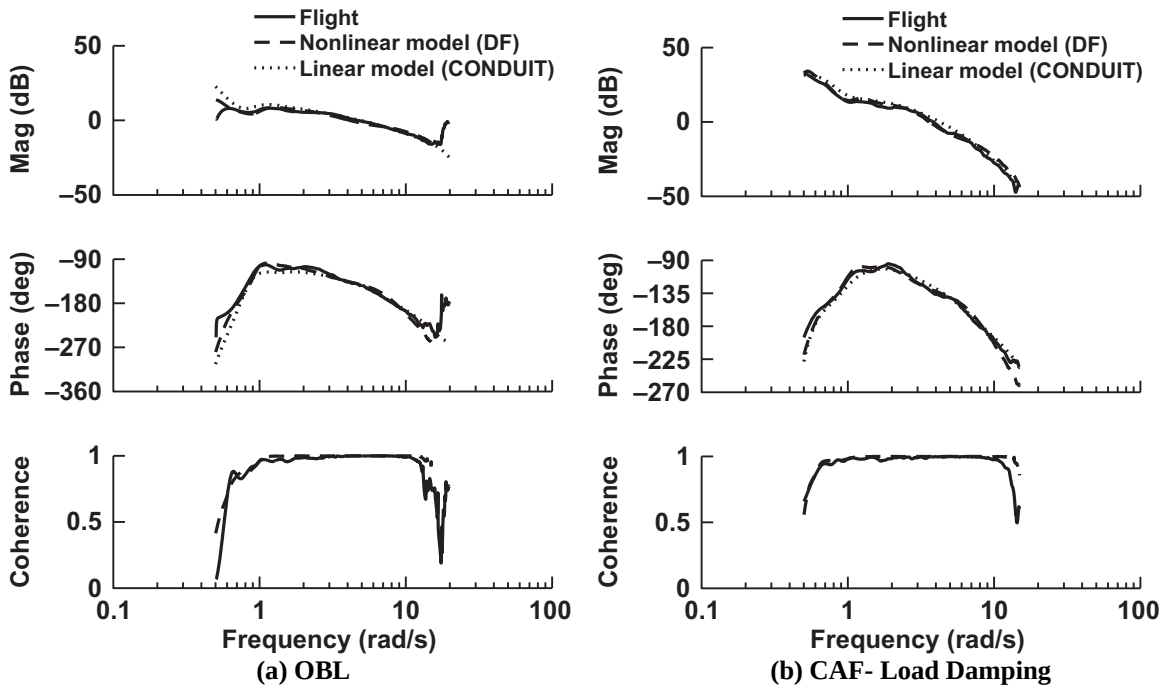

Figure 9-2. Broken loop responses from flight and simulation models (5K, 56ft sling).

The stability margins calculated from the broken loop responses at the actuator were also close to those expected from the model. The stability margins and cross-over frequencies determined from flight are compared to the linear model (CONDUIT®) and the development facility non-linear model (DF) in Table 9-1. The phase margin improvement in flight between the OBL and CAF from 37.77 degrees to 45.39 degrees is very close to the results predicted by the model.

The closed loop responses determined from flight change as expected with cable angle feedback. As an example, the pitch attitude response is shown for the 5K load with OBL and CAF as compared to the command model in Figure 9-3a. As expected, the CAF design for the 5K load has less magnitude and phase distortion as compared to OBL, because CAF is in Pilot Handling mode for piloted inputs. The closed loop CAF response with the 1K load in Figure 9-3b has slightly more distortion than OBL because CAF was optimized for the 5K load configuration. CAF overcorrects for the 1K load, causing some additional distortion in the Pilot Handling mode but more load damping.

Figure 9-4 and Figure 9-5 illustrate improvements in the load damping with CAF relative to OBL for both the 5000lb and 1000lb loads, respectively. The 5000lb load frequency response (ϕ_c) to an actuator chirp in PH mode is shown in Figure 9-4a, with CAF in Load Damping mode. The time response for acceleration to ~20kts and deceleration back to hover is shown in Figure 9-4b. The load damping is improved as the aircraft comes to a hover, as expected with the task tailored control laws (because this is where Load Damping mode is active). Figure 9-5a shows the 1000lb load damping has improved in the frequency domain for CAF in Load Damping mode as compared to OBL. As seen in Figure 9-5b, the load

response has greatly improved for the entire maneuver, as it was nearly undamped for the OBL control laws with this light load.

Table 9-1. Lateral stability margins from flight and models in PH mode (5K, 56ft sling).

Lateral Axis	Optimized Baseline (OBL)			Cable Angle/Rate Feedback (CAF)		
Data Source	Gain Margin (dB)	Phase Margin (deg)	Cross-over (rad/s)	Gain Margin (dB)	Phase Margin (deg)	Cross-over (rad/s)
FLIGHT	6.01	37.77	4.62	8.2	45.39	3.83
DF	5.93	38.46	4.56	7.02	46.53	3.68
CONDUIT	5.95	33.42	5.15	7.47	42.50	4.19

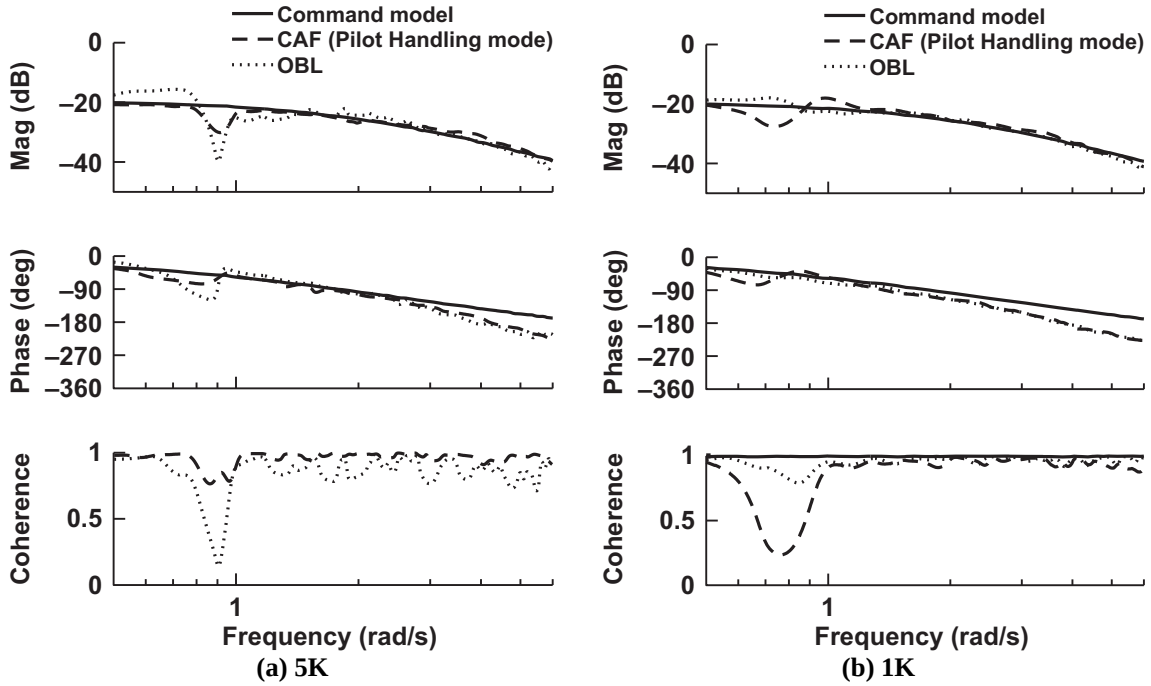

Figure 9-3. Flight closed-loop θ/δ_{lon} responses in attitude command mode (56ft sling).

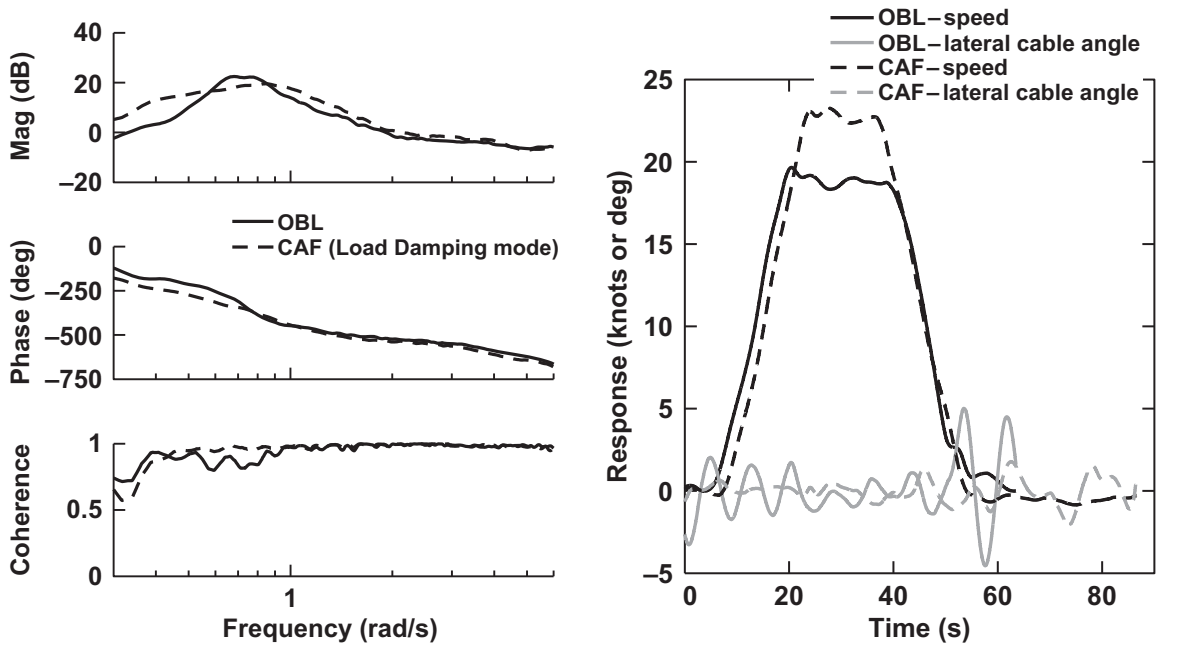

(a) Cable Angle (ϕ_c) Frequency Response **(b) Time Response**

Figure 9-4. Flight load response, position hold mode (5K, 56ft sling).

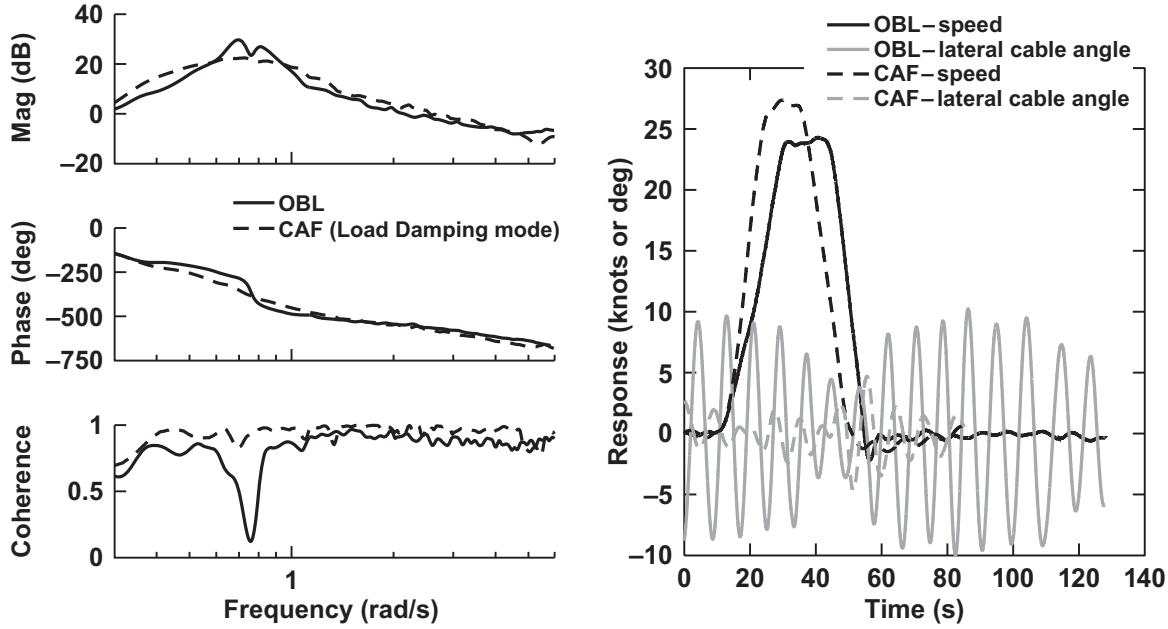

(a) Cable angle (ϕ_c / δ_{lat}) frequency response **(b) Time response**

Figure 9-5. Flight load response, position hold mode (1K, 56ft sling).

9.2 Handling Qualities Evaluations of Mission Task Elements

The military rotorcraft specification ADS-33E-PRF defines a selection of flight test evaluation maneuvers in the form of precisely defined Mission Task Elements (MTEs) [21]. These MTEs are stylized maneuvers which provide a standardized basis for an overall assessment of the rotorcraft's ability to perform certain critical tasks, and result in an assigned handling qualities rating (HQR). To allow for different standards of precision and aggressiveness, the performance standards for each task are listed separately for different rotorcraft categories and for slung load operations in Ref. 21. The handling qualities ratings are assigned based on the Cooper-Harper Rating Scale [32]. The Cooper-Harper Rating scale, which consists of a series of questions and aircraft flying qualities descriptions, helps the pilot determine an HQR in a standardized way. The ratings range from 10 (worst) to 1 (best). The ratings are also categorized into Levels:

- Level 1 for HQR 1-3.5 – 'satisfactory without improvement'
- Level 2 for HQR 3.5-6.5 – 'adequate performance obtainable with tolerable pilot workload'
- Level 3 for HQR 6.5-9 – 'controllable'
- HQR 10 – 'uncontrollable'

The interested reader can see Appendix B for the details of the scale.

Handling qualities evaluations with the OBL and CAF control laws were performed for selected hover/low speed mission task elements (MTEs) from ADS-33E-PRF [21]. These tasks were Hover, Lateral-Reposition, and Depart-Abort because these tasks tend to bring out the negative impact of the presence of a slung load on the HQR [2] and are most relevant to slung load operations. Additionally, a new MTE for precision load placement (described in Sec. 9.2.1) was developed herein and used for evaluation. This new task was developed to provide ADS-33E-PRF with an MTE in that focuses on precision load set-down, a high workload element of slung load operations. It has been proposed by the author that this MTE be included in the next update to ADS-33.

The handling qualities evaluation tests were performed in a single-blind study (e.g. the pilots were not told which control laws they were flying) with back-to-back comparisons between the two control laws, OBL and CAF. Four military experimental test pilots were involved in the flight tests, but only three sets of HQRs were collected for each task (not all pilots flew all tasks). Four tasks were flown: Hover, Lateral Reposition, Depart-Abort and the Load Placement MTE.

9.2.1 Load Placement MTE

The load placement mission task element (MTE) was developed to address the need for a task in ADS-33E-PRF [21] that focuses on load motions and load operations. For example, with a long sling and 1000lb load, the lateral-reposition maneuver for the UH-60 (LMR ~0.06) often causes the load to swing at an amplitude greater than 30 degrees and is nearly undamped. This swinging does not significantly affect the HQR for the conventional aircraft repositioning MTEs because the load is relatively light compared to

the aircraft and thus does not greatly distort the response to pilot inputs for this task. The load placement MTE addresses the motion of the load and how that affects the handling qualities while delivering a lightly damped load to a precise location on the ground within a finite time. The load placement task is described in the bullets below (in the standard ADS-33 format):

- **Objectives.** The objectives of the load placement MTE are to check the ability to translate with, stabilize, and set down an external load at a specific location, within a reasonable time limit. In addition, this task checks the ability to set load down without any residual motion of the load on the ground, such as dragging or swinging.
- **Description of Maneuver.** Initiate the maneuver at a ground speed between 6 and 10 knots, with a load clearance of 20 feet above ground level. The load placement target shall be oriented approximately 45 degrees relative to the heading of the rotorcraft. The load placement target is a ground referenced point, from which the deviation in the set-down point is measured. The ground track should be such that the rotorcraft will arrive over the target point (See Figure 9-6). Once the aircraft is stabilized in a hover over the load placement target, the crew chief will provide verbal instructions to assist the pilot in placing the load. These instructions should follow the form of *direction-count-hold* as in "Right, 3-2-1, hold" or "Down, 3-2-1, hold" to position the load and set it down.
- **Description of the Test Course.** The suggested test course for this maneuver is shown in Figure 9-6. Note that the desired and adequate boxes refer to the load set-down point, not the helicopter position during maneuver.
- **Performance Standards.** Accomplish the transition to hover in one smooth maneuver. It is not acceptable to accomplish most of the deceleration well before the load target point and then creep up to the final position. The load swing should be contained within the desired boundaries (or adequate if trying for adequate performance) before placing the load on the ground. The load should not perceptibly drift, swing, or drag after initial ground contact. All other performance standards are given in Table 9-2.

Table 9-2. Precision load placement Mission Task Element (MTE) standards.

	Externally Slung Load	
	GVE	DVE
Desired Performance		N/A
Attain a controlled hover within X seconds of initiation of deceleration:	10 sec	
Maintain altitude during translation and hover within +/- X ft:	4 ft	
Controlled set-down of external load within X seconds of hover:	50 sec	
Load set-down position should be within a box +/- X ft larger than the footprint of the external load on all sides:	3 ft	
The load should have no perceptible drift at touchdown	√	
Adequate Performance		N/A
Attain a controlled hover within X seconds of initiation of deceleration:	15 sec	
Maintain altitude during translation and hover within +/- X ft:	6ft	
Controlled set-down of external load within X seconds of hover:	120 sec	
Load set-down position should be within a box +/- X ft larger than the footprint of the external load on all sides:	6 ft	

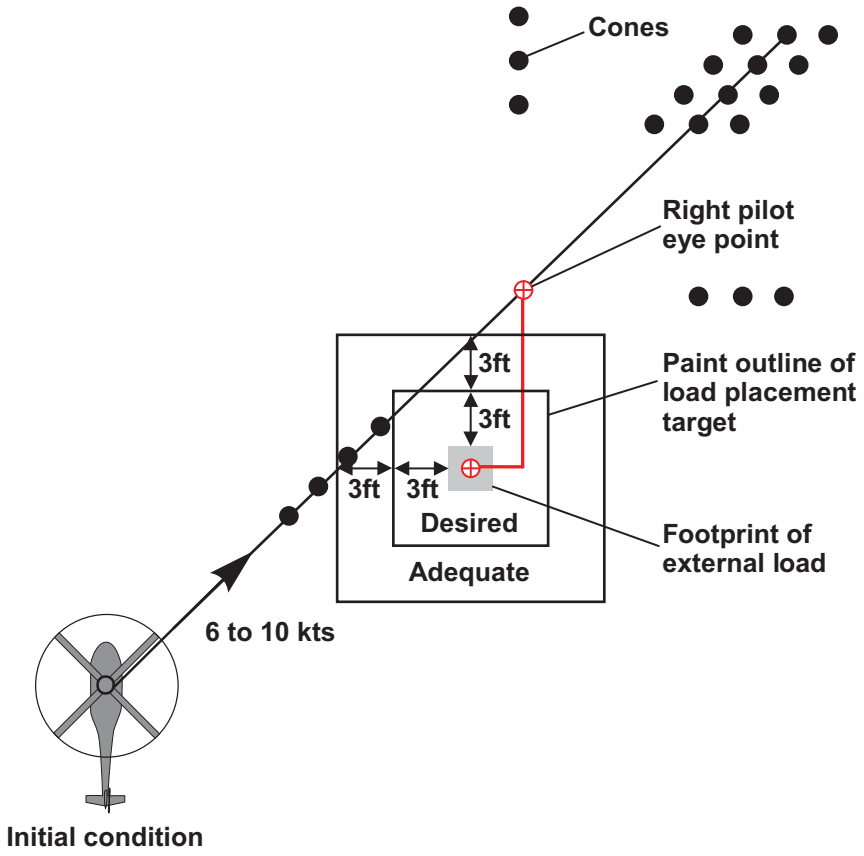

Figure 9-6. Load placement Mission Task Element (MTE) course.

9.2.2 Lateral Reposition and Depart Abort MTEs

The results of the handling qualities evaluations for lateral reposition and depart abort MTEs are shown in Figure 9-7 for the 56ft sling with 1000lb (1K) and 5000lb (5K) external loads. The average ratings are given by the square markers, and the range of individual pilot ratings are shown by the error-bars. From Figure 9-7, it is clear that the control laws were very similar and mostly provided Level 1

Handling Qualities Ratings (HQRs) for these large amplitude maneuvers. Additionally, the pilot cut-off frequencies (Eq. (6.1)) and pilot RMS (full throw +/- 5 inches) shown in Figure 9-8 indicate that there were not significant differences in pilot control strategy.

Handling qualities ratings for the lateral-reposition and depart-abort MTEs were not significantly affected by the presence of CAF, even though the load responses were vastly improved. During these maneuvers, the lateral cable angles were very poorly damped for OBL and well damped for CAF as shown for example runs in Figure 9-9. The overall results for load RMS during these maneuvers are shown in Figure 9-10, indicating that on average CAF had significantly lower load motion for all the maneuvers except the 5K depart-abort. The reason that the 5K depart-abort did not show as great a difference in load motion is due to the pilot skill at timing the maneuver such that the aircraft goes over the load in the end gate, effectively applying damping to the load in OBL and helping to decelerate the aircraft quickly. The pilots are not able to do this for the 1K depart-abort because the load is too light.

These results indicate that the CAF control laws were successful in providing an improved load response while maintaining good handling qualities for these larger-amplitude tasks. Improved HQRs were expected for CAF as compared to OBL because of reduced distortion of the magnitude curve of the piloted response as shown in Figure 9-3. However, there were no significant differences in the HQR for CAF versus OBL for these tasks. The improved distortion of the response in the Pilot Handling mode of CAF may not be large enough to result in a significant difference in task performance. Considering that both systems are in the HQR<4 region of the predicted handling qualities specification, as shown in Figure 7-5, the analysis is consistent with the results here which indicate Level 1 HQRs for both OBL and CAF. Still, there are compelling reasons to use CAF for the Lateral Reposition and Depart Abort tasks; to provide a better behaved load (in the CAF Load Damping mode), and to achieve improved stability margins (in both Pilot Handling and Load Damping modes) as compared to OBL. These are important flight safety improvements to consider.

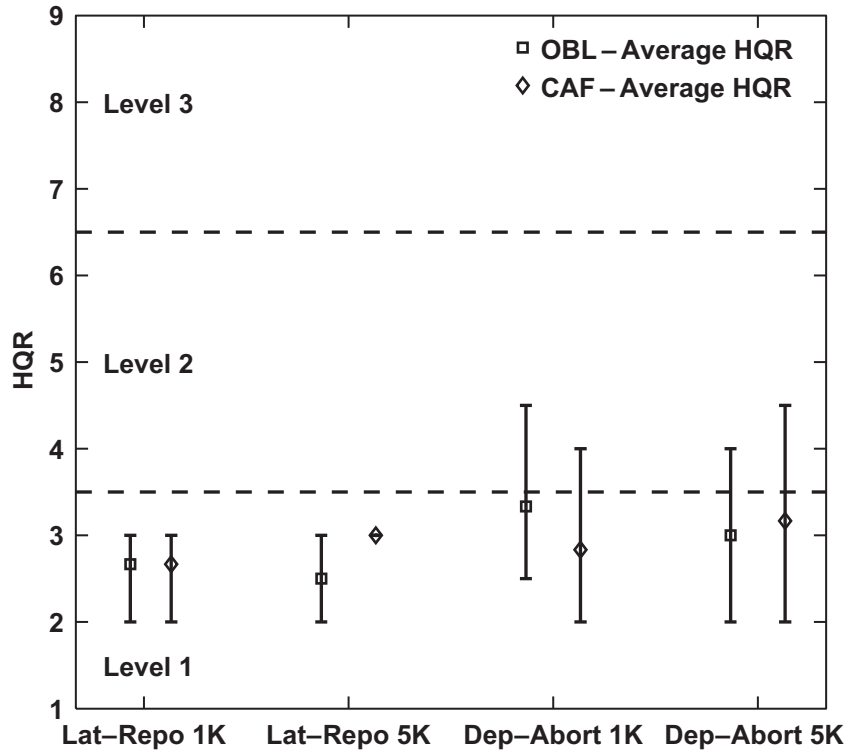

Figure 9-7. Handling qualities ratings for lateral-reposition and depart-abort MTEs (56ft sling).

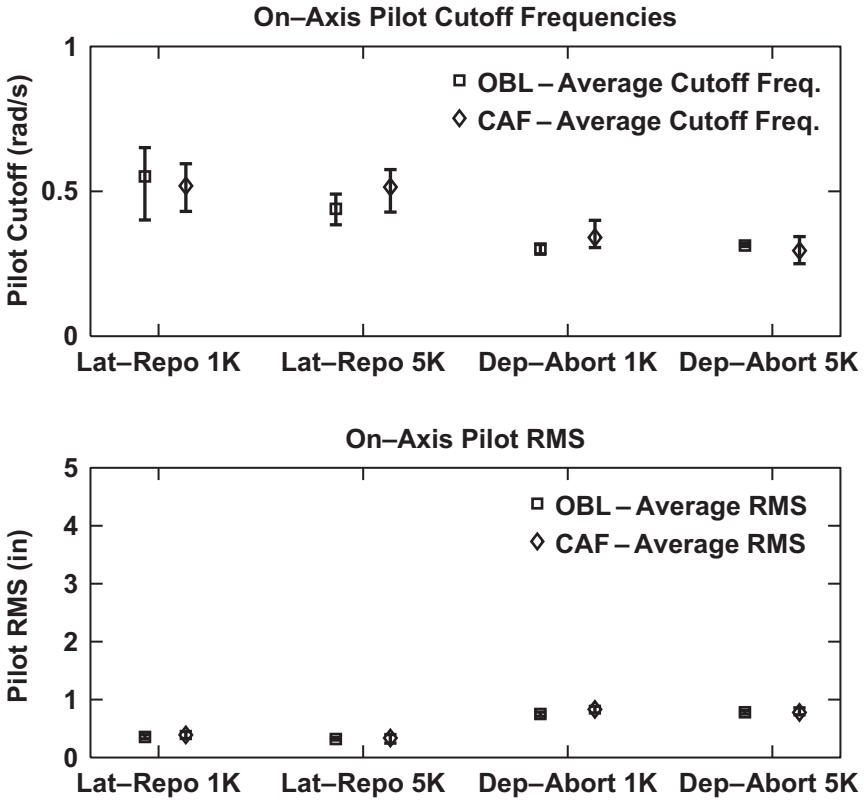

Figure 9-8. Pilot cut-off frequencies and actuator RMS for lateral-reposition and depart-abort MTEs (56ft sling).

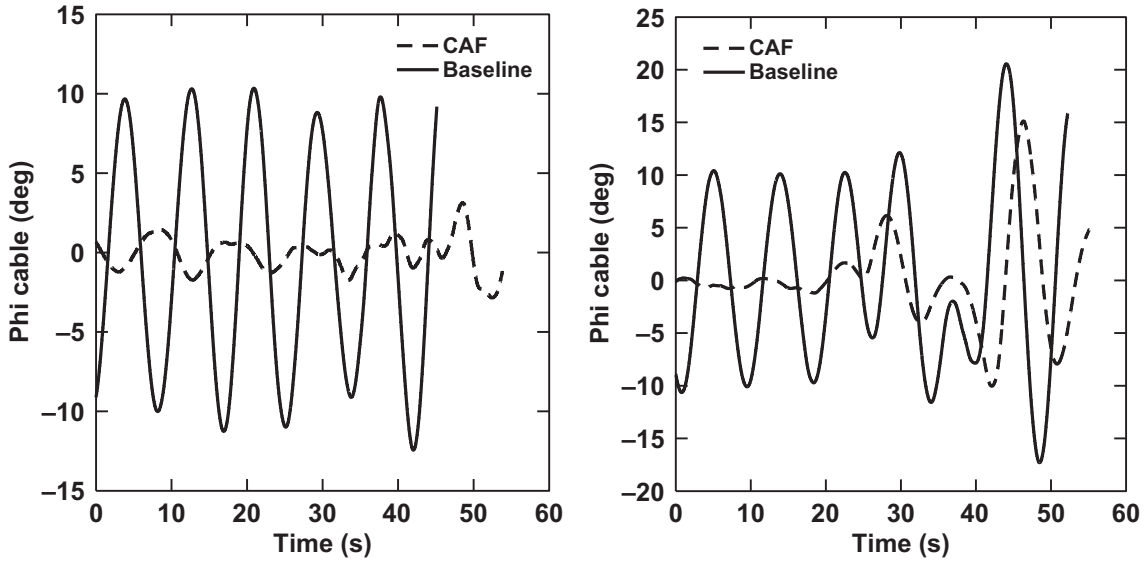

(a) Depart-abort cable angle **(b) Lateral-reposition cable angle**

Figure 9-9. Lateral cable angles (ϕ_c) during MTEs from flight (1K, 56ft).

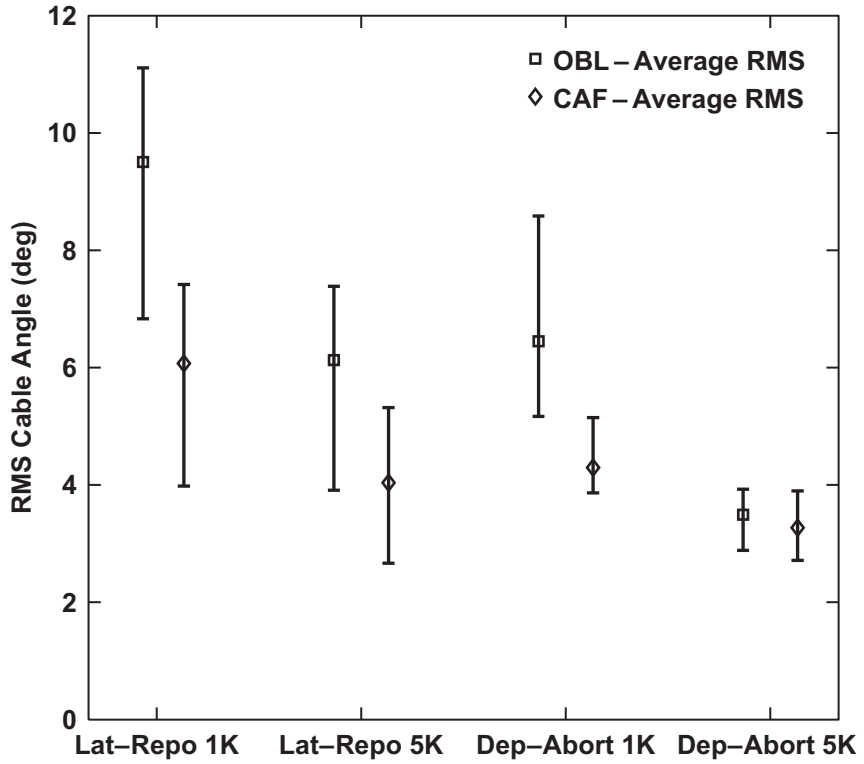

Figure 9-10. Cable Angle RMS for lateral reposition and depart-abort MTEs (56ft sling).

9.2.3 Hover and Load Placement MTEs

The results of the handling qualities evaluations for hover and load placement MTEs are shown in Figure 9-11. The areas where there were key differences in the ratings were for the precision hover task with the heavy load, and for the load placement with the light load. These results show that the key trade-off between load control and aircraft control is important in the handling qualities ratings. The CAF handling qualities rating improved to Level 1 for the load placement task, as compared to Level 2 for OBL. The CAF handling qualities rating for the hover task was slightly worse than the OBL, due to the trade-off between load control and aircraft control as described in the following paragraphs.

The pilot cut-off frequencies are not meaningful for these tasks because the RMS of the pilot inputs is very small, as shown in Figure 9-12. This means that the pilot was mostly relying on the hold modes of the aircraft to complete these tasks, which makes sense because the pilots used velocity hold mode for the run-in and position hold during the hover/load-placement maneuvers. Of course, the pilot is not moving the cyclic stick (it is in detent) during these portions of the task, which explains the low RMS stick values in Figure 9-12. Thus, the responses of the aircraft and load in the hold modes are the key to understanding the pilot ratings. During position hold, which is a critical element of both Hover and Load Placement tasks, the Load Damping mode is active for CAF. Therefore, the Load Damping mode characteristics drive the HQRs for these tasks. The characteristics of the Pilot Handling mode do not significantly affect the HQR because the critical portion of this maneuver is not performed in that mode.

Figure 9-13 explains the degradation in HQRs with CAF for the hover MTE with the 5K load (both systems are Level 2 for this task). For the CAF control laws, during the position maintenance portion of the task, there is a position excursion that exceeds the +/-3 feet requirement, which is caused by the Load Damping mode active in position hold. This causes the pilot to make some corrections in order to stay in the desired hover box, before returning to the position hold mode. In OBL, the pilot could leave the stick in detent and let the position hold mode maintain position without any correction. It is worth noting that the aircraft would typically stay in the adequate box for CAF in position hold mode without input from the pilot (+/- 6ft). The fact that the load is much better controlled for CAF during this hover maneuver does not improve the handling qualities ratings because it is a fuselage-based task.

Figure 9-14 shows that in general, the aircraft motion was larger during the final 30 second hover hold portion of the maneuver for CAF (because the system is also trying to damp the load), even though the pilot stick RMS was similar to OBL (Figure 9-12). This is consistent with simulation results shown in Chapter 7 (Figure 7-11), indicating that the aircraft moves over the load in order to provide load damping, which ultimately causes a greater position excursions with CAF than OBL in position hold mode (which is coincident with Load Damping mode for CAF). This indicates that the aircraft response to pilot inputs did not drive the HQR, but that the position hold performance was the critical element. In Figure 9-14 the 3-sigma position values are roughly on the adequate/desired boundary (+/-3 feet) for the hover maneuver

with CAF, which is consistent with the performance in flight and the degraded HQR. The 3-sigma values for OBL are within desired (less than +/-3 feet), as is also similar to observations from flight. The results of the hover MTE reflect the trade-off made in the Load Damping mode – that more aircraft motion is accepted in order to damp the load.

For the load placement task, the load can be set-down much more quickly and accurately on the ground with CAF. This is made possible by the improved load damping which becomes active in PH mode for the task-tailored control laws. However, this load damping comes at the cost of increased aircraft motion. This is consistent with analytical studies of this control system, as shown in Figure 7-9 and Figure 7-10, which show a clear trade-off between load damping and position maintenance of the fuselage. For the load placement task, two methods were tested for load set-down:

1. 'Low precision' maneuver in which the crew chief tries to predict when the load swings into the desired box and calls for the pilot to put down the load more quickly (but less accurately).
2. 'High precision' maneuver which required the load swing to be inside the desired box (a few feet above the ground) before the crew chief called the load to the ground, which gives higher accuracy but longer load set-down times.

For the low precision version of the task, the times for load set-down were roughly the same for CAF and OBL but the percentage of load deliveries to the desired box was reduced with OBL for both load configurations, as shown in Figure 9-15. The crew chief was required to time the load swing with the set-down for the OBL system, and because the load swing is larger and less predictable this ultimately resulted in fewer deliveries to the desired box than for CAF.

For the high precision load placement, the 1000lb load (which is poorly damped for the OBL design) set-down time is approximately twice as fast with the CAF control laws as compared to OBL, as shown in Figure 9-15. For the 1K high-precision load placement both control laws achieve a higher percentage of desired positioning than for the low-precision method. CAF had a 100% desired performance for the high-precision load placement method for the 1K load. The 5000lb load set-down times are also improved for CAF by 30% as compared to OBL for the high precision maneuver. For the 5000lb load both control systems had 100% desired load placement for the high precision maneuver.

Generally, the pilots preferred the high precision load placement method, as it gave them more information about the load motion, and eliminated the effect of variability in crew-chief skill that determines the placement accuracy in the low precision method. In the future, only the high precision method will be used for the load placement MTE, as written into the task in Sec. 9.2.1.

The handling qualities ratings in Figure 9-11 reflect the improvements for load placement with CAF. The 1000lb load HQR improved from Level 2 in OBL to Level 1 with CAF. Based on these results, the CAF task-tailored control law was successfully optimized for the load placement task (not the hover task)

to address this high workload aspect of slung load operations, and results in significant improvements for this task.

The relationship between load set-down time and increased load damping for the high precision load placement is further illustrated by Figure 9-16. The load motions are much more controlled for the CAF control laws and so the load set-down can be achieved more rapidly. Pilot comments indicate this is the reason for the improved HQR with the CAF control laws for the load placement task.

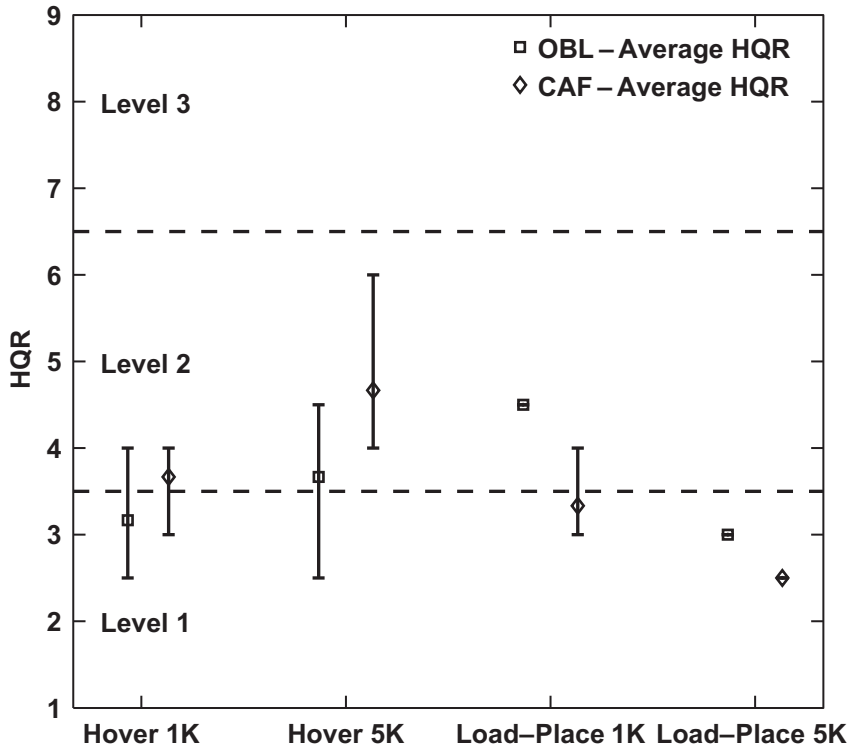

Figure 9-11. Handling qualities ratings for hover and load placement MTEs (56ft sling).

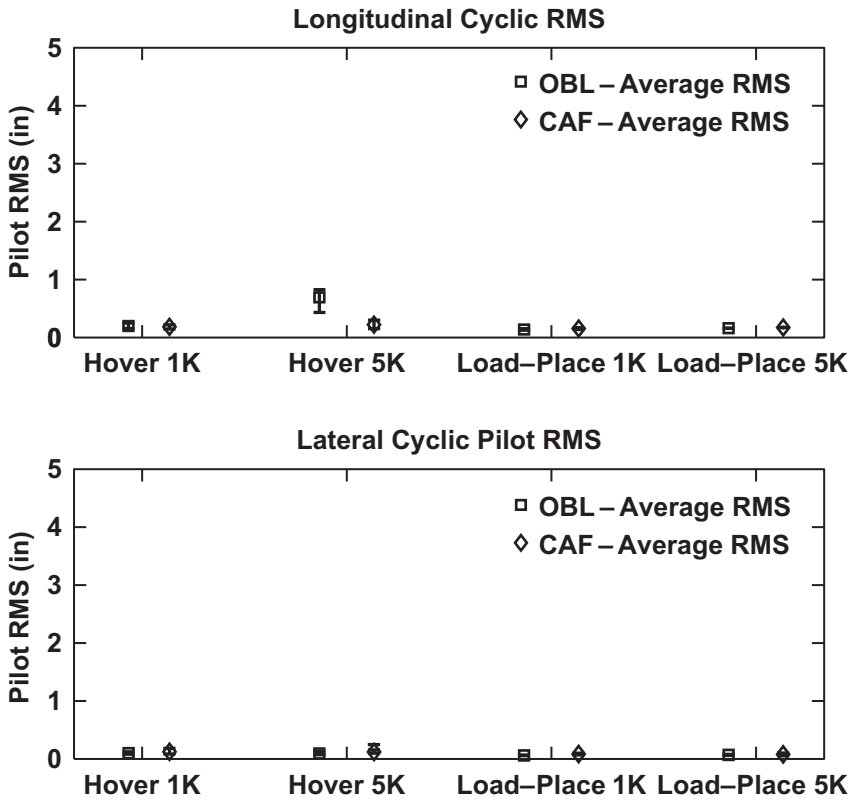

Figure 9-12. Pilot RMS for hover and load placement MTEs (56ft sling).

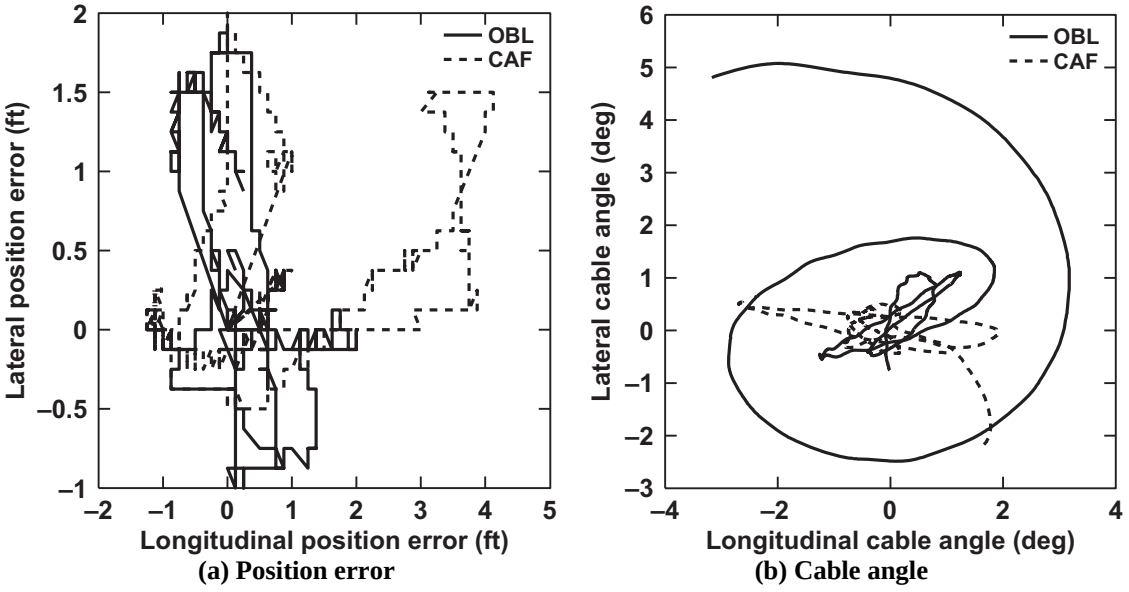

Figure 9-13. Hover MTE responses from flight (5K, 56 ft sling).

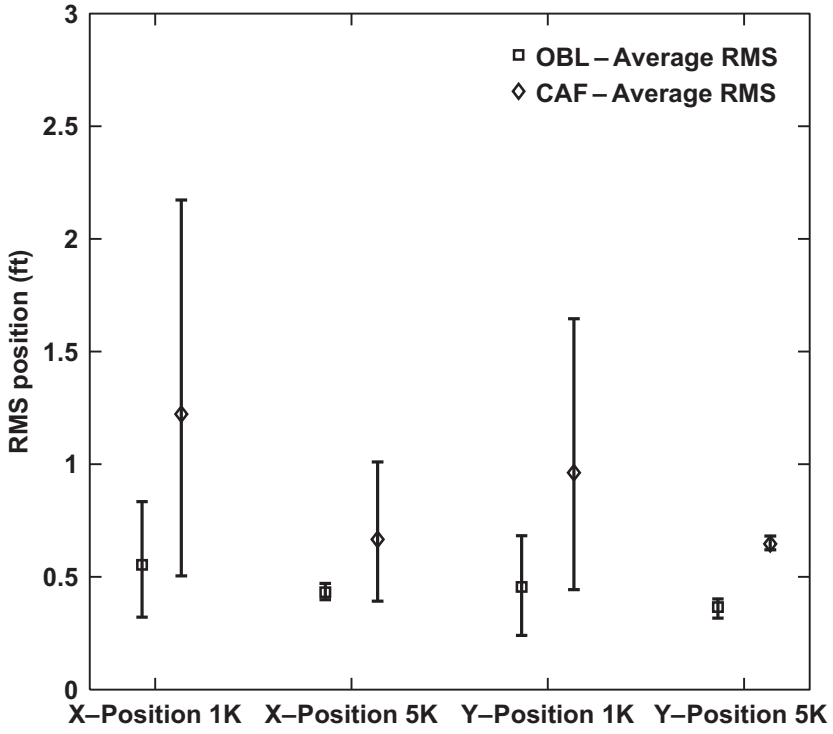

Figure 9-14. Position RMS during hover maneuver.

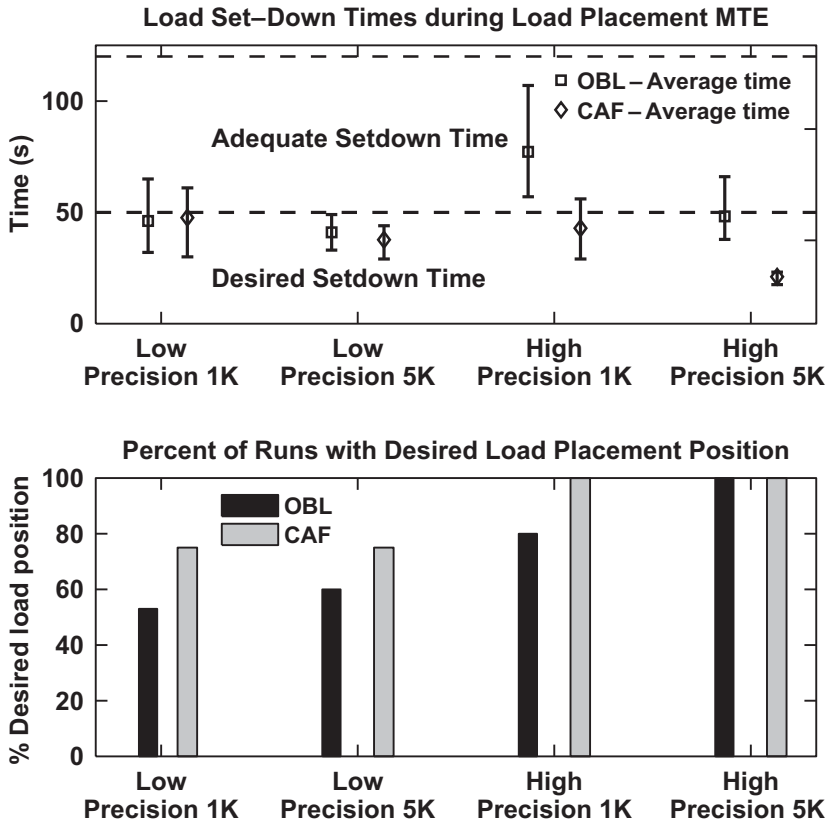

Figure 9-15. Load placement MTE performance (56ft sling).

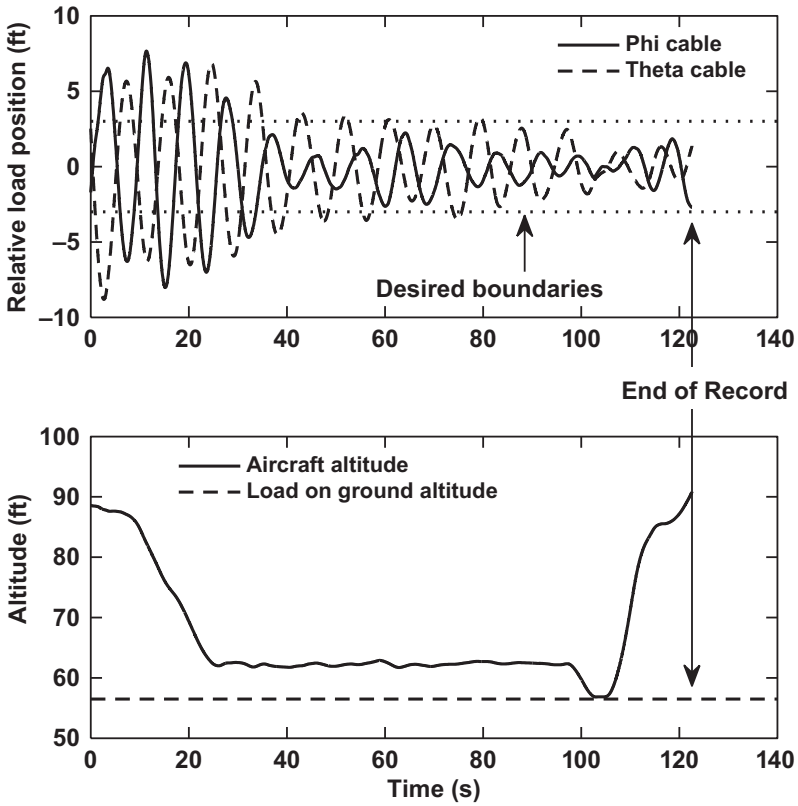

(a) OBL

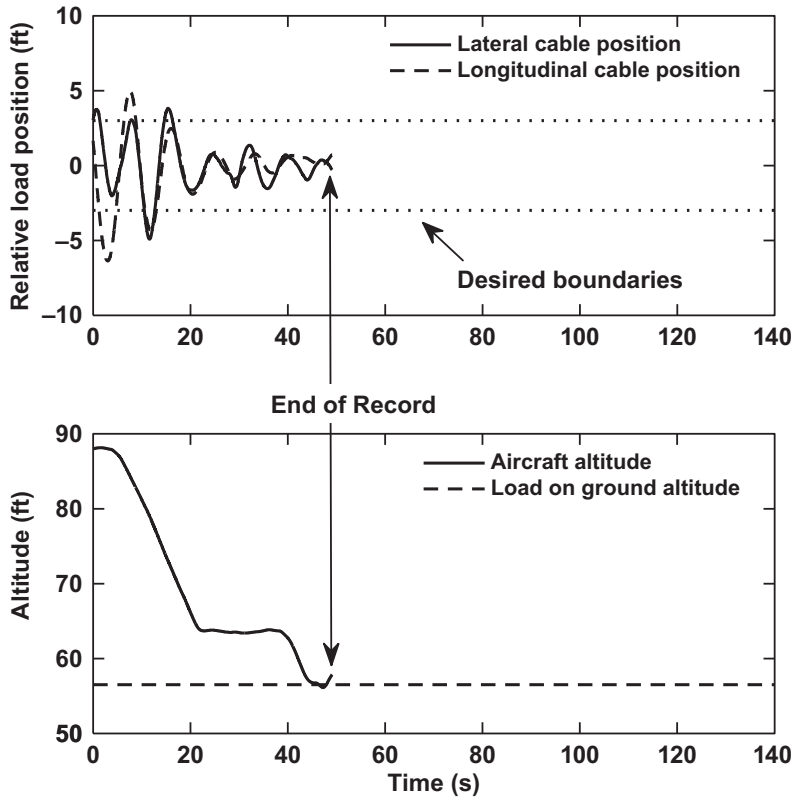

(b) CAF

Figure 9-16. Precision load Placement MTE responses from flight (1K, 56ft sling).

9.3 Summary of Chapter 9 – Discussion of Flight Results

The handling qualities ratings were similar for the depart-abort and lateral reposition tasks with CAF vs. OBL, and both systems were well within Level 1 (HQR<3.5). The result was not expected given the reduction in closed loop attitude distortion that was achieved by the CAF control laws, which was expected to translate to improved handling qualities as compared to OBL. Instead, both OBL and CAF demonstrated good handling qualities for the lateral reposition and depart-abort tasks. However, CAF provided a more controlled load response and improved stability margins, both of which provide improved flight safety. There were also some qualitative improvements noted by the pilots. One of the pilots commented that the key advantage is that "If the pilot stays in the loop a little longer (while the load damping settles down), during initial position capture, the result is a very stable aircraft, without residual oscillations due to the load." This is beneficial in providing the pilot with a more stable attitude response and better damped load behavior, and "could be helpful in degraded visual environments (DVE) to eliminate residual aircraft motion due to load oscillations".

The key drawback of the setup with the CAF task-tailored control laws, which use Load Damping coincident with the position hold mode, was for the precision Hover MTE. As discussed in the previous sections of this dissertation, the Load Damping mode degrades precision position maintenance of the fuselage in position hold to adequate (+/-6 ft) when the load is swinging. One pilot explained this very clearly remarking that "For aircraft maneuvers requiring tight control to capture a position, the workload with CAF was higher, however, CAF was superior for precision load placement." In operational environments, adequate performance for hover-hold may be an acceptable trade-off for improved load damping. The task-tailored CAF control laws provided a very clear improvement in the load placement task, especially for a lightly damped load. The load can be placed on the ground more quickly and with better accuracy using CAF. The operation is also much safer for ground crew because the load is more predictable and has less overall swing. In the future, it may be a better compromise to design the CAF Load Damping mode as a pilot selectable mode so it can be applied only when needed for load placement.

This work was motivated by poor handling qualities of the legacy UH-60A/L aircraft with a long sling and heavy load, as observed in Ref. 2. The CAF task-tailored control laws succeeded in providing improved handling qualities for maneuvering tasks and load placement as compared to the legacy UH-60 control laws, as shown in Table 9-3. (Note that only calm day ratings for precision hover were included in Table 9-3 in order to have a fair comparison with the legacy control law evaluations. One of the pilots performed the precision hover task for OBL and CAF in 12-15kts of wind.)

The legacy (operational) UH-60A/L has a partial authority SAS, which only features a rate command mode. Advanced modes such as altitude hold, velocity hold and position hold in the Optimized Baseline control laws provided a large improvement in the handling qualities as compared to the legacy UH-60A/L for maneuvering tasks, as shown by Table 9-3. However, CAF was required in order to get a major

improvement in the load placement task (Level 2 to Level 1), and also provided improved handling qualities for maneuvering as compared to the legacy UH-60A/L aircraft.

In the words of one of the evaluation pilots "overall, the CAF system is beneficial, but would require additional crew training in order to understand the best way to take advantage of the Load Damping mode." The pilots felt that CAF worked well behind the scenes to provide a more stable external load during low speed maneuvering. The most difficult aspect of external load operations, requiring the highest pilot workload, is the hookup and set-down of the load. The pilots felt that "CAF, when combined with well performing hold modes, effectively drives that workload down to minimal levels."

Table 9-3. Average HQRs for legacy UH-60A/L SAS vs. CAF and OBL (56ft sling).

	LAT REP, 5K	DEPART-ABORT, 5K	HOVER, 5K	LOAD PLACEMENT, 1K
LEGACY	4.50	4.00	4.50	5.00
OBL	2.50	3.00	3.25	4.50
CAF	3.00	3.17	4.00	3.33

10 Conclusions and Future Work

The importance of carrying external loads with helicopters, and the high workload involved with operations near hover calls for improved control systems to help minimize pilot workload during these operations. This dissertation studied the dynamics of the two-body helicopter-load system, evaluated the effects of fuselage and cable feedbacks, designed a task-tailored control system with cable angle/rate feedback, and flight tested the system on an experimental fly-by-wire Black Hawk (JUH-60A) with a slung load. This represented the first time that a modern fly-by-wire manned helicopter was flight tested with cable angle feedback.

10.1 Conclusions

In Chapters 2-6 of this dissertation, the dynamics and simple attitude command control responses of a cable angle/rate feedback control system were studied analytically and in fixed base pilot simulation. Two optimized attitude command cable angle/rate feedback control systems (Load Damping control system and Pilot Handling control system) were compared to a Baseline system (with fuselage feedback only) to determine the benefits that could be achieved as compared to a conventional control system. The following conclusions were reached in this analytical and simulation study:

1. The constrained coupling numerator responses can be expressed in a state-space solution for evaluation of the basic effects of fuselage and cable angle feedback on the helicopter/load coupling dynamics in a multi-loop single-axis feedback system.
2. The drawbacks of the Baseline that uses conventional fuselage feedback control system are degraded predicted handling qualities (HQR <4), and low lateral phase margins near the load mode.
3. Cable rate feedback provides damping to the load response. However, load damping is associated with poor aircraft attitude response and degraded predicted handling qualities.
4. Cable angle feedback combined with fuselage feedback provides improvement in the fuselage response of the aircraft, which improved the predicted handling qualities with an external load, but did not significantly improve load damping.
5. Pilots preferred the Pilot Handling cable angle feedback configuration over the Load Damping configuration in the fixed base simulator for maneuvering tasks. However, the Load Damping configuration was seen as potentially providing improvements in load placement.

In Chapters 7-9, a task-tailored cable angle/rate feedback (CAF) control system was developed in order to switch between Load Damping and Pilot Handling control systems depending upon the flight regime. A well designed Optimized Baseline (OBL) fly-by-wire control law (that does not use cable angle feedback) was developed for comparison with the cable angle system. A blind handling qualities flight-test evaluation was performed with army experimental test pilots on an experimental fly-by-wire Black Hawk helicopter. The following conclusions can be drawn from the results:

1. There is a key trade-off between load damping and piloted handling qualities, which can be exploited with a task tailored control law. This approach effectively mitigated the aircraft/load control problem in flight.
2. Both OBL and CAF control laws significantly improved the handling qualities relative to the legacy UH-60A/L with a partial authority SAS by providing advanced augmentation with hold modes including attitude command/ velocity hold, position hold, and altitude hold. The CAF control laws were required to improve the load placement task to Level 1 performance and the load set-down time was reduced by a factor of 2 for the 1000lb load.
3. The load placement mission task element (MTE) was useful for evaluating the handling qualities associated with the load set-down task. This is an important, high workload task for external load operations that is not captured by the current set of aircraft-focused ADS-33E-PRF tasks.
4. Cable Angle/rate Feedback control laws provided improvements in stability margins, load set-down times and load placement accuracy, as well as improvements in safety to ground personnel as compared to an Optimized Baseline fuselage feedback only control system.

10.2 Future Work

In the future, it would be useful to test the system for alternate sling lengths and load masses. The control system could be optimized to meet the requirements for all sling lengths with somewhat reduced performance, or scheduled for sling lengths. The JUH-60A Black Hawk is limited to 0.25 load mass ratio, but it would be useful to test the control system on a different model helicopter that could carry heavier load-mass-ratios.

The pilot comments and handling qualities results from flight test indicated that a pilot selectable Load Damping mode might allow for good handling qualities for the hover and load placement MTEs. There are multiple configurations that one could imagine for the mechanization of this; a plunger that would damp the load, then returns to the Pilot Handling mode once the load is stable or alternatively a switch that would allow the pilot to toggle between the two modes, etc. It would be interesting to explore various pilot selectable configurations in simulation and flight test in the future.

An area that could follow on to this work would be applying the methods used herein on an on-load actuation method (such as a moving hook or active sway arm). This configuration could allow for decoupling of load damping and handling qualities. The use of both cable angle/rate feedback to the on-load actuator and cable angle/rate feedback to the rotor could be used to maximize handling qualities and load damping simultaneously.

Additionally the development of operationally viable sensors for cable angle feedback should continue to be advanced. This dissertation has demonstrated the benefits of cable angle feedback, and it is a worthwhile effort to develop sensors that would allow the implementation of this type of control system with minimal maintenance and cost.

11 References

[1] Franklin, G.F., Powell, J.D., Emami-Naeini, A., *Feedback Control of Dynamic Systems 6th Ed.*, Pearson Prentice Hall, NJ, 2010, pp. 243 -247.

[2] Lusardi, J.A, Blanken, C.L., Braddom, S.R., Cicolani, L.S., Tobias, E.L., "Development of External Load Handling Qualities Criteria," Proceedings of the American Helicopter Society 66th Annual Forum, Phoenix, AZ, May 11-13 2010.

[3] Manwaring, J.C., Conway, G.A., Garrett, L.C*., Epidemiology and prevention of helicopter external load accidents*, Journal of Safety Research, 1998, Vol. 29, pp. 107-121

[4] Manwaring, J.C., Conway, G.A. "Helicopter Logging in Alaska – Surveillance and Prevention of Crashes," The International Mountain Logging and 11th Pacific Northwest Skyline Symposium, 2001.

[5] deVoogt, A.J., Uidewilligen, S., Eremenko, N.E., *Safety in high-risk helicopter operations: The role of additional crew in accident prevention*, Journal of Safety Science, No. 47, 2009.

[6] Key, D.L., "Analysis of Army Helicopter Pilot Error Mishap Data and the Implications for Handling Qualities," Proceedings of the 25th European Rotorcraft Forum, Rome Italy, Sept. 14-16 1999.

[7] Horcher, A., *Improving Helicopter Yarding with Onboard GPS*, PhD Dissertation, Virginia Polytechnic Institute, April 3 2008.

[8] Couch, M., Lindell, D., "Study on Rotorcraft Safety and Survivability," Proceedings of the American Helicopter Society 66th Annual Forum, Phoenix, AZ, May 11-13 2010.

[9] Garnett, T.S., Jr., Smith, J.H., Lane, R., "Design and Flight Test of the Active Arm External Load Stabilization System," Proceedings of the American Helicopter Society 32nd Annual Forum, Washington D.C., May 10-12 1976

[10] Asseo, S.J., Whitebeck R., *Control Requirements for Sling-Load Stabilization in Heavy Lift Helicopters*, Journal of the American Helicopter Society, 1973.

[11] Gera, J., Farmer, S.W., Jr., "A method of Automatically Stabilizing Helicopter Sling Loads," NASA Technical Note D-7593, July 1974.

[12] Liu, D.T., "In-Flight Stabilization of Externally Slung Helicopter Loads," USAAMRDL Technical Report 73-5, May 1973.

[13] Dukes, T.A., "Maneuvering Heavy Sling Loads Near Hover Part I: Damping the Pendulous Mode," Proceedings of the American Helicopter Society 28th Annual Forum, May 1972.

[14] Gupta, N.K., Bryson, A.E., Jr., "Automatic Control of a Helicopter with a Hanging Load," NASA Contractor Report 136504, June 1973.

[15] Gupta, N.K, Bryson, A.E., Jr., *Near-Hover Control of a Helicopter with Hanging Load*, Journal of Aircraft, Vol. 13, (3), March 1976.

[16] Hutto, A.J., "Flight-Test Report on the Heavy-Lift Helicopter Flight-Control System," Proceedings of the American Helicopter Society 31st Annual Forum, New York, NY, May 1975.

[17] Mconagle, J.G., "The Design, Test, and Development Challenges of Converting the K-MAX Helicopter to a Heavy Lift Rotary Wing UAV," Proceedings of American Helicopter Society 31st Annual Forum, Washington, D.C., May 9-11 2001.

[18] Bisgaard, M., la Cour Harbo, A., Bendtsen J.D., "Input Shaping for Helicopter Slung Load Swing Reduction," AIAA Guidance Navigation and Control Conference, Honolulu, HI, August 2008.

[19] Bisgaard, M., la Cour Harbo, A., Bendtsen J.D., "Swing Damping for Helicopter Slung Load Systems Using Delayed Feedback," AIAA Guidance, Navigation, and Control Conference, Chicago, Illinois, August 2009.

[20] Kang, K., Ottander, J.O., Prasad, J.V.R., Johnson, E., "Active Control of a UAV Helicopter with a Slung Load for Precision Airborne Cargo Delivery," Proceedings of the American Helicopter Society 66th Annual Forum, Phoenix, AZ, 11-13 May 2010.

[21] Anon., *Aeronautical design Standard, Handling Quality Requirements for Military Rotorcraft*, ADS-33E-PRF, U.S. Army Aviation and Missile Command (USAAMCOM), 2000.

[22] Sahasrabudhe, V., et al., "Balancing CH-53K Handling Qualities and Stability Margin Requirements in the Presence of Heavy External Loads," Prodeedings of the American Helicopter Society 63rd Annual Forum, Virginia Beach, VA, May 1-3 2007.

[23] Brenner, H., "Helicopter Sling Load Positioning," Proceedings of the European Rotorcraft 35th Annual Forum, Germany, Sept. 2009.

[24] Brenner,H., "Helicopter Sling Load Pendulum Damping," Proceedings of the European Rotorcraft 35th Annual Forum, Germany, Sept. 2009.

[25] Hamers, M., Bower, G., "Helicopter Slung Load Stabilization Using a Flight Director," Proceedings of the American Helicopter Society 61st Annual Forum, Grapevine, TX, 1-3 June 2005.

[26] Hamers, M., von Hinuber, E., Richter A., "CH53G Experiences with a Flight Director for Slung Load Handling," Proceedings of the American Helicopter Society 64th Annual Forum, Montreal Canada, April 29- May 1st 2008.

[27] DiCarlo, D.J., Kelly, H.L., Yenni, K.R., "An Exploratory Flight Investigation of Helicopter Sling-Load Placements Using a Closed-Circuit Television as a Pilot Aid," NASA TN D-7776, November 1974.

[28] Davis, D.M., Landis, K.H., Leet, J.R., "Development of Heavy Lift Helicopter Handling Qualities for Precision Cargo Operations," Proceedings of the American Helicopter Society 31st Annual Forum, Washington D.C., May 1975.

[29] McRuer, D.T., Ashkenas, I.L., Pass, H.R., "Analysis of Multiloop Vehicular Control Systems," DTIC Report AD434799, April 1964.

[30] McRuer, D., Ashkenas, I., Graham, D., *Aircraft Dynamics and Automatic Control*, Princeton University Press, Princeton, NJ, 1973.

[31] Hoh, et. al, "Development of Handling Quality Criteria for Aircraft with Independent Control of Six Degrees of Freedom," Technical Report AFWAL-TR-81-3027, April 1981, pp 223-226.

[32] Cooper, G. E., Harper, R. P., "The Use of Pilot Rating in the Evaluation of Aircraft Handling Qualities," Report TN-D-5153, April 1969.

[33] Leoni, R.D., *Black Hawk: The Story of a World Class Helicopter*, AIAA, Reston Virginia, 2007.

[34] Moralez III, E., Hindson, W.S., Frost, C.R., Tucker, G.E., Arterburn, D.R., Kalinowski, K.F., Dones, F., "Flight Research Qualification of the Army/NASA RASCAL Variable Stability Helicopter," Proceedings of the American Helicopter Society 58th Annual Forum, Montreal, Canada, June 2002.

[35] Fletcher et al., "UH-60M Upgrade Fly-By-Wire Flight Control Risk Reduction using the RASCAL JUH-60 In-Flight Simulator," Proceedings of the American Helicopter Society 64th Annual Forum, Montreal, Canada, April 29th – May 1st 2008.

[36] Fujizawa, B.T., *Control Law Design and Validation for a Helicopter In-Flight Simulator*, California Polytechnic State University Master's Thesis, San Luis Obispo, CA, February, 2010.

[37] Greenfield, A., et al, "CH-53K Control Law Risk Reduction Flight Testing on the Rascal JUH-60A In-Flight Simulator," Proceedings of the American Helicopter Society 68th Annual Forum, Fort Worth, TX, 1-3 May 2012.

[38] Tyson, P.H., *Simulation Validation and Flight Prediction of UH-60A Black Load Helicopter/Slung Load Characteristics*, Naval Post Graduate School Master's Thesis, Monterey, CA, March 1999.

[39] Howlett, J.J., "UH-60 Black Hawk Engineering Simulation Program: Volume 1 – Mathematical Model," NASA Technical Report CR-166309, 1981.

[40] Cicolani, L. S. "OVERCAST: Extension of FORECAST Linearized Equations to Include Slung Load DOF's," AFDD Internal Memo, POC:luigi.cicolani@us.army.mil, Feb 2009.

[41] Cicolani, L.S., Kanning, G, "Equations of Motion of Slung-Load Systems, Including Multi-lift Systems," NASA Technical Paper 3280, November 1992.

[42] Wolkovitch, J., Jonston, D.E., "Automatic Control Considerations for Helicopter and VTOL Aircraft with and without Sling Loads," STI Technical Report No. 138-1, Hawthorne, CA, November 1965.

[43] Kim, F. D., *Formulation and Validation of High-Order Mathematical Models of Helicopter Flight Dynamics,* Ph. D. Dissertation, University of Maryland, Aug, 1991.

[44] Johnson, W., "Rotorcraft Dynamics Models for a Comprehensive Analysis," Proceedings of the American Helicopter 54th Annual Forum, Washington, DC, 20-22 May 1998.

[45] Tischler, M.B, Remple, R.K., *Aircraft and Rotorcraft System Identification: Engineering Methods with Flight Test Examples 2nd Ed.*, AIAA, Aug 2012.

[46] Hoh, R.H., Mitchell, D.G., Aponso, B.B., Key, D.L, Blanken, C.L., "Background Information and User's Guide for Handling Qualities Requirements for Military Rotorcraft," USAAVSCOM Technical Report 89-A-008, Dec 1989.

[47] Cheng, R.P., *Rotorcraft Flight Control Design Using Quantitative Feedback Theory and Dynamic Crossfeeds*, Master's Thesis, California Polytechnic State University, San Luis Obispo, January 1995.

[48] Hess, R. A., *Coupling Numerators and Input-Output Pairing in Square Control Systems*, Journal of Guidance, Control, and Dynamics, Vol., 26, No. 2, March-April, 2003, pp. 367-368.

[49] Tischler, M.B, Ivler, C.M., Mansur, M.H., Cheung, K.K., Berger, T., Berrios, M., "Handling-Qualities Optimization and Trade-offs in Rotorcraft Flight Control Design," Proceedings of the RAeS Rotorcraft Handling-Qualities Conference, University of Liverpool, U.K., 4-6 Nov 2008.

[50] Horowitz, I., M., *Synthesis of Feedback Systems*, Academic Press, 1963.

[51] Landis, Kennth H. and Glusman, Steven I. "Development of ADOCS Controllers and Control Laws," NASA CR-177339, 1985.

[52] Berger, T., et al., "Longitudinal Control Law Design and Handling Qualities Optimization for a Business Jet Flight Control System," AIAA Atmospheric Flight Mechanics Conference Proceedings, Minneapolis, MN, 13-16 August 2012.

[53] Anon., *Aerospace - Flight Control Systems -Design, Installation and Test of Piloted Military Aircraft, General Specification For*, SAE Aerospace Standard, AS94900, July 2007.

[54] Blanken, C. et al., "Test Guide for ADS-33E-PRF," AMRDEC Special Report AMR-AF-08-07, July 2008.

[55] Duda, H., *Prediction of Pilot-in-the-Loop Oscillations due to Rate Saturation*, Journal of Guidance, Navigation, and Control, Vol. 20, No.3, May-June 1997.

[56] Tischler, M. B., Colbourne, J. D., Morel, M. R, Biezad, D. G., Cheung, K. K., Levine, W. S., and Moldoveanu, V., *A Multidisciplinary Flight Control Development Environment and Its Application to a Helicopter*, IEEE Control System Magazine, Vol. 19, No. 4, August 1999.

[57] Mansur, M.H., Dai, W., *RIPTIDE Installation and User's Guide*, University Affiliated Research Center.

[58] Anon, *Aircraft Internal Time Division Command/Response Multiplex Data Bus*, MIL-STD-1553b, Department of Defense, 21 September 1978.

[59] SBIR Contract # W911W6-10-C-0068, "Airworthy Cable Angle Measurement System For Slung Load Operations," AOS Inc., 2010.

[60] SBIR Contract # W911W6-10-C-0003, "Airworthy Cable Angle Measurement System For Slung Load Operations," Agiltron Inc., 2009.

[61] Hodgkinson, J., *Aircraft Handling Qualities*, AIAA Reston, VA, 1999.

A. Appendix-A

This appendix describes the development of generic nonlinear equations of motion for the helicopter/slung load system, described in Sec. 2.2.1. This model is used to derive the linear model structure described in Sec. 2.2.2. The forces and moments acting on the rotor and tail-rotor are treated as lumped forces and moments. The slung load is treated as a point mass (with no inertia) and the sling as a rigid cable.

Kane's notation is used throughout this section. Some general examples follow:

$r^{B/A}$ - the position vector starting at point A and ending at point B; position of point B relative to point A

${}^{N}V^{B}$ - Velocity of Point B in Reference Frame N

F^{A} - A force applied to body A

${}^{N}\omega^{B}$ - Angular velocity of reference frame B (attached to rigid body B) in reference frame N

A.1 Define Reference Frames

There are 3 relevant reference frames in this derivation:

1. Newtonian (N) (local vertical, north-east-down axes, $\hat{n}_x$, $\hat{n}_y$, $\hat{n}_z$)
2. Aircraft (A) (body axes, $\hat{a}_x$, $\hat{a}_y$, $\hat{a}_z$)
3. Cable (C) (z-axis is aligned with cable, $\hat{c}_x$, $\hat{c}_y$, $\hat{c}_z$)

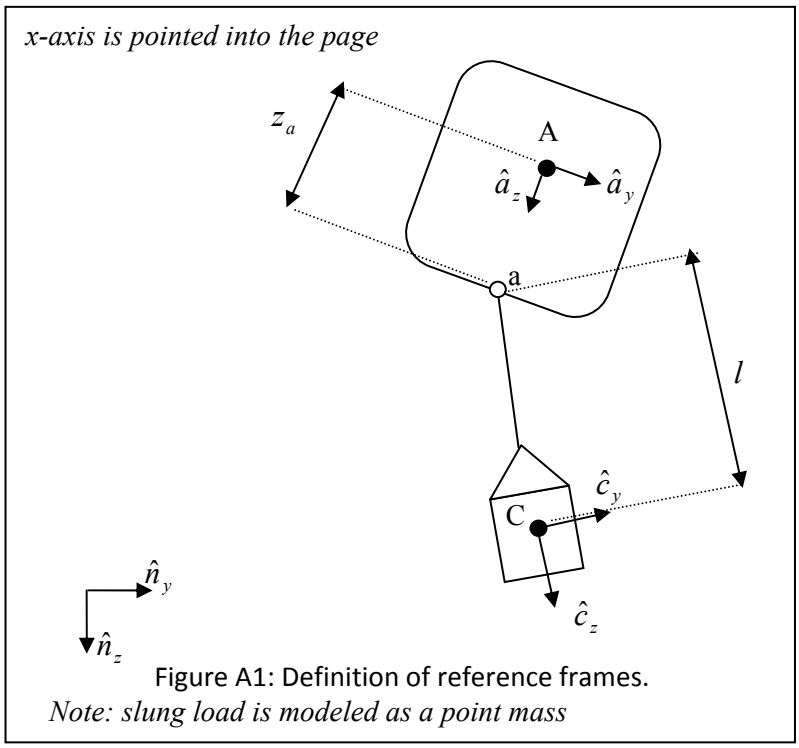

Figure A-1. Slung load geometry.

The rotation matrices give mappings between the two frames with Euler angles. The relationship between the Newtonian and Aircraft frames is defined in the conventional series of rotations: a rotation ψ about the Newtonian Z-axis, then rotation θ about the new rotated Y-axis, and finally a rotation ϕ about the rotated X-axis. This is expressed below:

$$ {}^{N}R^{A} = \begin{bmatrix} \cos\theta\cos\psi & \sin\phi\sin\theta\cos\psi - \cos\phi\sin\psi & \cos\phi\sin\theta\cos\psi + \sin\phi\sin\psi \\ \cos\theta\sin\psi & \sin\phi\sin\theta\sin\psi + \cos\phi\cos\psi & \cos\phi\sin\theta\sin\psi - \sin\phi\cos\psi \\ -\sin\theta & \sin\phi\cos\theta & \cos\phi\cos\theta \end{bmatrix} $$

Where:

$$ \begin{bmatrix} \hat{n}_x \\ \hat{n}_y \\ \hat{n}_z \end{bmatrix} = {}^{N}R^{A} \begin{bmatrix} \hat{a}_x \\ \hat{a}_y \\ \hat{a}_z \end{bmatrix} $$

The relationship between the aircraft reference frame and the cable reference frame is also defined in a series of rotations. To go from aircraft axes to cable axes, first rotate through longitudinal cable angle $\Delta\theta_c$ about the X-axis of the aircraft, and then rotate the lateral cable angle $\Delta\phi_c$ around the rotated Y-axis. The rotation matrix is expressed below in terms of cable angles expressed relative to the aircraft frame:

$$ {}^{A}R^{C} = \begin{bmatrix} \cos\Delta\theta_c & \sin\Delta\phi_c \sin\Delta\theta_c & \cos\Delta\phi_c \sin\Delta\theta_c \\ 0 & \cos\Delta\phi_c & -\sin\Delta\phi_c \\ -\sin\Delta\theta_c & c\sin\Delta\phi_c \cos\Delta\theta_c & \cos\Delta\phi_c \cos\Delta\theta_c \end{bmatrix} $$

Where:

$$ \begin{bmatrix} \hat{a}_x \\ \hat{a}_y \\ \hat{a}_z \end{bmatrix} = {}^{A}R^{C} \begin{bmatrix} \hat{c}_x \\ \hat{c}_y \\ \hat{c}_z \end{bmatrix} $$

And then:

$$ \begin{bmatrix} \hat{n}_x \\ \hat{n}_y \\ \hat{n}_z \end{bmatrix} = {}^{N}R^{A}\,{}^{A}R^{C} \begin{bmatrix} \hat{c}_x \\ \hat{c}_y \\ \hat{c}_z \end{bmatrix} $$

A.2 Aircraft Equations of Motion

F=ma:

Starting from the body-fixed velocities of the aircraft:

$${}^{N}v^{A} = (u)\hat{a}_x + (v)\hat{a}_y + (w)\hat{a}_z$$

Taking the derivative to get acceleration, and then forming F=ma:

$$m_a\,{}^{N}a^{A} = m_A\left(\frac{{}^{A}d}{dt}\left({}^{N}v^{A}\right) + {}^{N}\omega^{A}\times{}^{N}v^{A}\right) = F_G^A + F_{Aero}^A + F_C^A$$

Where:

$${}^{N}\omega^{A} = (p)\hat{a}_x + (q)\hat{a}_y + (r)\hat{a}_z$$

And where aerodynamic and gravity forces on the fuselage are represented by F_{Aero}^A and F_G^A terms, and F_C^A is cable tension T:

$$F_C^A = T\hat{c}_z$$

M=dh/dt:

Starting with the equation for angular momentum:

$$h^A = \underline{\underline{I}}^A \bullet {}^{N}\omega^{A} = (I_{xx}p + I_{xz}r)\hat{a}_x + (I_{yy}q)\hat{a}_y + (I_{zz}r + I_{xz}p)\hat{a}_z$$

Take the derivative of the angular momentum, to get the moment equation:

$$M_{Aero}^A + M_C^A = \frac{{}^{N}d}{dt}\left(h^A\right) = \frac{{}^{A}d}{dt}\left(h^A\right) + {}^{N}\omega^{A}\times h^A$$

Where:

$$M_C^A = r^{b/A}\times T\hat{c}_z + \left(K_{\Delta\theta_c}\Delta\dot{\theta}_c\right)\hat{c}_y + \left(K_{\Delta\phi_c}\Delta\dot{\phi}_c\right)\hat{c}_x$$

Then:

$$(I_{xx}\dot{p} + I_{xz}\dot{r})\hat{a}_x + (I_{yy}\dot{q})\hat{a}_y + (I_{zz}\dot{r} + I_{xz}\dot{p})\hat{a}_z + {}^{N}\omega^{A}\times(I_{xx}p + I_{xz}r)\hat{a}_x + (I_{yy}q)\hat{a}_y + (I_{zz}r + I_{xz}p)\hat{a}_z =$$
$$M_{Aero}^A + \left(K_{\Delta\theta_c}\Delta\dot{\theta}_c\right)\hat{c}_y + \left(K_{\Delta\phi_c}\Delta\dot{\phi}_c\right)\hat{c}_x$$

A.3 Slung Load Equations of Motion

Starting with the equation for the velocity of the point mass slung load in inertial space

$${}^{N}v^{L} = {}^{N}v^{A} + {}^{A}v^{L} + {}^{N}\omega^{A} \times r^{L/A}$$

Where:

$${}^{A}v^{L} = \Delta\dot{x}_c\hat{c}_x + \Delta\dot{y}_c\hat{c}_y$$

And:

$$r^{L/A} = z_a\hat{a}_z + l\hat{c}_z$$

Then taking the derivative of the velocity to get acceleration:

$${}^{N}a^{L} = \frac{{}^{N}d}{dt}({}^{N}v^{L}) = \frac{{}^{N}d}{dt}({}^{N}v^{A}) + \frac{{}^{N}d}{dt}({}^{A}v^{L}) + \frac{{}^{N}d}{dt}({}^{N}\omega^{A} \times r^{L/A})$$

$${}^{N}a^{L} = \frac{{}^{N}d}{dt}({}^{N}v^{L}) = {}^{N}a^{A} + \frac{{}^{C}d}{dt}({}^{A}v^{L}) + {}^{N}\omega^{C} \times {}^{A}v^{L} + \frac{{}^{N}d}{dt}({}^{N}\omega^{A} \times r^{L/A})$$

Finally setting F=ma, where cable forces on the slung load are equal and opposite to the cable forces on the aircraft:

$$m_L\,{}^{N}a^{L} = m_L\left({}^{N}a^{A} + \frac{{}^{C}d}{dt}({}^{A}v^{L}) + {}^{N}\omega^{C} \times {}^{A}v^{L} + \frac{{}^{N}d}{dt}({}^{N}\omega^{A} \times r^{L/A})\right) = F_G^L + F_{Aero}^L - F_C^A$$

Then:

$$\Delta\ddot{x}_c\hat{c}_x + \Delta\ddot{y}_c\hat{c}_y = \left(\frac{F_G^L + F_{Aero}^L - F_C^A}{m_L}\right) - {}^{N}a^{A} - {}^{N}\omega^{C} \times {}^{A}v^{L} - \frac{{}^{N}d}{dt}({}^{N}\omega^{A} \times r^{L/A})$$

The aerodynamic forces on the load are modeled as a drag force with fixed value of $\frac{D}{\bar{q}}$ in the direction of the velocity.

$$F_{Aero}^L = \frac{D}{q}\left(0.5\rho V^2\right)$$

A.4 Solution for Cable Tension

Solve for Cable Tension by assuming an inelastic cable, such that acceleration of the slung load in the $\hat{c}_z$ direction is equal to zero in the cable reference frame. First, solve the slung load equations of motion for the acceleration of the load in the cable reference frame:

$$\frac{{}^{C}d}{dt}({}^{A}v^{L}) = \frac{1}{m_L}\left(F_G^L + F_{Aero}^L - F_{F_y}\hat{c}_y - T\hat{c}_z\right) - {}^{N}a^{A} - {}^{N}\omega^{C} \times {}^{A}v^{L} - \frac{{}^{N}d}{dt}({}^{N}\omega^{A} \times r^{L/A})$$

Then, dot both sides of equation of motion of slung load with $\hat{c}_z$, and apply the inelastic cable assumption, $\frac{{}^{C}d}{dt}({}^{A}v^{L}) \bullet \hat{c}_z = 0$:

$$\left\{\frac{{}^{C}d}{dt}({}^{A}v^{L})\right\} \bullet \hat{c}_z = \left\{\frac{1}{m_L}\left(F_G^L + F_{Aero}^L - F_{F_y}\hat{c}_y - T\hat{c}_z\right) - {}^{N}a^{A} - {}^{N}\omega^{C} \times {}^{A}v^{L} - \frac{{}^{N}d}{dt}({}^{N}\omega^{A} \times r^{L/A})\right\} \bullet \hat{c}_z = 0$$

Where:

$${}^{N}a^{A} = \frac{F_G^A + F_{Aero}^A + F_C^A}{m_A} = \frac{F_G^A + F_{Aero}^A + F_{F_y}\hat{c}_y + T\hat{c}_z}{m_A}$$

Substitute the forces for acceleration:

$$0 = \left\{\frac{1}{m_L}\left(F_G^L + F_{Aero}^L - F_{F_y}\hat{c}_y - T\hat{c}_z\right) - \frac{F_G^A + F_{Aero}^A + F_{F_y}\hat{c}_y + T\hat{c}_z}{m_A} - {}^{N}\omega^{C} \times {}^{A}v^{L} - \frac{{}^{N}d}{dt}({}^{N}\omega^{A} \times r^{L/A})\right\} \bullet \hat{c}_z$$

And rearrange into an equation for the cable tension *T*:

$$-T = \frac{1}{\sigma}\left\{\frac{F_G^A + F_{Aero}^A}{m_A} + {}^{N}\omega^{C} \times {}^{A}v^{L} + \frac{{}^{N}d}{dt}({}^{N}\omega^{A} \times r^{L/A}) - \frac{\left(F_G^L + F_{Aero}^L\right)}{m_L}\right\} \bullet \hat{c}_z$$

Where:

$$\sigma = \frac{1}{m_A} + \frac{1}{m_L}$$

Since $\frac{F_G^A}{m_A} = \frac{(m_A g)\hat{n}_z}{m_A} = (g)\hat{n}_z$, and $\frac{F_G^L}{m_L} = \frac{(m_L g)\hat{n}_z}{m_L} = (g)\hat{n}_z$

Then these terms cancel out in the cable tension equation:

$$-T = \frac{1}{\sigma}\left\{\frac{F_{Aero}^A}{m_A} + {}^{N}\omega^{C} \times {}^{A}v^{L} + \frac{{}^{N}d}{dt}({}^{N}\omega^{A} \times r^{L/A}) - \frac{F_{Aero}^L}{m_L}\right\} \bullet \hat{c}_z$$

A.5 Final Non-Linear Equations

F=ma (aircraft):

$$(\dot{u})\hat{a}_x + (\dot{v})\hat{a}_y + (\dot{w})\hat{a}_z =$$

$$-{}^N\omega^A \times {}^N v^A + (g)\hat{n}_y + \frac{F^A_{Aero}}{m_A} + \frac{F_{F_y}}{m_A}\hat{c}_y - \left[\frac{1}{m_A\sigma}\left\{\frac{F^A_{Aero}}{m_A} + {}^N\omega^C \times {}^A v^L + \frac{{}^N d}{dt}({}^N\omega^A \times r^{L/A}) - \frac{F^L_{Aero}}{m_L}\right\} \bullet \hat{c}_z\right]\hat{c}_z$$

M=dh/dt (aircraft):

$$(I_{xx}\dot{p} + I_{xz}\dot{r})\hat{a}_x + (I_{yy}\dot{q})\hat{a}_y + (I_{zz}\dot{r} + I_{xz}\dot{p})\hat{a}_z + {}^N\omega^A \times (I_{xx}p + I_{xz}r)\hat{a}_x + (I_{yy}q)\hat{a}_y + (I_{zz}r + I_{xz}p)\hat{a}_z =$$

$$M^A_{Aero} + r^{b/A} \times \left[-\left(\frac{1}{\sigma}\left\{\frac{F^A_{Aero}}{m_A} + {}^N\omega^C \times {}^A v^L + \frac{{}^N d}{dt}({}^N\omega^A \times r^{L/A}) - \frac{F^L_{Aero}}{m_L}\right\} \bullet \hat{c}_z\right)\hat{c}_z\right]$$
$$+ \left(K_{\Delta\theta_c}\Delta\dot{\theta}_c\right)\hat{c}_y + \left(K_{\Delta\phi_c}\Delta\dot{\phi}_c\right)\hat{c}_x$$

F=ma (slung load):

Eliminating terms in the $\hat{c}_z$ direction because accelerations in this direction are equal to zero, and removing gravity terms that cancel out:

$$\Delta\ddot{x}_c\hat{c}_x + \Delta\ddot{y}_c\hat{c}_y = \frac{F^L_G + F^L_{Aero} - F_{Fy}\hat{c}_y}{m_L} - {}^N\omega^C \times {}^A v^L - \frac{{}^N d}{dt}({}^N\omega^A \times r^{L/A}) - (\dot{u})\hat{a}_x + (\dot{v})\hat{a}_y + (\dot{w})\hat{a}_z - {}^N\omega^A \times {}^N v^A$$

B. Appendix-B

This appendix describes the process for collecting pilot handling qualities ratings. First, the task is flown at least 3 times to ensure that the pilot is achieving consistent performance before giving a rating. After the task has been completed, the pilot goes through a questionnaire, and then gives a Cooper-Harper rating [32]. This is performed before moving on to another configuration or task, such that the flying qualities of the configuration on that particular task are fresh in the pilot's mind.

The questionnaire that was used to collect pilot comments is shown in Figure B-1. The pilot gives the answers to this questionnaire before giving a Cooper-Harper rating. This questionnaire prompts the pilot to think about the flight characteristics that were observed, which avoids hasty ratings, and also promotes better communication between the pilot and the engineer.

The Cooper-Harper Rating scale is shown in Figure B-2 (from Ref. 26). The Cooper-Harper scale was originally developed to provide a standardized rating scale that was focused on handling qualities. The scale has a series of questions on the left hand side that the pilot answers before moving to the right in the respective Level category to determine the rating.

Task Performance

1. Describe ability to meet DESIRED / ADEQUATE performance standards.
2. Describe aggressiveness / precision with which task is performed.
3. If trying for DESIRED performance resulted in unacceptable oscillations, did decreasing your goal to ADEQUATE performance alleviate the problem?

Aircraft Characteristics

4. Describe any objectionable controller force characteristics.
5. Describe predictability of initial aircraft response.
6. Describe any mid- to long-term response problems.
7. Describe any objectionable oscillations or tendency to overshoot.
8. Describe any non-linearity of response.
9. Describe any problems with harmony of pitch and roll, speed control, with height control, and with heading hold/turn coordination.

Demands on the Pilot

10. Describe overall control strategy in performing the task (cues used, scan, etc.).
11. Describe any control compensation you had to make you to account for deficiencies in the aircraft.
12. Describe any modifications you had to make to what you would consider "normal" control technique in order to make the aircraft behave the way you wanted.

MISC.

13. Please comment on anything else that may have influenced you.

Assign HQR for overall task.

14. Using the Cooper-Harper rating scale, please highlight your decision-making process and adjectives that are best suited in the context of the task. If assigned HQR is Level 2, briefly summarize any deficiencies that make this configuration unsuitable for normal accomplishment of this task.
15. What was the critical sub-phase of the task (e.g., entry, steady-state, exit) or major determining factor in the overall Handling Quality Rating (HQR).
16. For cases with external load, did the load have a significant impact on the assigned HQR?

Figure B-1. Pilot Questionnaire.

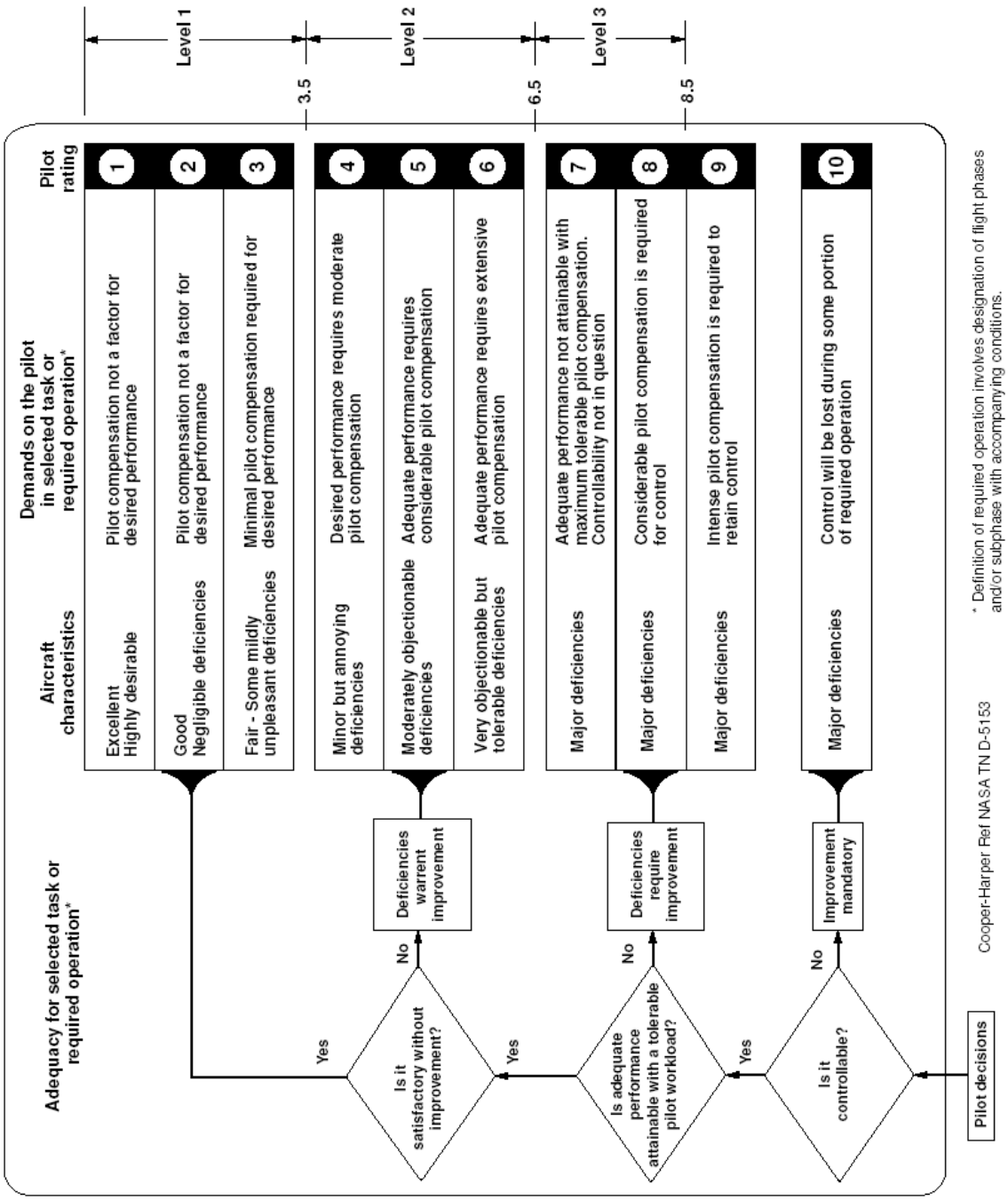

Figure B-2. Cooper-Harper Rating Scale [32].

INITIAL DISTRIBUTION LIST

		Copies
Defense Systems Information Analysis Center SURVICE Engineering Company 4695 Millennium Drive Belcamp, MD 21017	Ms. Jessica Owens jessica.owens@dsiac.org	Electronic
Defense Technical Information Center 8725 John J. Kingman Rd., Suite 0944 Fort Belvoir, VA 22060-6218	Mr. Jack L. Rike jackie.l.rike.civ@dtic.mil	Electronic
AMSAM-L	Ms. Anne C. Lanteigne hay.k.lanteigne.civ@mail.mil	Electronic
	Mr. Michael K. Gray michael.k.gray7.civ@mail.mil	Electronic
RDMR		Electronic
RDMR-CSI		Electronic
RDMR-ADF	Ms. Christina Ivler christina.m.ivler.civ@mail.mil	Electronic